ProQuest Number: 10131281

ProQuest 10131281

ProQuest LLC.
789 East Eisenhower Parkway
P.O. Box 1346
Ann Arbor, MI 48106 – 1346

The Characteristics and Low Level Counting Capabilities

of Ge(Li) Gamma Ray Spectrometers

by

Graham V. Walford

Abstract

The development of the Ge(Li) gamma ray spectrometer is incomplete in several areas, particularly those relating to low level counting. This thesis is an attempt to define their low level counting capabilities.

A Ge(Li) gamma ray spectrometer was developed and several aspects of its performance were investigated. In particular, emphasis was placed upon cryostat operation and the calibration, measurement, diagnosis and repair of detectors. Due to its significance in low level counting, the efficiency of detection of gamma rays has also been evaluated. It was found that some detectors had efficiencies of detection smaller than that expected from their size. Other problems associated in the optimisation of efficiency were also considered.

An expression has been derived, and experimentally verified, for the sensitivity limit of a Ge(Li) spectrometer and is found to depend upon the absolute efficiency of detection, background continuum, energy resolution, count time and the required statistical precision. This expression has been used to evaluate the significance of these parameters. The measurement of short lived isotopes has also been accounted for.

Several counting configurations (e.g. coincidence, anti-coincidence, and massive shielding arrangements) are available and have varying degrees of effectiveness when used for low level counting. A comparative method has been evolved to evaluate the usefulness of each technique. It is found that massive shielding, certain alpha-gamma and beta-gamma coincidence, and anti-coincidence methods have the best low level measurement capability and can reach levels of the order of 1 pCi.

Data is presented in certain cases to substantiate predictions. Such analyses are valuable in that they can allow performance predictions for spectrometers. Evaluation of additions of new counting configurations (or detectors) to an existing spectrometer is also feasible. No previous analysis of this type has been undertaken.

Acknowledgements

Contents

Chapter 7
The Low Level Counting Capabilities of Ge(Li) Detectors

Chapter 1

A Brief Description of the Principles of Ge(Li) Gamma Ray Spectrometers

1.1 Introduction

Ge(Li) gamma ray detectors are now well established in the field of gamma ray spectroscopy. Since their first experimental demonstration (Freck and Wakefield 1962) they have been successfully used for many applications. Current detectors can now reach energy resolutions* of 1.8 keV (Gibbons 1969), peak height to Compton edge ratios** of 37 to 1 (Canberra Industries Inc.) and drifted volumes of the order of 120 ccs (Henck, Siffert, Miehe and Coche 1969). In addition, timing resolutions (Quaranta, Martini and Ottaviani 1969) of the order of nanoseconds may be achieved.

A large volume of published material is available. This is well indexed by Bock (1967), Bornand (1968) (specialising on fabrication) and McKenzie (1969). The field is also well reviewed by Dearnaley and Northrop (1966), Adams (1966), Hollander (1966), Gunnersen (1967), Bertolini and Coche (1968) and Crouthamel, Adams and Dams (1970) and cover the major aspects of the development of Ge(Li) detectors. The more technical improvements in system performance have been achieved by the commercial companies and hence minimal detailed information is available. A study of the above literature yields a sound introduction into the principles and applications of Ge(Li) detector systems. At the beginning of the work for this thesis (1966) it was observed that there was, and still is, a marked lack of information regarding their low level counting capabilities. It was this point that led to the choice of this thesis subject.

1.2 The Development of the Ge(Li) Detector

The first use of semiconductors for radiation detection was demonstrated by McKay (1949), who constructed a p-n junction by placing a phosphor bronze needle point upon a germanium slice. The resulting sensitive volume, although only of the order 10^{-3} mm diameter, was sufficient to detect alpha particles. In the following decade considerable emphasis was placed

---

* Measured as full width at half maximum peak height (FWHM) for the 1.333 MeV gamma ray peak from ^{60}Co

** Measured for the 1.33 MeV peak of ^{60}Co

on the development of silicon and germanium for transistor manufacture, and this resulted in the availability of high purity semiconducting materials for radiation detector development.

Mayer and Gossick (1956) manufactured a germanium surface barrier detector, satisfactory for particle detection but inadequate for gamma rays due to the small sensitive volume. Both silicon and germanium p-n junction detectors were subsequently developed, the depletion layer being the sensitive region and hence inherently limited in this type of structure. Applications were thus limited to particle and X-ray measurement. At this stage, silicon detectors met wide use largely due to their ability to function at room temperature.

In 1960, Pell developed a means of achieving deeper depletion regions by the lithium ion drift process. Elliot (1961) managed to achieve sensitive depths of silicon of a few mm using Pell's technique. The ion drift principle was then applied to germanium, with its much higher gamma ray absorption coefficients and Freck and Wakefield (1962) demonstrated the first Ge(Li) gamma ray spectrometer. It was at this stage that relatively high energy resolution detectors, with workable efficiencies of detection, could be realised and this led to the wide-spread interest in the Ge(Li) detector as a gamma ray spectrometer.

Ewan and Tavendale (1964) fabricated devices with sensitive volumes of a few cubic centimetres, and demonstrated their use for several measurements in pair spectrometers, coincidence and anti-coincidence systems. The prime difficulties encountered then, as now, were in obtaining germanium ingots of appropriate quality (Coleman 1966, Muggleton 1967).

Fabrication techniques and results were highly dependant upon material quality and conditions frequently outside the control of the experimenters. This led to a large number of "recipe" type papers for detector fabrication (Bornand 1968). The principal effort was centred upon resolution and sensitive volume improvements. Malm and Fowler (1965), produced the first large volume coaxial detector with a volume of 54 cm^3. This was roughly equivalent to a 4 cm dia by 2.5 cm thick NaI(Tl) scintillator but with an energy resolution of 4.8 keV. In subsequent developments the detector quality was improved rapidly, but there were no large increases in sensitive volume. The germanium ingots were still the limiting factor to volume improvements.

It became appreciated that an increase in sensitive volume did not necessarily lead to an increase in efficiency (Walford and Doust 1968).

At the present time, detectors of all sizes are in use since it rapidly became apparent that smaller volume detectors are frequently more suited to certain applications (Camp 1967). The smaller detectors can offer simpler spectral analysis due to reduced peak interference (Gibbons 1968).

The Ge(Li) detector is well suited to timing measurements (Quaranta et. al 1969) and has been used in pair spectrometers (Tavendale 1964), coincidence arrangements (Shirley 1968), and anticoincidence systems, (Camp 1969).

Special arrangements of detectors have been made to extend the flexibility of systems and for special applications. Levey (1966) has fabricated annular detectors for nuclear reaction studies, while Saunders (1966), Ridley (1967), Lalovic (1969), Walford (1971) and Larsen and Strauss (1970) have stacked detectors together to increase the efficiency of detection. Dearnaley, Hardacre and Rogers (1968), have developed thin window detectors, suitable for high energy particles and X-rays. Guard ring devices (Tavendale 1966) and grooved detectors (Harchol 1969), result in high energy resolution performance and accurately define counting geometry while being relatively insensitive to handling. One major limitation remaining in detector flexibility is the unavoidable use of a cryostat, although some designs can allow considerable freedom of manipulation (Franke 1969).

The potential energy resolution of semiconductor spectrometers realised in the early 1960's placed severe demands on electronic requirements and in data handling. This demand helped to stimulate development of low noise amplifiers and multi-channel analysers. Low noise field effect transistors (FET) were used in the input of the preamplifier (Radeka 1965) and rapidly superseded the use of vacuum valves. Benoit (1969), has reviewed electronic considerations for semiconductor detectors and gives an adequate description of the problems confronted. Fairstein (1965), has also discussed main amplifier design for optimum noise performance. Electronic noise performances of less than 1 keV are now readily possible, and if the first stage F.E.T. is cooled then this can be reduced below 0.2 keV. High speed analysers having in excess of 4000 channels are now also available. It is also becoming common to use analogue to digital converters coupled directly to computers for direct data processing (Thompson 1969). This situation is a great advance from the mid 1950's when it was unusual to have analysers with more than 100 channels, these frequently being of prohibitive size.

There have been extensive applications of Ge(Li) spectrometers in nuclear physics and neutron activation analysis. The nuclear field itself if large and is briefly illustrated by measurement of neutron capture gamma rays (Shirley 1965 and Michaelis and Schmidt 1966), mesonic atoms (Nilsson 1966), short nuclear lifetimes (Allen 1966) and isomeric states (Yamazaki and Ewan 1968).

Neutron activation analysis has also been exploited (Sklavenitis 1967). Applications vary as widely as forensic study (Guinn 1967), geological sample assay (Gorden, Baedecker, Anderson and Dran 1968), detection of forged paintings (Schroeder, Kraner and Robley 1966) and trace element analysis in metals (Prussin, Harris and Hollander 1965) and human tissue (Perkins and Haller 1967).

There is also a steadily increasing range of other measurements in medical applications and in natural activity measurements where the activity levels are easily detectable as in the pitchblende measurements of Williams (1966) and fallout samples of Aakrog and Lippert (1965). It is noticeable that the low level counting capabilities have remained largely unexplored.

1.3 Charge Collection and Generation Applicable to Semiconducting Solids

The detector, for the purposes of this discussion, may be considered as analogous to a solid state ionisation chamber. For an incident gamma ray to be recorded in the full energy peak of the resulting spectrum, its entire energy must be deposited in the sensitive volume of the detector and then totally collected. Ignoring charge collection effects, the resulting pulse output will then be directly proportional to the incident gamma ray energy. The process of deposition and collection is considered in three parts, namely the primary gamma ray interactions, conversion to electron hole pairs and the collection of the generated charge.

1.3.1 The Conversion of Gamma Ray Energy to Single Electrons

Deposition of gamma ray energy occurs largely by three basic processes (Davisson and Evans 1951), Compton effect, pair production and photoelectric effect. Of these, the photoelectric effect and pair production result in entire deposition of the gamma ray energy. The Compton effect (Fig. 1.1) results in a varying percentage of the energy being deposited which adds a continuum to the spectrum observed (Fig. 1.2).

The collection of energy deposited by pair production however, is affected by secondary effects. The electron loses its energy in various processes (to be described), while the generated positron after losing its kinetic energy ultimately annihilates with an electron (Fig. 1.1), resulting in two 511 keV gamma rays which must be totally absorbed if a linear energy-response relationship is to be maintained. The loss of one or both gamma rays results in a 'single' or 'double' escape peak (Fig. 1.2) and if one or both of the escaping gamma rays interacts in a Compton interaction before escaping then the initial gamma ray will contribute to the continuum between the single escape peak and the full energy peak (Fig. 1.2).

Should the initial interaction be a Compton or pair production event, then the scattered photon and annihilation radiation must undergo total absorption to maintain the linear relationship. This involves total collection of multiple scatter events (Fig. 1.3), and is energy dependant, depending upon the absorption coefficients prevailing (Fig. 1.4). Below 500 keV, photoelectric events dominate, while above this figure multiple scatter contributes significantly to the full energy peak, being Compton dominated until 2 MeV, and thereafter by Compton and pair production events.

It is evident that, since the secondary interactions depend upon the spatial extension of sensitive volume, its shape has some effect upon the full energy peak efficiency. For significant contribution to the full energy peak efficiency by multiple scattering, the sensitive volume should be compact depending upon the energy range of interest (Section 5.2.2.2).

1.3.2 The Generation of Electron Hole Pairs

The energetic electron (energised by the gamma ray) loses energy to the crystal lattice, by repeated collisions. This results in a large number of lattice excitations and electron-hole pairs. Some energy is also lost by the generation of bremsstrahlung that may be re-absorbed by the processes described in Section 1.3.1. Ultimately, the entire energy is deposited in the form of electron hole pairs and localised lattice heating. As the average energy required to create an ion hole pair (w) in germanium is small (2.94 eV), a large number of pairs are generated. The division of energy between electron and lattice excitations and electron hole pairs is statistical and hence there is a variance associated with the total number of pairs collected for the same energy input. The

Fig. 1.1
Three Basic Interactions of Gamma Rays with Matter

Compton
Scatter

Photoelectric

Pair Production

.511 MeV

e^+

e^-

γ

e^-

e^-

.511 MeV
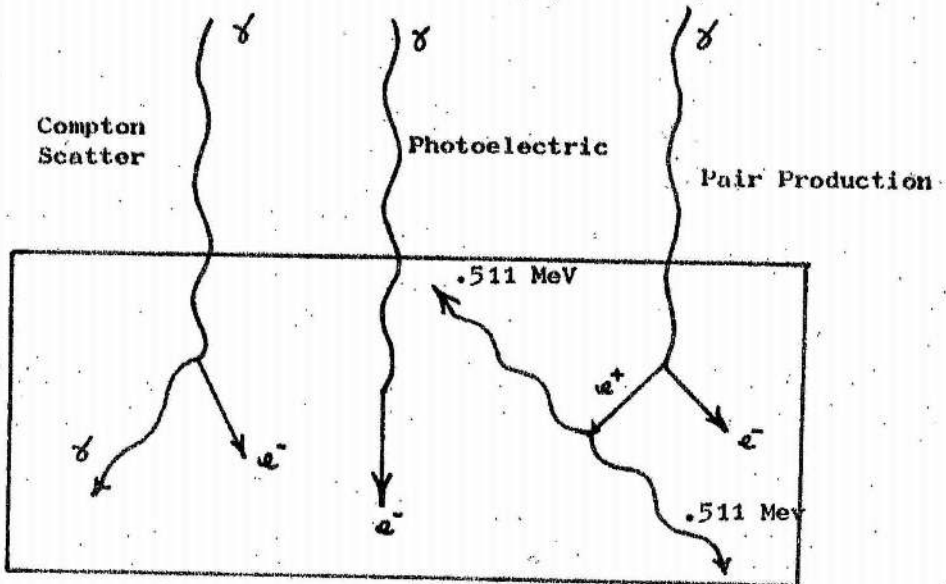
Fig. 1.2
Line Spectrum Showing Energy Deposition in a Solid from Gamma Rays

Intensity

Both 0.511 MeV quanta
interacting before escape

Full Energy
Deposition

Compton
Continuum

Single escape
line

double escape
line

One 0.511 MeV quanta
interaction before
escape, also multiple
Compton scatter with
a γ escape
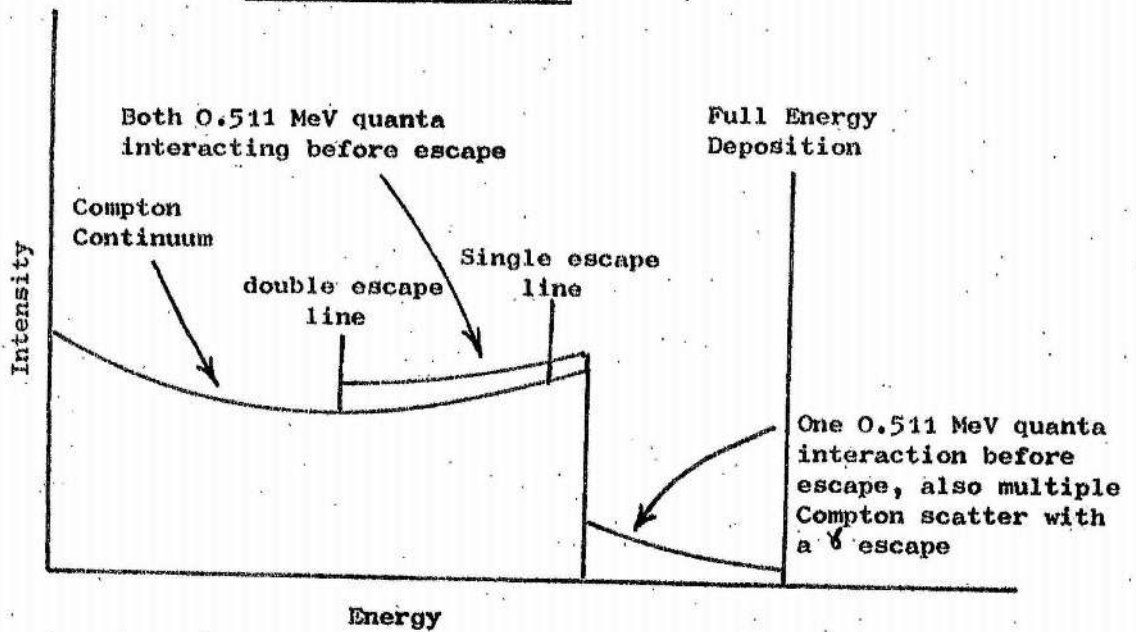
Energy

Fig. 1.3
Two Examples of Multiple Scattering in a Solid, Resulting in Total Energy Deposition

P.E. = Photo Electric Effect

C.S. = Compton Scatter

P.P. = Pair Production
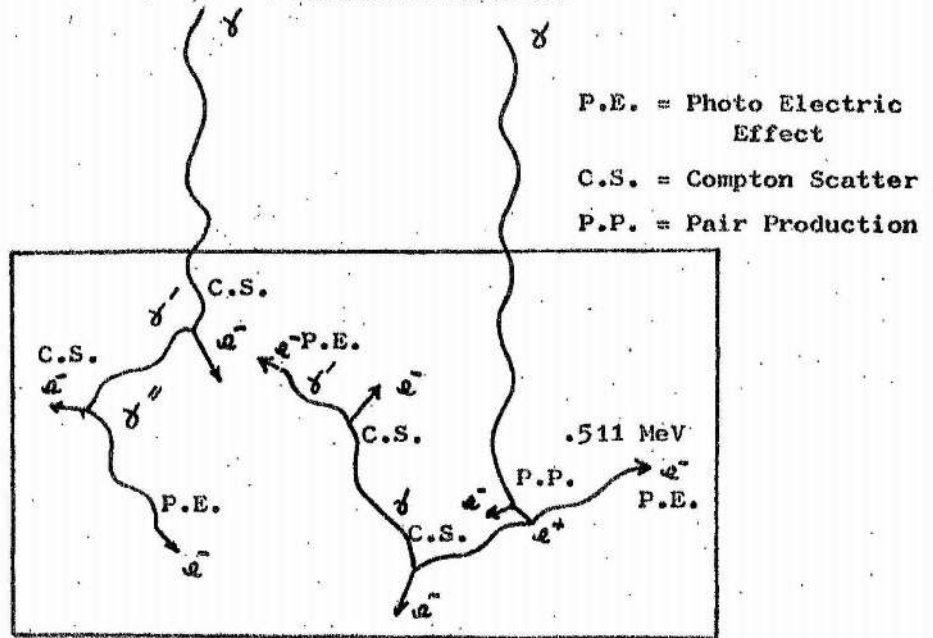
Fig. 1.4
The Photon Absorption Coefficients of Germanium with Silicon shown for Comparison (Chapman 1968)
(Electron ranges also shown)
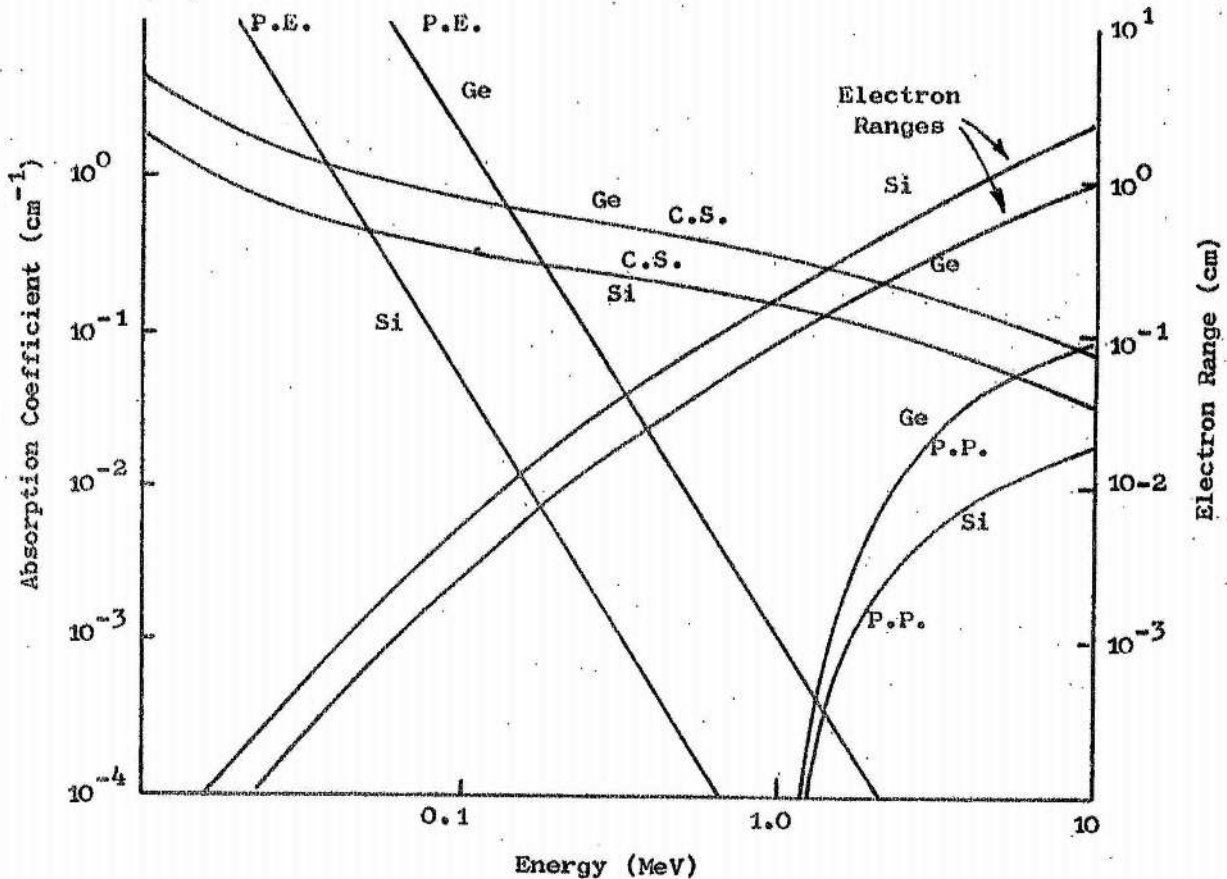
theoretical treatment has been considered for gases by Fano (1947).
Theoretical determinations for w and Fano's theory have been considered
in detail by Restelli and Rota (1968), Klein (1966), the Gatlingburg
Conference (1967), Pehl and Goulding (1970) and Zulliger and Aitken (1970)
and hence is only briefly considered here.

The variance may be expressed as follows:-

Let E = energy of incident ionising radiation,

then $N = \dfrac{E}{w}$ where N = average number of ion pairs generated.

If σ = root mean square of the ion pair yield then

$F = \dfrac{\sigma^2}{N}$ where F (Fano factor) is a figure used to express
the degree of correlation between the process
producing ion pairs and excitations.

If $F = 0$, then there is no lattice excitation and only ion hole pairs are
generated.   If w is large and the number of pairs generated is small,
then Poisson statistics hold and $F = 1$.   Hence $\sigma^2 \sim N$.   This is the case
for scintillators.

The factor, F, may be measured and has been found to be a
function of germanium quality, the lower the value, the better the quality.

It is this phenomenon that provides the ultimate limitation to
the energy resolution obtainable from the semiconductor detector.

1.3.3 Phenomena Involved During Charge Collection in Semiconductors

The semiconductor detector is operated under a reverse bias
voltage and charge liberated by gamma rays being swept to the electrodes
(p and n layers), by the electric field across the intrinsic region
gives rise to an output pulse.   Ideally, the intrinsic region should be
free of mechanisms (traps) that cause charge loss but this is never
completely achieved in practice (Mayer 1969 and Restelli 1968).

Charge is lost by recombination of ion pairs either by chance
meeting or by capture of an electron at an impurity site, or structural
defect that is also sensitive to hole capture.   These centres are termed
recombination centres.   From a consideration of energy levels, the
recombination centres have deep energy levels in the forbidden gap which
can exist in one of two states of electronic charge.   These states, if
empty, can capture an electron from the conduction band and can then
either release the electron to the original band or, by capturing a hole
from the valence band annihilate both carriers.   As the centre is left

in its original condition after the recombination it is capable of
recombining a large number of carriers.

Recombination also occurs at surfaces where the band structure
may be distorted and contamination considerable. This can be considered
as a special case of the bulk recombination mentioned above.

Localised levels, in addition to the above mechanisms, exist
which capture carriers but do not cause recombination. These are indicated
as shallow trapping levels. A trapping level such as this only exchanges
carriers with one band and holds them for a limited time. The carrier then
returns to its original band (detrapping). This process affects the appar-
ent carrier mobility.

In practice, the performance of the semiconductor detector is
entirely dominated by its trapping and carrier lifetime and the carrier
mobility is trap dependant rather than material dependant. The criterion
is whether the amount of trapping present can be tolerated in its effect on
a particular detector. The nett effect of the above processes is the loss
of charge and some delay in its collection, giving longer pulse rise times.

The reverse bias across a detector (ideally $>$ 100 volts/mm
depleted region), generates leakage current from a number of sources, (Ellis
1968), in particular the bulk and its surfaces. In imperfect detectors,
this may be considerable, but whatever the order of magnitude, the accurate
measurement of the gamma ray generated charge is perpetually impaired by a
background flow of electron and holes.

1.4 The Choice of Semiconductors and Techniques for Solid State Detectors

Semiconducting solids have been widely exploited for use as
particle detectors by the manufacture of a p-n junction and use of the
depletion region. By selection of suitable solids, and techniques of
achieving effectively intrinsic material, the depletion region depth may be
increased. The efficiency of particle detection is optimised by using the
deepest possible depletion region coupled with the highest Z material pos-
sible. The Ge(Li) drift process gives the best results at present.

Three basic techniques may be used for the production of intrinsic
material. The first is that of acceptor compensation by the drifting of
suitable donors into the material (for example lithium drifting in germanium
and silicon, Pell 1960).

The second technique, also one of compensation of existing impurity centres, relies upon compensation by production of radiation induced defects (Ryvkin and Matveev, 1966 and 1968). These workers have managed to produce sensitive depths of the order of 3 mm in germanium. They have also attempted fabrication of similar detectors using cadmium telluride. However, the technique has been found to be inherently limited by the large numbers of trapping centres also generated by the induced defects. In addition, the technique is insensitive to small inhomogenietes in acceptor concentration in the bulk material.

The third technique, now starting to show promise (Tavendale 1970) is the direct pulling of high purity ingots (Hall 1966, 1968). The best material so far achieved using depths of the order 2 - 3 mm for germanium, has given an energy resolution of 2.06 keV for ^{60}Co. This material has the great advantage of rapid detector fabrication in comparison with the lithium drift process. However, it will be several years before this process is directly competitive with the highly successful drift process.

The possibilities of using other semiconducting compounds have been considered (Brown and Wagner 1966, Mayer 1968). Several materials show promise (Gunnerson 1967) but lack the intensive development that silicon and germanium have enjoyed. Working detectors have been made from cadmium telluride by Akutagawa and Zanio (1968) and Zanio, Akutagawa and Mayer (1968) who also used gallium arsenide. Weisberg and Goldstein (1968) have also used gallium phosphide as well as gallium arsenide. To date, the maximum sensitive depth produced with these materials has been of the order of 2 mm and with relatively poor performance. These materials also have inherently poorer ultimate resolutions from considerations of their band gap and Fano factor. However, further development is required since these materials have the important potential of the ability to operate at room temperature.

1.5 The Characteristics of Ge(Li) Detectors

The requirements and characteristics of Ge(Li) detectors, are best understood by consideration of the fabrication processes. These considerations also form the basis of the processes and phenomena discussed in chapters 4 and 5.

1.5.1 The Fabrication Process

The process is commenced by the selection, shaping and etching of a suitable ingot of p type germanium. One face of the ingot is then lithium diffused at 380°C for approximately 20 minutes. The return of the crystal to room temperature results in a supersaturated lithium rich n type layer diffused approximately 0.5 - 1 mm deep. The application of a reverse bias to the newly formed p-n junction causes the highly mobile lithium ions to drift into the crystal. This process is such (Pell 1960) that the lithium ions form a spatial distribution, according to the prevailling electric field, to automatically compensate for the distribution of acceptor sites. The germanium, usually boron doped for drifting purposes, is not only compensated for the p type boron sites, but any other nett variations in acceptor density throughout the crystal.

The temperature during drift is usually of the order of 30°C. As the drift depth increases, the reverse bias leakage current also increases. This is due to the overall increase of bulk generated current and is indicative (Ellis 1968) of the drift progress. The bulk generated current distorts the lithium compensation (Lauber 1969) in the following manner.

Fig. 1.5a shows the generated charge flow in the drifted region under reverse bias. Fig. 1.5b shows the resulting space charge density. This results in the distortion of the electric field from uniformity as shown in Fig. 1.5c due to thermally generated bulk currents. This distortion generates the distorted lithium profile of Fig. 1.5d. The dotted level represents that expected with perfect acceptor compensation in the drifted region. If this detector is now cooled for use, the performance will be poor due to poor electric fields and excess trapping in the poorly depleted regions. This may be remedied by drifting the detector after the main drift at a lower temperature where the bulk current is much reduced and there is still sufficient lithium mobility for effective compensation. The drift is sustained for about four days at about 0°C to -10°C and at as high a reverse bias as possible. This results in the lithium distribution being levelled to the ideal dotted line profile of Fig. 1.5d.

The detector is now mounted in a vacuum cryostat where it is usual to perform a further short cold drift in order to outgas the intrinsic surfaces as well as to complete the compensation process. The detector should be ready for use after cooling to liquid nitrogen temperatures.

Fig. 1.5

Characteristics Observed in the Lithium Drifting of Germanium

a) Charge Flow in the Intrinsic Region

b) Resulting Charge Density

c) Electric Field Distortion due to Thermally Generated Current Flow

d) Resulting Lithium Distribution

——— after drift

- - - - after cold drift
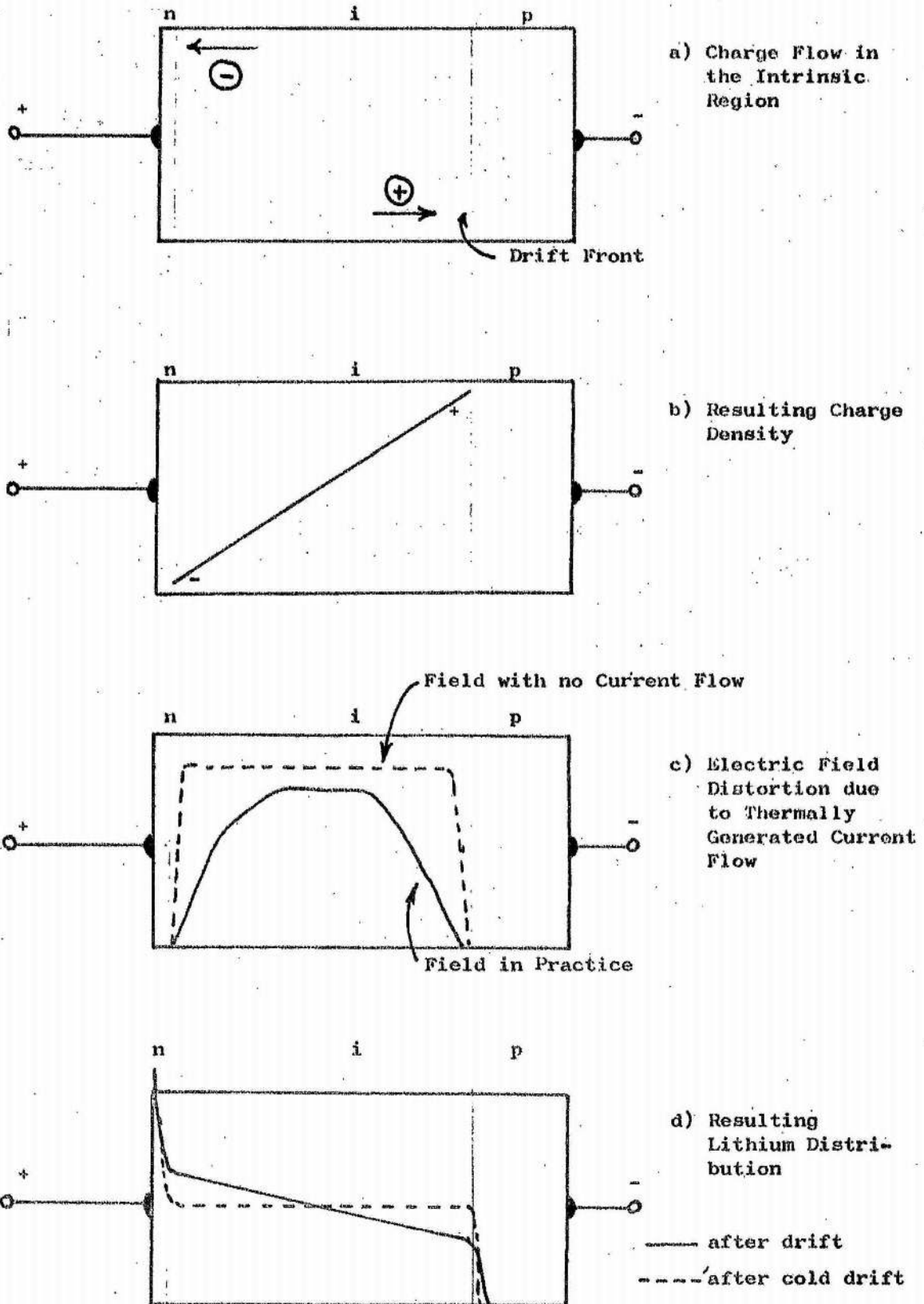
1.5.2 The Environmental Requirements and Characteristics

The detector must be cooled for two reasons. The first is due
to the large leakage current at room temperature, destroying any high
resolution potential. The second is due to the high lithium mobility at
room temperature. The p-i-n structure is not preserved (Webb 1968) and
any time the detector spends unbiased at room temperature results in degra-
dation of detector quality and loss of lithium through precipitation pheno-
mena. The detector must always be stored and used below -60°C. This is
conveniently effected with a vacuum cryostat with a thin entry window for
minimum gamma ray absorption.

Several workers have investigated the choice of working temperature
for the Ge(Li) detector. El-Shinshini and Zobel (1966) have measured per-
formance changes down to 77°K while Sakai and Malm (1967) and Elad and
Nakamura (1968) have measured performance changes down to 5°K. The lowest
temperatures are not suitable due to the cost of maintaining helium cryostats
and the presence of a slow rising charge collection component below 20°K.
The optimum temperature has been found to be near that of liquid nitrogen
(Martin, McMath and Fowler 1970) and for convenience, liquid nitrogen is
invariably used.

For the optimum performance, the detector capacity and leakage
current must be as small as possible. In this way the preamplifier noise
is minimised. The capacity is a function of the fabrication technique, the
lower capacity indicating the better quality detector. The better quality
detectors will also have lower bulk leakage. However, surface currents are
also critical and to date, they are best minimised by keeping the intrinsic
surfaces exposed only to vacuum. Detectors typically available from the
major manufacturers operate at reverse bias voltages as high as 3500 volts
at leakage currents of 0.1 to 1.0 nA. It is thus evident that the operating
conditions of the detector can only be sustained by an ultra clean vacuum
environment in the cryostat, maintained permanently at liquid nitrogen
temperature.

Chapter 2

Cryostats for Ge(Li) Detectors

2.1 Introduction

The cryostat requirements deduced from section 1.5.2 are:-

1) Scrupulously clean internal cryostat walls inside the cryostat and a vacuum better than 10^{-6} torr.

2) Efficient cooling with minimum heat loss.

and from section 1.3.1:-

3) Thin entry window and a minimum of bulk materials near the detector to reduce unwanted scatter contribution in the gamma ray spectrum.

The first two requirements are essential for maintenance of crystal condition, while the third is to obtain optimum spectral response. It is also important to provide sufficient electrical feedthroughs for the use of a test pulse and thermocouple for temperature measurement in addition to the signal output.

Cryostats fall into two categories, those that cool the detector by a dripfed supply of liquid nitrogen and those that cool via a copper conduction rod (dipstick cryostat) inserted into a dewar of liquid nitrogen. This chapter is descriptive of the cryostats used and the precautions taken to obtain optimum performance.

2.2 Basic Constructional Requirements

Where possible, all cryostat materials should be of stainless steel (with the possible exception of the aluminium end cap) due to its potential cleanliness and outgassing properties. All joints should be argon arc welded. The use of rubber 'O' rings is avoided with the possible exception of that of the end cap. For an effective performance to be maintained the cryostat is internally scoured, leak tested and baked to at least 200°C.

It is advantageous to nickel plate the copper or aluminium cold finger of the cryostat to reduce heat loss and reduce surface outgassing.

For effective evacuation, the pumping port should be at least 1.5 cms diameter. If an ion pump is fitted, care should be taken in its

Fig. 2.1
Schematic Diagram of Vertical Dripfeed Cryostat

10 Litre Dewar

Electrical Feed-throughs in Screened Box

To Pump

Liquid Nitrogen

Stainless Steel End Cap

Cooling and Spacing Block

Thermocouple

Detector Clamp

Signal and E.H.T. Lead

Be Window
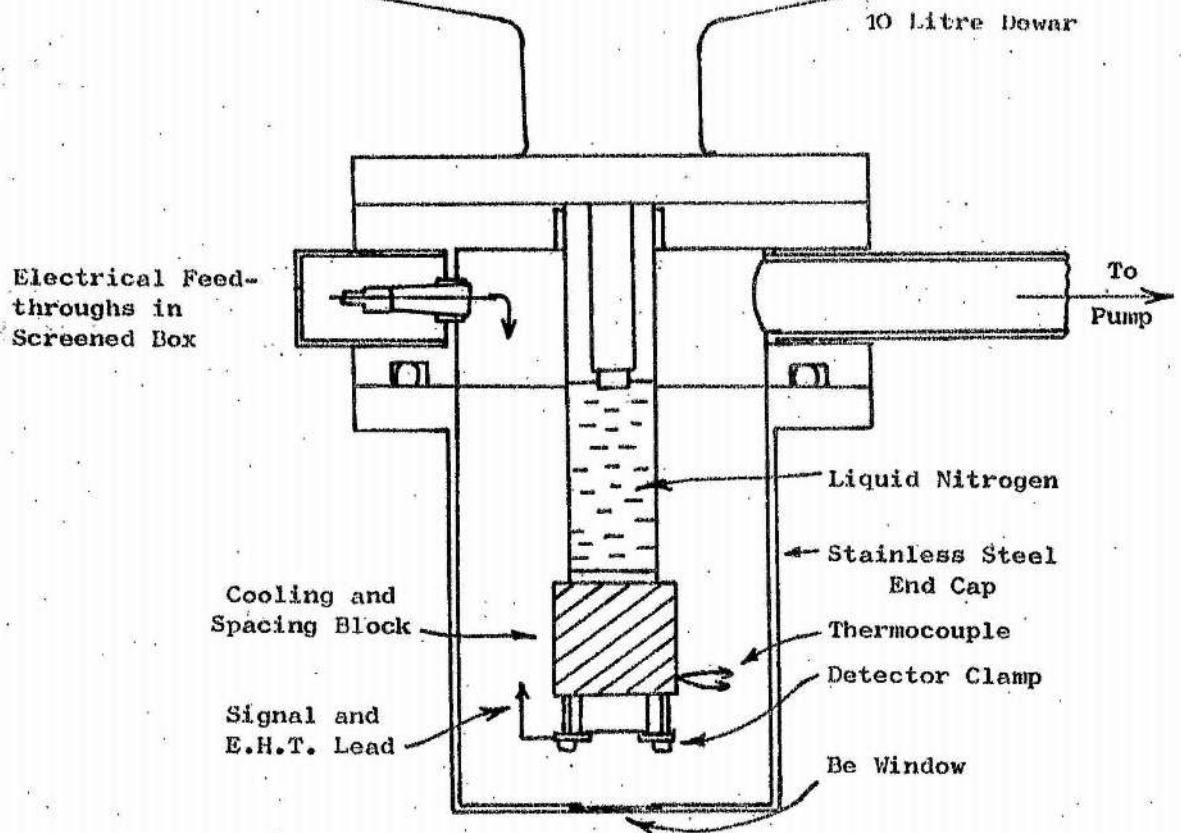
Fig. 2.2
Extension Cold Finger to Extend Crystal into an Anticoincidence Shield

Aluminium End Cap with 1.5 mm wall

30 cms

Aluminium Extension Finger
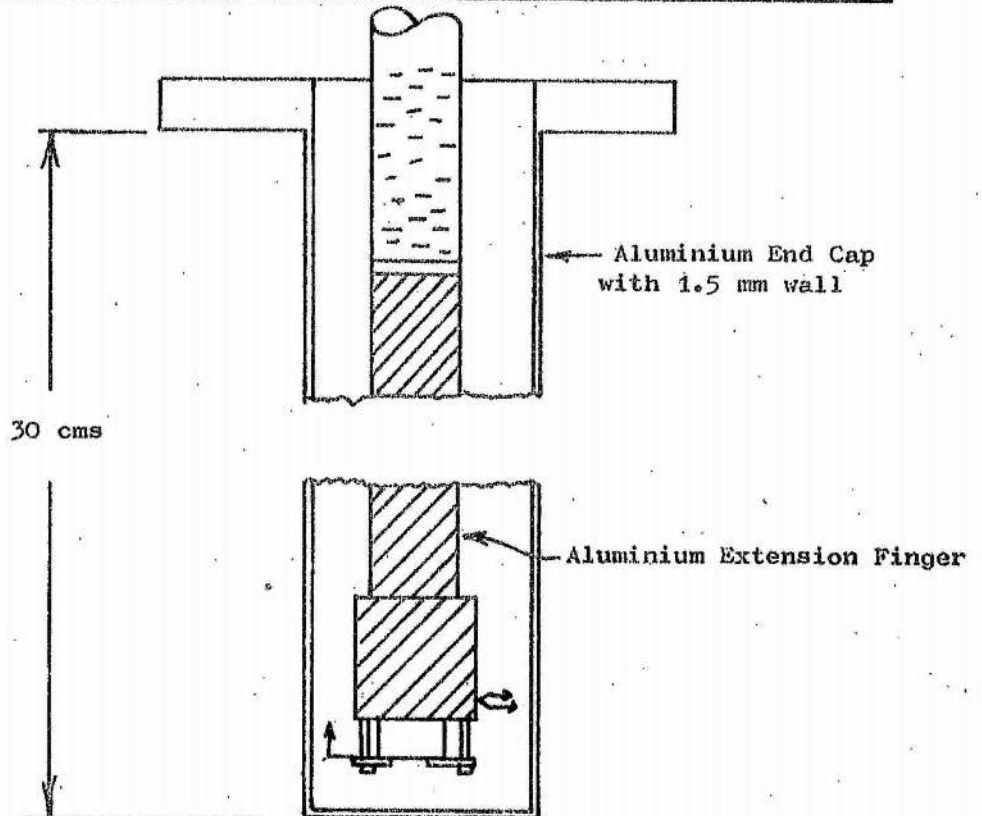
Fig. 2.3

Schematic Diagram of Horizontal Dripfeed Cryostat

To 10 litre Dewar

To Pump

Sloped to
Prevent Nitrogen
Bubbling

Copper Cold
Finger

Feedthroughs in
Screened Box

Aluminium Cold Finger

Crystal

Aluminium End Cap
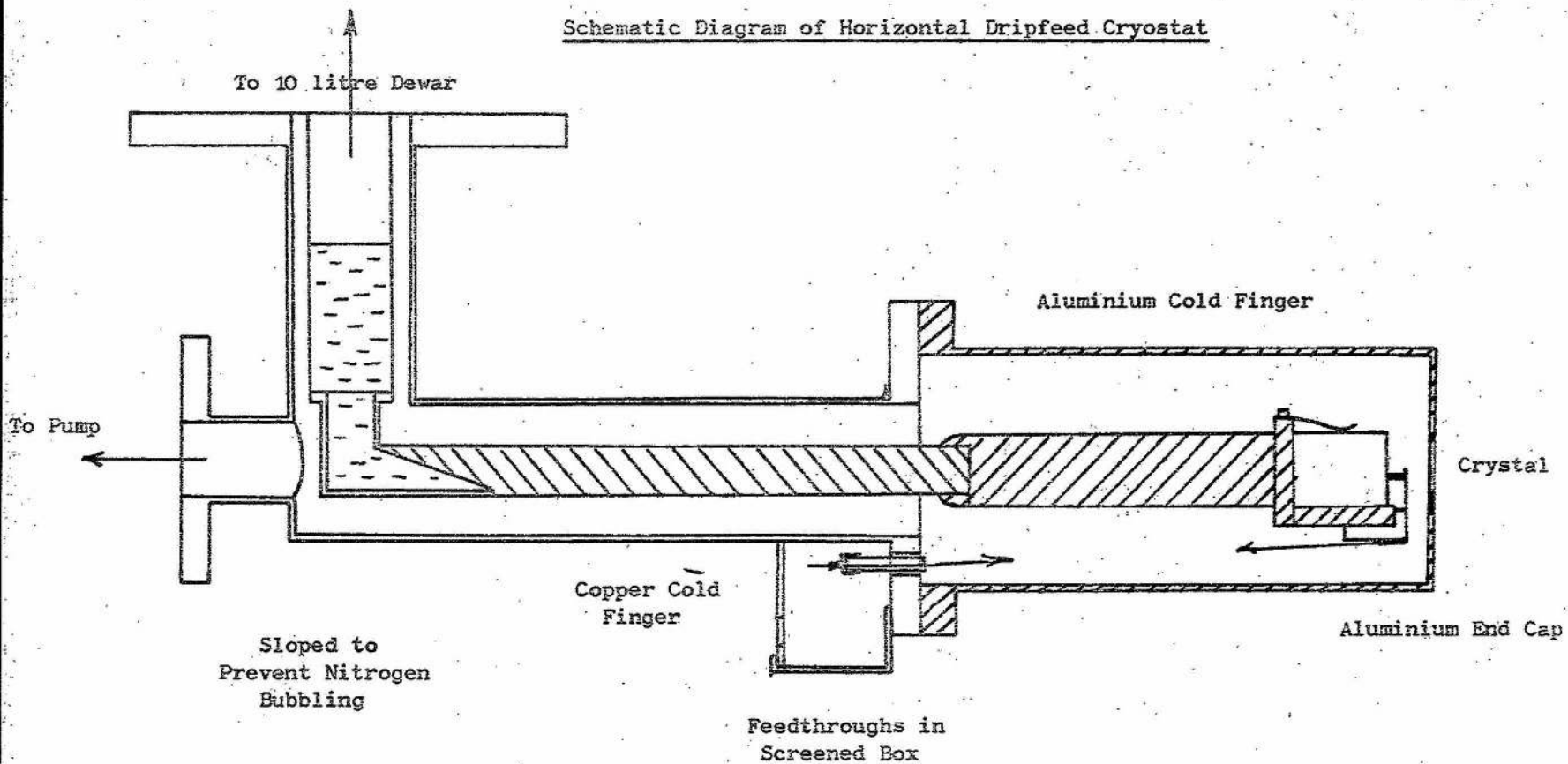
positioning. Ellis (1969) has pointed out that in certain conditions (usually when pumping out a cryostat after a detector mounting) titanium ions may escape and be deposited on the crystal. This effect is enhanced if the pump and detector are in direct line and operate at opposite potentials. Ridley (1969) has reduced this problem using a wire grid over the ion pump outlet port, and by changes in the evacuation and cooling procedure.

2.3 The Dripfeed Cryostat

The constructional principles outlined above are illustrated by reference to several designs developed in this present work.

Fig. 2.1 shows the general layout of the vertical dripfeed cryostat used. Liquid nitrogen fills the detector supply tube (termed cold finger) to the bottom of the reservoir supply tube. This level is maintained automatically by an excess pressure between the reservoir and detector supply tubes. Heat loss, by conduction, is minimised by using 0.15 mm wall stainless steel tube with internally polished surfaces. A removable end cap with rubber 'O' ring seal facilitates the mounting of the detector. This end cap (of stainless steel) has a thin entry window of 0.5 mm thick berellium let into its end face.

The cryostat was subsequently modified to allow the detector to be inserted into an anticoincidence shield (Fig. 3.5). Fig. 2.2 shows the stainless steel end cap replaced with an extended aluminium end cap. The cold finger is also extended with an aluminium conduction rod. The nitrogen bubbling is no longer near the crystal and hence microphony is reduced.

The vertical dripfeed cryostat may be adapted to position a detector horizontally. Fig. 2.3 shows the system adopted which is modified from a design used by A.E.R.E. Harwell. The nitrogen supply tube is extended sideways with a copper rod and terminated in aluminium to reduce backscatter. Microphony, introduced by nitrogen bubbling is at a minimum. Fig. 2.4 shows the cryostat after the mounting of a detector (Fig. 4.14 a,b) during a cold drift operation. Fig. 2.5 shows the complete system assembled with preamplifier and liquid nitrogen dewar after the detector had been cooled.

This cryostat similarly incorporates an aluminium end cap, but with the end wall thickness thinned to 0.5 mm as a thin entry window. In this case, an indium wire vacuum seal was used for the end cap. However, the detector mounting technique must be both rapid and effective and the

Fig 2.4

Photograph of Dripfeed Cryostat Taken During the Cold Drifting

of a Newly Mounted Detector
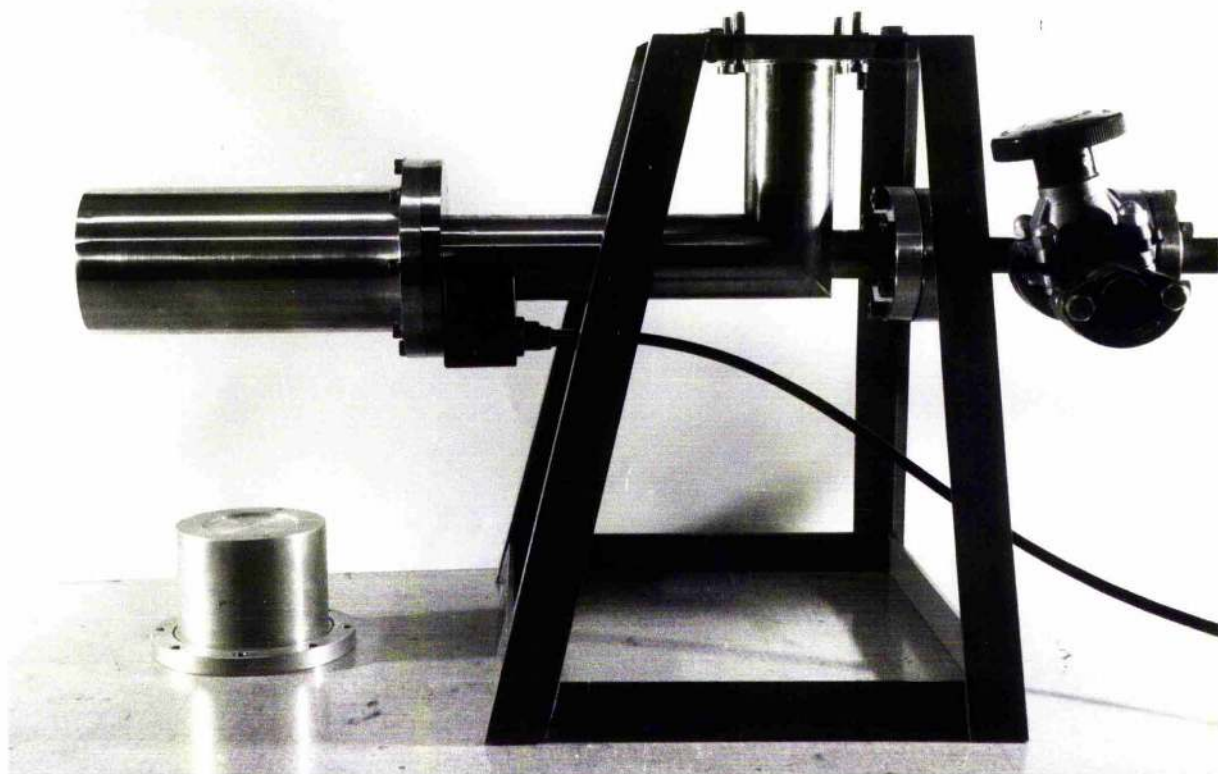
Fig 2.5

Photograph of the Completed System with a Liquid Nitrogen

Dewar Attached and the Preamplifier Connected
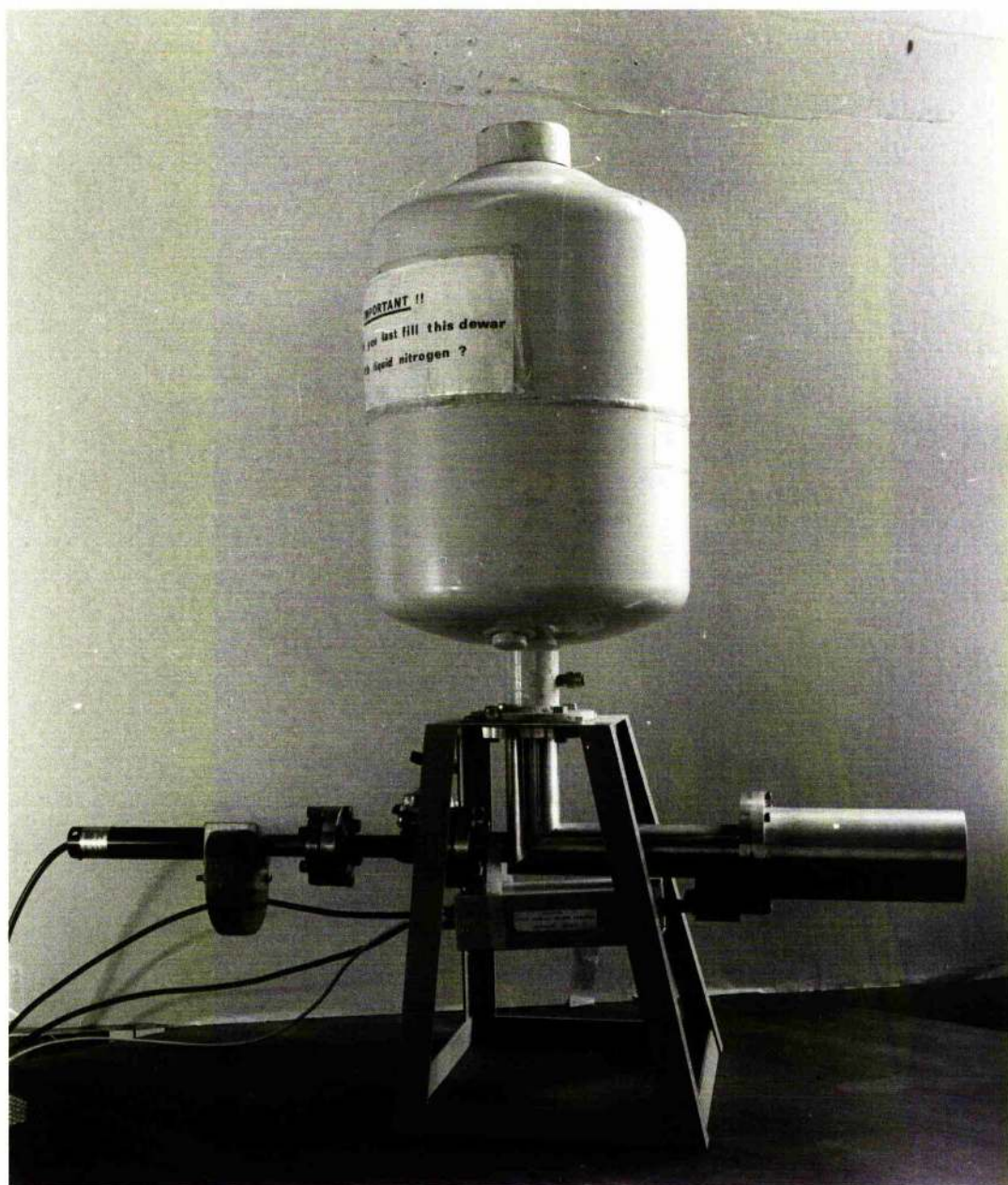
establishing of the indium seal was found to be clumsy and a rapid evacuation was seldom achieved. For this reason Viton 'O' rings are generally preferred in the end cap seal.

2.4 The Dipstick Cryostat

This cryostat was designed along similar lines to that of Buhler and Marcus (1967). Fig. 2.6 shows a sectioned side elevation of the cryostat. Two pumping facilities are available, namely that of an ion pump, and molecular sieve introduced between the outer case and cold finger. An extension rod is available to allow the cryostat to be used with 10 or 25 litre dewars. Fig. 2.7 shows the cryostat in normal use in a 25 litre dewar.

2.5 Vacuum Pumping

The pumping of cryostats is separated into the following categories.

2.5.1 Rough Pumping

Since the crystal surfaces are highly susceptible to any contamination, it is essential to use an ultra clean pumping system. Molecular sorption pumps inherently fulfil this requirement. They have the disadvantage however, that the pump can readily saturate if several evacuations from atmosphere are required. A rotary and diffusion pump system can be used for initial pumping provided that an effective cold trap is incorporated.

In this instance a sorption pump was used not only for cleanliness but for simplicity in use, and its independence from mains power supplies. The sorption pump, when evacuating a cryostat from atmosphere, reduces the pressure to approximately 5×10^{-3} torr in about 15 minutes. This pressure is low enough to allow ion pumping to commence.

No trouble was experienced with this pump provided that it was well baked prior to use.

2.5.2 High Vacuum Pumping

Ion pumps are preferred, due to their cleanliness and the compactness when compared with diffusion pumps. A pumping capacity of 1 litre/sec is adequate and this size pump was used for all three cryostats discussed. The resulting pressures were usually of the order 10^{-7} torr, well below the stated minimum in section 2.1. These pumps have a limited duration due to

Fig. 2.6

Schematic Diagram of the Vertical Dipstick Cryostat

with Copper Extension for use in Larger Dewars
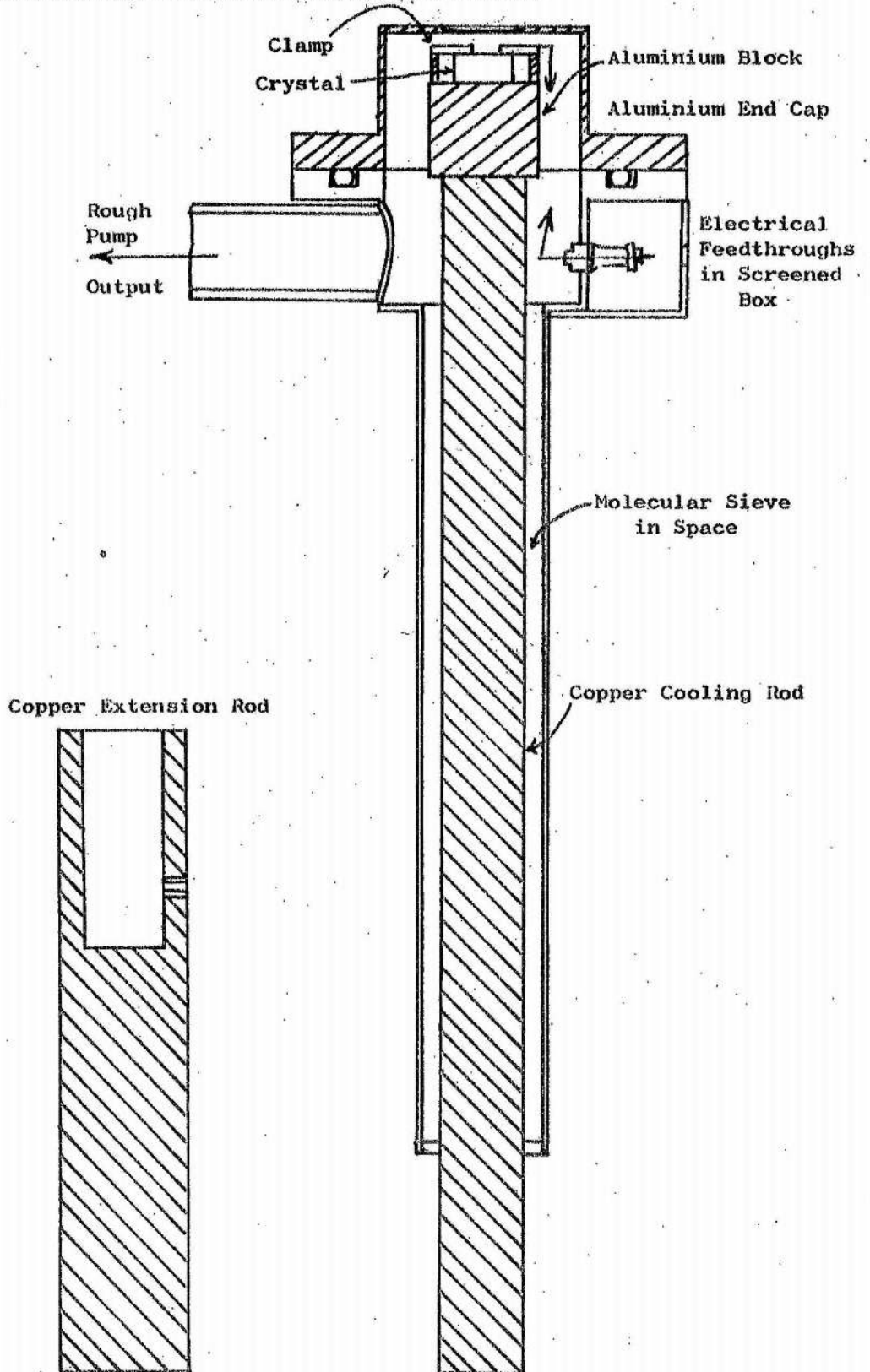
Fig 2.7

Photograph of the Dipstick Cryostat in Normal Use
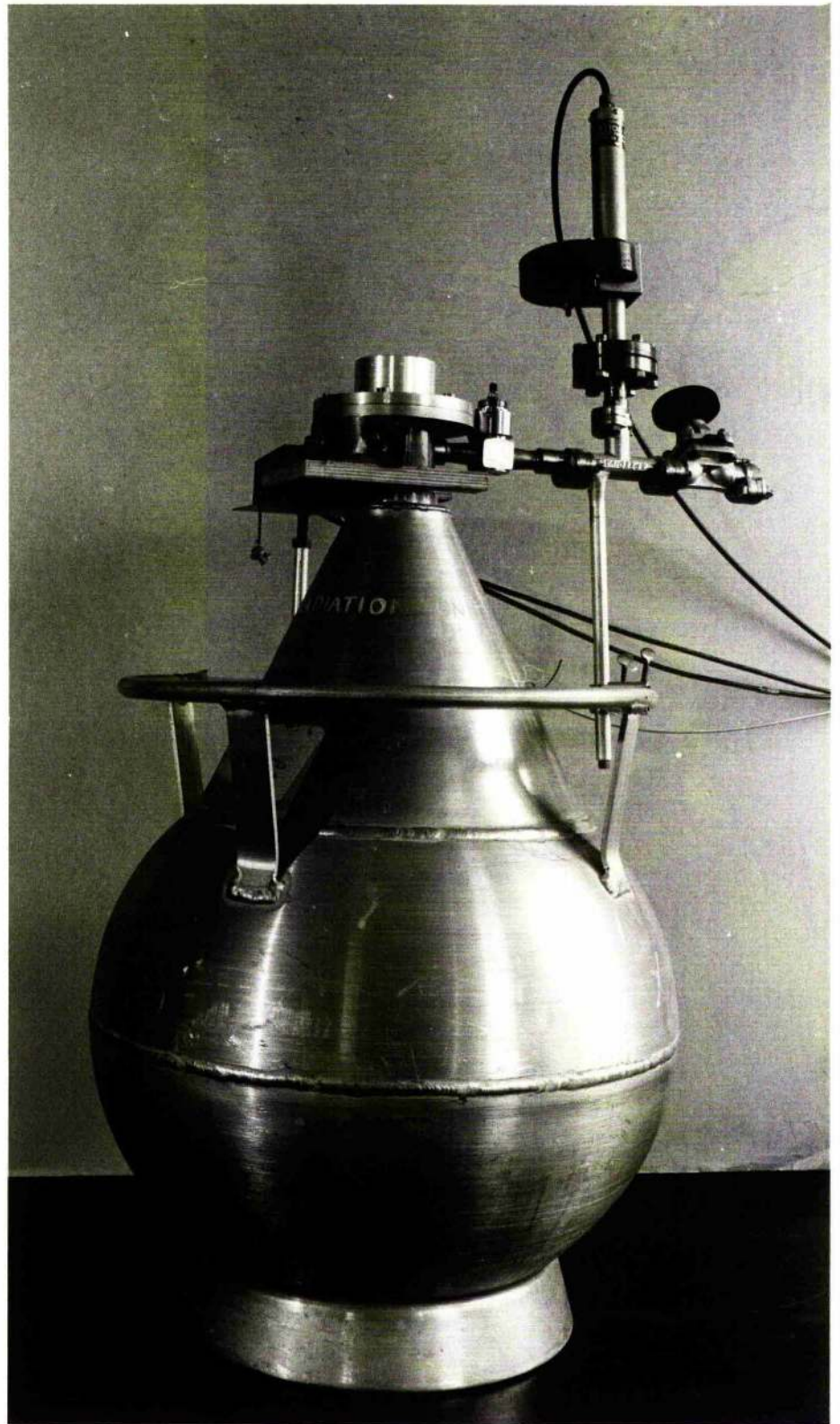
the limited quantity of titanium available on the pump electrodes. However, at 10^{-7} torr, this life is considered indefinite. At higher pressures the life becomes limited due to rapid use of titanium. Hence early pump failure is caused by the presence of leaks or considerable out-gassing. Care must be taken where a cryostat is cycled to room temperature many times, to prevent the ion pump from pumping high pressures ($> 10^{-4}$ torr) for long periods of time. The problem of titanium sputtering described in section 2.2 is rarely observed with new pumps but is quite common with older ones which have been maltreated in the manner described. The older pump electrodes are near saturation, and absorbed gas and titanium are very easily ejected from their surfaces when fresh ions hit the electrode surfaces.

The above condition can lead to outgassing from the electrodes sometimes at a rate greater than the pumping speed of the pump causing a rise in pressure. In particular, this can happen through accumulations of argon in the system, built up over a period of time due to difficulty in pumping this gas. The pressure rise subsequently results in an oscillating current in the pump. Fig. 2.8 shows a trace recording from one of the pumps in this laboratory in this condition (termed argon instability). The pressure oscillates between 5×10^{-3} torr to 5×10^{-5} torr, over a period of hours. This problem is remedied by heating the pump to 200°C and rough pumping using the molecular sorption pump only. Most gases should be removed from the ion pump in this way.

Old pumps, in addition to this instability, can build up deposits between the electrodes causing increased current readings (although the pressure may be quite low) and even near short circuit. This is easily diagnosed by observing if a current is still recorded after removal of the magnet. If this is so then the following steps may be taken:-

The deposits may be dislodged by sharp tapping on the pump body with a wood block. The current through the pump will be observed to jump and if the operation is successful, the current will rapidly fall. If this is unsuccessful, a high voltage supply, (6000V), is attached across the pump (Muggleton 1969) blowing away any deposits.

A final, and rather more drastic action, is to remove the pump from the cryostat and fill it with nitric acid for a few seconds (Coles 1968). After quench-ing and drying with a compressed nitrogen jet the pump is remounted.

Fig. 2.8

Trace Recording of Argon Instability showing an Oscillation
in the Pressure Recorded from the Ion Pump Control Unit

5×10^{-4} torr

Pressure

1×10^{-4} torr

Time (hours) ⟶

|← 1 hour →|
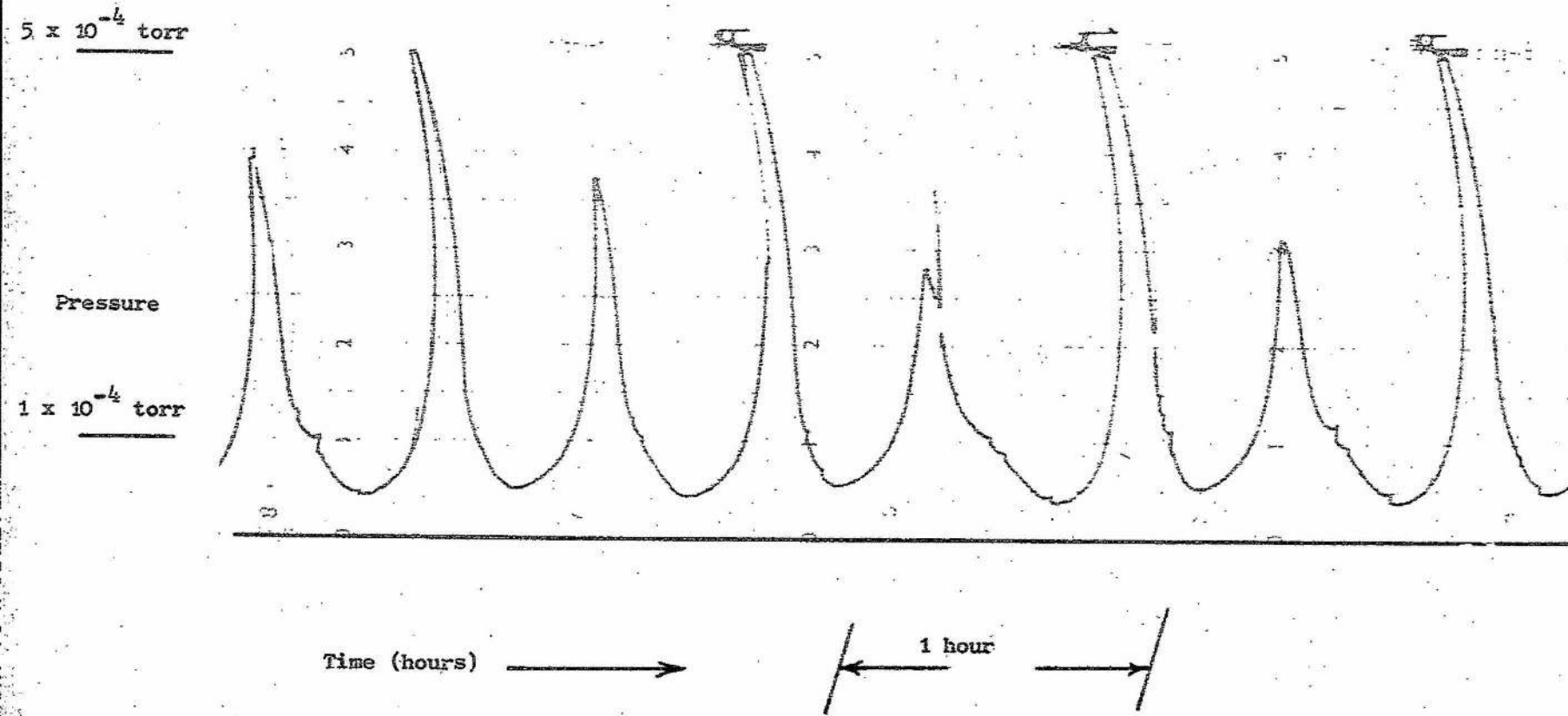
Provided that the pump is carefully used on a well prepared cryostat the above actions should be unnecessary for at least several years.

2.5.3 Molecular Sieve as the Sole Means of Pumping

Molecular sieve has none of the problems of ion pumping, but is limited in its ultimately achievable pressure ($\sim 10^{-5}$ torr). This pressure is a function of cryostat cleanliness and the state of saturation of the sieve.

The vertical dipstick cryostat (section 2.4) was designed initially for use with the molecular sieve. Measurements on the obtainable pressures showed that it is essential to perform a rough evacuation before cooling the cryostat to maintain the sieve in as good a condition as possible. For protection of crystal surfaces at 10^{-5} torr it is advisable to use encapsulation, or inner shielding round the crystal. The absence of an ion pump results in a neat and portable cryostat assembly.

Problems are encountered if the sieve becomes saturated, accelerated by leaks and outgassing. The result is a sudden vacuum failure once saturation is reached and when the cryostat returns to room temperature, pressures above atmospheric can result with the possibility of explosion. Thus the design should embody a pressure release valve. In systems required for low energy measurements the thin Be end window may act as the blow out valve.

2.5.4 Emergency Power Supplies

The use of ion pumps necessitates the continual supply of mains power. Power failure may result in a cryostat pressure rise which can cause a deterioration of the crystal surfaces well before the loss of thermal insulation properties becomes significant. This problem is avoided by the use of an auxiliary power supply unit. Mains power failure causes a relay to switch the ion pump supplies to the lighting circuit, this being a different supply for these laboratories. Should both circuits fail, then a second relay operates a D.C. to A.C. rotary converter, driven by a heavy duty 12 volt battery. When the battery is charged, the unit is capable of ten hours supply at 250 watts. This is sufficient for most power failures. A battery charger is incorporated in the system. This unit has proved its worth on several occasions.

This auxiliary power supply is also useful when transportation of cryostat assemblies is attempted.

2.6 Modern Cryostat Design

It is generally accepted that the unavoidable use of a cryostat is a significant limitation for several aspects in the use of semiconductor detectors. However, modern cryostat design has improved flexibility such that in many respects, this no longer represents a serious limitation.

The first improvements in cryostats were ones of maintenance, in that pumps could be changed without a break in the vacuum. Turcotte and Moore (1969) have developed systems in which the molecular sieve can also be changed in this manner.

Williamson and Alster (1969) appreciated the value of small compact cryostats in limited access areas and developed a miniature cryostat. Nuclear Diodes Inc. have developed systems suitable for insertion into bore holes, while Princetown Gamma Tech, Kevex, Nuclear Enterprises and Quartz et Silice have developed small systems suitable for use with electron microscopes. Meyer and Heinz (1970) have investigated the use of encapsulated detectors immersed directly in liquid nitrogen.

The problems of ease of detector positioning have also been improved by Nitche (1969) who has developed a demountable system capable of use as a dripfeed or dipstick system without disturbing the crystal. Franke (1969) has built a flexible arm cryostat made from armoured hose that is capable of a wide range of positions. The most versatile design has been developed by Harshaw Inc. that allows the detector to be pointed in any direction. The filling tubes of the reservoir are so arranged that no spillage of nitrogen occurs during tilting. This cryostat is a combination of dripfeed and dipstick designs.

The rigorous demands of cryostat conditions and pump operation can be relaxed if the detector is satisfactorily encapsulated (Gibbons, Howes and Pyrah 1966). Fowler and Toone (1964) initially investigated the use of encapsulation, and in 1965, Stab, Henck, Siffert and Coche produced a satisfactory system with minimal system degradation attributable to the encapsulation. Webb, Green, Fowler and Malm (1966) also developed a satisfactory technique for encapsulation. However, the technique has not met extensive use as the problems with crystal surfaces are now better understood and the techniques of internal cryostat design and preparation have been well developed.

Chapter 3

The Electronic Pulse Analysis System

3.1 Introduction

A large amount of research and development on nuclear pulse electronics has been undertaken by many workers. A good appreciation of this may be gained from the bibliography compiled by McKenzie (1969). It is due to this activity that research in this sphere was not undertaken. In addition, commercial units are available from which a high performance pulse analysis system may be constructed.

A knowledge of the most important aspects of pulse analysis systems is gained from Dearnaley and Northrop (1966), Chase (1967) and Siegbahn (1966). Fairstein (1965, 1966) has published an instructive set of papers on pulse amplifiers. More recent developments are considered by Benoit and Bertolini (1968) and another good source is the IEEE Transactions on Nuclear Science.

This chapter is descriptive of the spectrometer and the units used in its construction. The precautions taken to optimise performance are also considered.

3.2 Some Spectrometer Counting Configurations

Depending upon the particular experiment under consideration, several counting configurations, such as coincidence and anticoincidence arrangements are available. Only those used experimentally during this work are considered here. The spectrometer may be simply represented by the block diagram of Fig. 3.1. It is split into four fundamental blocks, these being the detector (or detectors if this represents a coincidence spectrometer), the pulse amplifying system, the pulse height analyser and the data processing and output facility.

The counting configurations used are now discussed.

3.2.1 Singles Counting

Singles counting was the most commonly used mode in these studies. Fig. 3.2 shows a schematic diagram of the spectrometer used. Charge pulses are collected from the detector, fed to a charge sensitive preamplifier, (Ortec 118A or NE 5287), and are converted to voltage pulses

Fig. 3.1

Functional Diagram of a Ge(Li) Spectrometer
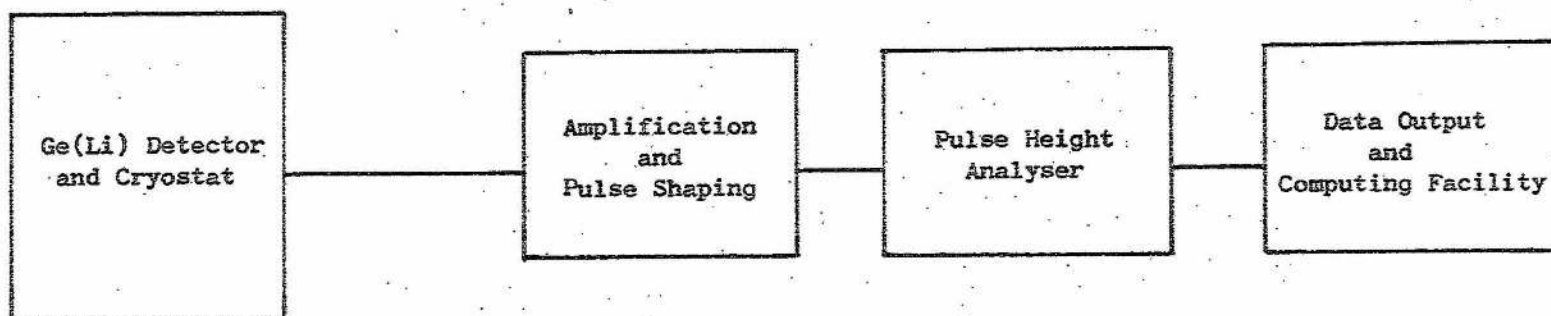
Fig. 3.2

Block Diagram of the Singles Spectrometer used in this Laboratory
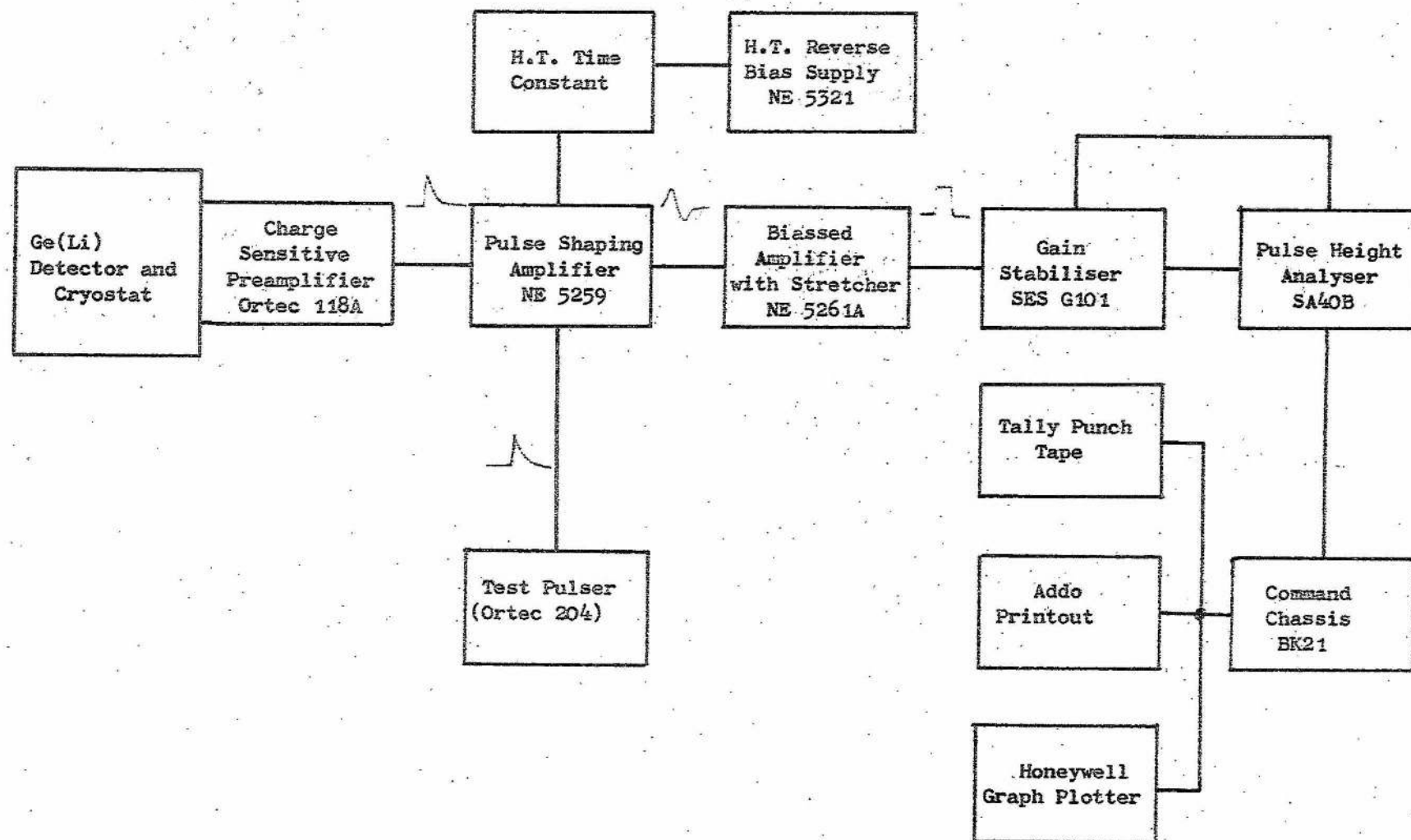
whose heights are proportional to the charge collected from the detector.
The detector reverse bias is supplied from an H.T. unit, (NE 5321), via
the preamplifier. The preamplifier is A.C. coupled to the detector, with
the H.T. being applied via the signal lead. To prevent damage to the sen-
sitive input stage of the preamplifier, due to H.T. transients, the bias is
applied via a large RC time constant (88 seconds).

Output pulses from the preamplifier are fed to a main amplifier
(NE 5259) which uses integrating and differentiating networks to shape the
pulses. This optimises the signal to noise ratio by restricting the band
width of the amplifier to allow only those frequencies relevant to the pulse.

If only a limited portion of the energy spectrum is of interest,
this is selected and expanded using a biassed amplifier (NE 5261A).

A digital gain stabilizer (see Fig. 3.2) is incorporated (S.E.S.
Stabimat G101) which operates when coupled with the pulse height analyser.
The stabiliser depends upon the measurement of a standard input pulse,
supplied either by a gamma ray source or pulse generator, and adjusts the
system gain accordingly to account for drift. The pulser (Ortec 204) is
used for calibration and noise measurements of the spectrometer.

The pulses from the main amplifier are sorted into channels repre-
senting different heights (and hence energy) by the pulse height analyser.
This information is stored in a magnetic core memory in the analyser, which
is read to give a visual display on the oscilloscope screen, or printed
(using Addo printer), plotted (using Honeywell chart recorder), or punched
out (using Tally punch), via a command chassis for data processing.

3.2.2 Coincidence Counting

Several sophisticated coincidence configurations are available
that have resolving times of the order of nano seconds (Pigneret, Samueli
and Sarazin 1966, Miehe, Ostertag and Coche 1966 and Brandenberger 1969).
However, this degree of timing resolution was not necessary for the present
experiment in mind (section 7.3). Fig. 3.3 shows the experimental config-
uration adopted. The gamma source being studied is placed in between two
Ge(Li) detectors. The pulse amplification units and H.T. supply for each
detector is as shown in Fig. 3.2. Pulses from the two systems are fed
into a dual parameter analogue to digital converter (termed ADC) incorpor-
ating a coincidence unit with a 1.0μ sec resolving time (NS 625). The out-
put information is displayed by an NS 630 display unit capable of either

Fig. 3.3

Block Diagram of Ge(Li) Coincidence Spectrometer
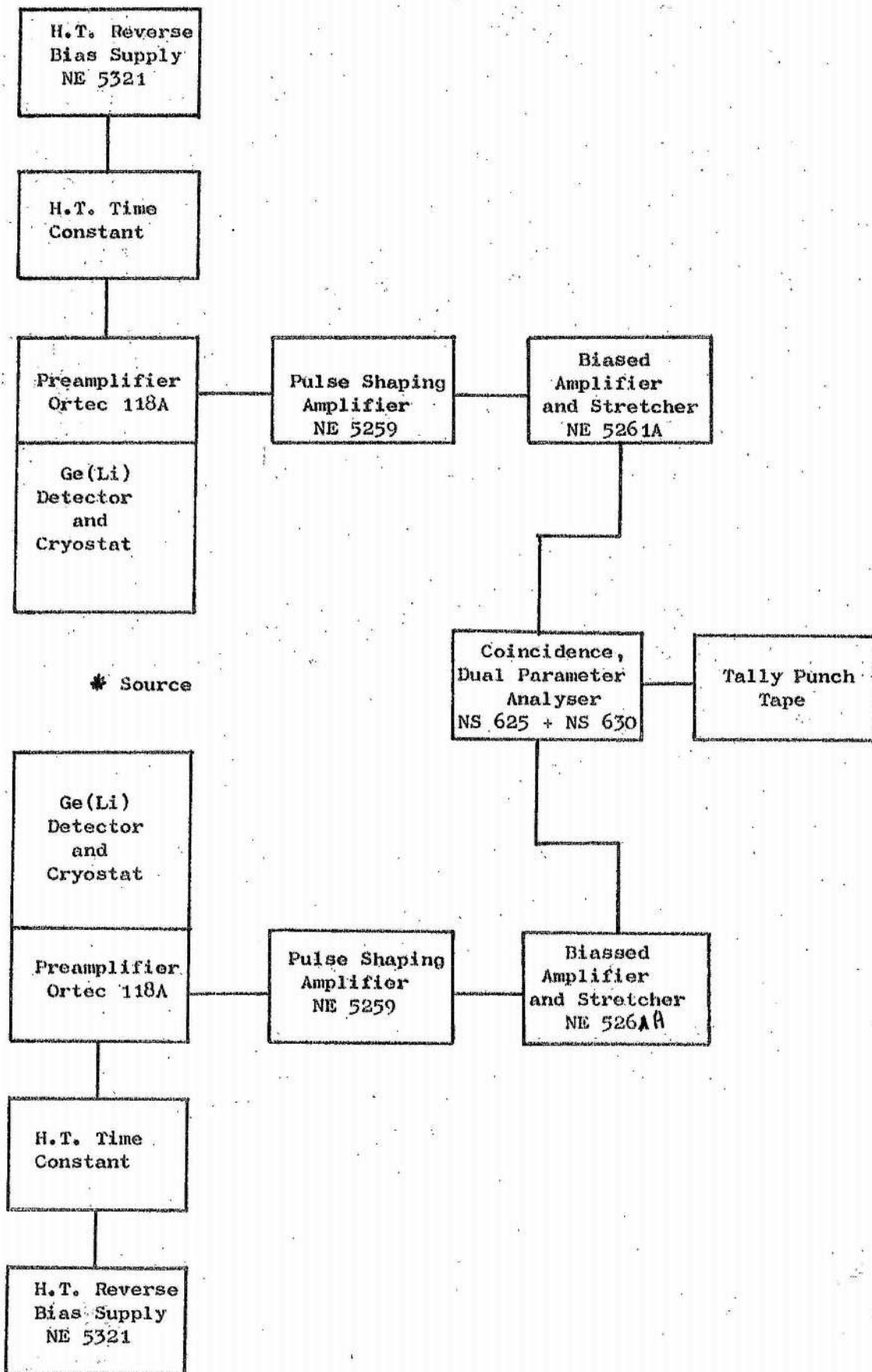
Fig. 3.4

Anticoincidence Configuration
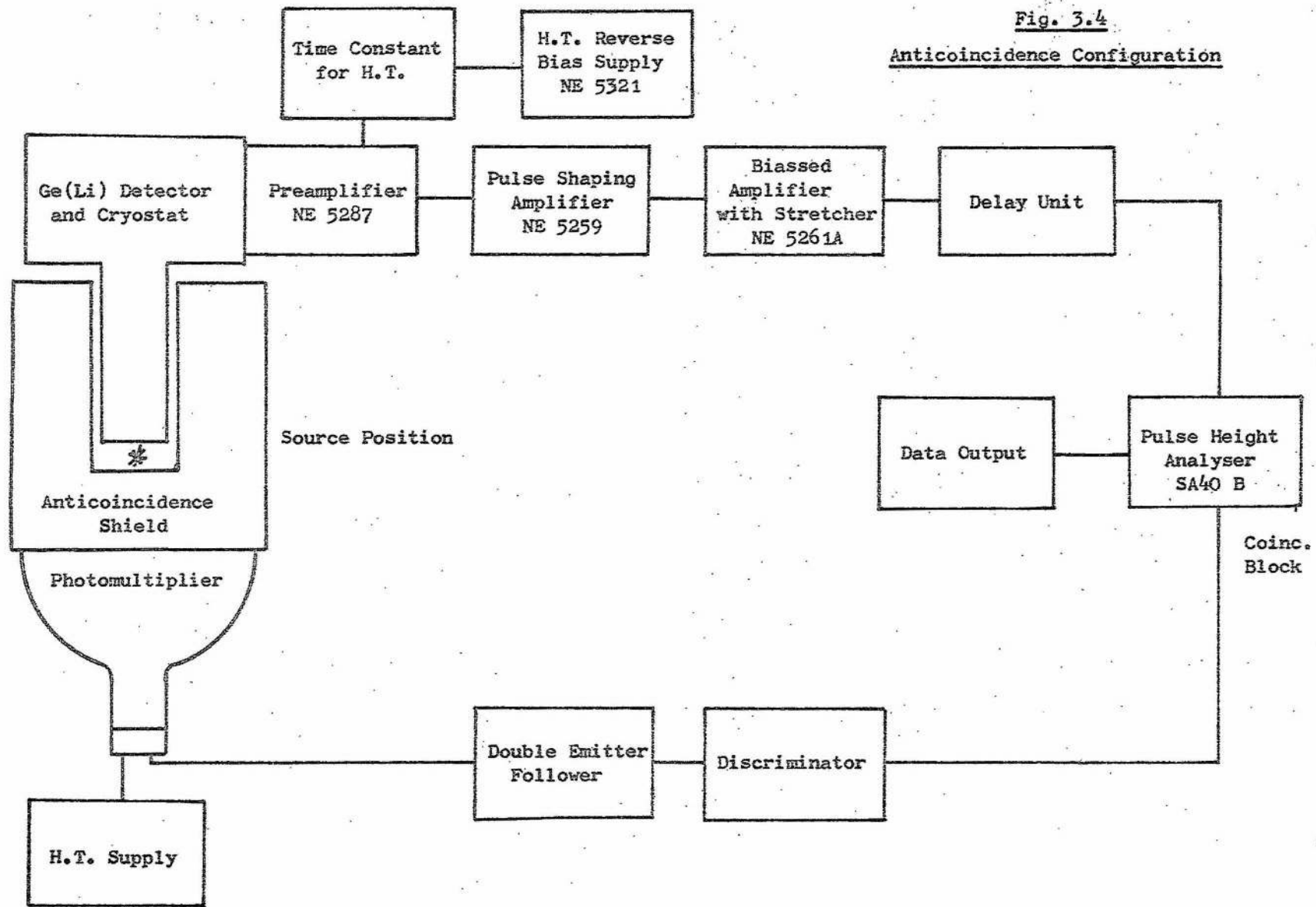
contour or isometric display.   The display unit also controls data output
to a teletype punch printer.

Several experiments were performed in the coincidence mode.
Fig. 3.3 shows the system used for two germanium detectors in coincidence.
Coincidence counting was also performed using a NaI(T1) scintillator and a
germanium detector.   In this instance one of the germanium detectors in
Fig. 3.3 was replaced by a scintillator and photomultiplier together with
one amplifier (NE5259).   An α - γ coincidence experiment was also perfor-
med using a silicon surface barrier with the germanium detector.   In all
coincidence experiments, the NS625 analyser was used.

3.2.3 Anticoincidence Counting

Fig. 3.4 shows a schematic diagram of the arrangement used in this
laboratory.   When the shield is used to reduce natural background events,
the reduction process relies on the principle that the incident particle
deposits some energy in both the shield and the detector.   When pulses
arrive simultaneously at the analyser coincidence units they are rejected by
the analyser.   When Compton events in the Ge(Li) detector are rejected, the
Compton scattered photon from the detector interacts in the shield and the
coincidence event is also rejected.   In both cases, the mode of operation
of the equipment is the same although the effect on the background continuum
is different.   The distinction lies in the different origins of the radio-
activity.

The use of this shield has been evaluated by Parish (1971) as
part of an M.Sc. project, and hence it is only very briefly described here.

Fig. 3.5 (a) and (b) show the Ge(Li) detector withdrawn and
inserted into the shield.   The shield is made of 3" thick Naton 136 plastic
scintillator viewed by a 7" photomultiplier tube.   The tube output pulses
are amplified and fed to a discriminator.   Discriminator output pulses are
directed into the blocking input of the Intertechnique SA40B analyser.

Pulses from the Ge(Li) detector are processed as described
previously, except that a delay unit is added to bring coincident events
into overlap.   Fig. 3.6 shows a general view of the whole spectrometer,
arranged for anticoincidence work.   Fig. 3.7 shows a general view of the
dipstick cryostat arranged in a spectrometer with a 256 channel NS630
analyser.
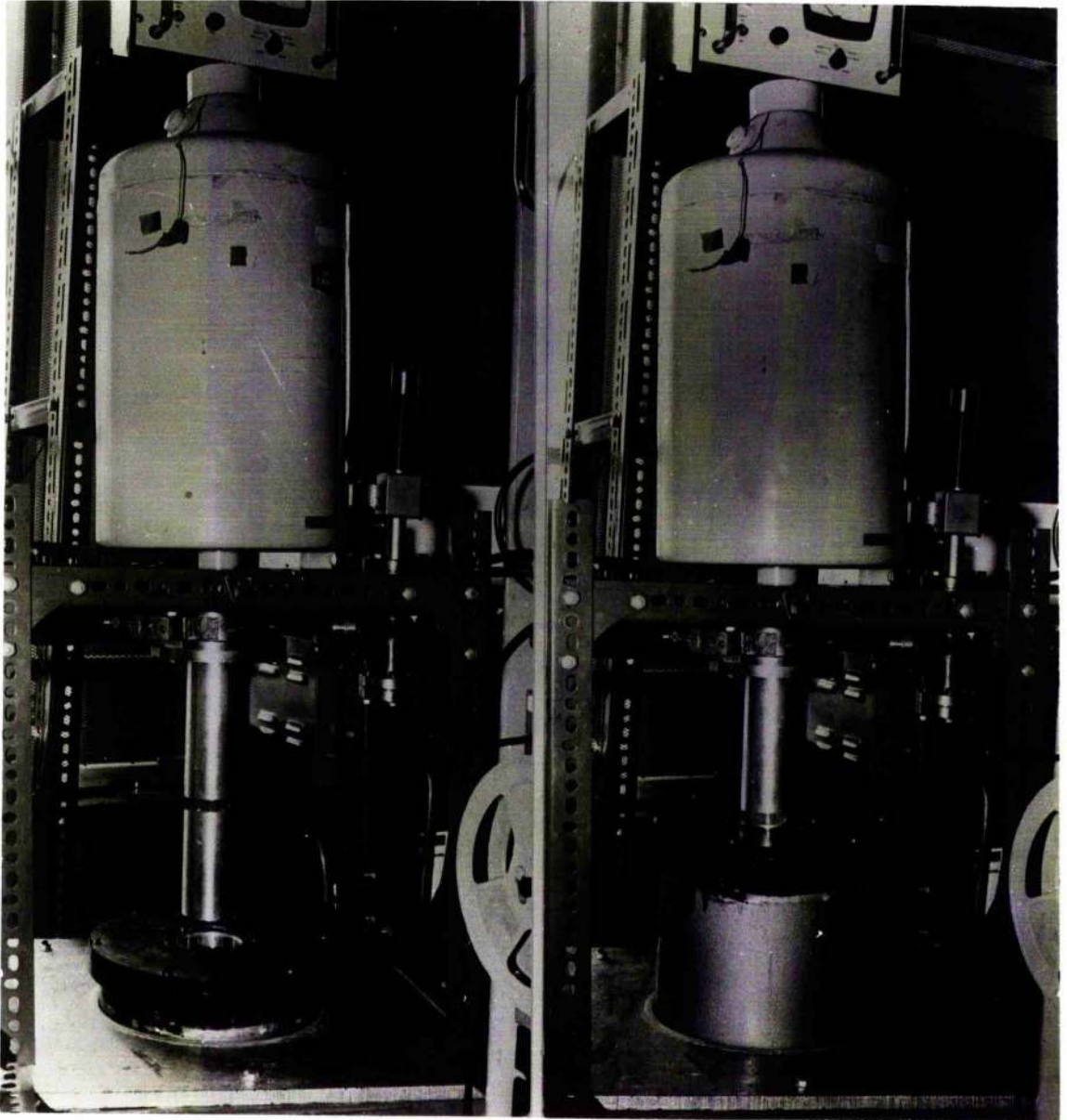
a)   b)

Fig 3.5

Ge(Li) Detector a) Withdrawn From the Anticoincidence Shield
b) Inserted into the Anticoincidence Shield

Fig 3.6

General View of the Gamma Ray Spectrometer Arranged
for Anti-Coincidence Counting
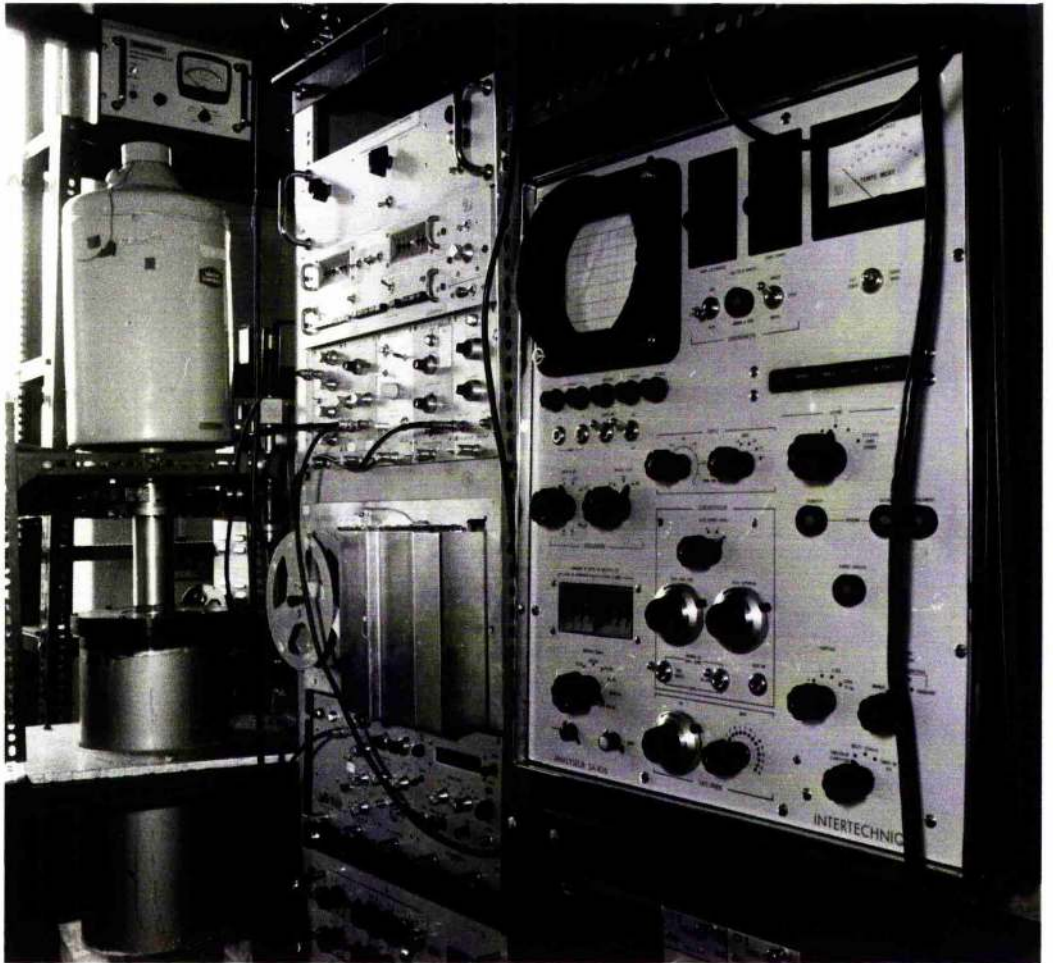
Fig 3.7

General View of a Gamma Ray Spectrometer Using the Dipstick

Cryostat with the 256 Channel NS 630 Analyser
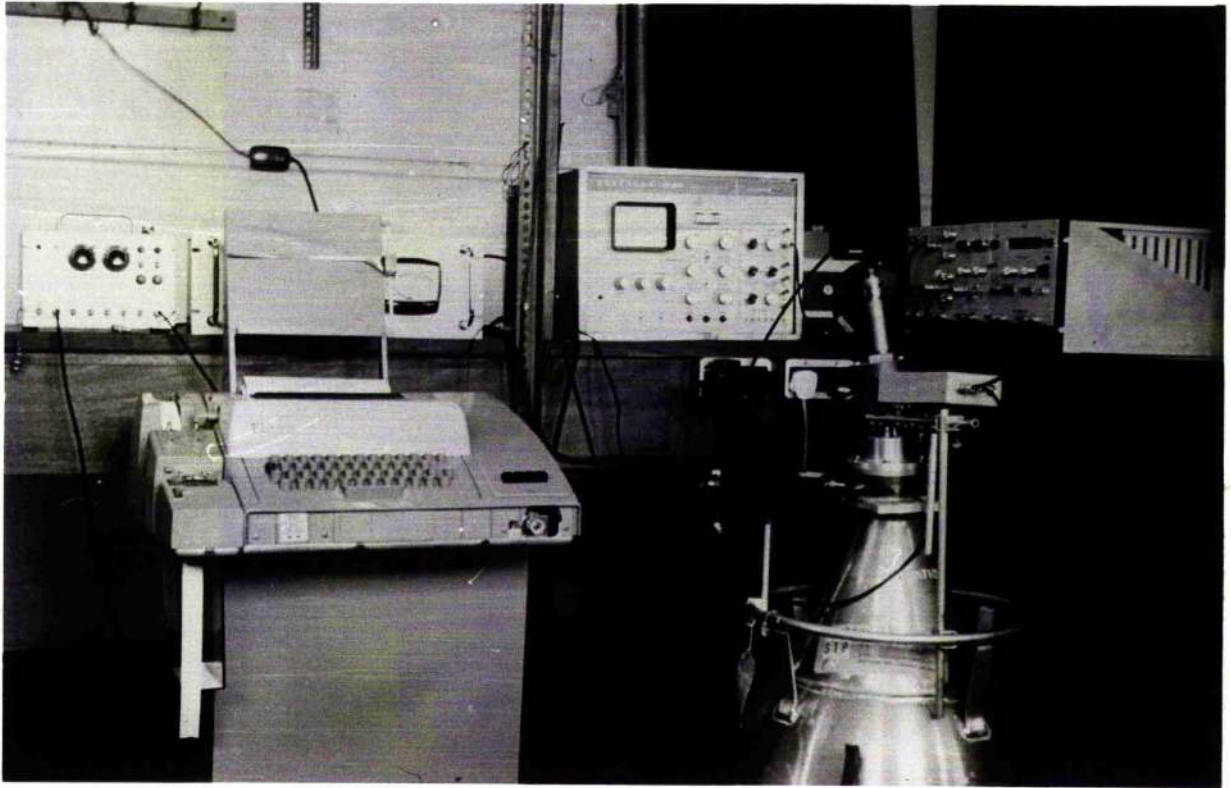
3.3 <u>Some Features Considered in the Optimisation of the Pulse</u>
<u>Analysis System</u>

The performance of the pulse analysis systems used in this
laboratory are governed by the following parameters:-

(i) Preamplifier noise

(ii) Gain stabilisation

(iii) Choice of the analyser and amplifier operating conditions.

This section is descriptive of these parameters and their adjustment for
optimum performance.

3.3.1 <u>Preamplifier Performance</u>

The preamplifier performance dominates the overall noise perfor-
mance of the pulse analysis system (McDonald 1971). This in turn is dom-
inated by the capacity and leakage current presented to the preamplifier
input (Goulding 1961, 1964, Monteith 1964 and Heath, Black and Cline 1966a).
The preamplifier is a wide band device used to amplify all frequencies
associated with the input charge pulse. Integrating and differentiating
filters in the main amplifier (NE5259) are used to restrict the band width
to optimise the signal to noise ratio at the output. These filters are
also adjusted to minimise the leakage (dominating at low frequencies) and
capacity (dominating at higher frequencies) noise contributions.

Fig. 3.8a shows the noise performance of the NE5287 preamplifier
as a function of input capacity. This was measured with amplifier time
constants of 1.0 μ sec and using Texas Instruments D1546 FETs. It is
observed that the addition of FETs in parallel increases the noise at zero
capacity input but reduces the characteristic slope. The optimum number
of FETs is decided by the detector capacity.

Fig. 3.8b shows the noise performance of the NE5287 preamplifier
as a function of input leakage current. The frequency dependance of this
noise source is shown by the variation of energy resolution with filter
time constant. The optimum choice of the time constants is a balance
between the capacity and leakage contributions, Fig. 3.9 showing a typical
variation measured for a spectrometer. The minimum shown is sometimes
shifted to a shorter filter time constant if the cryostat is significantly
microphonic, since microphony gives an essentially low frequency noise
contribution.

Fig. 3.8a

Variation of Preamplifier Noise
with Input Capacity

Fig. 3.8b

Variation of Preamplifier Noise with Input Leakage

48
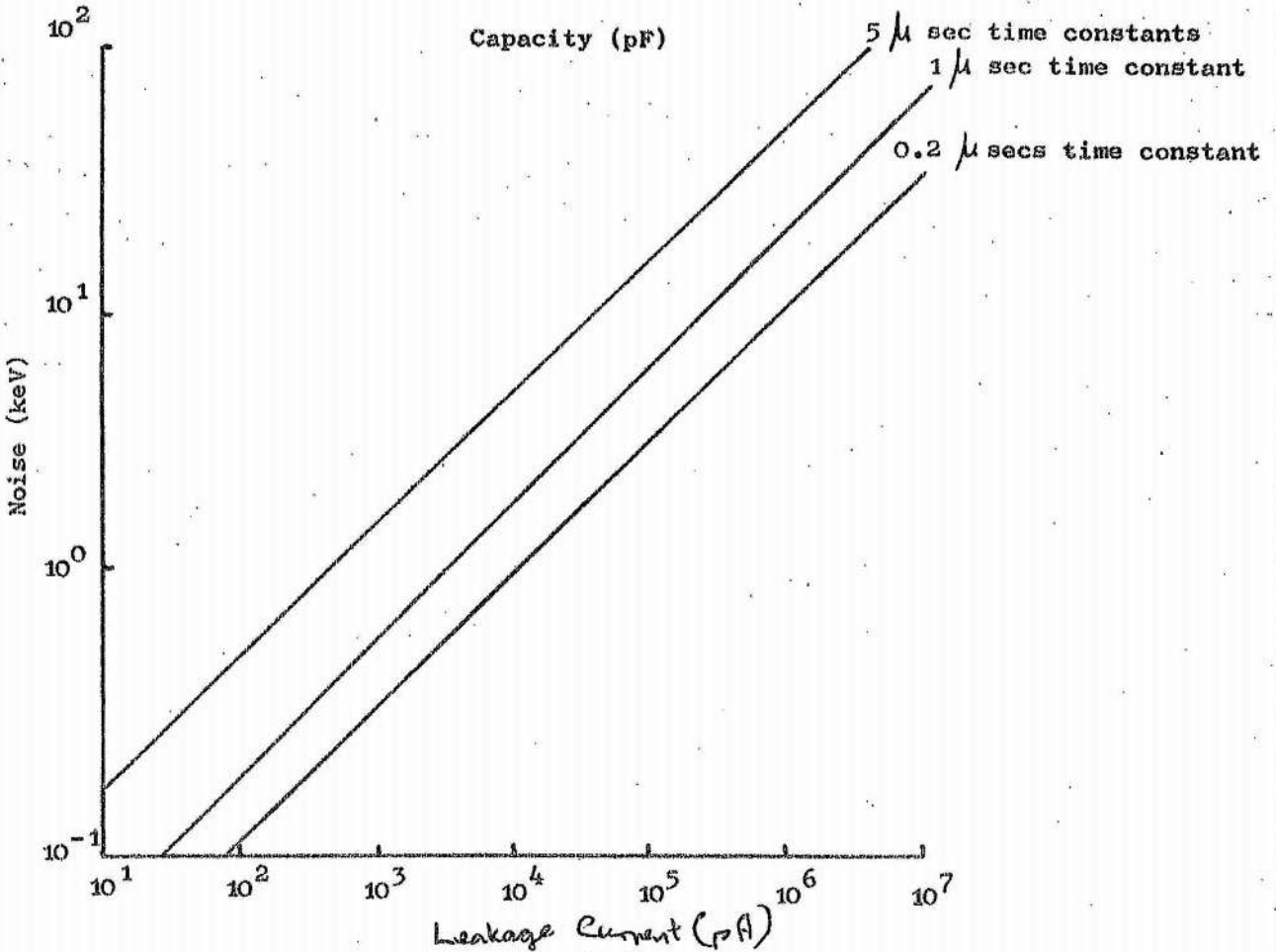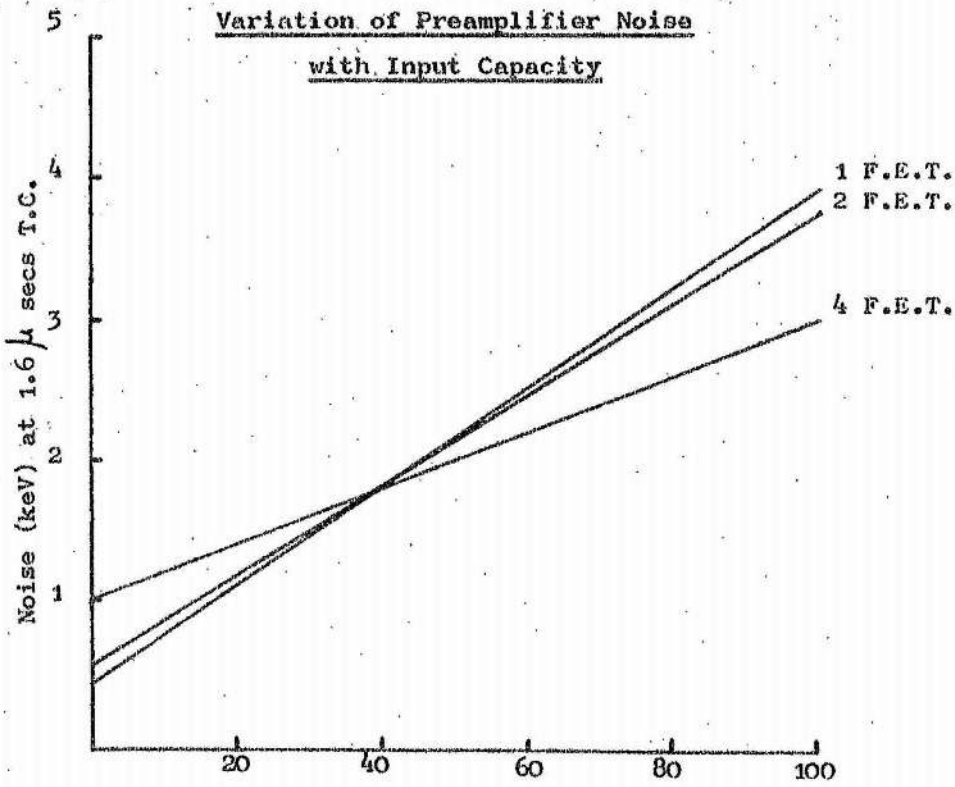
Fig. 3.9

Variation of Overall Spectrometer Resolution
with Amplifier Time Constants showing Capacity and
Leakage Components for a Typical Spectrometer
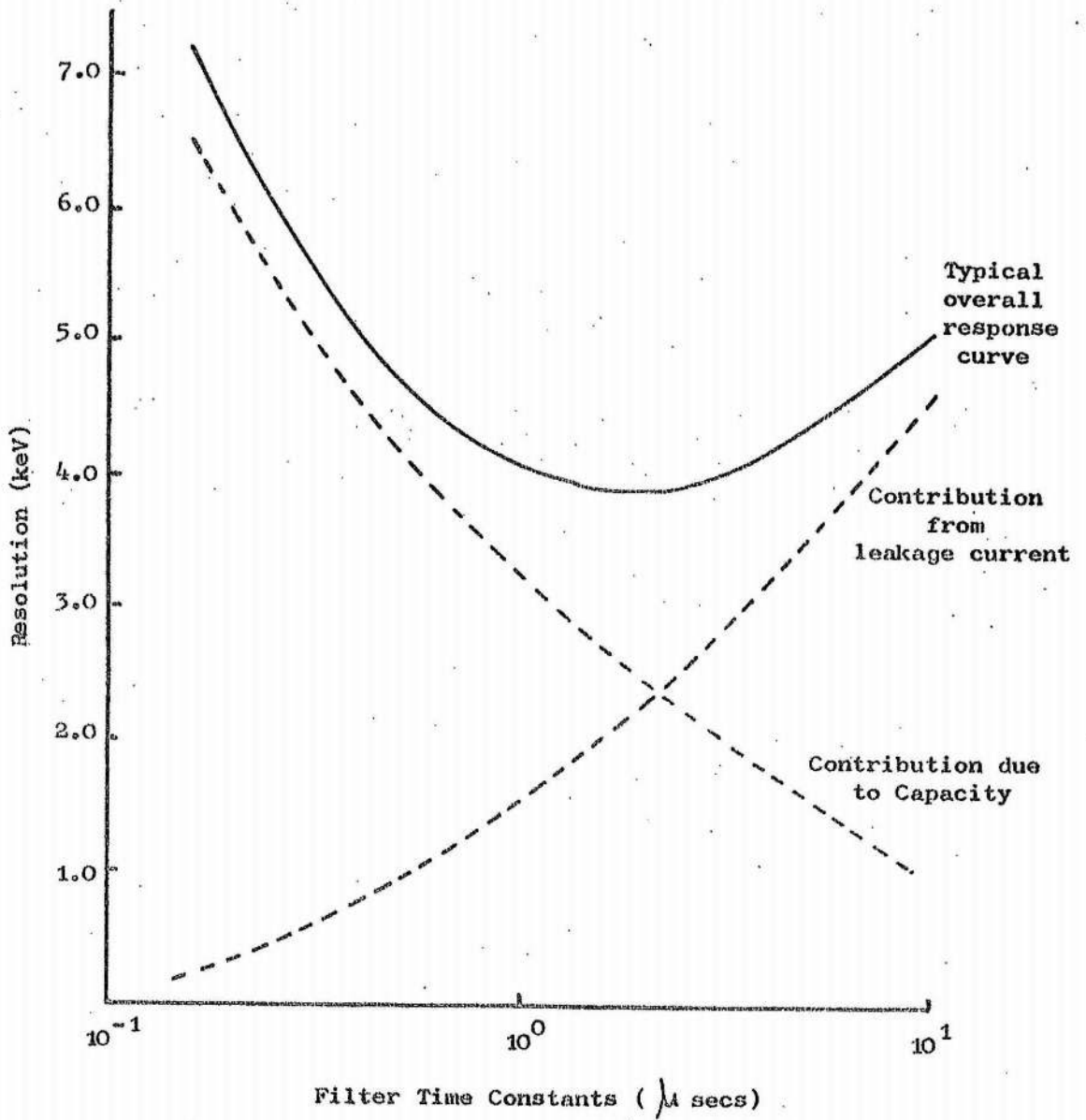
3.3.2 Gain Stabilisation

A gain shift of as little as 0.1% during the course of a counting experiment results in a resolution broadening of 1.3 keV for ^{60}Co. To avoid this spectrum degradation, an SES Stabimat G101 gain stabiliser was used. Zero stabilisation devices are also commercially available but were not used here as their effects are generally small compared with gain drift effects.

The stabiliser functions by locking a standard peak (generated by a precision pulse generator or gamma ray) onto a set channel in the analyser spectrum. An unwanted gain change is observed by summing counts from two "windows", one set on each side of the peak. A difference between the sum counts from each window is indicative of a gain change in the system. This difference generates a signal which adjusts a servo controlled amplifier in the stabiliser unit to oppose the gain shift. In this way the standard peak is returned to its chosen channel.

The intensity of the standard peak controls the count accumulation rate of the two windows and hence the correction ability of the stabiliser. The window width and position, preset contents and the content difference, are selected by the experimenter. Care and a knowledge of counting statistics are required to ensure an effective and rapid correction of gain drift without generating spurious corrections due to natural statistical fluctuations.

Without the use of the stabiliser, it was found that gain shifts in excess of 0.1% were common. The use of the stabiliser radically improved this figure. This is typified in one experiment where the overall spectrum drift was restricted to 0.01% for a period of eleven days continuous counting.

3.3.3 The Pulse Height Analyser

Three analysers were used in this laboratory. Two of these, the Intertechnique SA40B and the Northern Scientific NS630 are single parameter analysers while the third, the Northern Scientific NS625 (kindly loaned by Nuclear Measurements Ltd.), is a dual parameter analyser.

The Intertechnique analyser with a 400 channel capacity was used for the bulk of the research work. The analyser memory is cycled by an 8MHz crystal oscillator, giving a maximum dead time of 60 μ secs. Fig. 3.6

Fig 3.10
The Northern Scientific NS 630 Analyser Together
With its Teletype Output
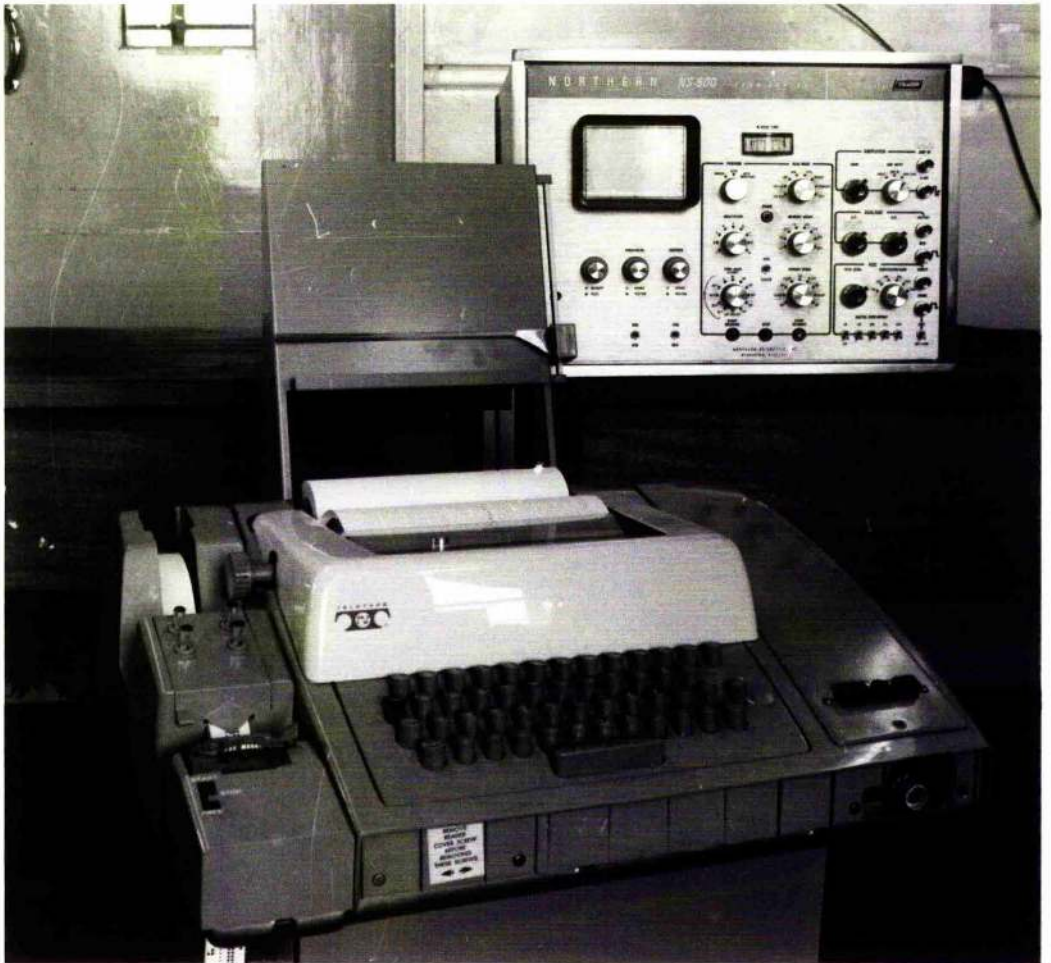
Fig 3.11

Northern Scientific NS 625 Dual Parameter Analyser
Used for Coincidence Measurements in this Laboratory
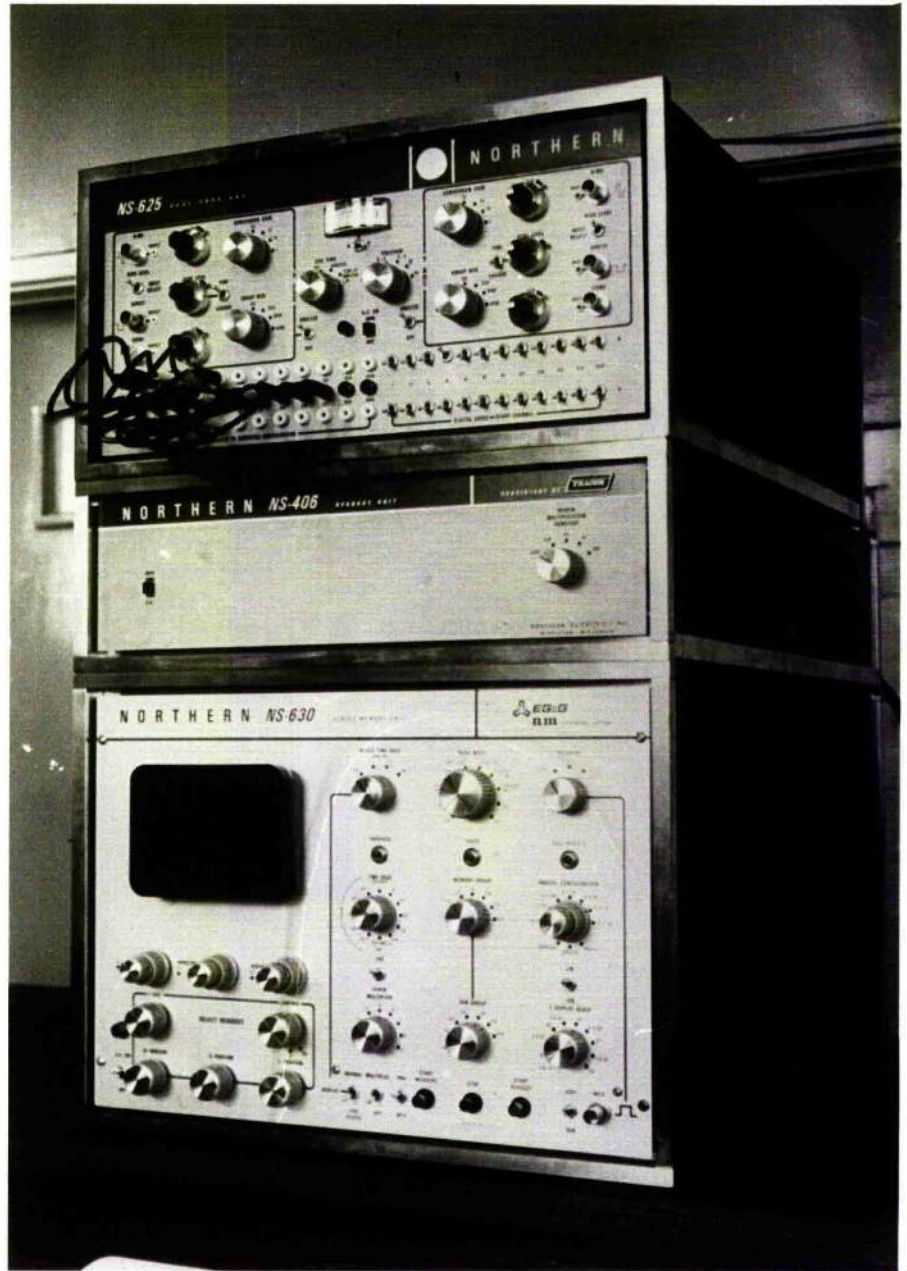
Fig 3.12a

Isometric Coincidence Spectrum of ^{60}Co Using a Ge(Li)
and NaI(Tl) Detector

Fig 3.12b

Contour Display of the Above Spectrum

NaI(Tl)

Ge(Li)
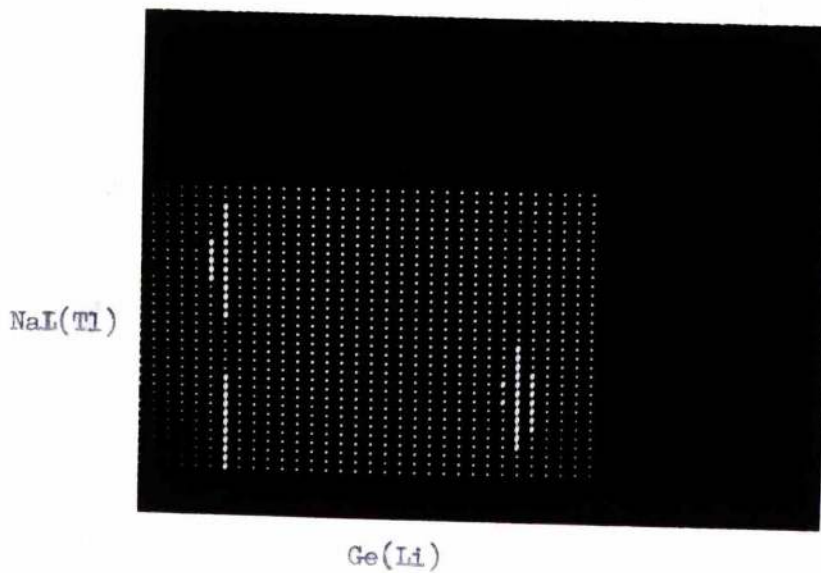
shows the analyser together with the anticoincidence shield. The NS630 analyser, although having only 256 channels, has a 40MHz memory cycle time giving a maximum dead time of approximately 10 μ secs. It is suitable for poorer resolution systems, (due to the lack of channels), fast count rates, or experiments where only a limited energy range is necessary. This analyser has a 2048 channel ADC together with a digital back bias facility which results in simpler energy alignment when examining a spectrum in sections.

Fig. 3.10 shows the analyser together with its Teletype data output unit. The dual parameter analyser (Fig. 3.11) is intended primarily for coincidence experiments. Two ADCs are incorporated and stores pairs of pulses that are within the coincidence resolving time of 1 μ secs. The memory contents may be displayed either in isometric or contour form. The 1024 available channels may be arranged in any two dimension combination from 1 x 1024 to 32 x 32 channels.

Dual parameter analysers in use with Ge(Li) detectors have one major problem (Alberger 1967), namely the increased requirement for channels. Heath, Black and Cline (1966b) have shown that a minimum of five channels are required in the full width at half maximum of a peak for adequate definition. For two dimensional spectra this rises to 25 channels. For a 1 MeV energy range in each dimension with 5 keV resolution detectors, a total of 10^6 channels are necessary.

Fig. 3.12a and 3.12b demonstrate the results of a coincidence experiment with ^{60}Co. A NaI(Tl) and a Ge(Li) detector were used and the spectrum is shown both in isometric and contour display. For the 32 x 32 display, the scintillator has sufficient channels, but the Ge(Li) detector suffers from poor definition.

It is essential to provide sufficient channels compatible with the detector resolution otherwise considerable spectral information will be lost.

Chapter 4

Problems and Evaluation Procedures Encountered in Establishing Operational Ge(Li) Detectors

4.1 Introduction

An appreciation of the characteristic of Ge(Li) detectors helps the user obtain optimum performance and longer life from a given system. In part, this includes evaluation, diagnostic measurements, and detector repair procedures. This chapter represents the experience gained in the course of establishing, evaluating and repairing operational detectors.

4.2 Detector Faults and their Effects

Problems associated with Ge(Li) detectors are considered under three headings, bulk, surface and contact problems. These require quite separate treatments, although when one defect is remedied, consideration is often required of the other two groups of phenomena to retain optimum performance.

4.2.1 Bulk Defects

Bulk defects arise from imperfections in the fabrication process and imperfections in the germanium used. Defects due to the fabrication process arise from a high temperature drift (Armantrout 1970, Armantrout and Thompson Jr. 1970), ineffective cold drift conditions (Gibbons and Iredale 1967, Lauber 1969) and excess time spent at room temperature (Armantrout 1966a, Sakai and Fowler 1968). The resulting imperfect compensation also results in the inability of the compensated material to support a high collecting field.

Many defects due to the germanium originate from substitutional impurities in the lattice (Fox 1966, Armantrout 1966a,b, Tavendale 1970b, Schell and Nienhuis 1968, Cappellani and Restelli 1968), principally oxygen, copper, iron and silver. Crystal defects and strain (Hansen, Pehl, Rivet and Goulding 1969, Armantrout 1970a) also degrade the detector performance. These impair the lithium drift mobility (Henck, Stab, Lopes da Silva, Siffert and Coche 1966) making the possibilities of good compensation remote.

Trapping effects of the type discussed in section 1.3.3 as well as being generated by poor acceptor compensation are caused by precipitated

lithium, lithium defect interactions, lithium-impurity interactions and complexes, impurity centres, crystal defects and regions of lattice strain. Their effect is enhanced by poor collecting fields.   These phenomena create both shallow and deep energy levels in the energy gap to cause ion pair recombination (Day, Dearnaley and Palms 1967) and the extension of the charge collection time (Trammell and Walter 1969, Sakai 1968 and Zanio and Akutasawa 1968).

It is interesting to note that the traps themselves do not cause significant peak broadening (Day et. al. 1967, Sakai 1968) as their effect has a small statistical variance.   The broadening is due to the position of the generated charge in that each group of freshly generated electrons and holes have different distances to travel to the electrodes (depending upon the position of the initial gamma ray interaction).   This results in varying amounts of charge loss from each pulse.

The overall effects of the above phenomena have considerable influence upon the detector characteristics.   The full energy peak effic- iency may be much reduced when compared with high performance detectors of equivalent volume (section 5.2.1).   This is accompanied by non symmetric shape peaks, slow rise time pulses and a poor full energy peak height to Compton edge ratio.   The reverse bias leakage will be excessive ($> 10^{-10}$A) and probably show a low voltage breakdown characteristic (Fig. 4.1) due to distorted regions of field at junction irregularities (Armantrout 1966a). The detector capacity will also be larger than that calculated from detector geometry considerations and show a large variation with reverse bias (Fig. 4.2).   The curves of Figs. 4.1 and 4.2 were plotted after two successive cold drifts on a $1.5 cm^3$ volume* Ge(Li) detector.

4.2.2 Surface Effects

The performance of a detector is highly sensitive to the condition of its intrinsic surfaces.   The dominant contribution to reverse bias leak- age is invariably generated by surface currents (Dearnaley 1967).   A signi- ficant proportion of this can be thermally generated (McIntyre 1968).   Care is essential in the minimisation of this and the defects that arise in intrinsic surfaces (Armantrout 1966a, Ellis 1968 and McKenzie and DeWit 1967).

* All detectors, for the remainder of this thesis, are referred
   to by their calculated (by copper staining, section 4.3.4.1)
   sensitive volume.

Fig. 4.1

The Variation of Leakage Current with Reverse Bias
for a 3 mm drift depth Planar Ge(Li) Detector
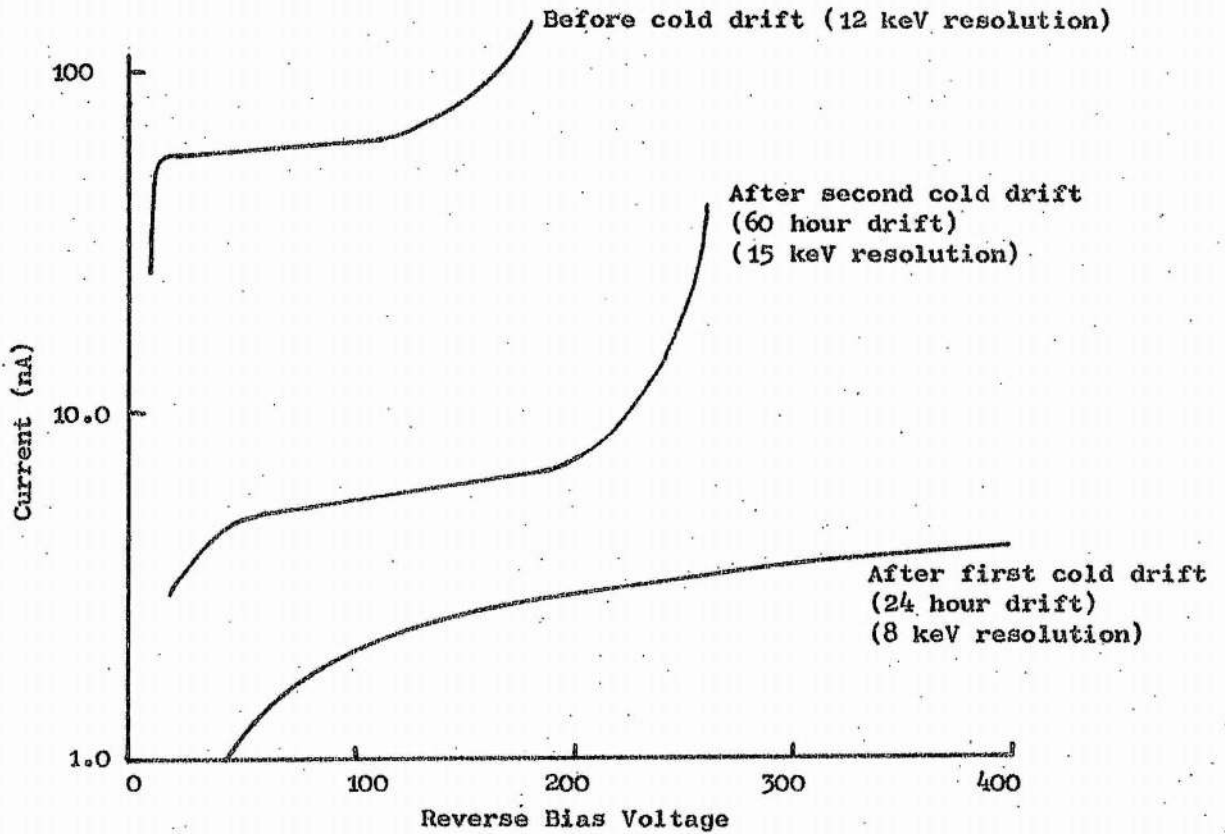
Fig. 4.2
Variation of Capacity for the Detector used in Fig. 4.1
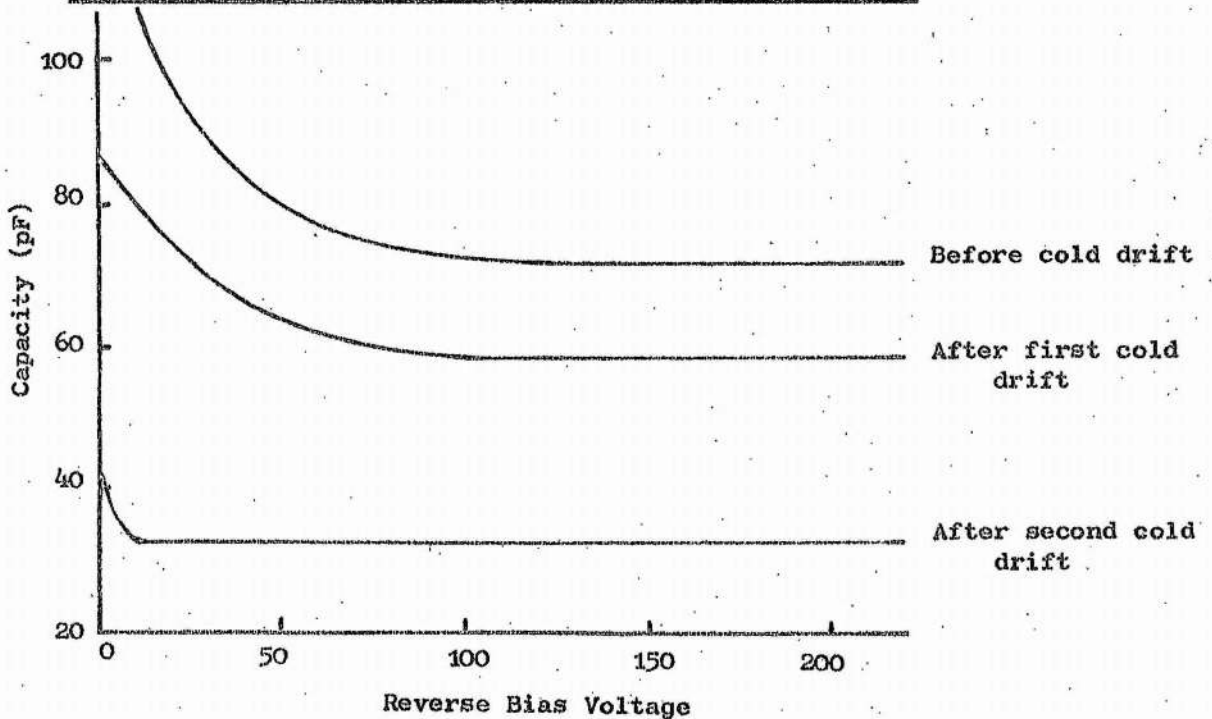
In addition to defects typical of the bulk material surfaces contain a concentration of crystal damage (Armantrout 1966a, Goulding 1964), extra impurities, precipitated lithium and other lithium complexes giving a distorted energy band gap structure (McIntyre 1965). Surfaces are highly susceptible to impurities and particular impurities result in n and p layers on the compensated germanium. Kingston (1956) has shown that 10^{13} impurity atoms cm^{-2} can dominate the surface state of intrinsic germanium. These "inversion" semiconducting junction layers may extend over the entire surface and if they cross the p-i and i-n junctions, they shunt these, contributing additional capacity to the detector (Armantrout 1966a). This additional capacity is frequently accompanied (McIntyre 1965) by low breakdown voltages and excess current. The charge storage capability of this surface condition (Davies and Webb 1966 and Elliot 1966) may result in slow charge collection. Surfaces with these phenomena generally exhibit poor collecting fields coupled with significant charge trapping.

Careful lapping, etching and mounting techniques are critical for the achievement of low leakage characteristics and the minimisation of charge trapping. The reverse bias leakage current variation with voltage (i.e. Fig. 4.1) of a detector generally reflects a combination of diode and resistive curves. Its use in detector defect diagnosis requires care in that any one of a number of bulk, surface or contact defects can give rise to similar characteristics (Goulding 1961, Ellis 1968). Ellis (1968) has extensively studied the use of leakage current characteristics for evaluating detector defects. The curves from Fig. 4.1 were measured between cold drifts. Fig. 4.2 shows the reduction of capacity after each cold drift. The current characteristic change shows that this detector was dominated by its surface conditions.

4.2.3 Contact Effects

Contact problems are those arising from the n and p layers of the detector and those from the electrical and thermal contacts to the detector.

Poor condition n and p layers result in excess charge injection, increasing the reverse bias leakage current. Strauss and Larsen (1969) and Mayer (1969) have shown that slow rising pulses result from charge generation in the proximity of the junctions due to diffusion of charge from regions with low collecting fields. Unnecessarily thick n and p layers result in loss of counting efficiency (section 5.2.2.1).

High resistance ohmic contacts to the detector cause slow risetime detector pulses. In addition, the resultant poor thermal contact prevents adequate cooling of the detector. Hansen and Jarrett (1964) have optimised contact performance, using indium foils painted with indium-gallium eutectic. These foils must be of minimum thickness due to their high gamma ray absorption.

Optimum detector performance can only be achieved when effective minimum thickness non-injecting n and p layers are achieved.

4.3 Measurement of the Detector Characteristics

This section describes the measurements made to obtain pertinent data on crystal condition both before and after the crystal is installed in the cryostat.

4.3.1 The Measurement of Leakage Current

Typical detectors at $77^{\circ}K$ have reverse bias leakage currents of the range 10^{-8} to 10^{-10} amps. The technique of Dearnaley and Northrop (1966) is used for this measurement. Fig. 4.3 shows the circuit used for measuring the leakage current of a planar detector. The current flows through a standard 10^7 ohm resistor, one nanoamp generating 10 millivolts. This voltage is measured with a high internal impedance, ($>> 10M\Omega$), digital voltmeter, or vibrating reed electrometer. The curves of Fig. 4.1 were obtained with this technique.

Careful attention must be paid to the earthing of the circuit and to electrical pick-up to avoid the measurement of additional stray currents. When these are eliminated, the precision depends upon the standard resistor and the voltmeter used. Emphasis is also placed on recording the shape of the current-voltage characteristic due to its significance in the diagnosis of crystal faults.

4.3.2 The Measurement of Detector Capacity

In practice, the capacity measured is a combination of stray and detector capacity. Dearnaley and Northrop (1966) use a pulse technique to measure capacity, sharing the charge from a pulse between a known capacitor and the detector. Fig. 4.4 shows the circuit used for measuring the detector capacity as a function of reverse bias voltage. Pulses at 50 pps are fed from a precision pulse generator (Ortec 204) to a standard capacitor C_s and the detector input.

Fig. 4.3

Circuit Diagram for Leakage Current Measurement

cryostat wall

n   i   p

cooling block

+

O
HT supply
+ Ve

feed
through

standard
resistor

to
digital voltmeter
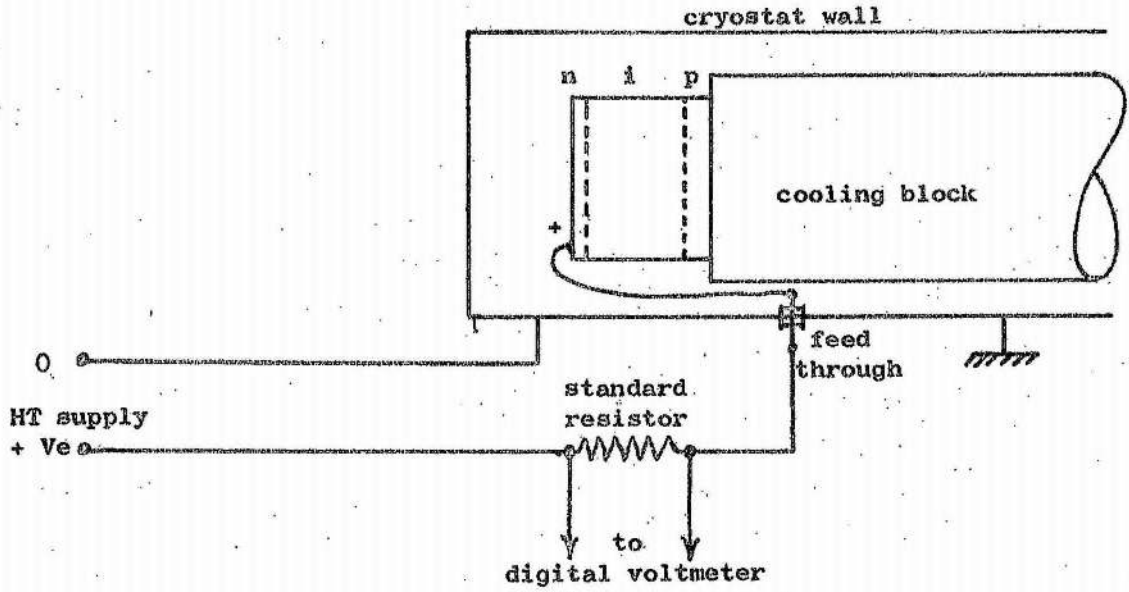
Fig. 4.4

Circuit Diagram for Detector Capacity Measurement

cryostat wall

n   i   p

cooling block

O
HT supply
÷ Ve

10M

to pulser

C_1

to
oscilloscope
or
voltage sensitive
amplifier
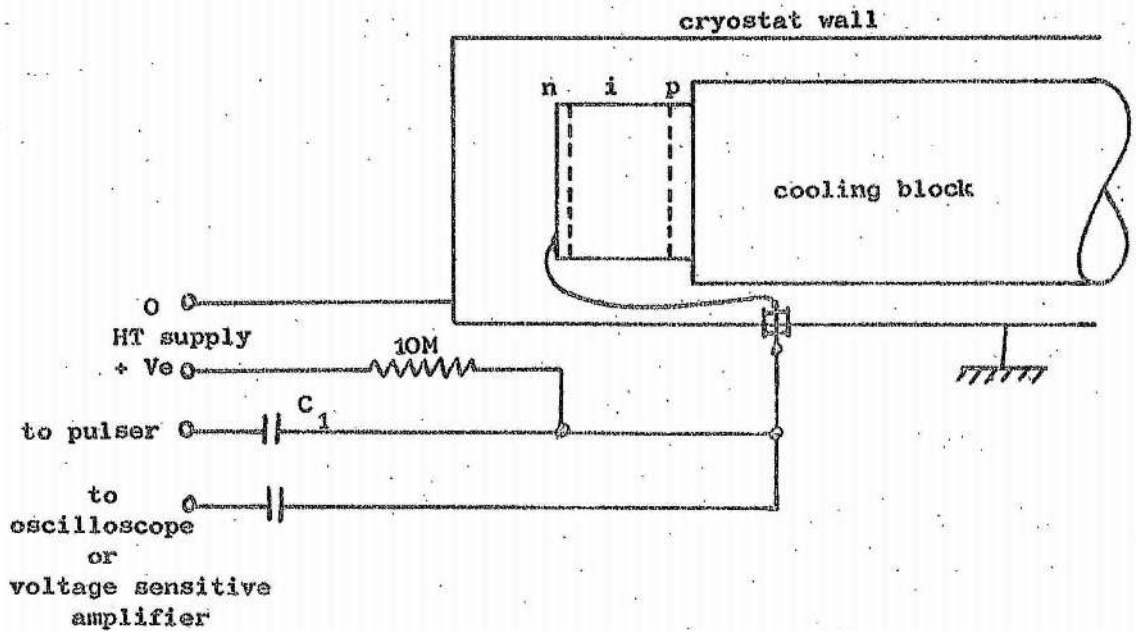
If C_T = detector capacity (C_D) + stray capacity (Cs)

V = voltage pulse height of pulse

V_D = voltage developed across C_D

Then $C_T = \dfrac{C_1(V-V_D)}{V_D}$ .... (4.1)

Measurement with and without the crystal in circuit allows accurate calculation of C_D. Fig. 4.2 shows curves of the variation of capacity measured with this technique. Typical measured values of capacity vary from 5 - 200 pF and are dependant upon the magnitude of the reverse bias voltage. Again, emphasis is placed upon measuring the shape of the capacity - voltage characteristic as well as its magnitude due to its significance in fault diagnosis.

4.3.3 Observation of Full Energy Peak Shape

Observations are made after the energy resolution has been optimised as far as possible as described in section 3.3. The peak shape is observed at different filter time constants. Slow charge collection becomes evident by increased peak assymmetry at the shorter time constants. The peak has both random and symmetric sources of broadening which can be usefully considered.

The symmetric components are due to leakage current and capacity contributions. The non symmetric components are due to the trapping mechanisms discussed in section 1.4.3 caused by the phenomena described in section 4.2. An approximate measure of the assymmetric component is obtained by comparison of the energy resolution at full width at half maximum and one tenth maximum peak height. The ratio of the two should be approximately two* for a good detector. Larger ratios show that significant trapping is taking place and the compensation should be improved. Fig. 4.5 shows two full energy peaks. The higher resolution peak is from a well compensated detector operating at 100V/mm in the depletion region, and shows an acceptable degree of tailing. The poorer peak is from a detector that had been accidentally returned to room temperature with a corresponding loss of compensation (also at 100V/mm bias). The observable tail complicates precise intensity measurements in a complex spectrum.

4.3.4 The Measurement of the Detector Volume Sensitive to Gamma Rays

Several techniques are available for determination of the sensitive volume of a detector. These are divided into two groups, those used

* On the assumption of Gaussian statistics

Fig. 4.5

Comparison of Peak Tailing Between a Good Detector
and a Degraded Detector
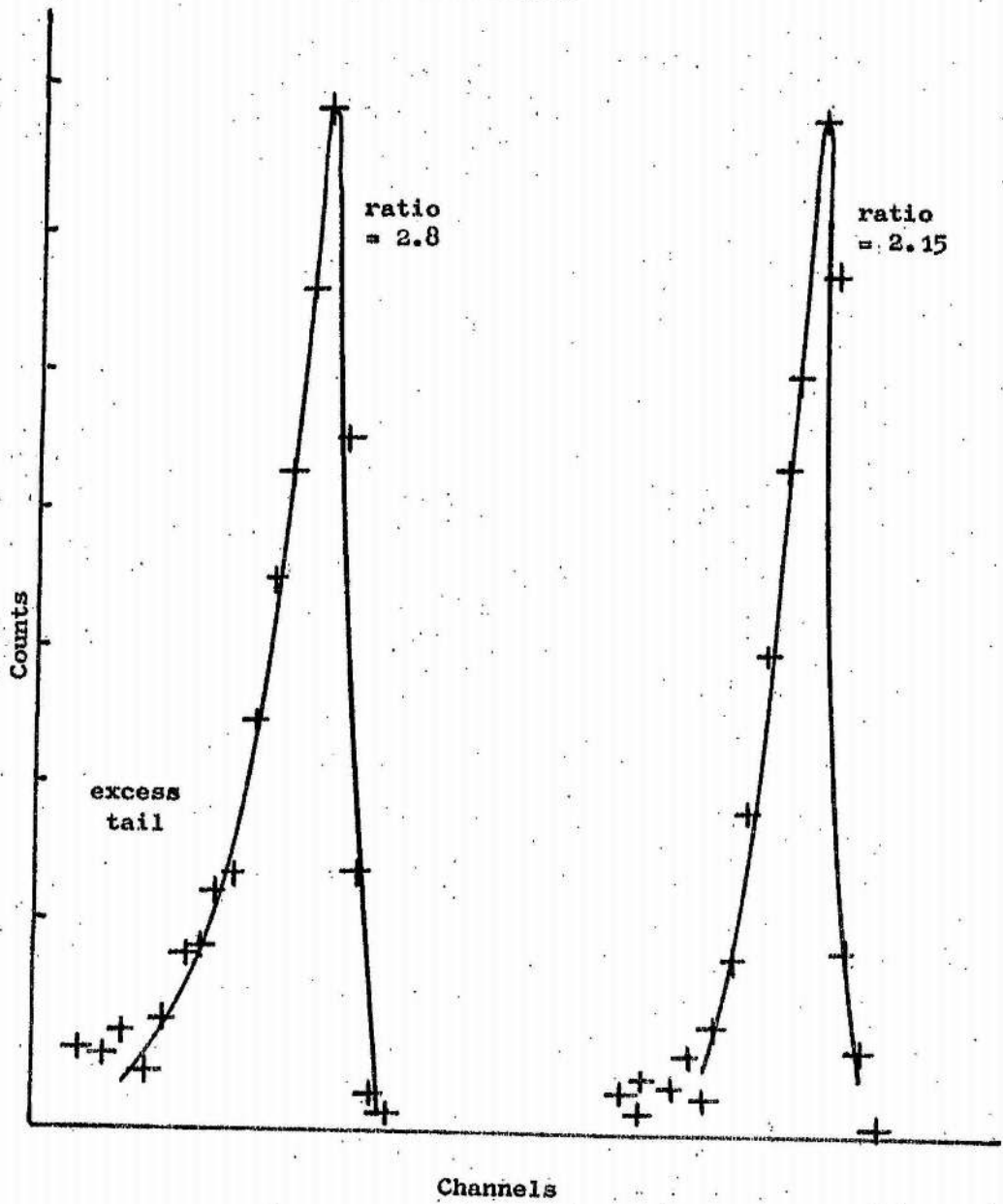
before installation of the detector and those used when the detector is operational.

4.3.4.1 Measurement before Installation

The following techniques are available for detector volume measurement:-

    (i)   Thermoelectric probe (Henck et. al. 1966)

  (ii)   Surface Resistivity Probe (Goulding and Hansen 1964)

(iii) Photoconductance Analysis (Brownridge and McLoughlin 1968)

 (iv) Copper Staining (Hansen and Jarrett 1964)

  (v) Eddy Current (Walford and Doust 1968).

All methods rely on the assumption that the boundaries of the drifted region coincide with the sensitive volume. Webb, Malm, Chartrand, Green Sakai, Fowler (1968) have confirmed this for high quality detectors. For poorer detectors there is some doubt as to whether this assumption is accurate. Methods (i) - (iv) measure surface p-i-n contours while (v) has some degree of depth measurement in the crystal. All methods leave the operator to estimate the sensitive volume by estimating the internal contours of the crystal. This may be satisfactory for small planar crystals, but for large coaxial detectors considerable errors can be incurred.

No satisfactory direct method is at present available. While each technique has its limitations it is unwise to disregard them, since they are useful for various diagnostic measurements. For example, the surface resistivity probe can be applied to the n layer to determine the lithium concentration. Photoconductance techniques allow analysis while the crystal is still drifting. Copper staining is simple and in addition its appearance gives a rapid indication of the quality of the intrinsic region (Ellis 1968). If the stain is indistinct and copper also deposites upon the intrinsic region then poor compensation is suspected. Fig. 4.6 is a photograph of a copper stained 30 cm^3 coaxial crystal showing delineation of the p core. An additional less distinct stain may be seen, indicating that areas of the intrinsic region have reverted in part to p type material. This crystal required considerable reprocessing before it could be used as a detector.

Method (v) was suggested as an attempt to determine the internal junction contours of a detector. This method relies on the different effective resistance of n, i and p material. The technique should also be adaptable to monitoring the detector while it is still in the drift bath.

Fig. 4.6

Copper Stained 30 cm³ Coaxial Detector Showing Delineation of
the p Core and Additional Staining in the Intrinsic Region
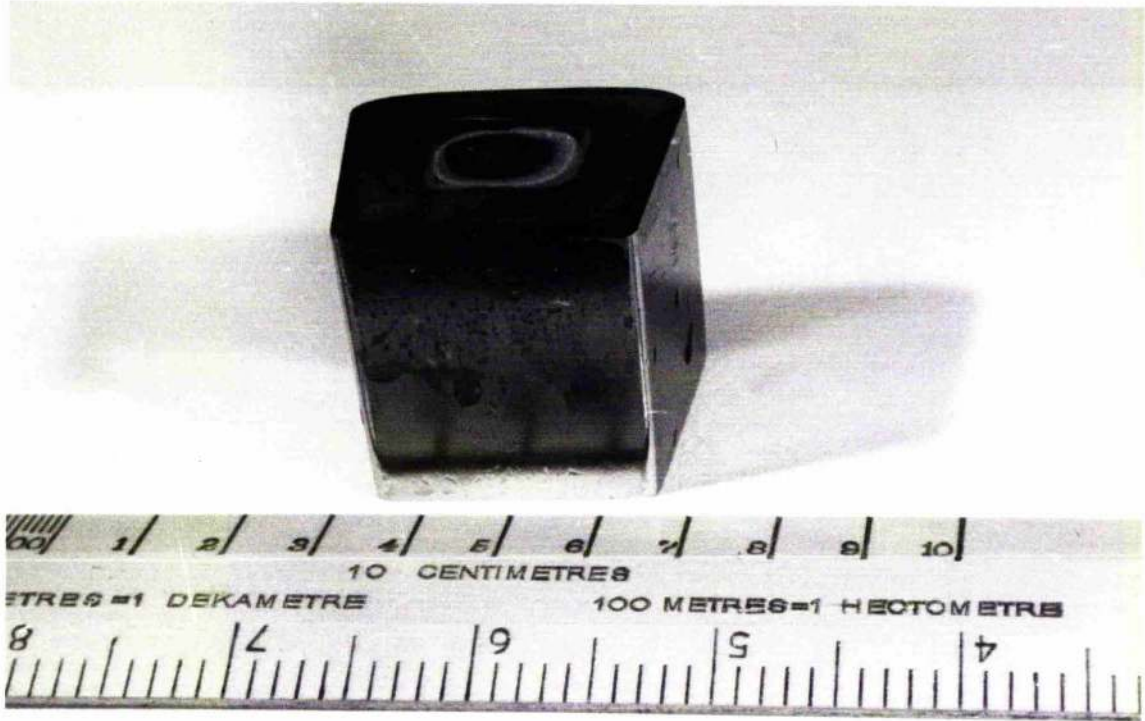
4.3.4.2 Volume Measurement on an Operational Detector

Two techniques are available:-

(i) Capacity measurement (Pell 1960)

(ii) Collimated Gamma Ray Beam (Webb et. al. 1968).

Method (i) equates the measured value of capacity with an expression con-
taining the dimensions of the detector. As has been discussed, the true
capacitance of a detector is influenced by several factors in addition to
its geometry. Unrealistic results for volume determinations can be obtained
thus limiting this approach.

Method (ii) is the only technique that measures the detector in
operational conditions. A finely collimated gamma ray beam is moved across
the cryostat until the detector is observed to respond. In this way, the
sensitive volume may be delineated. Webb et. al. (1968) have developed the
use of the collimator to a high degree, and have used it to measure crystal
property variations. The precision of the technique is dependant upon the
degree of collimation, choice of source and the collimator positioning equip-
ment. Campbell, Smith and MacKenzie (1971), by the use of annihilation
gamma rays and coincidence equipment, have achieved a spatial resolution of
0.1 mm, a factor of ten better than that obtained in the present work using
conventional collimation techniques. However, this precision is unnecessary
due to the thickness of material required in complete absorption of gamma
rays (section 5.2.2.2).

Fig. 4.7 shows a detailed scan that was taken on a $7.4 \, cm^3$ crystal.
In this case the collimator was also used to record sensitivity variations
throughout the crystal. A ^{137}Cs source was used with a lead collimator
($\frac{1}{2}$mm hole diameter and 13 cms long) mounted on a lathe bed for accurate
positioning. The sensitive volume edges could be located to 1 mm. The
non-uniformity of sensitivity observed is discussed in section 5.2.2.3.
To obtain a volume measurement the crystal must be scanned in orthogonal
planes. The sensitivity will always be reduced at the edges of a crystal
due to charge loss caused by electron escape and other energy losses
(Cline 1968). As a result the sensitive volume is never more well defined
than the range of the secondary electrons induced by gamma ray interactions.

4.3.5 Location of the Sensitive Volume within the Cryostat

To a first approximation, this information may be obtained by
measurement just before installation. Remeasurement is necessary for the

Fig. 4.7

Collimated Gamma Ray Scan of a 7.4 cm^3 Detector

The Superimposed Shape Shows the Physical Crystal Outline

counts/min in ^{137}Cs peak
Direction of γ beam
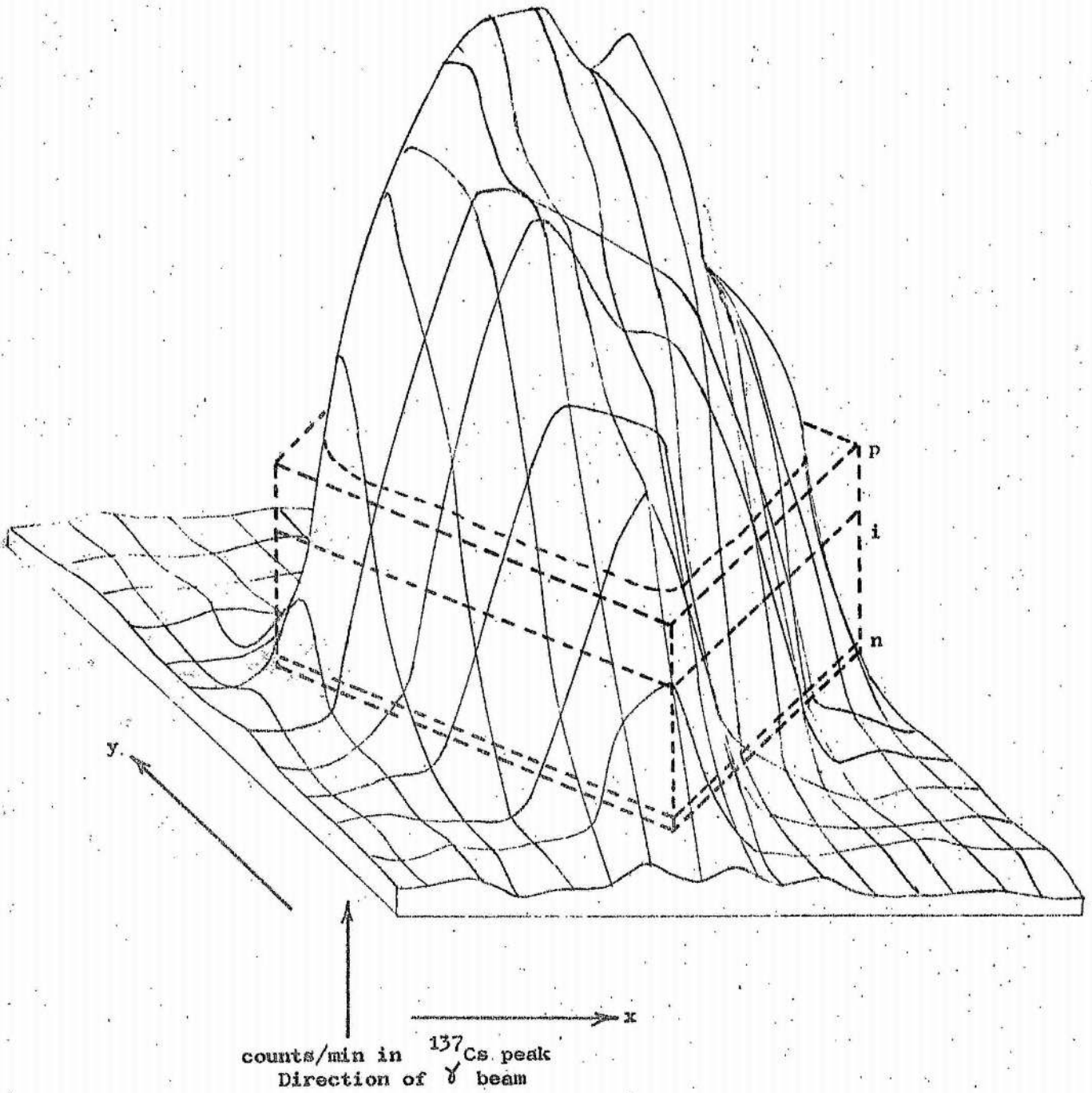
following reasons. Contraction of the cold finger on cooling can move the detector up to 2 mm (Heath et. al. 1966). This can be accompanied by distortion of the finger causing the detector to move off centre by as much as 5 mm (Muggleton 1969). Furthermore, the sensitive volume contours do not necessarily coincide with the crystal's physical external dimensions.

Three techniques are available for volume location; collimated gamma ray beam, radiography of the cryostat and a source distance variation technique.

4.3.5.1 Volume Location with a Collimated Gamma Ray Beam

This technique is as described in section 4.3.4.2. When the scan is performed the volume may be located by measuring relative to a fixed reference point on the cryostat end cap. The choice of gamma ray energy is significant.

In the scan demonstrated in Fig. 4.7, 622 keV gamma rays were used to obtain some degree of penetration for additional data. If a volume location and measurement only is required, then the choice of a low energy gamma ray delineates the surface layers only.

The use of ^{241}Am (60 keV gamma rays with an H.V.L. of .54 mm Ge), allows better spatial resolution, not only due to the shorter range but also to improved collimation at lower energies. The boundaries of the sensitive volume in this instance can be located to 0.5 mm.

4.3.5.2 Radiography of the Cryostat

If an appropriate X-ray machine is available then such a technique is possible. The resultant radiograph will show the position of the crystal. However, unless the crystal is almost entirely sensitive material, or is expected to have an accurately known p-i-n structure then radiography is not satisfactory. Hence, this method has not been considered in detail.

4.3.5.3 The Distance Variation Method

This technique, developed in this laboratory, involves the placing of a source of the energy range of interest at a known distance from a fixed point near the crystal (usually the cryostat end cap window, Fig. 4.8). The area of the full energy peak is measured for that distance and the source adjusted to new position.

Fig. 4.8

Source Detector Geometry for Determination of the Detector Position

detector

source

$\ast$

$\leftarrow t \rightarrow$

l
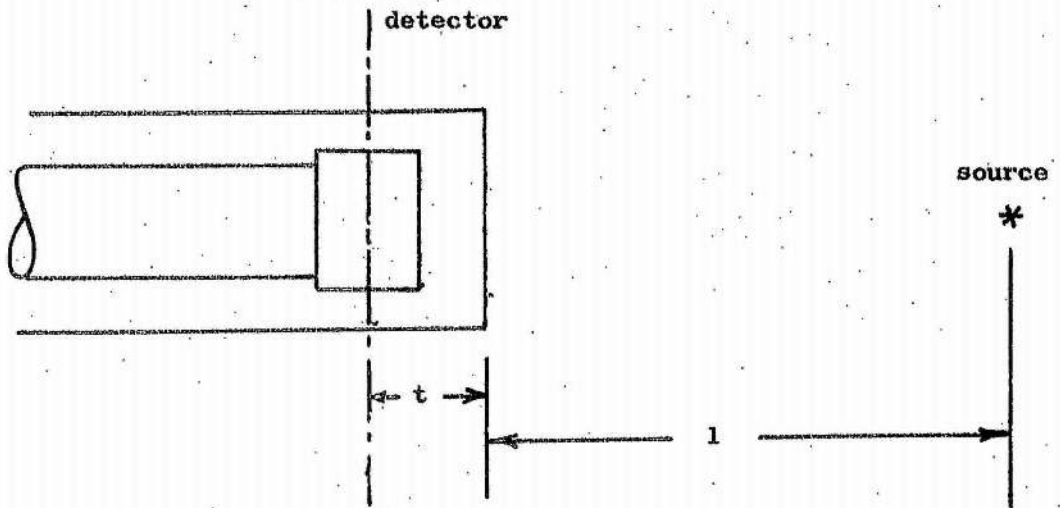
Fig. 4.9

Graph of l against $D^{-\frac{1}{2}}T^{\frac{1}{2}}$ Used to Determine

the Detector Position in the Cryostat

(for energy of 662 keV)

slope = $K^{\frac{1}{2}}$

least squares fit

l

t

100

80

60

40

20

0

0.1   0.2   0.3   0.4   0.5

$D^{-\frac{1}{2}}T^{\frac{1}{2}}$
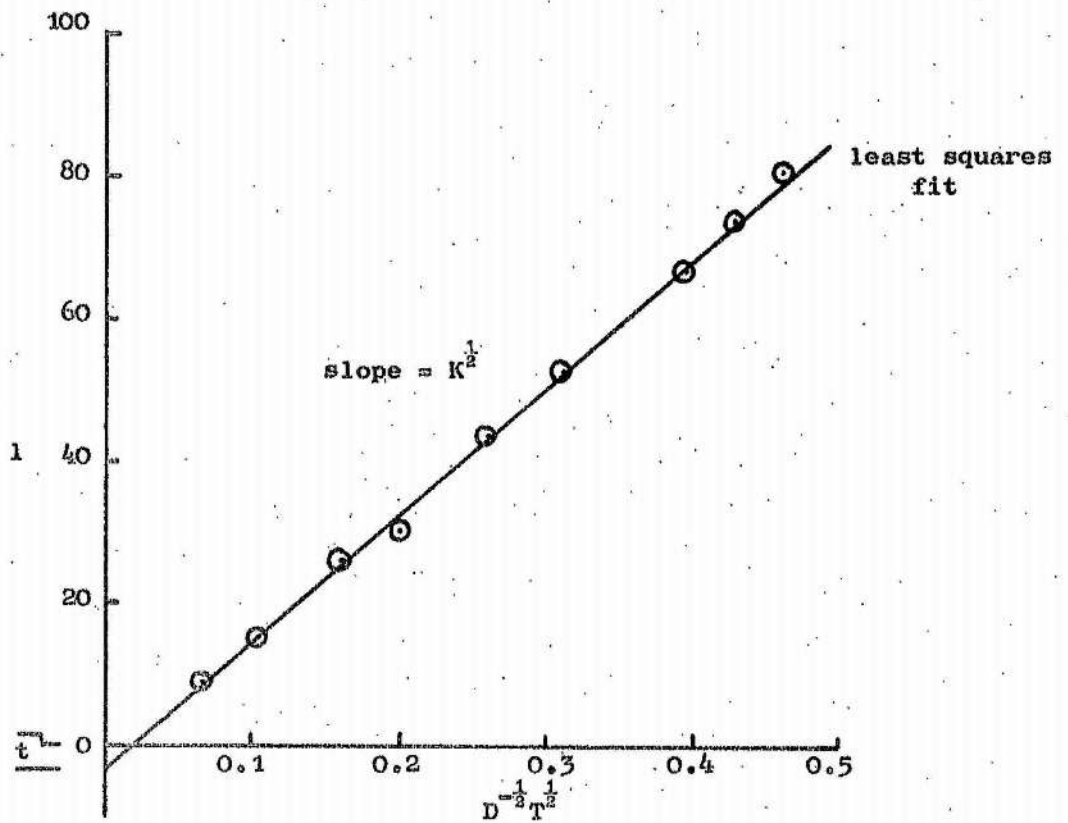
If D = number of counts in the full energy peak

       l = distance of source from end window, or some other fixed point

       t = distance between the fixed point and the plane in the active volume such that the full energy peak receives equal contributions from each side of the plane

Then, to a good approximation:-

$$D = \frac{KT}{(1+t)^2} \qquad\qquad \dots\dots\dots\dots 4.3$$

Where K = constant, and T = count time.

If D is measured for several values of l then a graph is plotted of slope $(K)^{\frac{1}{2}}$ with an intercept of $-t$. Fig. 4.9 shows the graph obtained for the $7.4\,\text{cm}^3$ crystal in the extended dripfeed cryostat of Fig. 2.2. t is energy dependant, but if the thickness of the active volume is small compared with the H.V.L. of germanium for the energy used, then t gives the centre of the effective volume. As the gamma ray energy decreases, t decreases as more of the incident beam is stopped in the first layers of the crystal. The minimum t is just greater than the distance from the fixed point to the crystal front face (ignoring the effect of dead layers).

The position of the front face of the active volume can be readily calculated if low energy gamma rays are used (i.e. 60 keV from ^{241}Am). The dominant interaction is photoelectric (Fig. 1.4) so that the calculation of the position of the front face may assume total absorption for each gamma ray.

If μ_P^E = photoelectric linear absorption coefficient for gamma rays of energy E

    I_o = number of gamma rays in incident beam

    ϕ = distance between crystal front surface and "central plane"

Then $I_o e^{-\mu_P^E \phi} = I_o - I_o e^{-\mu_P^E \phi}$ (equating interactions on each side of the plane)

And $\mu_P^E \phi = 0.639 \qquad\qquad \dots\dots\dots\dots 4.4$

The distance to the front face is thus $t - 0.693/\mu_P^E$ for 60 keV gamma rays, reducing to $t - 0.54$ mm.

The results obtained using these techniques relate to parallel beam conditions and are also useful for apparatus configurations with

difficult experimental access and where the source of gamma rays is some
distance from the detector.

The accuracy of the technique ultimately depends upon the accuracy
of the distance measurements and in the present work was approximately 1 mm.

4.4 Calibration of a Ge(Li) Spectrometer for Efficiency and Linearity

The use of gamma emitting isotopes of accurately known energies
and intensities allows determination of efficiency of detection, and the
response with energy (linearity), simultaneously. Calibrations have been
reported using various radioisotopes, the desirable criteria being a long
half life, a well known decay scheme, and easily and cheaply obtainable in
standard forms and quantities. Appendix II lists some sources that have
been found suitable for calibration.

For a wide energy range (188 keV to 2448 keV) with one source, the
use of ^{226}Ra in equilibrium with its daughter products allows a rapid cali-
bration (Walford and Doust 1968). The energies and relative intensities
(Table 4.1), of ^{226}Ra in equilibrium with its daughter products* have been
determined by Dzelepow and Zhukovsky (1958), using electron recoil measure-
ment techniques and more recently by Wallace and Coote (1969) and Lingeman,
Konijen, Polak and Wapstra (1969) who measured the gamma ray intensities
directly.

The use of radium has the following advantages:-

1) There are at least 46 peaks available for use and the calibration
   may be undertaken with one pulse amplitude spectrum, thus avoiding
   errors due to cross calibration of spectra.

2) Its use is more rapid than that of multiple sources and does not
   require the maintenance of a large stock of sources.

3) The half life of ^{226}Ra (1620 years), is sufficient to eliminate
   any problems due to radioactive decay, so long as equilibrium has
   been established.

However, there are the following disadvantages:-

1) The radium source available has Pt/10%Ir encapsulation so that
   a substantial correction has to be made for attenuation of the
   gamma rays. In addition, the encapsulation causes a continuum
   in the spectrum, due to primary interactions in the encapsulation
   reaching the detector.

* Hereafter termed ^{226}Ra source

<u>Table 4.1</u>

The Principle[a] Energies and Intensities of the Gamma Rays observed

from ^{226}Ra in Equilibrium with its Daughter Products

Energy (keV)	γ s per ^{226}Ra disintegration	Energy (keV)	γ s per ^{226}Ra disintegration
* 188.0	0.04	*1120.4	0.116
* 241.9	0.105	1155.3	0.018
286.9	0.052	1207.8	0.006
* 295.2	0.189	*1238.2	0.060
* 352.0	0.377	1281.1	0.017
396.3	0.013	*1377.7	0.048
417.0	0.008	1403.1	0.040
450.0	0.010	1509.3	0.022
465.0	0.150	1543.3	0.008
485.0	0.015	1583.3	0.011
511.0	0.013	1605.5	0.004
535.0	0.009	1668.8	0.010
* 609.4	0.471	*1729.8	0.024
665.6	0.023	*1764.6	0.163
703.1	0.008	1847.6	0.020
719.9	0.007	1862.1	0.008
740.0	0.004	1900.0	0.004
* 768.4	0.053	2016.1	0.001
786.0	0.012	2090.1	0.001
806.2	0.015	*2118.7	0.014
837.1	0.009	*2204.3	0.052
885.0	0.004	*2294.3	0.004
* 934.2	0.033	2423.7	0.002
960.0	0.005	*2448.0	0.016
1052.0	0.005		

* Signifies those used for efficiency measurements

2)   Due to the 46 principal gamma emissions, there is a large Compton continuum to be subtracted from the full energy peaks.

4.4.1   Energy Versus Response Calibration (Linearity)

Fig. 4.10 shows a radium source spectrum obtained with a 20.5 cm^3 crystal from which 46 peaks may be identified.   The 32 most prominent of

Fig. 4.10

^{226}Ra in Equilibrium with its Daughter Products
Measured with a 20.5 cm^3 Ge(Li) Detector
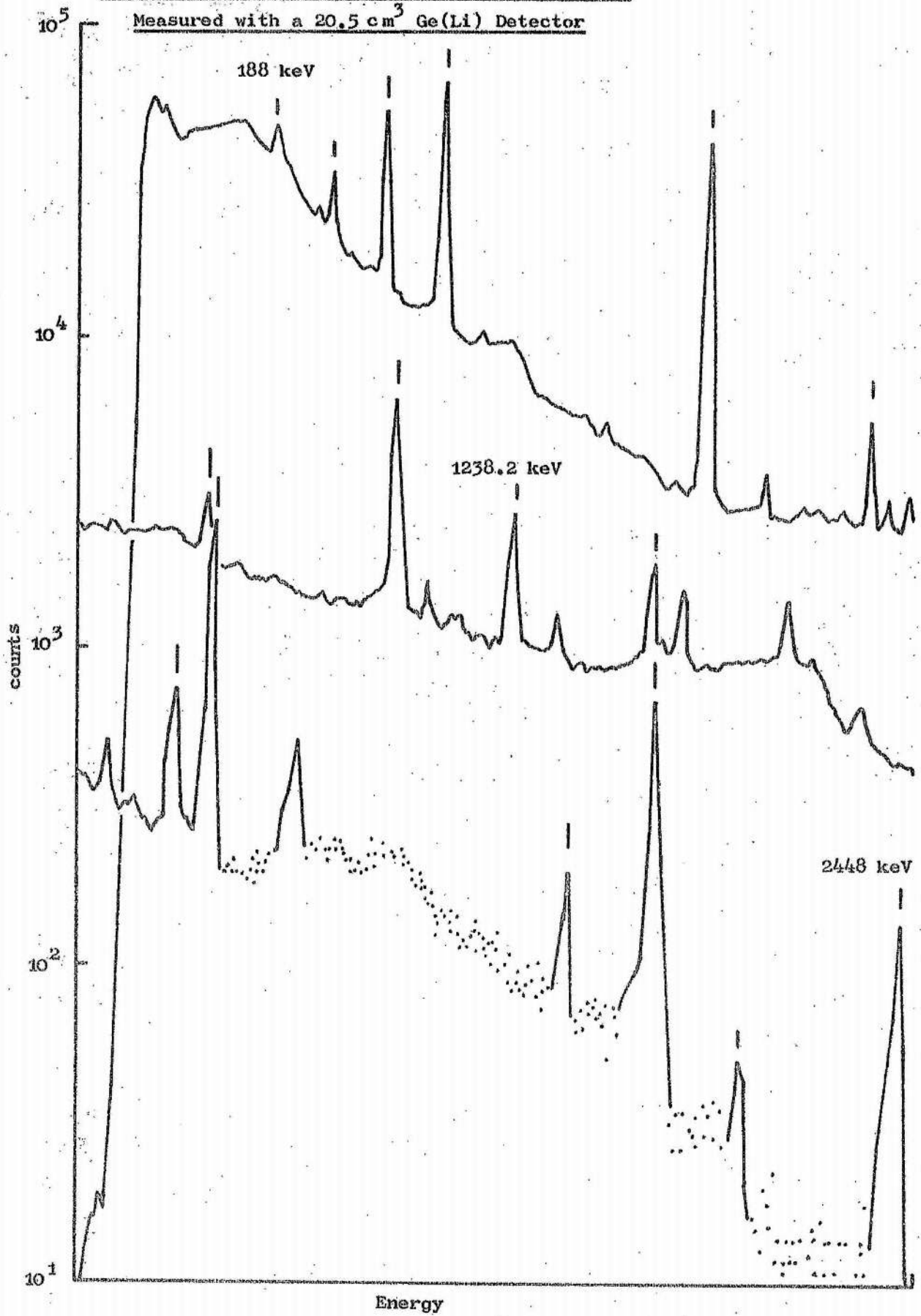
these covering the energy range 188 keV to 2448 keV are used for the energy
calibration of the spectrometers.   For example, for one spectrometer using
a crystal of 4.0 keV energy resolution and an active volume of 0.6 cm^3, a
linear regression analysis yielded a coefficient of 0.999 but showed a slight
curvature in the plot of energy against channel number.   A second order
polynomial equation fitted by least squared analysis gave the equation:-

$$E = .0000017 8i^2 + 0.640i + 2.845$$

Where E = energy of gamma ray in keV

   i = channel number

The difference between the energy of a gamma ray calculated from this
equation and that used in the derivation of the equation was in all cases
less than 1.0% and was in 24 cases less than 0.25%.   These results illustrate
the validity of using a ^{226}Ra source to determine the variation of energy
with channel number of a germanium spectrometer.

4.4.2 Full Energy Peak Efficiency

For the calculation of the full energy peak efficiency of the system
only the 16 most prominent peaks are used.   The intrinsic full energy peak
efficiency is calculated by determining the total number of counts in each
peak (excluding those counts due to the continuum upon which the peak was
situated) and dividing this by the number of gamma ray photons of that
energy incident upon the crystal.   For an absolute full energy peak effic-
iency calibration, the calibrating source must be in the same position, have
the same shape and encapsulation as the unknown sources to be measured.

Fig. 4.11 shows efficiency calculations for five typical crystals
measured with radium.   To verify the use of ^{226}Ra, and the wall attenuation
calculations, one detector (37 cm^3 sensitive volume) was remeasured with
^{54}Mn, ^{56}Co and a further ^{226}Ra source encapsulated in monel* metal.   Fig.
4.12 shows the efficiency calculation for this detector.   It can be seen
that there is good agreement of results.

The errors of this technique originate in the accuracy of peak measure-
ments and source calculations.   In the worst case, (a small crystal with a
poor peak to Compton ratio) the errors vary from $\pm$ 10% for a low intensity
peak on a high continuum to $\pm$ 2% for a more prominent peak.   For larger
crystals the deviations reduce to the range 7% to 1.5%.   Of this, the wall
attenuation tolerances contribute $\pm$ 3% at 188 keV reducing to $\pm$ 1% at
2448 keV.   An experimental technique to verify the source wall attenuation
factor by angling the source proved unsatisfactory.

* 50%Cu + 50%Ni encapsulated source borrowed from R.E. Coles,
                A.W.R.E. Aldermaston.

Fig. 4.11

The Intrinsic Efficiency Measured for Five Detectors
using the ^{226}Ra Source
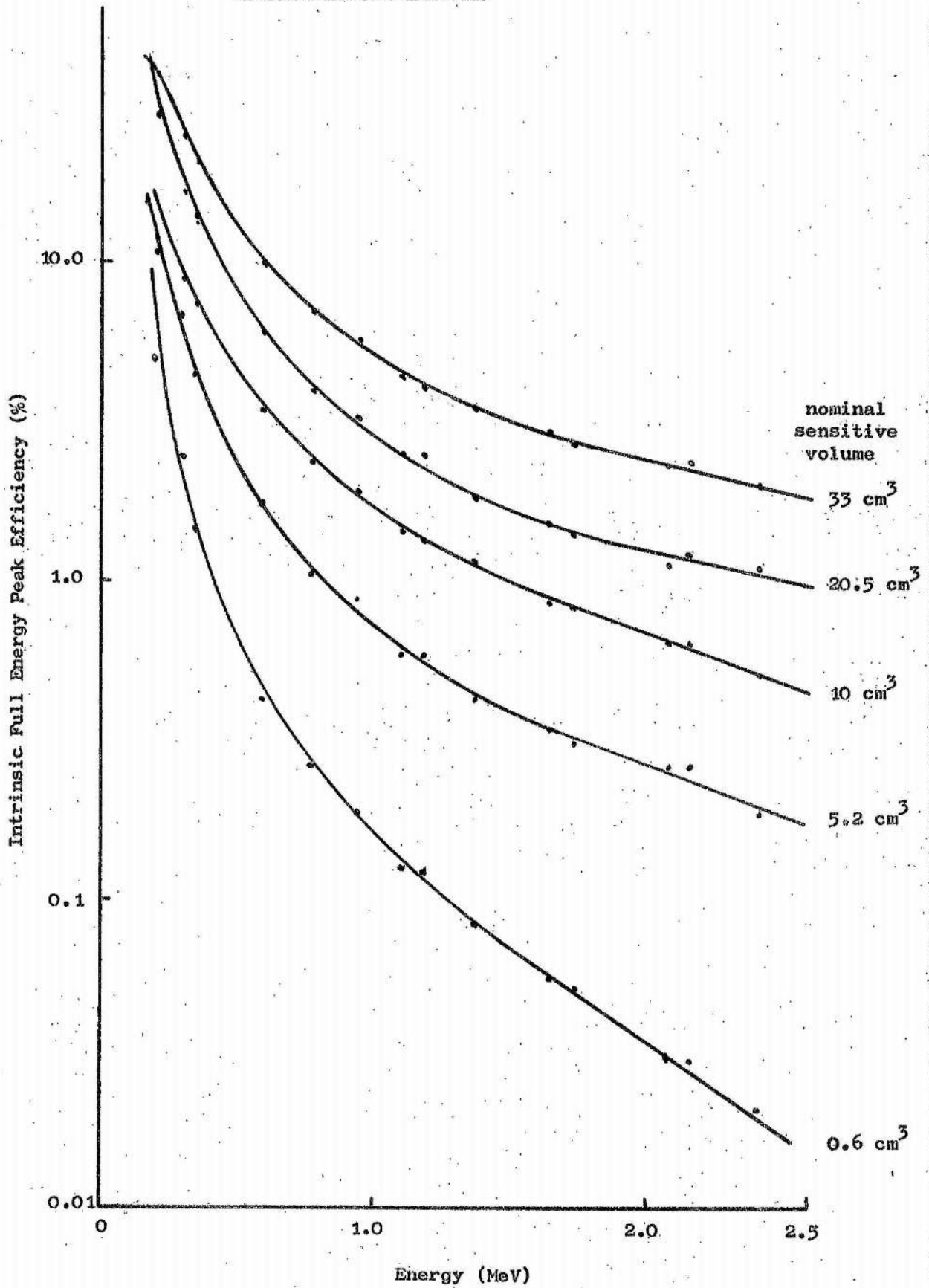
Fig. 4.12

Efficiency Calibration of a 37 cm^3 Detector
with ^{54}Mn, ^{56}Co and Two ^{226}Ra Sources

∇ ^{226}Ra - Pt/Ir encapsulation

⊙ ^{226}Ra - Monel encapsulation

▯ ^{54}Mn

△ ^{56}Co
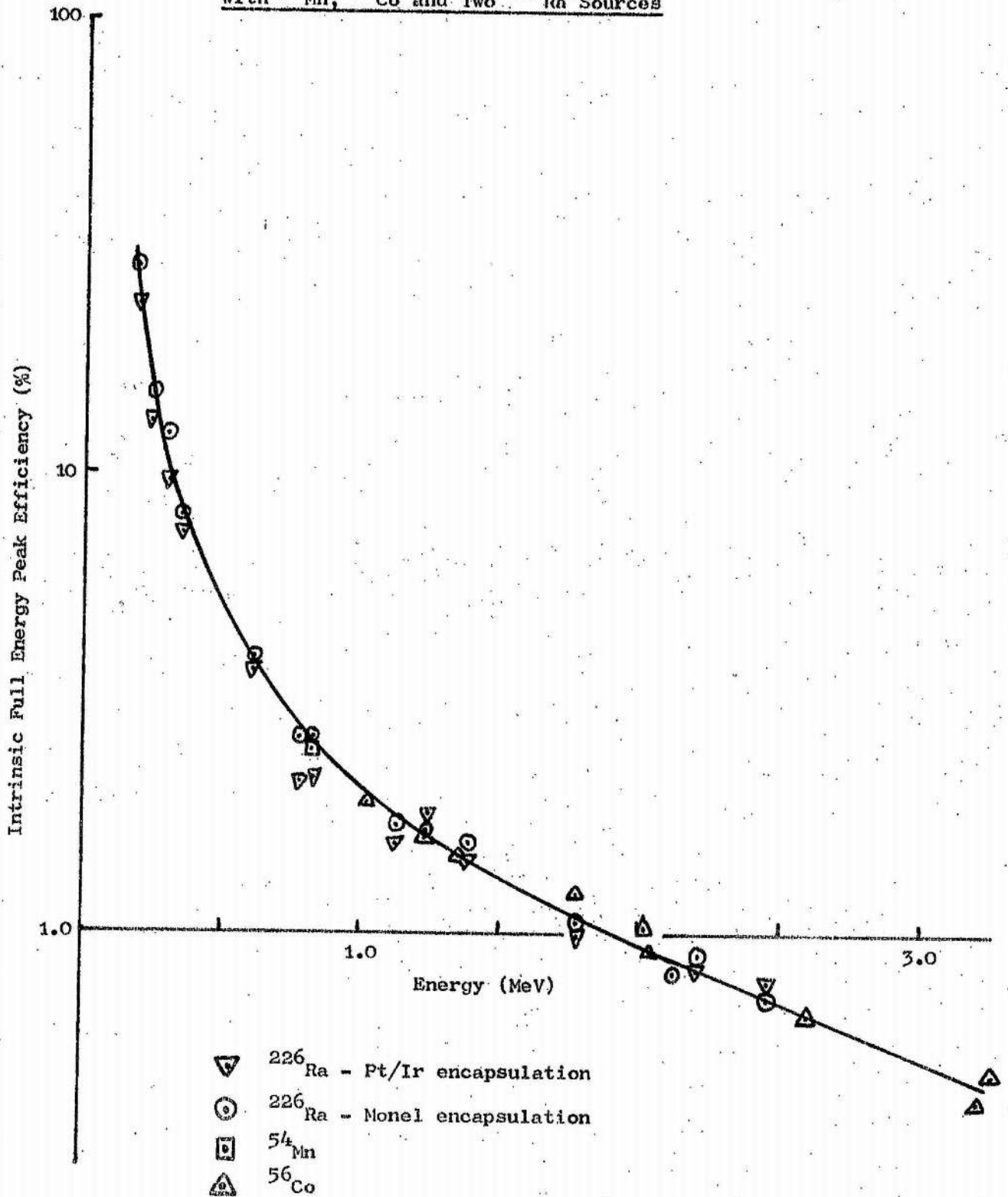
Dolev, Adam and Katriel (1969) point out that some gamma rays emitted from a ^{226}Ra source are in cascade thereby giving rise to possible sum coincidence peaks. The consequence is that events may be removed from one peak and superimposed onto another in the spectrum. For example, a gamma ray of energy 609 keV interacting at the same time as one of 769 keV results in a sum energy being recorded of 1378 keV. Nearly all the cascaded gamma rays are due to ^{214}Bi. Corrections in excess of 8% would have to be applied to the efficiency curve if all the coincident gamma rays from ^{214}Bi were incident upon the detector. This would be so if all the cascade gamma rays were emitted in exactly the same direction. However, the angular correlation of ^{214}Bi is such (Bishop 1958) that this is not the case, and the true correction to be applied is less than 0.001%.

In conclusion, the use of a ^{226}Ra source provides a cheap and rapid method for the calibration of a germanium spectrometer. The long standing use of ^{226}Ra for medical and instrumental calibration has resulted in these sources being readily available in standard forms in many laboratories.

4.5 Experimental Techniques for Crystal Repair and Processing

The following procedures were adopted for use in this laboratory in the mounting and optimisation of Ge(Li) detectors.

4.5.1 Etching

This process is used to prepare the surfaces of a detector just before it is mounted in a cryostat. All etch techniques have the following features:-

1) Strict cleanliness must be maintained for all beakers and equipment used.

2) The crystal surfaces must be free of surface contamination, grease and finger-prints. This may be implemented by prior washing of the crystal in methanol and handling with tissues.

3) All chemicals used are "analar" grade, and all other liquids (e.g. deionised water) are maintained as pure as possible.

4) The time between the etching and mounting of the crystal is a minimum and always less than 5 minutes.

5) The final etched surface must under no circumstances be touched. Paris and Treherne (1968) have investigated the use of protective

varnishes sprayed on the detector after etching. These
have met with partial success and have potential if
developed further.

Etching was always performed in the clean environment of the
polythene tank shown in Fig. 4.13. Deionised water is supplied from an
"Elgastat" on top of the tank. On the left are the power supplies for
detector drifting and on the right are the asbestos cabinets containing
the drifting apparatus.

A number of etch techniques are available, two of which have been
used with average success. The first is that used by Dearnaley (1967).
The second is that devised by De Wit and McKenzie (1969) and adopted in this
laboratory by Baker (1970).

The first etch is as follows:-
The detector is placed in a polythene beaker such that the intrinsic
surfaces are free of any physical contact. The beaker is now filled with
etch (consisting of 3:1, HNO_3:HF) to cover the crystal. A large volume
should be used to prevent the etch boiling rapidly. Etching is continued
(with continual agitation) until it is just starting to give off brown fumes
(about 3 - 5 minutes). Methanol is now flooded into the beaker to quench
the etch. It is essential not to expose the crystal to atmosphere at this
stage. If this occurs, then the process must be repeated. Deionised water
is now poured into the beaker, flooding away the methanol. The resistance
of the overflow water is monitored until it is above 1MΩ. All liquids
should be poured so as to avoid air bubbles in the beaker.

The crystal is removed and laid on tissues, ensuring that no
intrinsic surfaces are touched. Drying is effected by a jet of oxygen free
nitrogen. The crystal is now mounted in the cryostat. The curves shown
in Fig. 4.1 were obtained using this etch.

The second etching procedure used in this work is similar to the
above technique. The crystal is flooded with an etch fluid consisting of
1:1, HNO_3:HF, for about 3 minutes. Again, no exposure to atmosphere must
occur throughout the etching and quenching. The etch is washed away by
several litres of a solution of 10gms KaCl per litre of deionised water.
After removal from the beaker the crystal is placed on tissues, and dried
with oxygen free nitrogen. A milky deposit is observed over the crystal,
in contrast with the clear surfaces of the first etch. The detector is
now ready for mounting.

Fig. 4.13
Detector Processing Equipment Showing Drift Power Supplies
(Left), Etch Tank (Centre) and Drift Apparatus (Right)
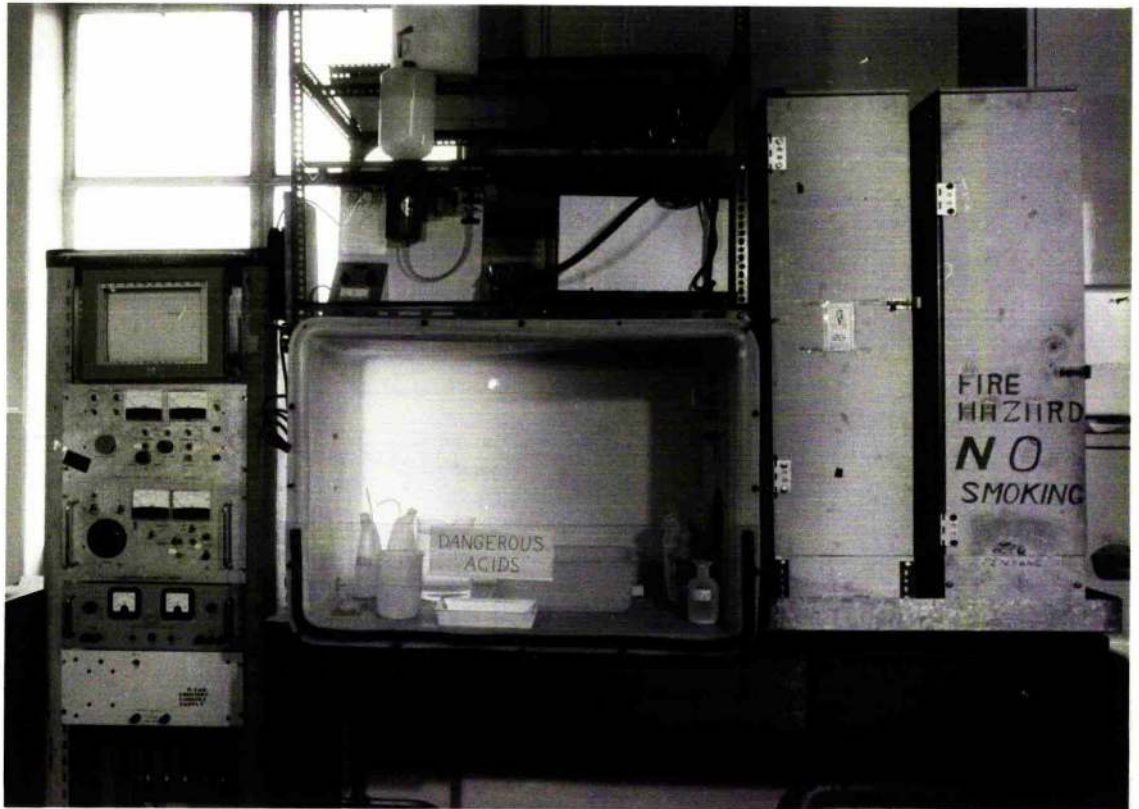
4.5.2   The Mounting of the Detector in the Cryostat

The principle of mounting is simple, but is critical in achieving the full potential performance of the detector.   The two essential features are cleanliness in handling and the time taken in mounting.

Goulding (1966) has observed that the final etched surfaces are sensitive to the atmosphere in which the detector is mounted.   Excessive humidity results in degradation and non-reproducibility of performance, and clearly the time the crystal spends at atmosphere should be minimised to avoid these effects.   Hence the cryostat should be near the etching facility and attached to a pumping system so that it may be evacuated immediately the end cap is bolted on.

Fig. 4.14a is a photograph of a mounted 50 cm^3 coaxial detector. Diagram 4.14b shows the mechanical arrangement.   The detector is pressed into the indium pads for good thermal and electrical contact, and a spring on a perspex block establishes a high tension electrical contact to the p-core.   The detector was placed in the cradle with tissues, contact with the intrinsic surfaces being absolutely avoided.   The cryostat is that discussed in section 2.3.

When the detector is under vacuum it is advantageous to perform a short electrical cold drift to allow a thorough outgassing of surfaces, as well as improvement of compensation.

Liquid nitrogen is added when the cryostat pressure falls below 10^{-4} torr after the ion pump has been switched on.   The detector can take several hours to stabilise at 77°K and is left overnight before continuous use is considered.

4.5.3   The Electrical Cold Drift

The principle of cold drifting has been discussed in section 1.5.1 and is carried out at a temperature approximately -10°C to 0°C, with a voltage of about 100 volts/mm in the depletion region.

When a detector is brought above -20°C, lithium precipitation is always in evidence at a rate depending upon the condition of the detector. During a cold drift the compensation is improved at a rate which is dependant upon the effectiveness of the cold drift conditions, and the rate of precipitation.   The leakage current under reverse bias is thus a combination of two components, one increasing due to precipitation, causing loss of compensation, the other decreasing due to the cold drift improving compensation.

Fig. 4.14a

A 50 cm³ Detector Mounted in its Cradle in the Cryostat
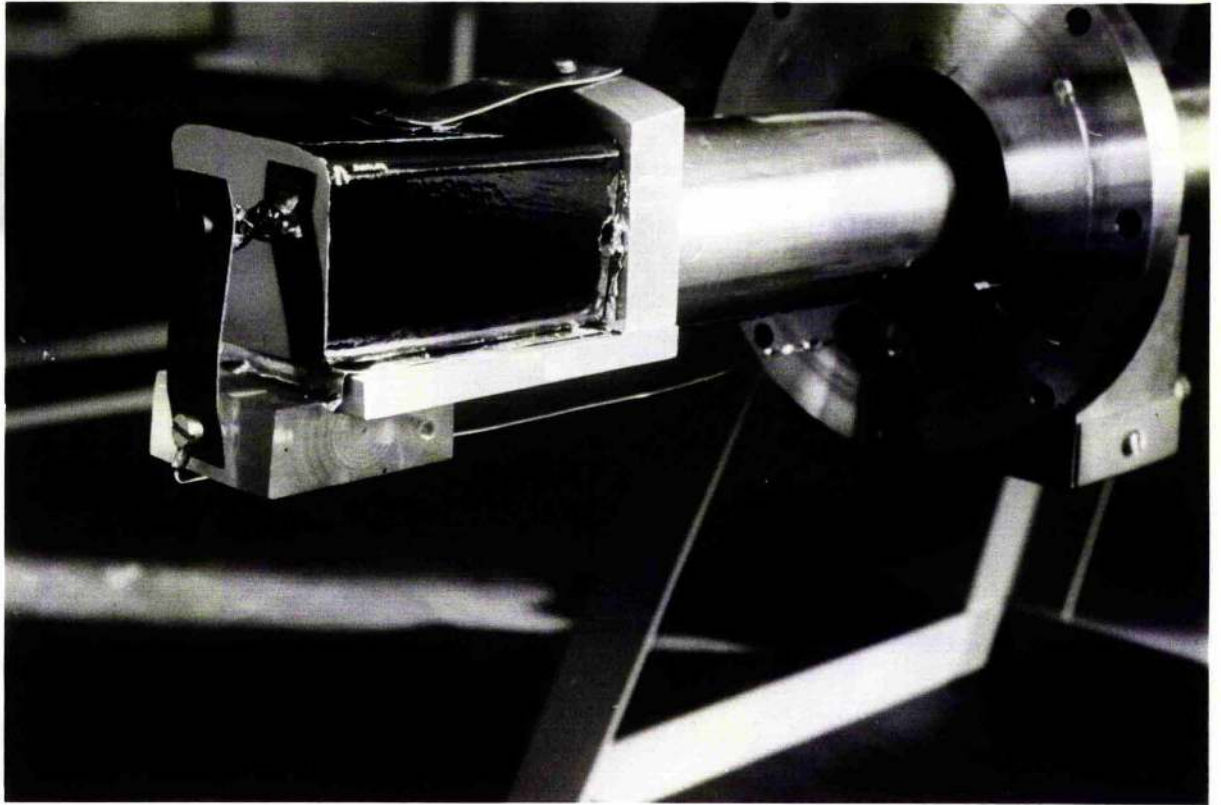
Fig. 4.14b

Explanatory Diagram of the Detector Mount Shown in Fig. 4.14a
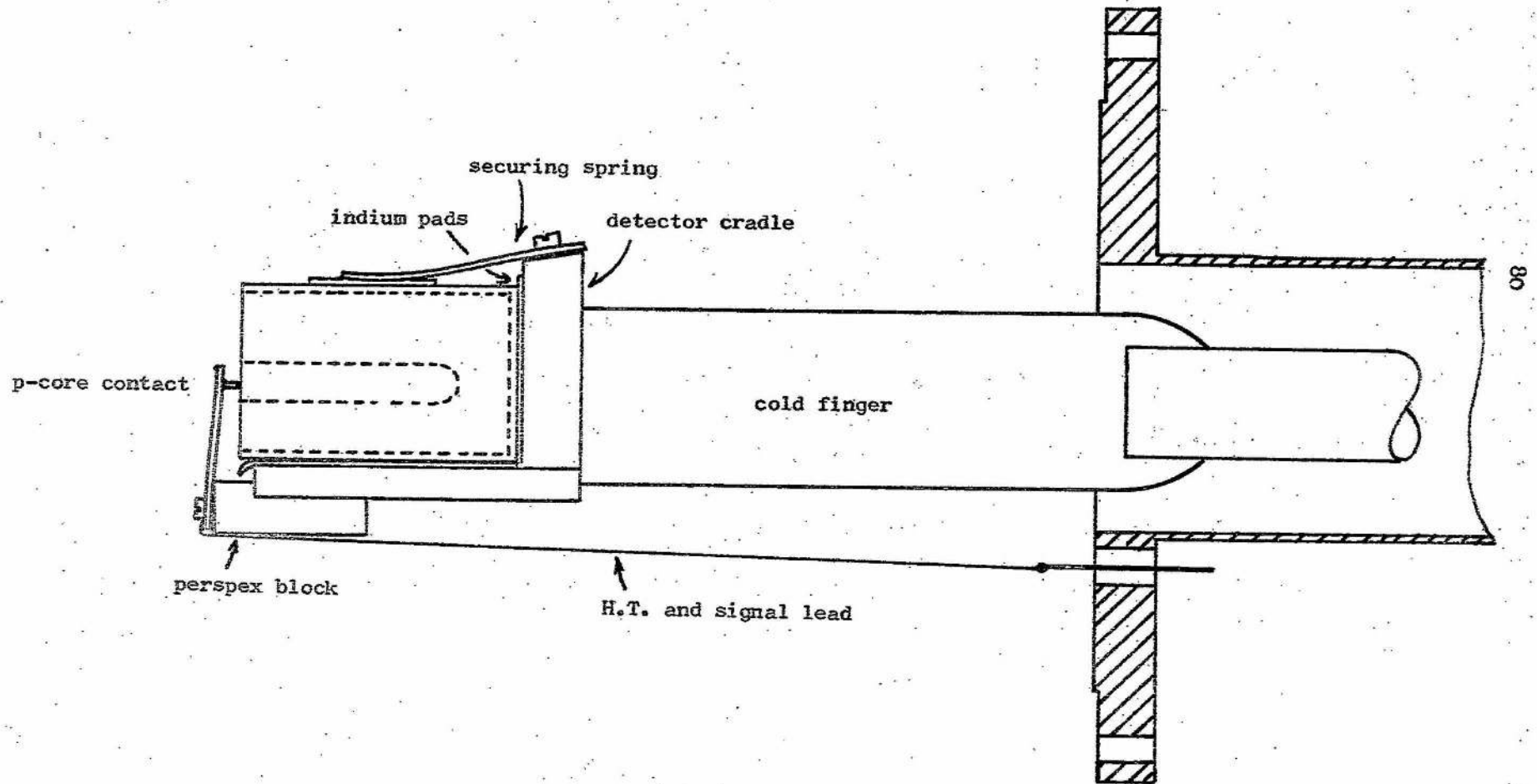
The continuation of cold drifting is advantageous while the nett current falls. Ultimately the degree of compensation reaches a maximum for the drifting conditions when the current reaches a minimum and then slowly rises. The drift is terminated at this point and the crystal cooled to 77°K.

The current flowing during the cold drift has been found to be approximately 1 - 2 mA/cm^2 of i - p junction area. Near perfect diode characteristics must be obtained if good results are to be expected. A resistive slope indicates excess leakage paths not associated with a good diode structure. A detector may commence cold drifting with a positive slope which should be flat at the termination of drift. This is indicative of improved compensation.

Fig. 4.15 shows the variation of leakage current with time during a cold drift, applied to a detector that had accidentally returned to room temperature. The minimum current level may be clearly seen. The detector, a 0.6 cm^3 crystal with 4 keV resolution at ^{60}Co, had remained at room temperature unbiased for about 8 hours with a resultant resolution degradation to 8 keV. The detector characteristic was fully restored to 4 keV resolution.

The duration of the cold drift is difficult to decide in advance as it depends entirely on the germanium and the history of the detector. In general, about 30 minutes cold drift is applied for every hour the detector remains unbiased at room temperature. For freshly drifted detectors cold drift times of a few days may be applied. Periods in excess of this can degrade the crystal due to the increasing amount of precipitation.

An exact control on a clean-up drift is possible if the crystal can be maintained at a precise temperature. For larger crystals this may be difficult as an appreciable amount of power ($\sim$30 watts) may be dissipated (Ridley 1968). Constant power supplies are required to balance the power dissipated in the crystal with the available cooling. Unless this is achieved, no current minimum is observed and the time of cold drift becomes indefinable. In this instance, care has to be taken to avoid excess drifting, resulting in gross precipitation. This was the case for one detector in this laboratory. The detector shown in Figs. 4.1, 4.2, was cold drifted when freshly mounted for approximately 30 hours at a current approximately 1 - 2 mA with a 250 volt bias. The detector was maintained with difficulty at about 0°C using salted ice water and no current minimum

Fig. 4.15

Variation of Leakage Current with Time at 240 Volts Bias
for a 0.6 cm³ Detector at -10°C to Recover Loss of Compensation
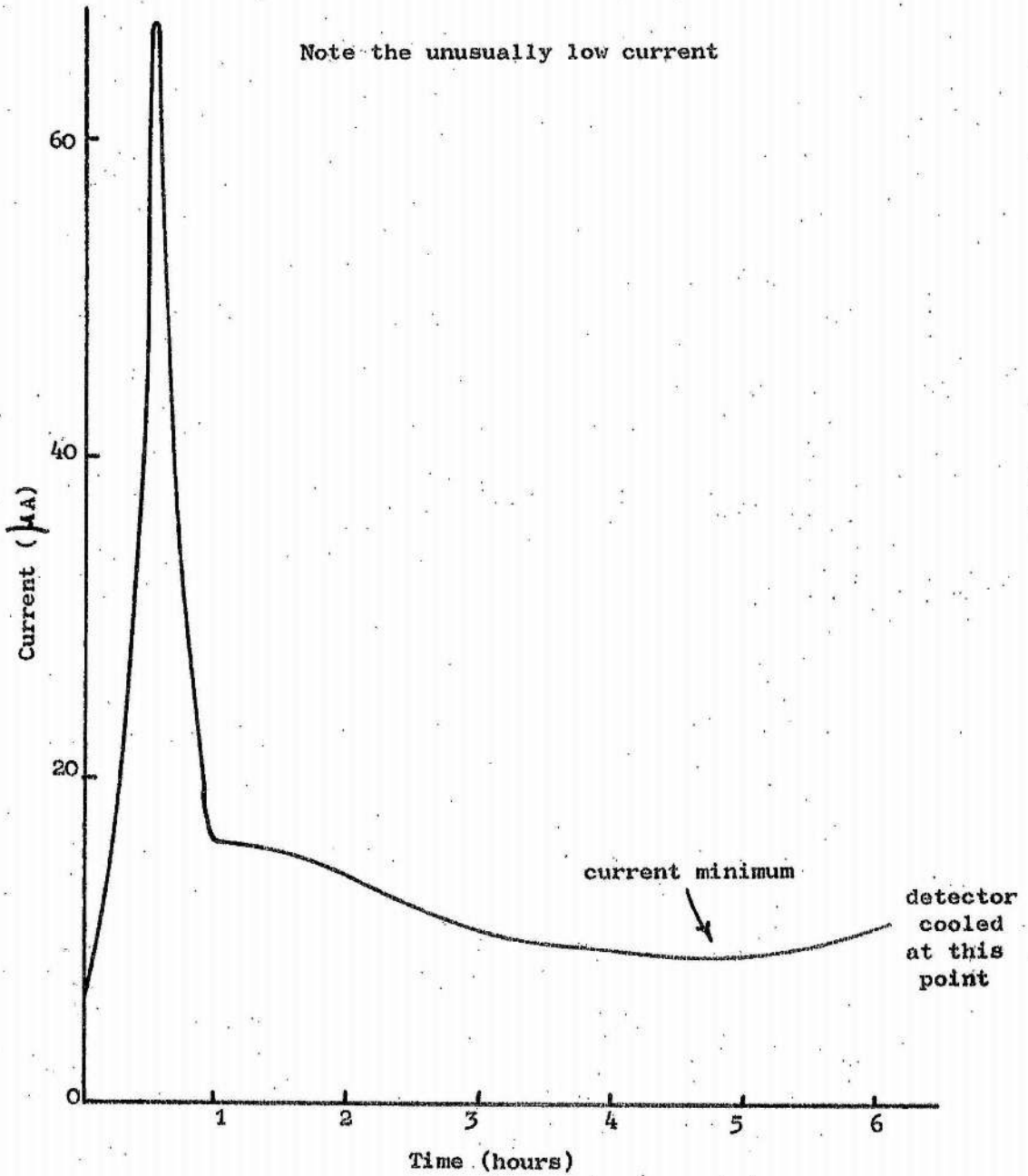
was observable.   However, the detector condition was much improved. Fig. 4.1 and 4.2 show the changes in capacity and leakage resulted in a resolution improvement from 12 to 8 keV.   A further cold drift of 3 days duration resulted in excess precipitation and the resolution being degraded to 15 keV.

4.5.4 Reactivation of Lithium

The phenomenon of lithium precipitation is described in section 4.2.1.   When this has caused a loss of performance it is necessary to re-activate the lithium by breaking the lithium-defect and lithium-impurity bonds by heating the detector to approximately 380°C.   As this temperature is sufficient for the diffusion of lithium into the n-layer, it is advan-tageous to do this at the same time.   In this case, the detector may be electrolytically rediffused with lithium as described by Baker (1970).

Fig. 4.16 shows the diagram of a furnace constructed for the reactivation of precipitated lithium.   The main design requirements are uniform heating, cleanliness to prevent the diffusion of impurities into the crystal and an inert atmosphere to prevent oxidation of crystal surfaces. Thermocouples are embedded in the furnace winding and the windings are arran-ged to give a uniform heating profile over the centre portion of the tube.

The detector is steadily heated to 380°C over 30 minutes, to reduce stressing of the crystal.   Helium is passed through the quartz tube, the rate of which is varied to give fine heating control.   The coarse control is via a Variac transformer in the heating circuit.   This temperature is maintained for approximately 20 minutes (recommendations from panel discus-sion at Ispra conference 1968) and then the detector is cooled slowly to room temperature over the course of an hour.

In the discussions at the Ispra Conference 1968, it was considered that the lowest possible temperature should be used in diffusion and re-activation ($\curvearrowright 380^{o}$C).   All heating cycles have been found to be detrimental to the germanium ingot qualities and hence the temperature used and the number of cycles must be minimised.

Fig. 4.17 is a photograph of the completed furnace showing the quartz tube protruding from the end wall.

When the crystal has cooled, it is etched, re-drifted for a short time (approximately six hours), and then cold drifted for two to three days prior to its mounting in the cryostat.

Fig. 4.16

Furnace used for Lithium Reactivation in a Ge(Li) Detector

aluminium case

thermocouple

detector inserted through
end on quartz shovel

end winding

quartz tube

gas
inlet

gas
inlet

stainless steel
tube

end windings to stabilise
temperature profile

main winding

fibre glass filling

2'0"
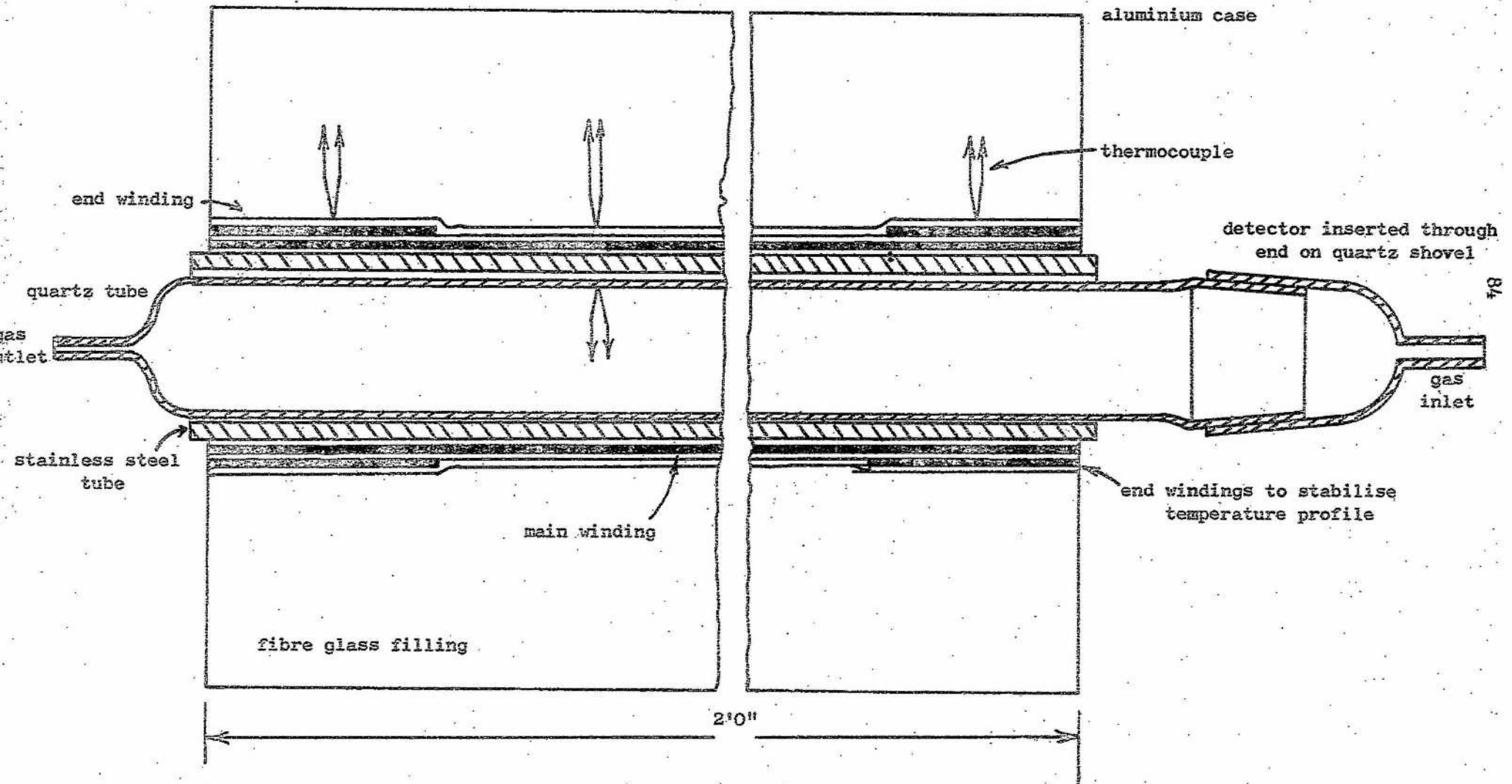
Fig. 4.17

Photograph of the Furnace Used for Lithium Reactivation
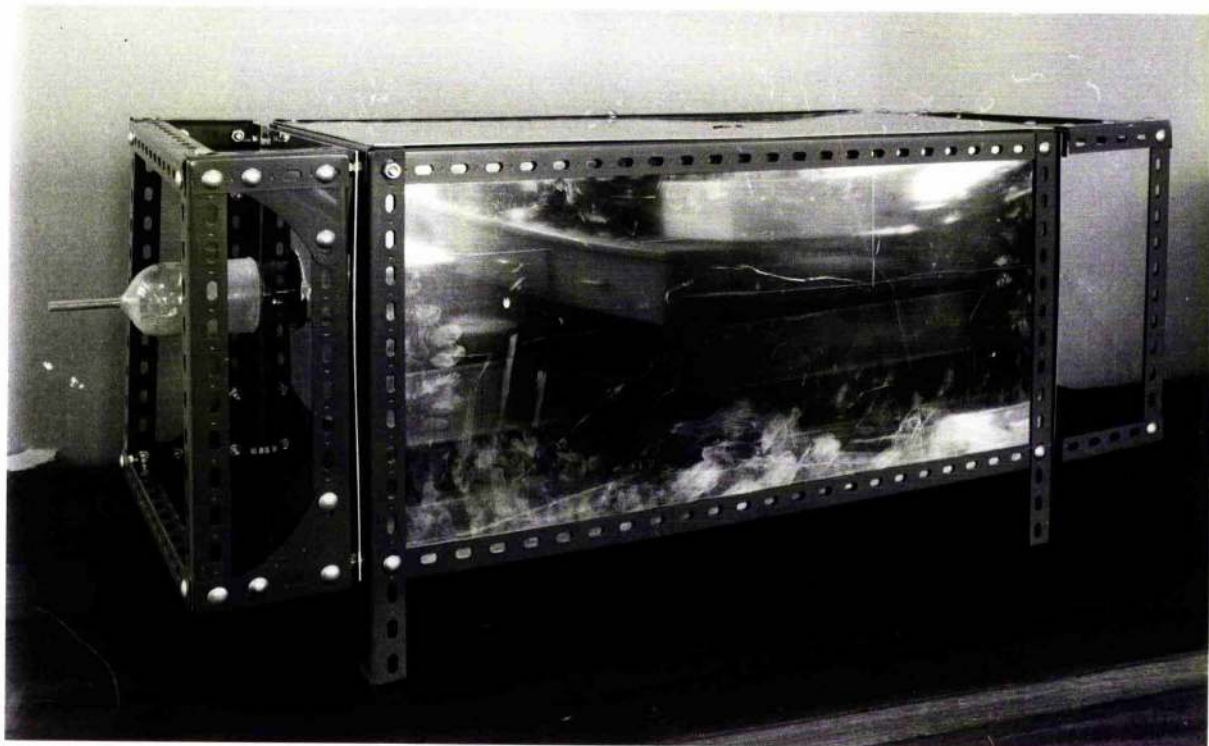
4.6 Operational Running Experience

The stability of a Ge(Li) spectrometer is of great significance when it is considered that a gain drift of 0.1% can seriously degrade the expected resolution. Variations of this kind originate from electronic components of the spectrometer. It is also important to consider the possible changes due to the variation of characteristics of a mounted detector.

4.6.1 Short Term Variations

These may be expected from a detector in the first few hours of its mounting due to its stabilising to liquid nitrogen temperature. After a week, the detector should be reasonably consistent in performance.

No random short term variations in performance have been observed in established Ge(Li) spectrometers that are directly attributable to the detector.

4.6.2 Long Term Variations

If a detector is maintained continuously at liquid nitrogen temperatures then there can be no increase in trapping levels observed (excluding the effects of radiation damage). No detector failure of degradation with time has been observed. Anders (1969) has observed a reduction of pulse height output for his detectors of 1% per year. However, all detectors in this laboratory have undergone slow improvement. This is attributed to outgassing of the detector surfaces and a very gradual compensation improvement due to the continuously applied bias. Fig. 4.18 shows a graph of the leakage current of one crystal at constant voltage measured over a period of months. It was generally found to be roughly halved in two months, a performance typical of the other detectors used.

Fig. 4.19 shows the performance variation of a 40 cm^3 trapezoidal detector. Initially, the working voltage was 1300 volts with 2.0 nA leakage current and a resulting performance of 3.2 keV with a peak height to Compton edge ratio of 16:1. In one week the current had reduced to 0.15 nA and the breakdown point was 400 volts higher. As a result, the performance of the detector was improved to 2.5 keV with a peak to Compton ratio of 22:1.

4.7 Detector Accidents and Repair

Any disruption of the liquid nitrogen filling routine may lead to the detector returning to room temperature. This is frequently accom-

Fig. 4.18

Variation of Leakage Current with Time at Constant Voltage
for a Mounted Detector

Time (months)
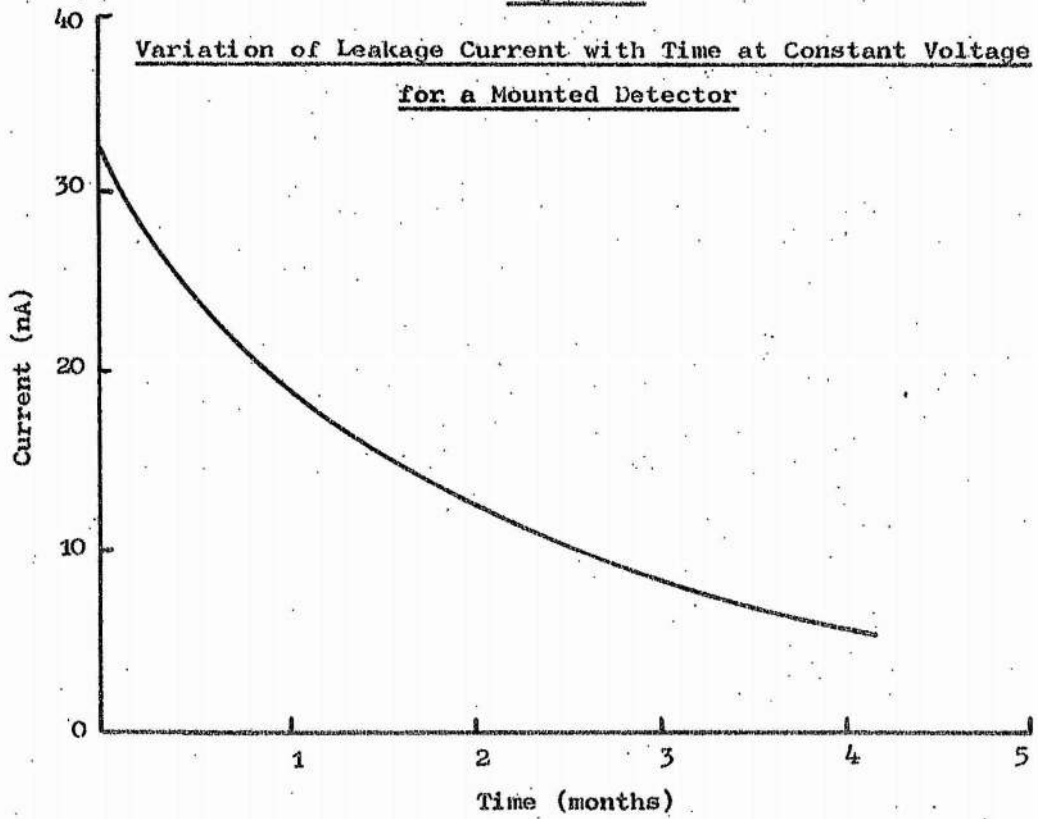
Fig. 4.19

The Change in Characteristics for a 40 cm^3 Detector from
a) 4 hours after Mounting to b) one week after Mounting

Reverse Bias Voltage
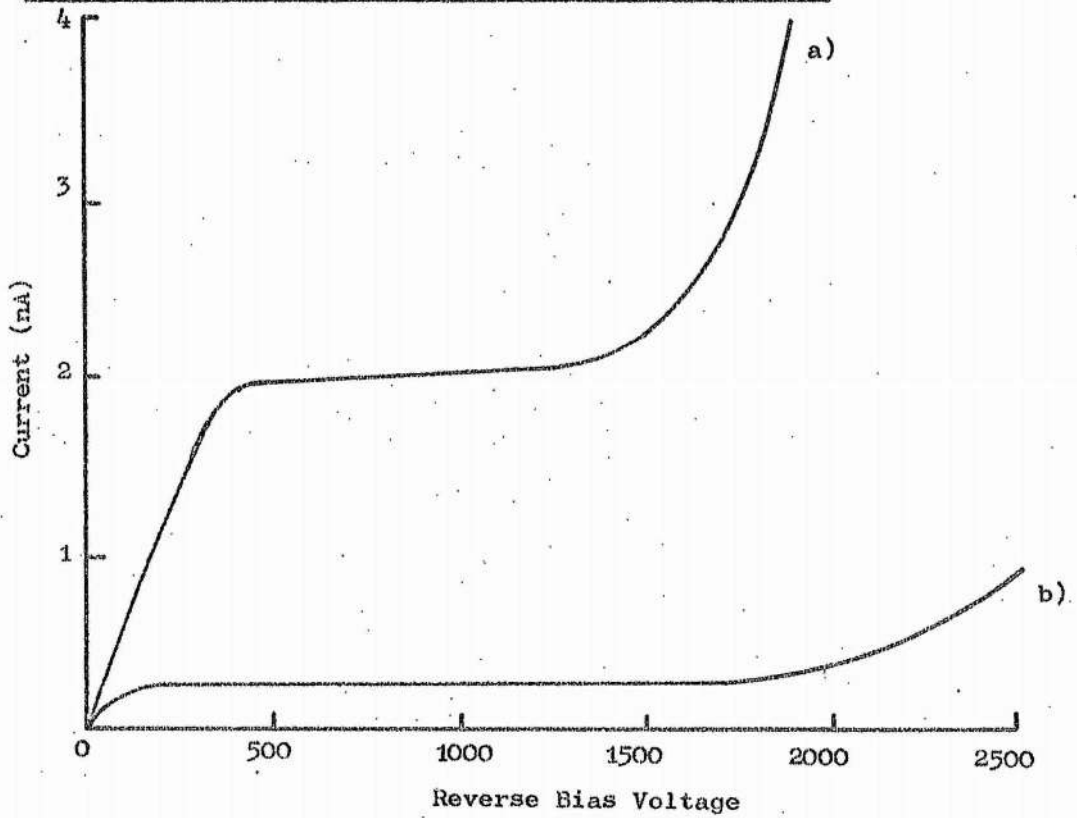
panied with a resultant degradation of vacuum. Accidental warm-ups have occurred twice in this laboratory and in each case the detector was satis-factorily recovered.

Recovery depends upon either a rapid fault diagnosis and immediate treatment, or a rapid return to liquid nitrogen temperature for an exact assessment of the damage to performance. In the first case the 0.6 cm^3 detector (described in section 4.5.3) was immediately cooled and a spectral analysis taken. The cold drift (Fig. 4.15) completely recovered its perfor-mance. In the second case, a 7.4 cm^3 detector, a short half-hour clean up was performed on the detector while it was still at room temperature. It was found on cooling that no loss of performance had occurred. It is inter-esting to note that no re-etching was necessary in either case due to the 0.6 cm^3 detector being encapsulated and the second detector being mounted in a thoroughly cleaned and outgassed cryostat.

Detector repair is possible with the diagnostic and processing techniques discussed in this chapter. Recovery is simplified considerably with the initial use of good cryostats and well etched detectors.

Chapter 5

Problems on the Efficiency of Detection of Ge(Li) Detectors

5.1 Introduction

In the early measurements on Ge(Li) detectors in this and other laboratories it has become apparent that some detectors had an efficiency smaller than that expected from their size. This is now experimentally confirmed (Walford and Doust 1969). The efficiency of a Ge(Li) detector is low compared with NaI(Tl) detectors and hence an additional efficiency reduction represents a significant counting limitation (section 6.5.4).

Monte Carlo calculations are satisfactory for NaI(Tl) detectors (Zerby 1960 and 1963, Zerby and Moran 1962 and Heath 1964) where the shape is accurately specified and the physical processes satisfactorily understood. Their use in prediction of efficiency and other parameters has now been applied to Ge(Li) detectors (Wanio and Knoll 1966; de Castro Faria and Levesque 1967; Hotz, Mathiesen and Hurley 1965) but these require accurate knowledge of the dimensions of the sensitive volume and certain assumptions about the detector material. In particular, unknown factors such as trapping and possible losses in distorted electric fields invalidate the theoretical approach. Consequently, an experimental method has been used to measure the efficiencies of a number of crystals. As only a few crystals were available in the laboratory it was necessary to co-operate with other workers to collect additional data. Further experiments with certain crystals and collimated gamma rays were then made to attempt a determination of the origin of the efficiency defect.

The efficiency of detection is a significant parameter particularly in the detection of weak activities (section 6.5.4) and merits investigation. Experiments were undertaken to measure the variation of efficiency with source volume. It is also shown that careful design in source-detector geometry can result in considerable improvement.

5.2 Efficiency Defects in Ge(Li) Detectors

Confusion often arises due to the loose definition of efficiency. In this thesis, the following definitions are used:-

1) Absolute Full Energy Peak Efficiency (ϵ_{PA}) $= \dfrac{N1}{N2}$

Where N1 = number of counts received in the full energy
peak per unit time representing energy E.

N2 = number of gamma rays of energy E emitted from
the source per unit time.

2) Intrinsic Full Energy Peak Efficiency $(\varepsilon_{px}) = \frac{N1}{I_o}$

Where I_o = number of gamma rays of energy E incident
upon the crystal per unit time.

3) Geometric Efficiency $(\varepsilon_G) = \frac{G}{4\pi}$

Where G is the solid angle subtended by the source to the
detector.

5.2.1 Relationship Between ε_{px} and Sensitive Volume

Efficiencies were measured using definition 2) to avoid as far
as possible the effects of differing detector geometries. The measurement
technique is that described in section 4.4.2 with a ^{226}Ra source placed one
metre from the detector. The source strength was 0.8 mCi and this resulted
in an adequate count rate without pulse pile-up. At this distance, the
gamma rays incident upon the detector under test could be considered to be
parallel. All crystals tested had previously undergone copper staining to
estimate their sensitive volumes.

Three factors complicate the results:-

1) Each detector was mounted in a different cryostat with its own known
window thickness. The gamma rays would also have to traverse vary-
ing dead layers of unknown thickness in the crystal. Hence, the
gamma ray beam was attenuated to an unknown extent with each detector.
At high energies this is usually insignificant, but at lower energies
such attenuation may exceed 10%.

2) In three cases the source-detector distance was less than the standard
one metre because of the design of the apparatus.

3) Some of the crystals were planar and others coaxial, so that there
was some variation in the shape and cross sectional areas of active
volumes (Table 5.1). Shape is significant for energies above
250 keV, when a significant contribution to the full energy peak is
through multiple scatter. To test the effect of shape, a trapezoidal
detector was measured from two different directions (Fig. 5.1).

Fig. 5.1

Trapezoidal Detector Measured from Two Directions to Test the Effect of Detector Shape

3.2 cm

4.1 cm

3.1 cm

γ rays in front face (direction A)

γ rays perpendicular to plane of largest cross section (direction B)
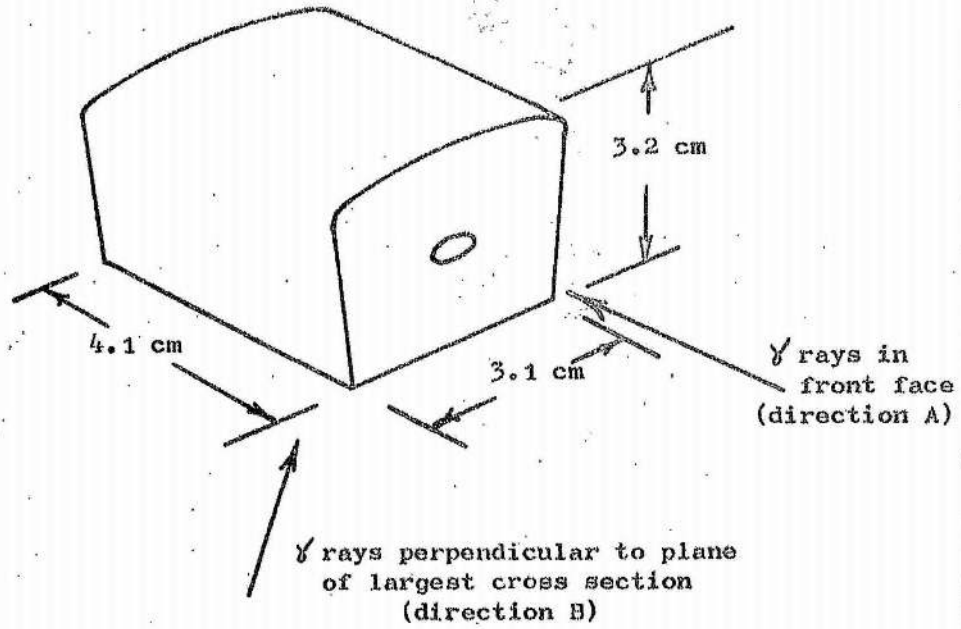
Fig. 5.2

Variation of ϵ_{PI} with Energy for the Detector Shown in Fig. 5.1

Measured for Direction A

Measured for Direction B

ϵ_{PI} (%)

Energy (MeV)
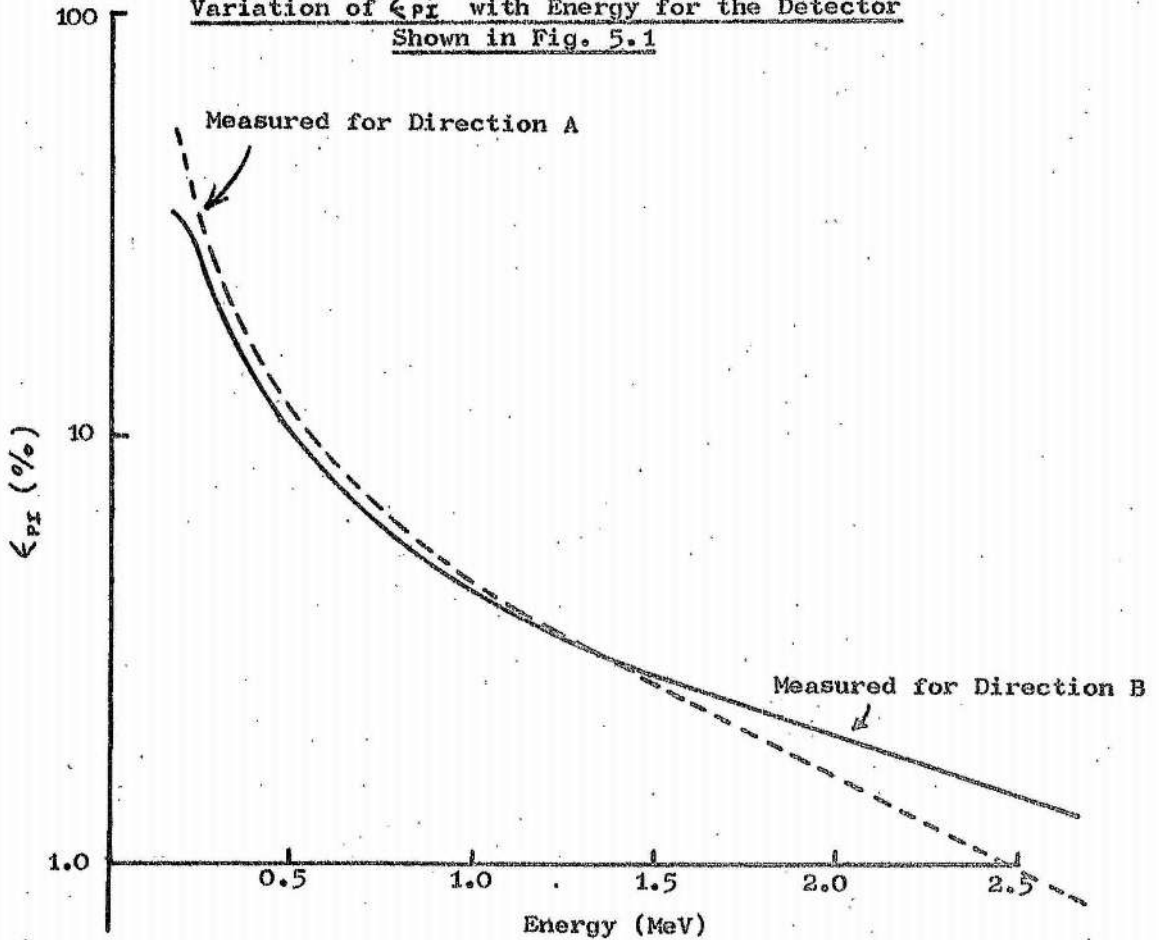
Fig. 5.2 shows the variation of ϵ_{PI} with energy for this crystal measured from the directions shown in Fig. 5.1. It will be observed that the maximum differences for the energy range shown are below 20% for this compact geometry detector, this being at the higher energy. All crystals were measured with the end face geometry shown in Fig. 5.1. However, for simplicity, differences in shape have been ignored although better correlation might have been achieved if a parameter combining shape and the volume had been plotted against the efficiency.

Nineteen crystals with sensitive volumes ranging from 0.6 cm^3 to 42 cm^3 were measured. Fig. 4.11 shows typical efficiency curves obtained with this technique. Values for ϵ_{PI} were read from each curve and tabulated for the nineteen crystals (Table 5.1). The table also shows the estimated active volume, shape and the energy resolution. Figs. 5.3a and 5.3b show the variation of efficiency with volume at 2.0 MeV and 1.0 MeV for all the crystals measured. It will be observed from these figures and Table 5.1 that those detectors with resolutions better than 5.5 keV have the highest efficiencies. There is agreement among the higher resolution crystals, but the detectors with poorer resolutions fall considerably below the lines. Fig. 5.4 shows the variation of ϵ_{PI} with sensitive volume for the high resolution detectors.

The following observations are made on the above results:-

1) The higher resolution detectors (5.5 keV and better) have a high degree of correlation between volume and efficiency.

2) All the poorer resolution detectors have lower efficiencies compared to those with higher resolutions. The magnitude of the reduction varies from detector to detector. The maximum reduction of efficiency observed was for a 23 cm^3 detector having one quarter that expected for a good detector. The minimum reduction observed was for a 34 cm^3 crystal having roughly half the expected efficiency. All poor detectors had losses varying between these limits.

3) In Fig. 5.4 the curves for high energy radiation can plausibly be extrapolated to go through the origin. However, for lower energies, extrapolation through the origin necessitates a change in curvature. It is notable that a linear extrapolation would

Table 5.1

ϵ_{PI} for all Detectors at Several Energies

Estimated Sensitive Volume (cm^3)	Shape	Energy Resolution (keV)	ϵ_{PI} % (0.5 MeV)	ϵ_{PI} % (1.0 MeV)	ϵ_{PI} % (1.5 MeV)	ϵ_{PI} % (2.0 MeV)	ϵ_{PI} % (2.5 MeV)
0.6	circular planar	4.0	0.70	0.17	0.072	0.037	0.019
1.4	rectangular planar	7.0	2.10	0.44	0.20	0.125	0.08
1.5	square planar	9.0	1.22	0.31	0.165	0.094	0.55
5.2	circular planar	5.0	2.35	0.68	0.37	0.24	0.185
7.4	trapezoidal planar	4.5	3.40	1.10	0.62	0.41	0.285
8.2	trapezoidal planar	8.0	3.15	0.99	0.58	0.38	0.25
10.0	trapezoidal coaxial	5.5	4.5	1.57	0.99	0.69	0.48
20.5	trapezoidal coaxial	5.0	7.6	2.8	1.65	1.20	0.97
23.0	cylindrical coaxial	7.0	2.85	0.97	0.56	0.39	0.30
23.0	cylindrical coaxial	5.0	9.5	3.0	1.7	1.15	0.88

Table 5.1 (cont.)

25.0	cylindrical coaxial*	8.5	9.2	3.4	2.1	1.35	1.2
25.0	cylindrical coaxial	2.5	9.6	3.80	2.20	1.70	1.11
26.0	cylindrical coaxial	4.0	9.7	3.85	2.45	1.78	1.25
28.0	trapezoidal coaxial	15.0	3.7	1.43	0.82	0.54	0.41
30.0	cylindrical coaxial	5.5	11.5	4.60	2.90	2.20	1.75
33.0	trapezoidal coaxial**	3.6	12.1	4.95	3.23	2.40	1.75
34.0	cylindrical coaxial***	5.0	7.6	2.90	1.79	1.39	1.22
37.0	trapezoidal coaxial	7.5	5.20	2.05	1.25	0.92	0.69
41.7	trapezoidal coaxial	10.0	6.20	2.45	1.45	1.02	0.78

* Resolution due to poor electronics

** Detector shown in Fig. 5.1

*** Unavoidable use of thick perspex absorber in system

94

Fig. 5.3a

Variation of ϵ_{px} with Sensitive Volume at 2.0 MeV for all the Measured Detectors

Estimated Sensitive Volume (cm^3)
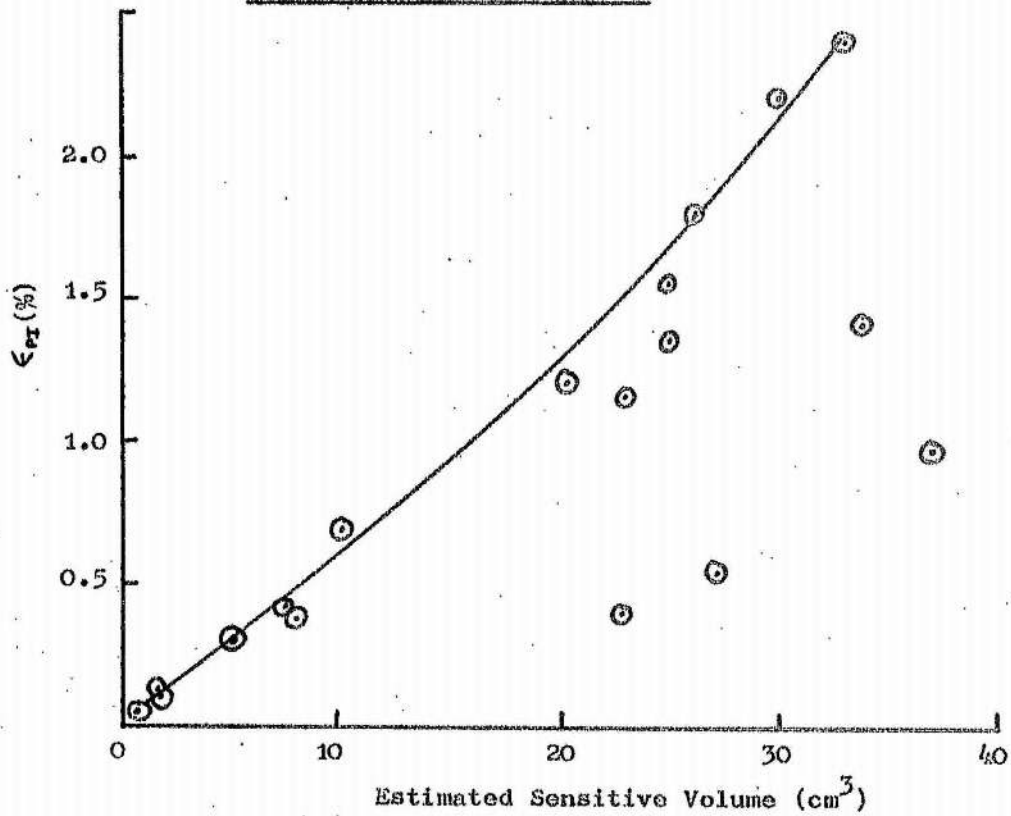
Fig. 5.3b

Variation of ϵ_{px} with Sensitive Volume at 1.0 MeV for all the Measured Detectors

Estimated Sensitive Volume (cm^3)
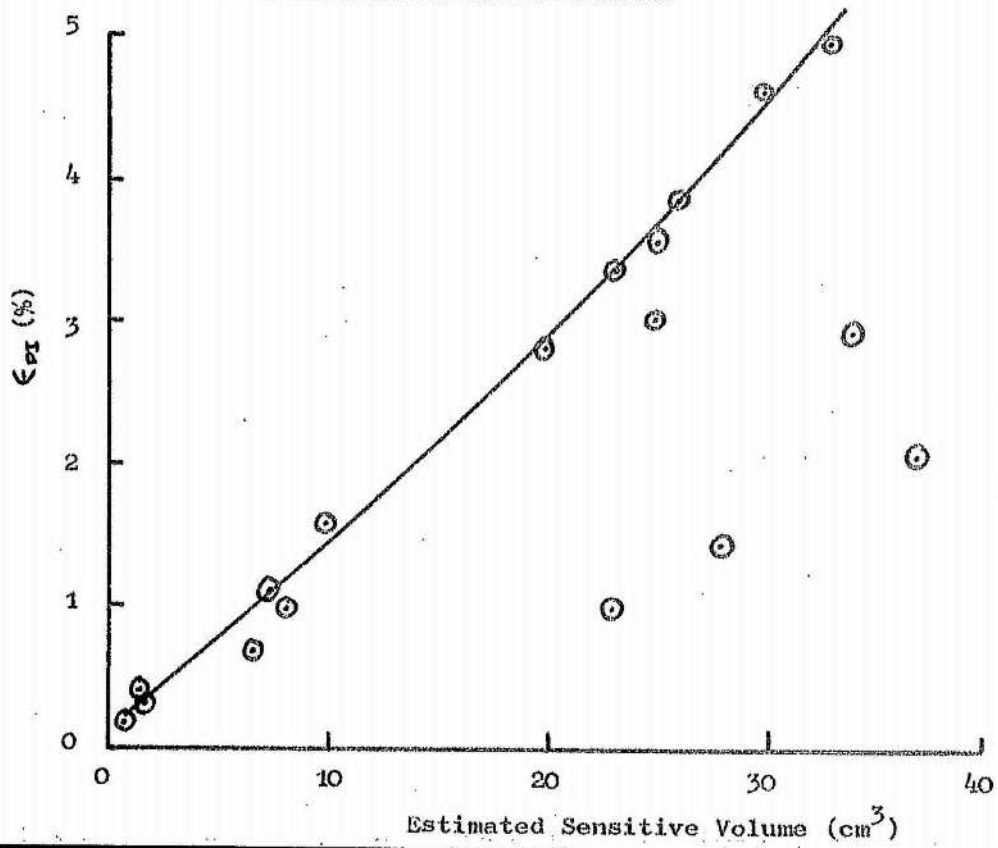
Fig. 5.4

Variation of ϵ_{pr} with Sensitive Volume at Different Energies
for the Higher Resolution Detectors
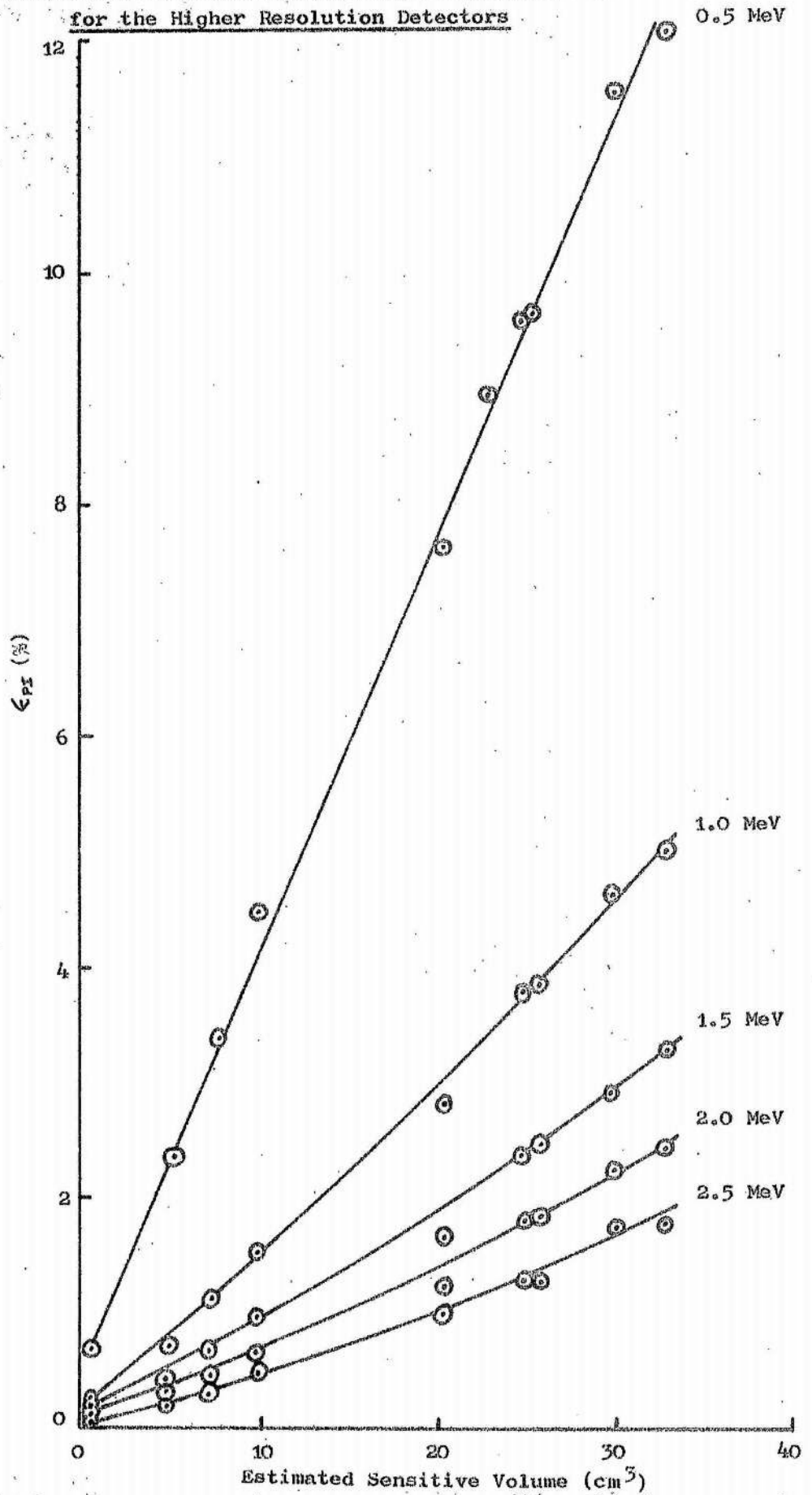
intercept the efficiency axis and not the volume axis as might
be expected.   The phenomenon is energy dependant and therefore
probably a function of photon range in germanium.

The explanation may lie with the relation between the amount of
multiple scattering and crystal size.   Above 250 keV a significant contri-
bution to the full energy peak is that due to multiple scattering.   For a
particular energy, there is a mean path length of the scattered gamma rays
for total absorption to be likely.   At low energies, this path length is
small (about 1 - 2 mm at 200 keV incident energy) so that as the crystal
size decreases below 0.5 cm^3 there is still a significant contribution from
multiple scattering to the full energy peak.   For crystals with dimensions
shorter than this mean path length the full energy peak height is small,
because of the absence of multiple scatter.   At high energies the path
lengths for multiple scatter increase and becomes greater than 10 mm at
several MeV so that the minimum volume for a significant contribution to
the full energy peak increases with increasing energy.   Hence the sharp
curving to the origin below 0.5 cm^3 decreases with increasing energy (Fig.5.4).

5.2.2   Factors Relevant to a Reduced Efficiency of Detection

Several factors contribute to the reduction of efficiency in a
detector.   Design and technique considerations may reduce them but not
eliminate them.

5.2.2.1   Insensitive Layers on the Detector

Insensitive material on a Ge(Li) detector is unavoidable due to
the necessary presence of the n and p layers.   Their effect, however, can
be minimised in two ways:-

1) If possible, the source-detector arrangement is designed to allow
    incident photons to enter directly into sensitive material.

2) The detector geometry can be fabricated so that the p layer (or
    core) is as thin as possible.   Lithium is diffused into the det-
    ector very carefully during fabrication to maintain the n layer
    thickness at about 0.5 mm or less.

Fig. 5.5 shows the variation of half value layer (H.V.L.) of germanium with
energy.   NaI(Tl) is also shown for comparison.   Any interaction in the
insensitive layer will remove a potential event from the full energy peak.
A scatter continuum is also added to the spectrum.   Fig. 5.6 shows the

Fig. 5.5

Variation of H.V.L. for Germanium and Sodium Iodide
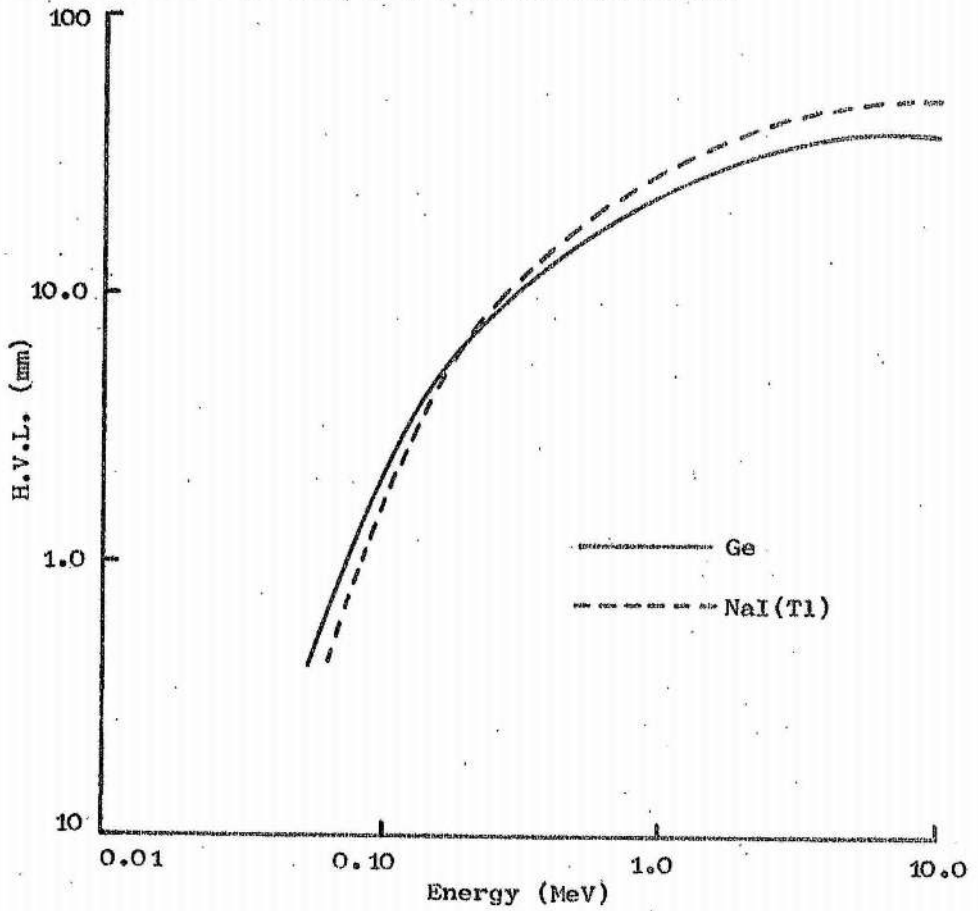
Fig. 5.6

Peak Efficiency Loss for Varying Thickness Insensitive Layers
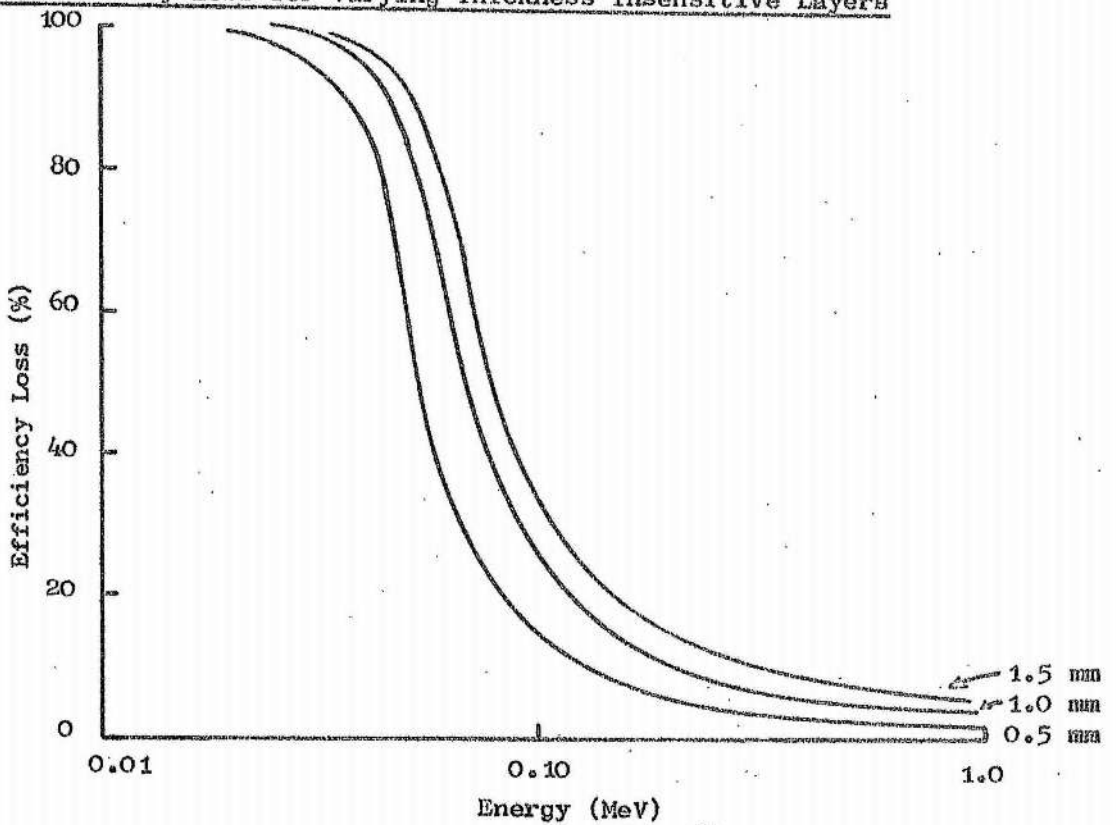
variation of full energy peak efficiency loss with energy for three thick-
ness dead layers.   Large sensitivity losses at lower energies are observed.

These losses can be reduced by grinding away or drifting through
the p layer.   The p layer is then re-established either by ion implantation
of boron or gallium (Dearnaley 1969) or by gold plating a thin surface
barrier contact of the order of 0.5 microns (Nuclear Enterprises).

5.2.2.2   The Optimum Detector Shape

A qualitative treatment is attempted due to the complexity of an
exact mathematical approach.

It is important to specify the source-detector geometry.   If this
is not possible, due to a wide range of shapes and orientations to be en-
countered, then a compact detector is required to present the maximum depth
of sensitive material to all possible source positions.

Shape effects are very sensitive to gamma energy since the propor-
tions of the various interactions change rapidly with energy.   For simpli-
city, parallel beam irradiation is considered.   Energy loss from the detec-
tor through bremsstrahlung is significant above 2 MeV (Camp 1967) but negli-
gible in the region where photoelectric interactions predominate.   Only a
few millimetres of germanium are required to absorb the energy from the
energetic electron.

Compton scatter events dominate in the region 0.5 - 2.0 MeV and
are the origin of the multiple scatter contribution of full energy peaks.
Wainio and Knoll (1966) have deduced that on average there are one to two
Compton collisions in these total absorption events.   On this assumption,
a simple estimate of optimum detector shape is made.   Photons are scattered
at calculable angles and energies (Davisson and Evans 1951).   Fig. 5.7
shows the angular distribution of the scattered photon as a function of
incident photon energy.   Consideration of Fig. 5.5 and Fig. 5.7 allows a
determination of the half value layer (H.V.L.) with angle for germanium
(Fig. 5.8).   Fig. 5.9 shows a coaxial detector with Compton interactions
occurring in the detector surface.   This detector is fitted onto the shape
of Fig. 5.8 with the dimensions 2r and h maintained in the same proportion.
An increase of the detector size in the same proportions will reduce surface
escape.   The ratio of $2r/h$ (=R) is energy dependant (Fig. 5.10) and reaches
a maximum of $2r \sim 0.7h$.

Fig. 5.7

The Variation of Energy with Angle of Scatter for Several Incident Energies
(Each Curve Normalised for Comparison)
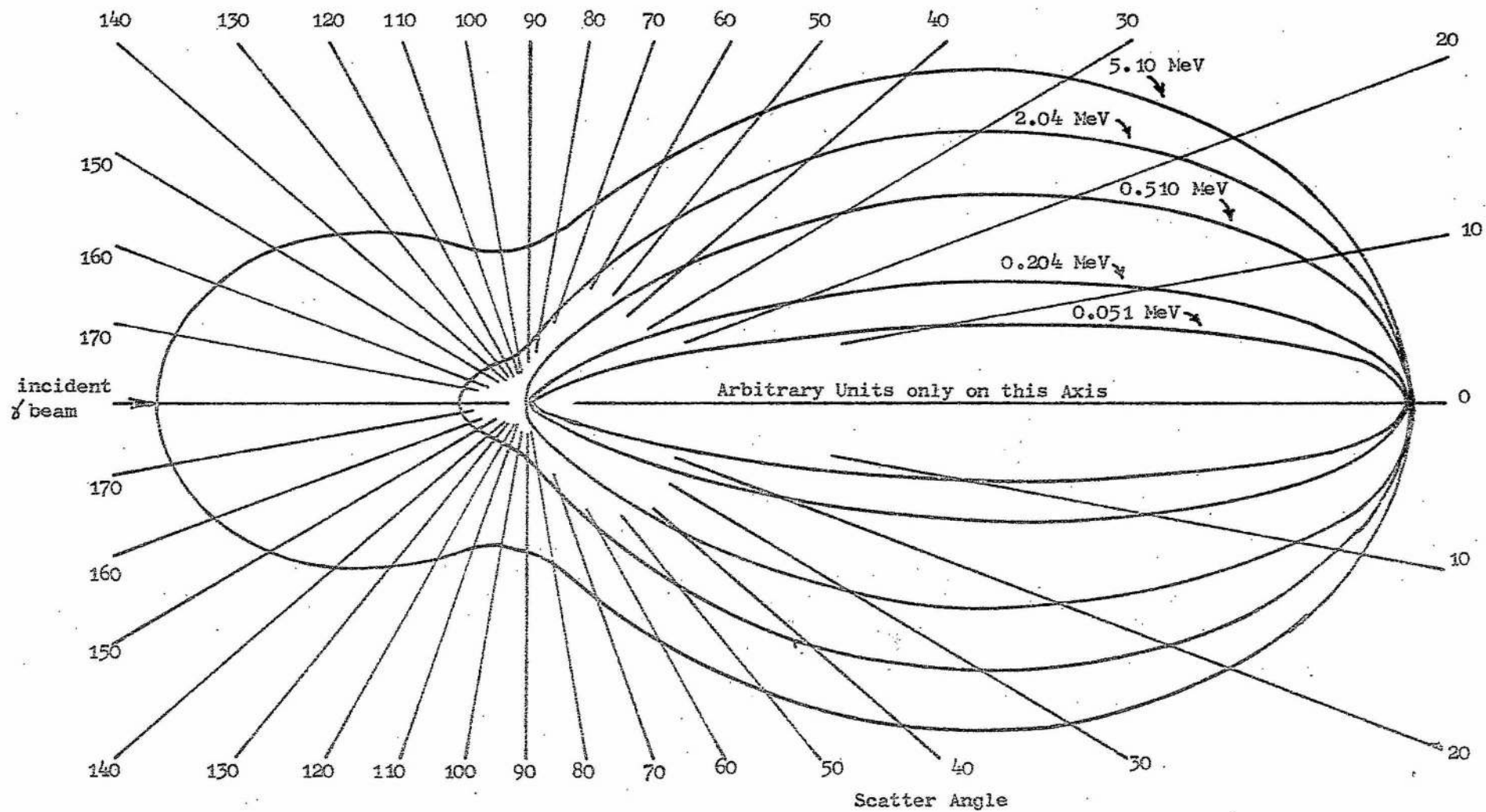
Fig. 5.8

The Variation of H.V.L. (of Germanium) with Scatter Angle Shown for 510 keV incident Energy

h (16 mm at 510 keV)

incident γ
beam (510 keV)

101
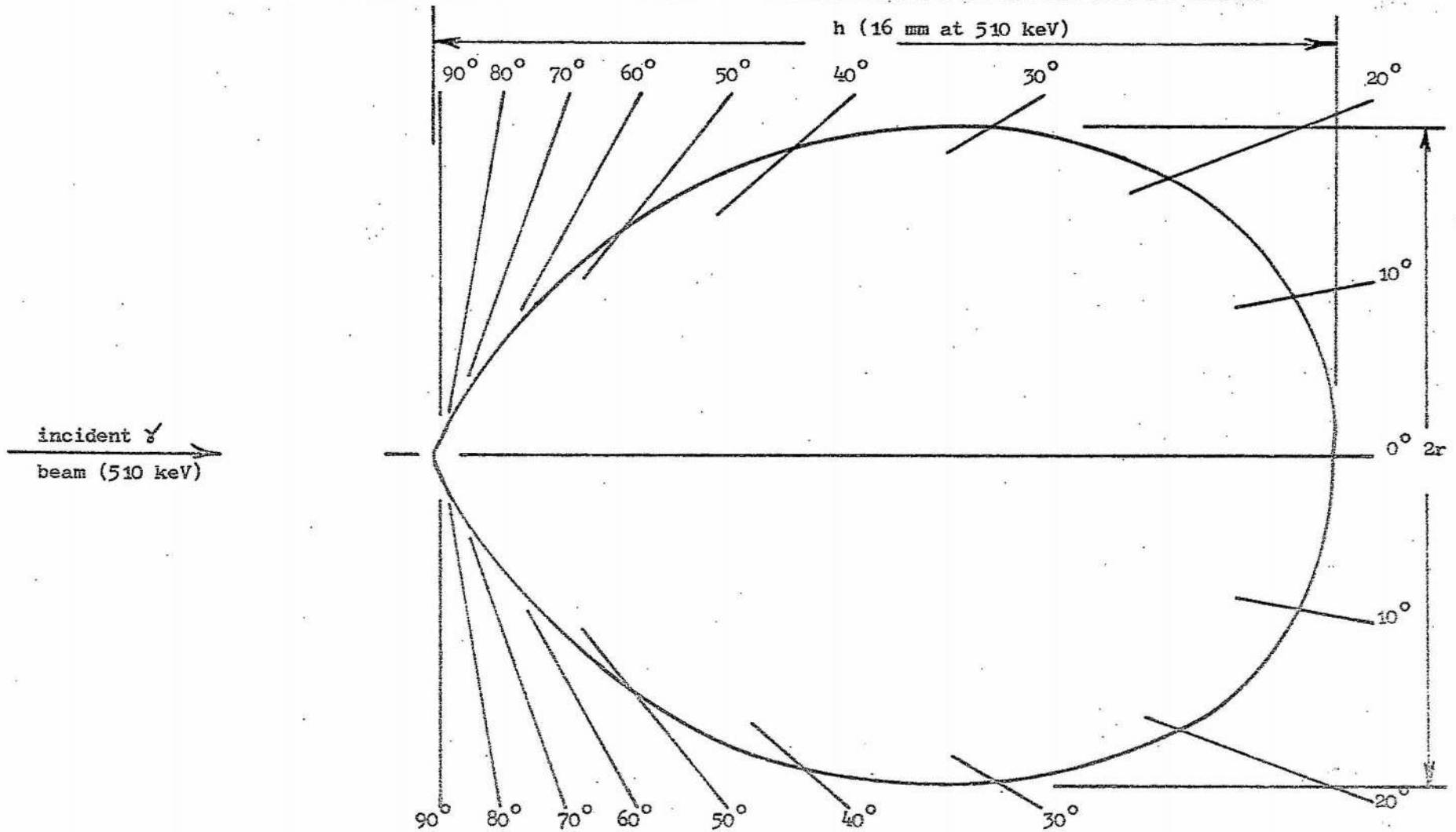
Fig. 5.9

Cylindrical Coaxial Detector Fitted onto the Shape in Fig. 5.8 Extended to Allow for Edge Loss

$$\frac{2r}{h} = R = \frac{2r'}{h'}$$

Fig. 5.10

The Variation of 2r, h and R with Energy
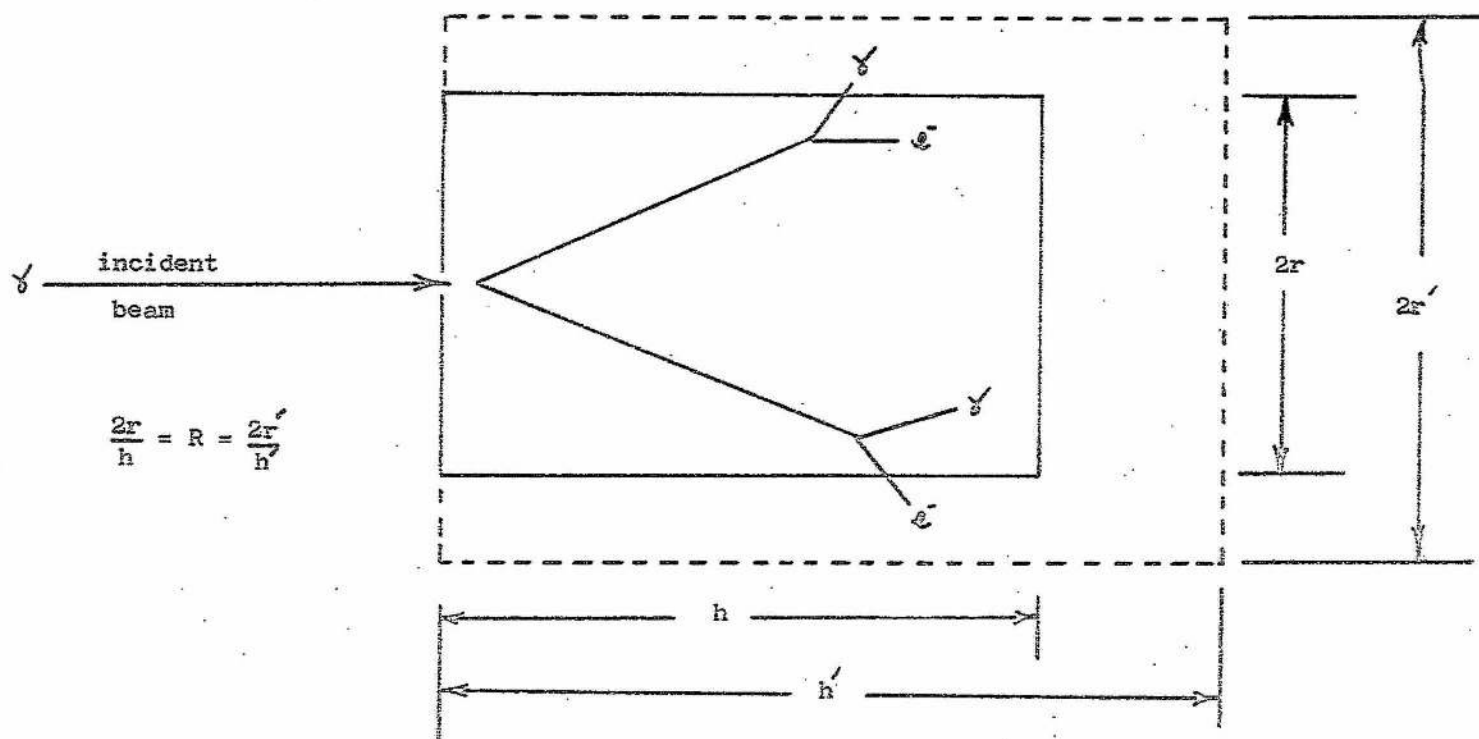
Fig. 5.10
The Variation of 2r, h and R with Energy
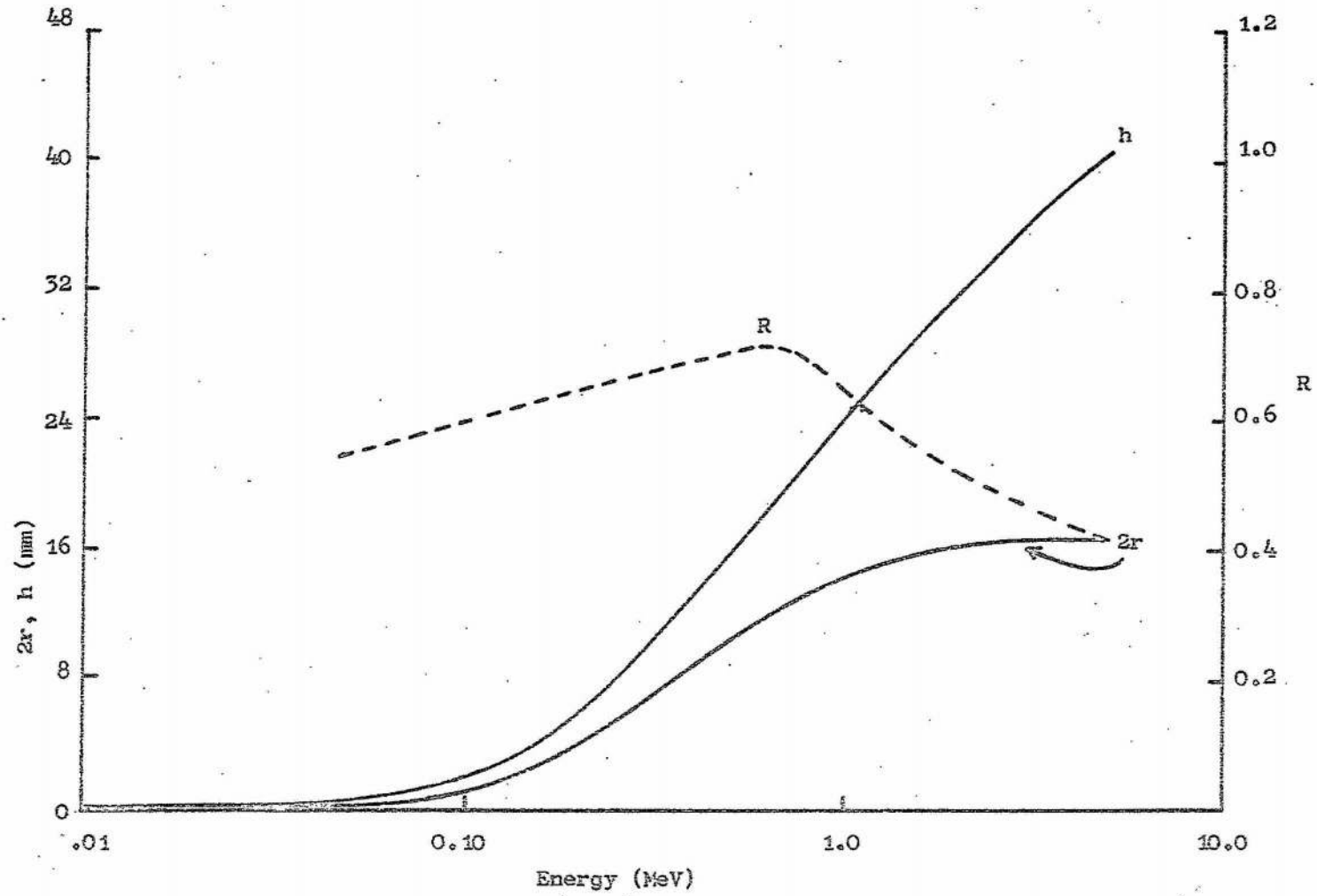
Pair production events only contribute to the full energy peak by total absorption of the annihilation quanta. As their orientation is random with respect to the orientation of the incident gamma ray, absorption is optimised by the smallest surface area to volume ratio (a sphere). In practical terms, this is approached by a cylinder whose diameter and length are equal.

The above considerations indicate that many of the requirements are fulfilled by a coaxial detector whose length and diameter are equal.

5.2.2.3 Collection in the Sensitive Volume

Charge loss is significant in the consideration of the efficiency defects shown in section 5.2.1. It is considered in two parts, namely that due to a uniform distribution of traps and that due to a non-uniform distribution of traps.

5.2.2.3.1 The Origin and Effect of Uniform Trap Distributions

The mechanism of trapping has been briefly considered in section 1.3.3 and its origin and structure in sections 1.3.3 and 4.2.1. The major uniform and uniformly varying trap distributions generally originate from poor compensation, caused by poor drift conditions. This is frequently accompanied by a poor collecting electric field. Therefore, such trap distributions are a function of drift direction and are uniformly distributed (neglecting material defects) parallel to the n layer in planar and true coaxial detectors.

It is difficult to obtain an accurate and direct measure of the degree of compensation. The final detector characteristics are sometimes the most sensitive means of measuring compensation variations (Lopes Da Silva, Henck and Siffert 1968, Schell 1970). The variation of ϵ_{PI} with reverse bias is an effective test of compensation in that poor collection rapidly becomes evident below 100V mm^{-1} reverse bias by a rapidly falling ϵ_{PI}. Fig. 5.11 shows typical results for the 7.4 cm^3 detector, this being an average performance detector.

Measurement of the electric field across a detector is also indicative of the degree of compensation. The field may be simply measured using the arrangement shown in Fig. 5.12. The electric field profile expected for a perfect planar detector is uniform across the intrinsic region. Poenaru (1967) has calculated that for a coaxial detector with perfect compen-

Fig. 5.11

The Variation of ϵ_{px} with Reverse Bias for the 7.4 cm^3 Detector
(9mm Drift Depth)

Energy Resolution

Leakage Current

ϵ_{px} (1.17 MeV)

ϵ_{px} (1.33 MeV)

Reverse Bias (Volts)
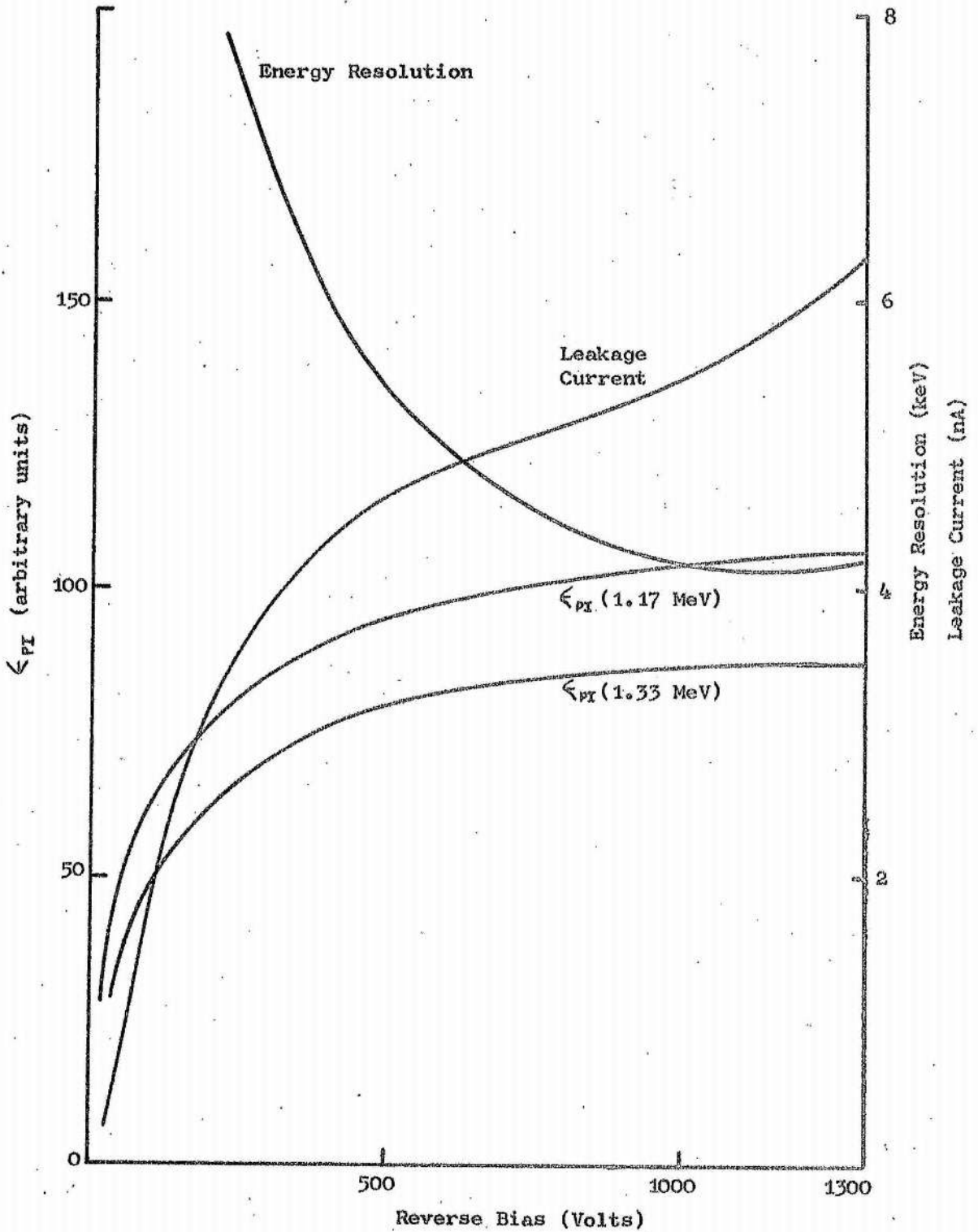
sation, the electric field $\mathcal{E}$ (r) varies as the radius (r) where

$$\mathcal{E}_{(r)} = \frac{V_a}{r_i \, \ln\left(\frac{r_e}{r_i}\right)} \cdot \frac{r_i}{r}$$

and V_a = detector bias

r_i = p core radius

r_e = external radius

There is a similar field variation for trapezoidal and cylindrical geometries. As a demonstration of field measurement, the electric field was measured for a 30 cm^3 trapezoidal detector. Fig. 5.13 shows the variation observed compared with that expected for perfect compensation. Poorly fabricated coaxial detectors tend to have excess lithium towards the n layer and this results in the poor field of Fig. 5.13. This results in the formation of poor collection regions towards the n layer.

5.2.2.3.2 Origins and Effects of Non-uniform Trap Distributions

Anomolous performance variations with the position of irradiation were first observed in this laboratory in 1967 and by Chartrand and Malm (1967) and were considered by Gibbons (1968) as potentially significant in the evaluation of the efficiency defect. Armantrout (1969, 1970), Schmidt-Whitley (1969), Cappellani, Ostidich and Restelli (1970) and Henck, Gutknecht, Siffert, De Laet and Schoenmaekers (1970) have also observed regions of poor response in Ge(Li) detectors but have not satisfactorily explained these findings.

Schell and Nienhuis (1968), Cappellani and Restelli (1968) and Armantrout (1969) have observed that certain impurities form clusters in the crystal lattice. The clusters are not necessarily associated with dislocations or vacancies (Armantrout 1970). These impurity and defect clusters are probably the origin of the anomolous variations considered above.

These clusters are difficult to compensate and result in regions of excess trapping. This may be brought about in two ways.

1) The impurity generated traps are in sufficient strength in the drifted regions to absorb most of the generated ion pairs formed in or passing through the cluster.

2) The cluster remains uncompensated due to the degradation of the lithium mobility by the impurities. Fig. 5.14 shows a proposed model for the formation of this region. The region remains essentially uncompensated as the lithium drift front proceeds

Fig. 5.12

Schematic Arrangement of the Voltage Probe

Used for Measuring the Detector Electric Field

D.C. Volts

0   ÷Ve

Detector Axis

Freon at -20°C

(V)

p ←———— i ————————→

n

1.0

Curve expected for
perfect compensation

0.8

0.6

measured field for
trapezoidal detector

0.4

0.2

0.0

Fields Normalised to 1.0

12   10   8   6   4   2   0

Depth in Detector (mm)
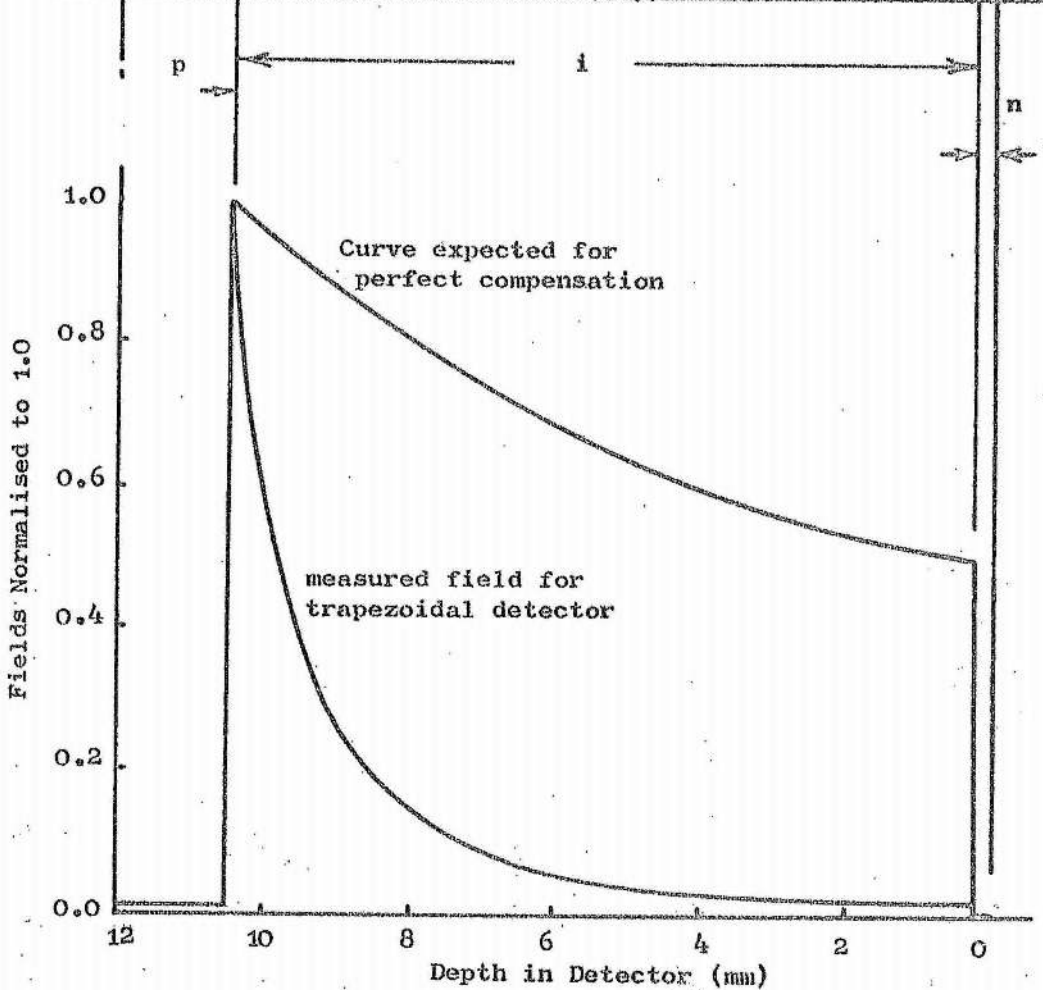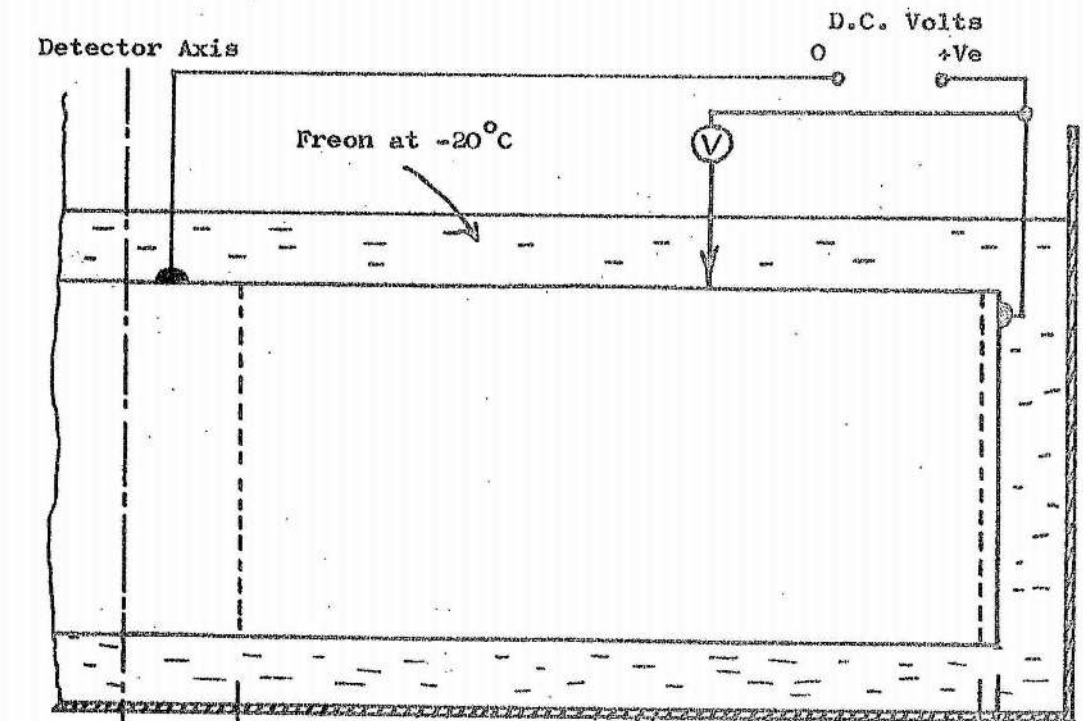
Fig. 5.13

The Measured Electric Field Across a Coaxial Detector

Fig. 5.14

Proposed Model of the Formation of Insensitive Regions

in the Detector
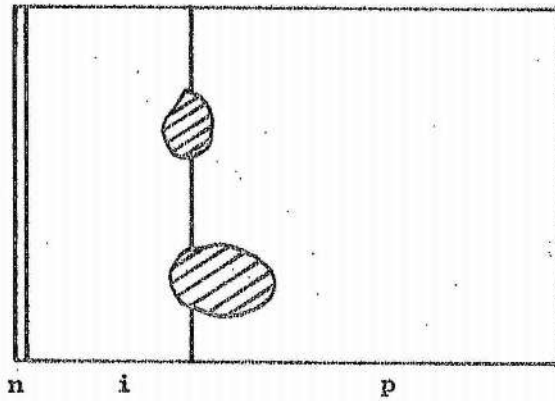
1) Drift front passing the impurity cluster in the germanium
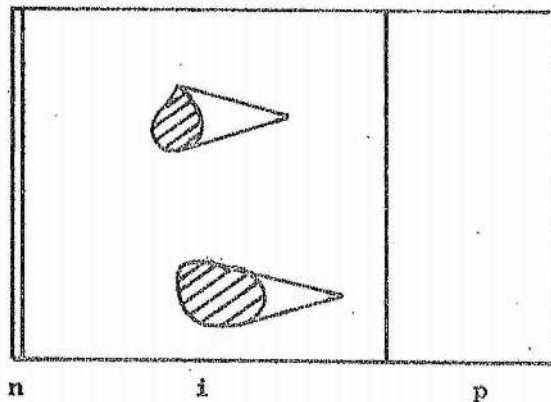
2) Drift nearly complete and cluster shadows formed
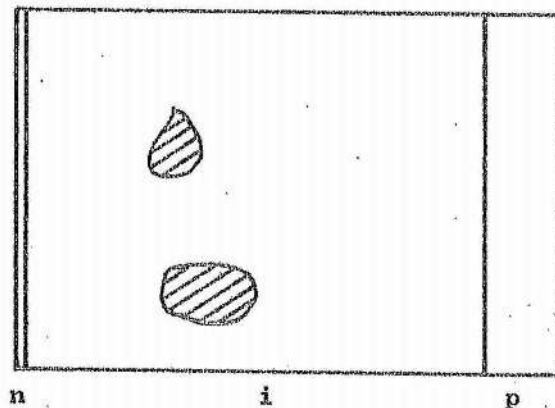
3) Shadows removed after cold drifting leaving inactive regions in the intrinsic region

through the crystal.   Precipitated lithium (and hence
additional trapping) is added to each cluster.   "Shadows"
of uncompensated germanium are left behind which may be
removed by cold drifting.   The final cluster formation is
relatively unaffected by drifting and is considered as
inherent to the detector characteristics.   Recently, Walford
(1971) has directly observed the formation of such a region
in a large planar detector.   Poor collecting fields and
local field distortions accompany the defect cluster.

Some gamma rays will undergo total collection, while others, interacting
near the cluster, will lose a considerable portion of energy.   The overall
effect is a detector with a small $\xi_{\rho I}$ and not necessarily showing peak
assymmetry.   The regions, being inherent to the germanium ingot as opposed
to drift defects are independant of drift direction and may be considered
to be randomly situated in the detector volume.

5.2.2.3.3   Experimental Observations with Collimated Gamma Ray Beams

Multiple scatter events in the detector degrade the spatial
resolution of a collimated gamma ray beam.   To overcome this Dearnaley (1969)
suggested the use of a highly collimated proton beam with energies up to
200 MeV.   The region responding would then be little greater than the
particle beam diameter.   However, this facility was not available and a
collimated gamma ray beam using ^{137}Cs as described in section 4.3.4.2 was
used.

Typical detector responses may be expected to reflect a combination
of the effects of section 5.2.2.3.1 and 5.2.2.3.2.   Fig. 4.7 shows a scan
of the 7.4 cm^3 detector, scanned with the beam perpendicular to the n layer.
The response variations are due to edge losses and trapping variations
independant of the drift direction.

Fig. 5.15 shows a scan taken of a 20 cm^3 poor quality trapezoidal
coaxial detector.   The observed variations are considerable both radially
and parallel to the detector axis.   There is difficulty in observing the
position of the p core.   This detector had been ineffectively cold drifted
and had undergone some precipitation.   The detector was reprocessed by
heating to 380°C for 20 minutes and then redrifted according to the tech-
niques discussed in section 4.5.4.   Fig. 5.16 shows the scan taken of this
detector after treatment.   The response is considerably improved and is

Fig. 5.15

Gamma Ray Scan of the 20 cm^3 Detector before Treatment

counts/min in ^{137}Cs peak

400

200

0

γ beam direction

2.5 mm steps

2.5 mm steps

detector axis

0

3.4 cms

3.0 cms

2.3 cms
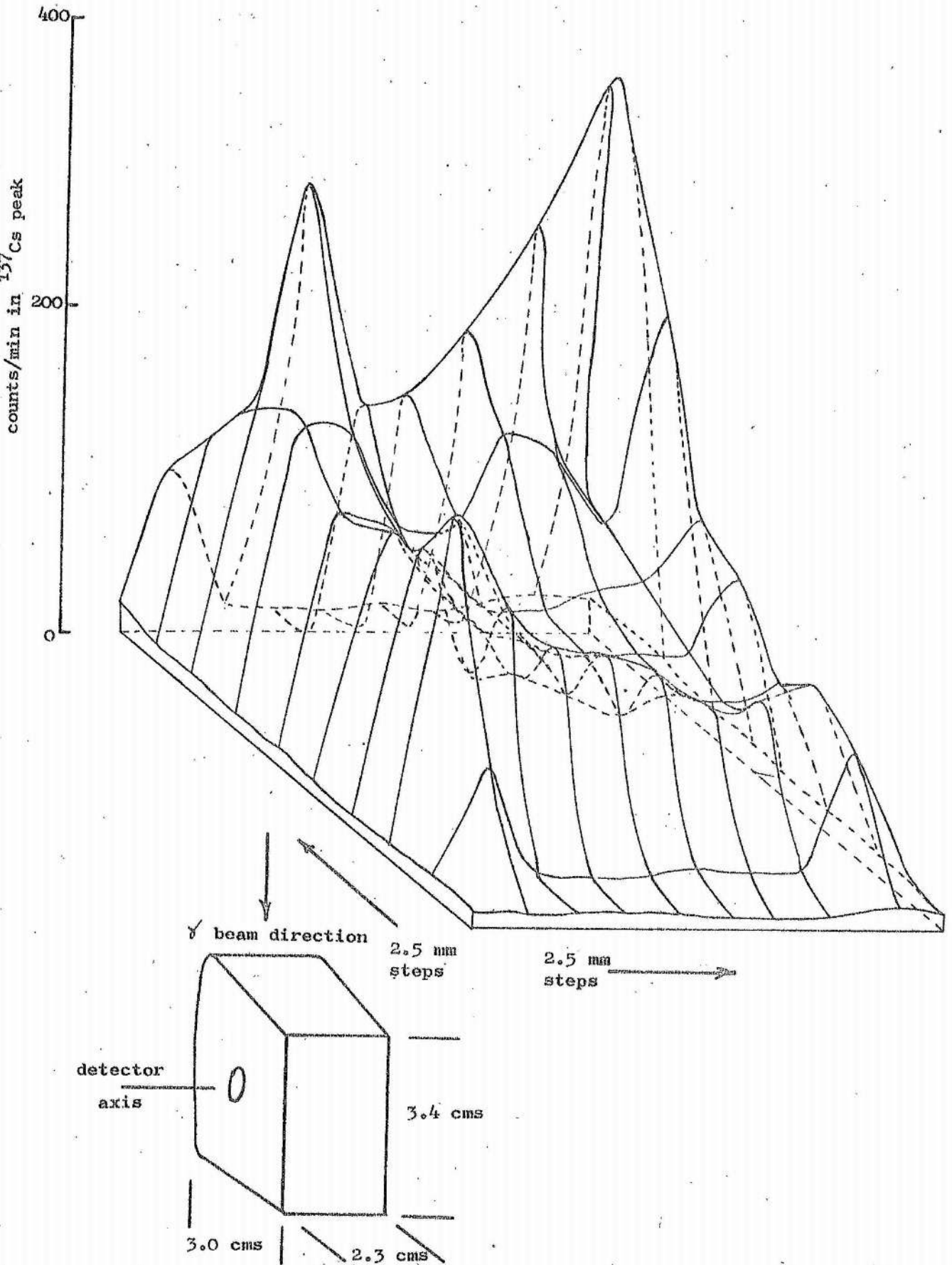
Fig. 5.16

Gamma Ray Scan of the 20 cm^3 Detector after Treatment

1000

counts/min in ^{137}Cs peak

500

scan orientation as
for Fig. 5.15

2.5 mm scan intervals
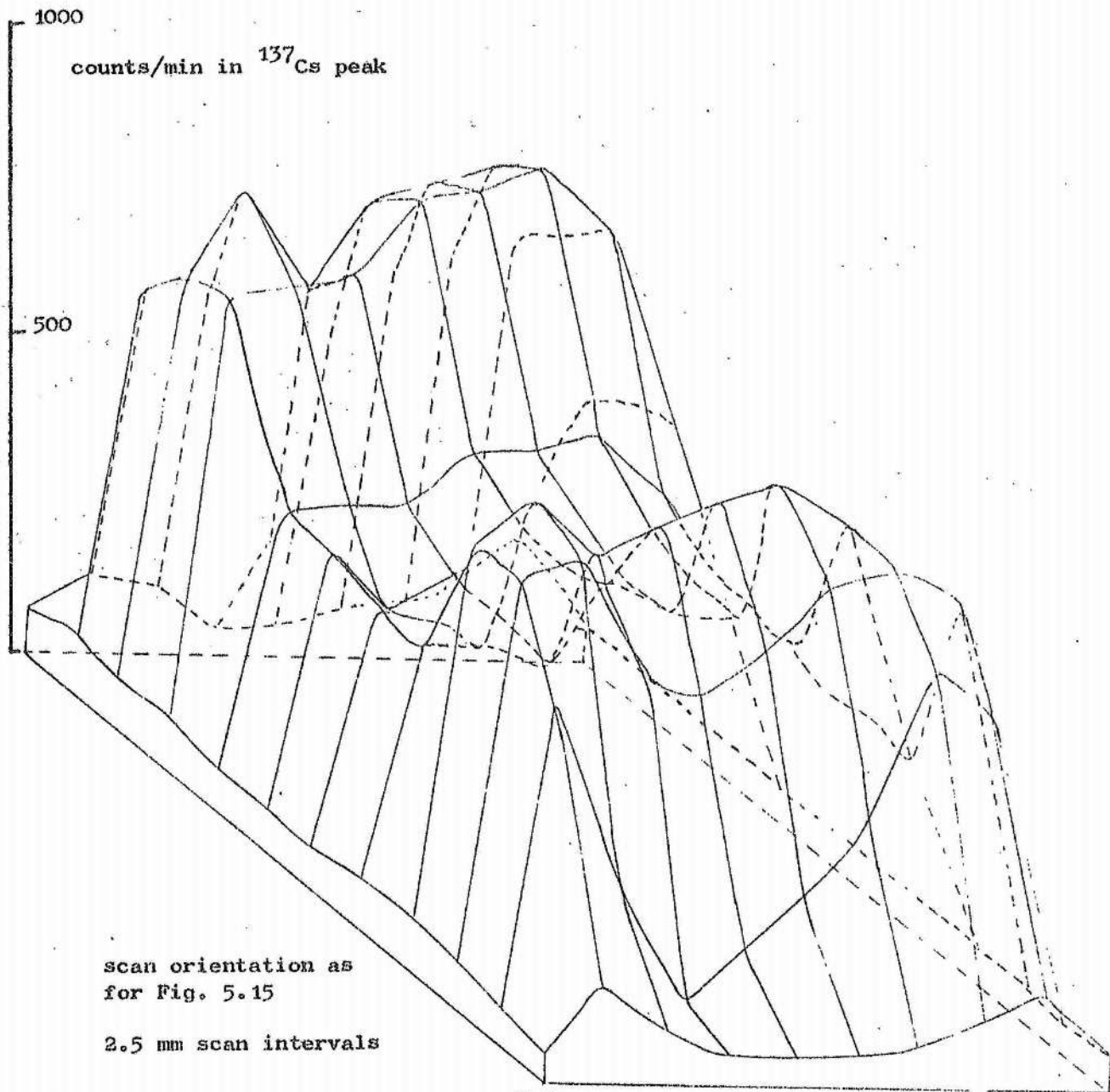
more uniform over the drifted volume (measured by copper staining).
Fig. 5.17 shows the improvement observed in ϵ_{pI}. These curves were
compared with the data of Fig. 5.4 to give the dotted curve of ϵ_{pI} expected
for a good quality detector.

Fig. 5.18 shows the comparison of the cross-section scans for a
particular plane from Fig. 5.15 and 5.16. In addition to the improved
radial response and uniformity, the detector is much more sensitive near
the n layer. Compensation is considerably improved and reference to Fig.
5.13 shows that the material near the n layer is most sensitive to drift
defects.

The response variations parallel to the detector axis are still
considerable, though to a lesser extent and reflect the contours of Fig.
5.15. These non-uniformities are due to preferential precipitation regions,
whose effects are reduced by the detector reprocessing.

This detector suffers from drift and material defects though the
material effects are capable of being minimised by careful processing.

These results are illustrative of the variations observable in
Ge(Li) detectors. The efficiency defect considered in section 5.2.1 may
be accounted for by the above results.

Previous measurements on Ge(Li) detectors have assumed that
drifted and sensitive volume contours coincide. Fig. 5.18 illustrates
that this is not necessarily so. Large efficiency defects are always
possible as the fine degree of compensation attempted in the cold drift is
difficult to judge and is very sensitive to fabrication technique and the
condition of the starting material.

5.3 Variation of the $\epsilon_{p\beta}$ with Source Volume

Once a detector has been optimised as far as possible in the
cryostat, any change in the measured peak efficiency is due to variation
of ϵ_g. This requires some consideration as large improvements in ϵ_g
can be obtained by careful system design (Kemmer 1968). In practice, a
wide range of source volumes are encountered. Their measurement is con-
sidered in two groups, namely small ($\sim 1 - 2 \, cm^3$) and large volumes.

5.3.1 Optimisation of $\epsilon_{p\beta}$ for Small Volume Sources

Many measurements (such as those in this laboratory) are made

Fig. 5.17

$\in_{PI}$ Measured for the 20 cm^3 Detector before and after Treatment

$\in_{PI}$ expected for
a good quality
detector

after
treatment

before
treatment

Energy (MeV)
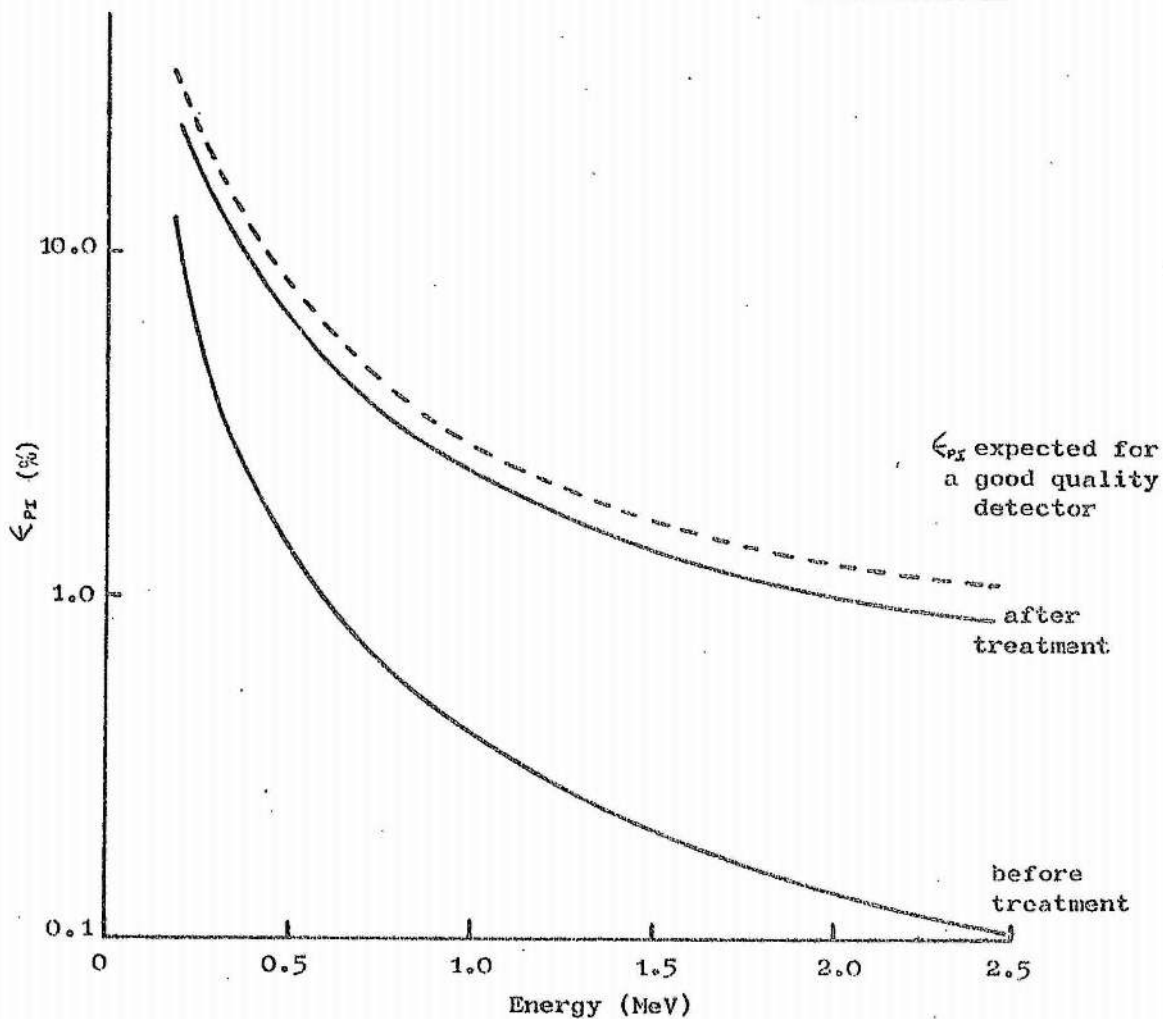
Fig. 5.18

Comparison of the Scan Cross Sections from Figs. 5.15 and 5.16

copper stained
dimensions

Distance in Detector (mm)
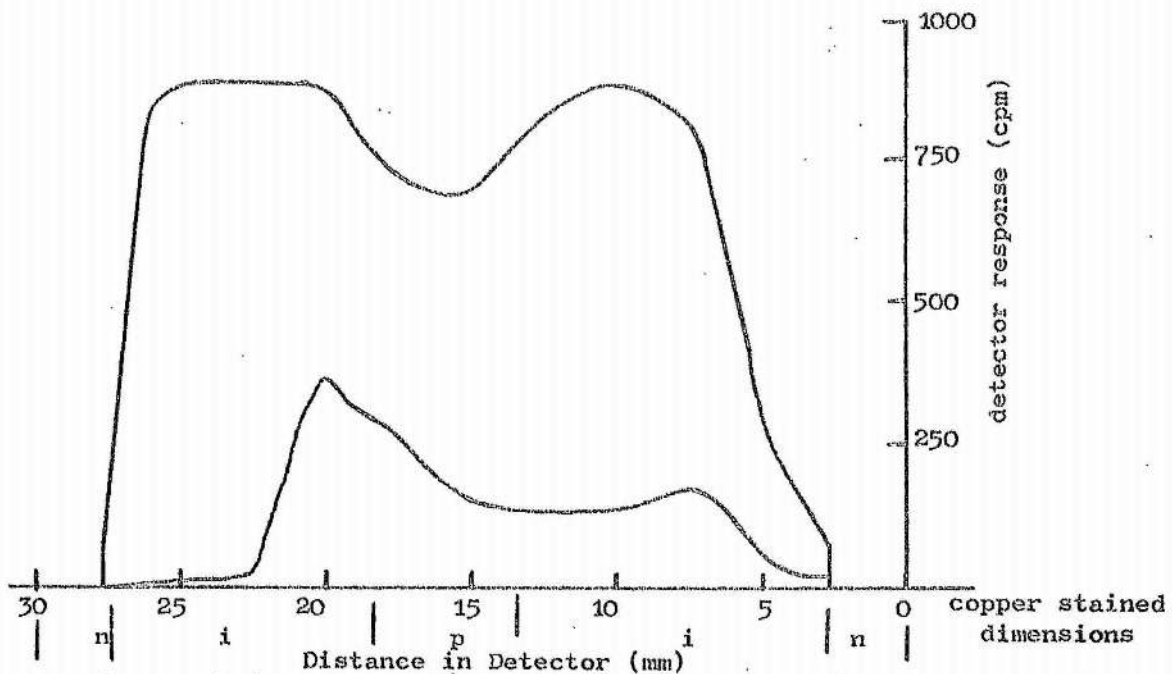
with small sources placed against the cryostat end window. Kemmer (1968) has developed a well-shaped detector allowing suitable insertion of small sources to give $\leqslant g \geqslant 0.5$. Since then, the design has been optimised by Santhanam, Webb and Monaro (1969), Glasgow (1970), Forcinal and Meuleman (1970) and Verplanke and Verheijke (1970) who have made systems capable of accepting sources up to 8 mm diameter and with detector dead layers of the order of 5 microns.

The detector used by Kemmer (1968) has similar overall character-istics to the 7.4 cm^3 detector used in this laboratory. However, his well crystal has a value of 0.012 for $\leqslant_{p\Lambda}$ for ^{137}Cs whereas the value for the 7.4 cm^3 detector is .0008, a factor of 15 lower. Clearly, when the source shape and size permits the use of this design, its value in low level count-ing (Glasgow 1970) is considerable.

5.3.2   The Measurement of Large Volume Sources

There are many common applications where large volume sources are available (e.g. contamination monitoring of milk and other foods, Potter, McIntyre and Pomery 1968). Sample reduction, by ashing and other techniques, may be used to improve $\leqslant_{p\Lambda}$ but is not always feasible and results in the destruction of the sample. This section evaluates the variation of $\leqslant_{p\Lambda}$ when measuring large volume sources.

This measurement is complicated by the great variation of detector shapes commonly encountered, so that no standard geometry is available. However, as a demonstration of the effect on a medium size detector, an experiment was performed using the 7.4 cm^3 volume detector.

A liquid source containing 0.50 μCi of ^{134}Cs and 0.50 μCi of ^{60}Co of 0.5 ml volume was manufactured. An absolute efficiency calibration was performed using energies and intensities from Lederer, Hollander and Perlman (1967) with the source placed just by the cryostat end window. The source was diluted with distilled water to form sources of increasing volume sur-rounding the detector. Fig. 5.19 shows the arrangement adopted. The distances marked were kept identical in an attempt to maintain a near optimum and uniform geometry. The absolute full energy peak efficiency was measured at each successive dilution and plotted in Fig. 5.20. Fig. 5.21 shows the measured variation of $\leqslant_{p\Lambda}$ with volume for different energies.

The following observations are made from Fig. 5.20 and Fig. 5.21:-

Fig. 5.19

Schematic Diagram of the Arrangement Used for
Measurement of Large Volume Sources
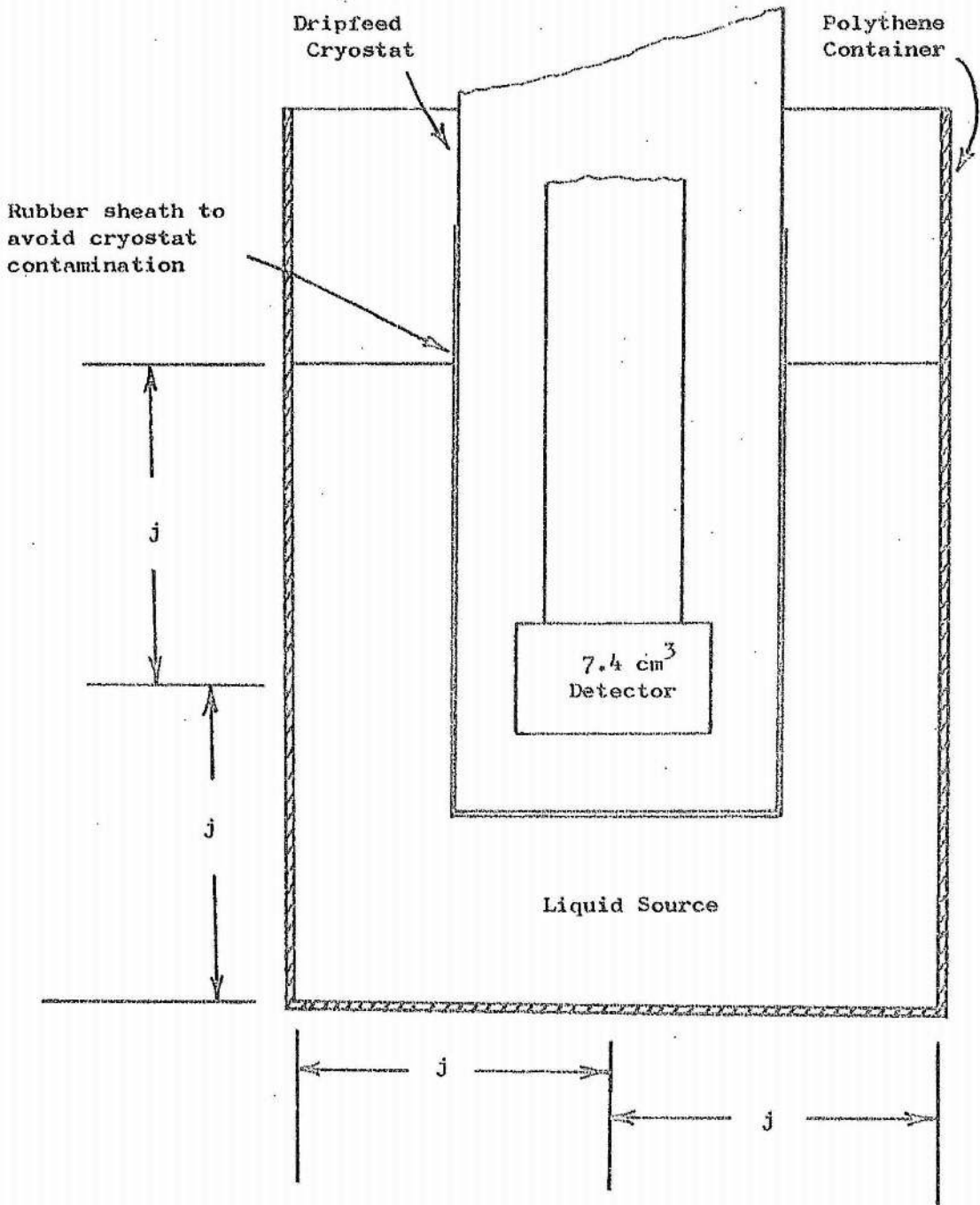
Fig. 5.20

The Variation of $\leqslant_{PA}$ with Energy for Differing Source Volumes
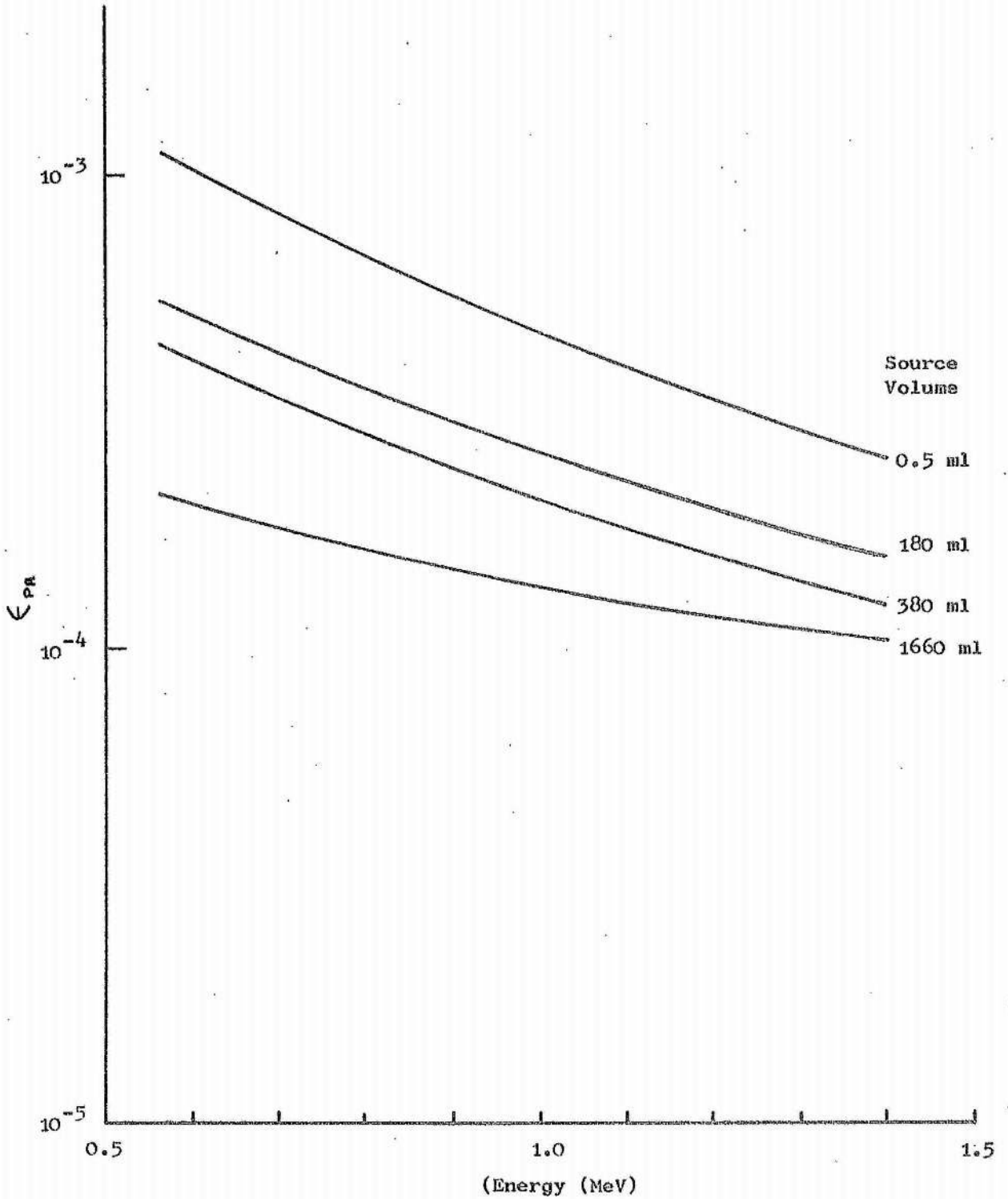
Fig. 5.21

Variation of ϵ_{PA} with Source Volume for Different Energies
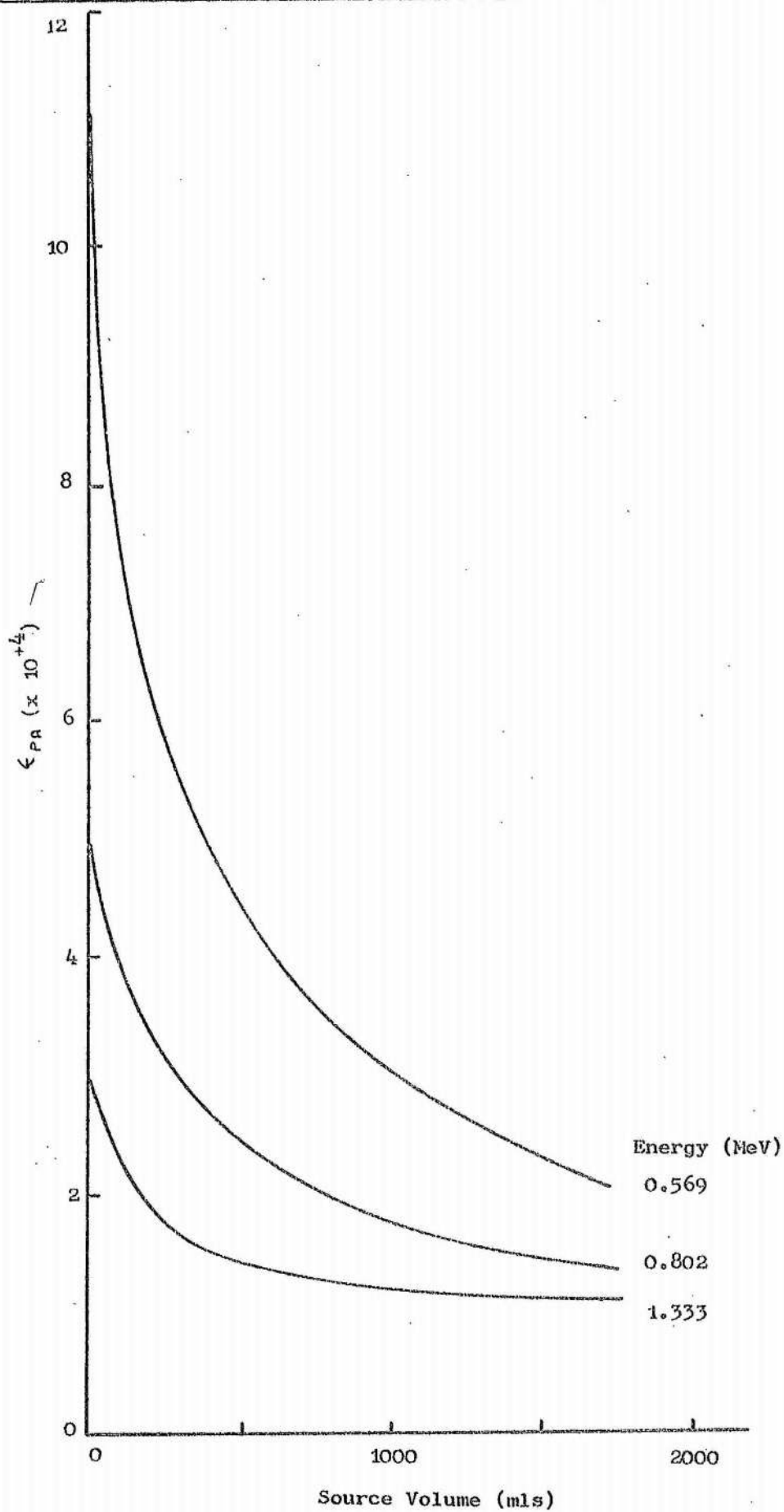
Source Volume (mls)

Fig. 5.22

Increase in Peak Counts with Source Volume,
Assuming a Constant Activity per Unit Volume
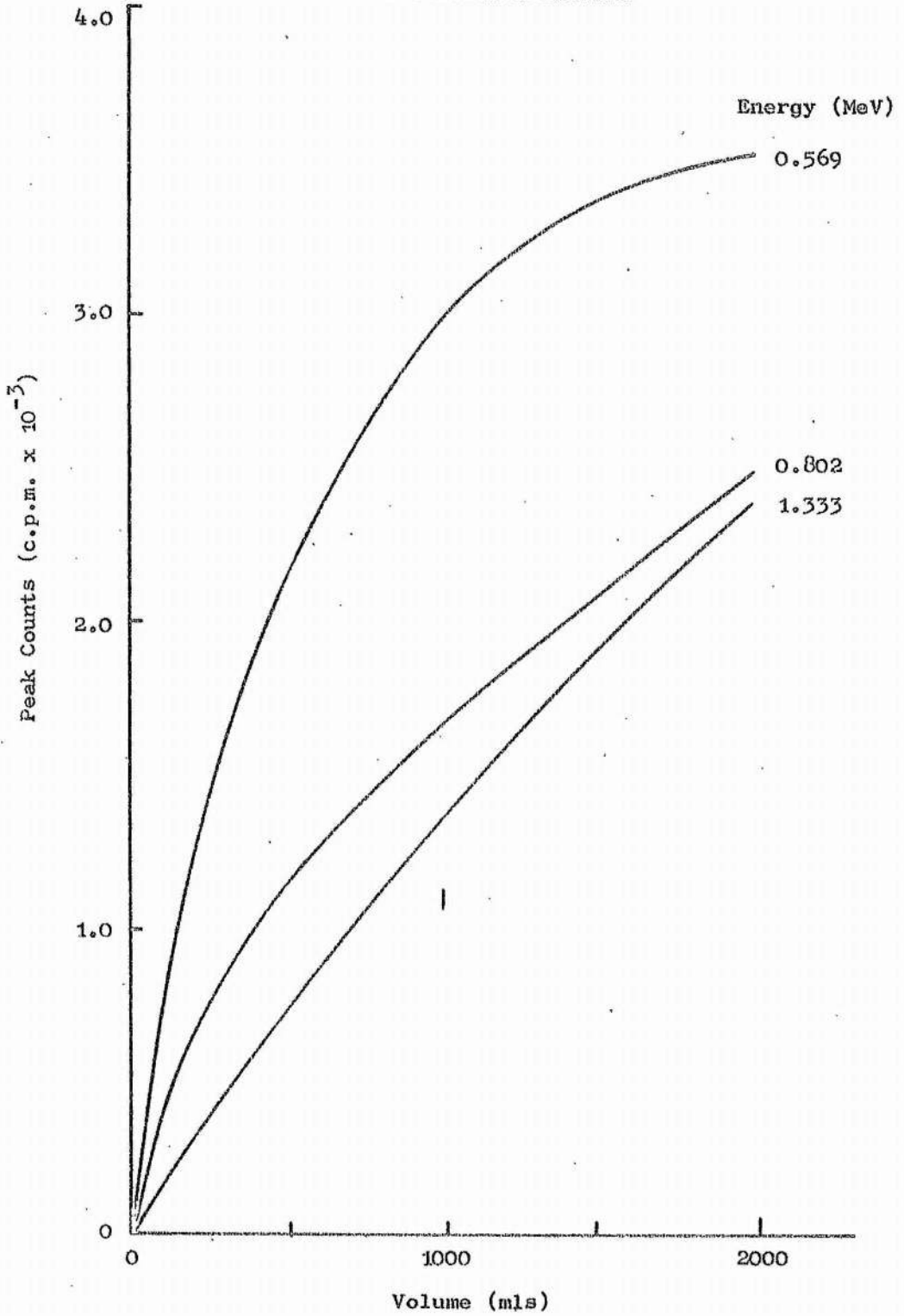
1) Self absorption in the source causes a stronger variation of efficiency with volume for the lower energies.

2) Because of self absorption, the efficiency vs energy curve (Fig. 5.20) becomes flatter with larger volumes.

If the liquid source surrounding the detector were of a fixed activity per unit volume, the full energy peak count rate would increase with increasing source volume. Fig. 5.22 shows the relative increase calculated from the data of Fig. 5.21. The rate of increase in peak count rate diminishes with increasing source volume due to the poorer geometry and greater self absorption. In this instance there is little point in exceeding a source volume of two litres due to the diminishing return obtained.

In general, the optimum volume of source is dependant upon the source material, the energy of interest, material inhomogenieties and detector size. The above data illustrates the behaviour of this particular counting configuration for the measurement of liquid sources.

Chapter 6

Determination of the Sensitivity Limits of a
Ge(Li) Gamma Ray Spectrometer

6.1 Introduction

In spite of the widespread use of Ge(Li) spectrometers over the
last few years, their low level counting capabilities have remained largely
unexplored. The studies attempted to date are limited in their basic
assumption and application in several respects. Werner (1966) sets arbitary
confidence limits on the minimum detectable peak area. Pauly, Buzzi, Girardi
and Borella (1966) use a similar approach and in addition rely on the measure-
ment of symmetric peaks. Cooper (1970) has used a similar approach to that
in this thesis, but restricts its precision and application by neglecting
peak fitting errors and using the one peak measurement technique. The tech-
nique developed in this chapter allows any peak measurement technique, any
preset precision and accounts for errors in the peak fitting technique used.

The expression derived for the sensitivity limit allows the pre-
diction of the low level counting capabilities of Ge(Li) spectrometers and
an evaluation of their parameters.

There are several methods available for measuring the peak area.
In this chapter, a projection technique is developed and used to demonstrate
sensitivity limit calculations.

6.2 Definition of the Sensitivity Limit of Ge(Li) Spectrometers

There are two definitions, with fundamentally different uses, of
the sensitivity limit which are not distinguished in the published literature.
These are defined as follows:-

1) For any given experiment, a certain minimum precision is required.
   The sensitivity limit is reached (minimum acceptable activity)
   when it is just possible to obtain the desired precision in a
   given count time. It is quite possible that due to the required
   precision, the peak may still be quite clear above the background
   continuum.

2) The minimum detectable activity is reached when it is just possible
   to distinguish and measure the peak area in question above the back-
   ground continuum. In this case the resulting statistical precision
   is out of the control of the experimenter.

Both definitions are evaluated using the same definition of statistical precision. This is defined as C,

where $C = \dfrac{\text{standard deviation of peak area}}{\text{peak area}} = \dfrac{\sigma_b}{D}$ 6.1

If B = background counts under the peak accumulated in a time T

and S = measured peak plus background counts accumulated in a time T

then S = B + D

Ignoring any systematic errors, equation 6.1 is rewritten as

$$C = \frac{(S + B)^{\frac{1}{2}}}{D} = \frac{(S + B)^{\frac{1}{2}}}{S - B} \qquad \dots\dots\dots 6.2$$

B is measured indirectly and allowance must be made for the additional variance (σ_w^2) incurred by the estimation of B from statistically varying data. Equation 6.2 is hence rewritten as

$$C = \frac{(S + B + \sigma_w^2)^{\frac{1}{2}}}{D} \qquad \dots\dots\dots 6.3$$

The minimum detectable activity is determined by putting $C \sim \frac{1}{3}$ (section 6.4.2). This may be considered as the limiting case of the minimum acceptable activity and hence C can assume all values less than $\frac{1}{3}$.

6.2.1 Under Stable Conditions

Assuming a high stability spectrometer, the peak counts measured over a time T is

$$D = \frac{1}{C} (S + B + \sigma_w^2)^{\frac{1}{2}} \; counts \qquad \text{from equation 6.3}$$

and when the desired value of C is just obtained for the peak

then $J \, \mathcal{D}_{min} = \dfrac{1}{CT} (S + B + \sigma_w^2)^{\frac{1}{2}}$ counts per minute

From the definition of absolute efficiency (ϵ_{PA}) in section 5.2 the sensitivity limit in gamma rays emitted from the source per minute is Λ_E where

$$A_E = \frac{1}{\epsilon_{PA} C T} \left(S + B + \sigma_w^2 \right)^{\frac{1}{2}} \qquad \text{gamma rays per min.} \quad \dots\dots\dots 6.4$$

where suffix E dontes energy dependance.

It is useful to determine Λ_E for a given background continuum by a direct measurement of B, energy resolution and ϵ_{PA}. Hence substituting for S in equation 6.4 from 6.3 we obtain

$$\Lambda_E = \frac{1}{\epsilon_{PA} C T}\left(2B + \frac{1}{2C^2} + \sigma_w^2 + \frac{1}{2C}\left(\frac{1}{C^2} + 8B + 4\sigma_w^2\right)^{\frac{1}{2}}\right)^{\frac{1}{2}} \quad \ldots\ldots\ldots 6.5 \quad *$$

Equation 6.5 may be used to predetermine a minimum acceptable or detectable activity for a given spectrometer, provided that the parameters remain constant or calculable with and without the source in position. B is determined by measuring those counts that fall in the peak base region of interest in a prior test on the spectrometer with no source present.

If R_E = energy resolution of the spectrometer at energy E then the peak base width in channels = $\qquad$ $\ldots\ldots\ldots 6.6$

where v = ratio of peak base width to R_E

$$\frac{v R_E}{d}$$

d = keV per channel

This peak base width is used in calculating the value of B in equation 6.5.

In certain circumstances, the peak base width is a function of the background counts and peak to background ratio (Pauly et. al. 1966). This is because the peak edges are more easily confused with the background continuum as the magnitude of the continuum increases (table 6.3). This effect should be allowed for in the use of equation 6.5 and by the particular peak fitting technique used.

6.2.2 The Influence of Gain Shift

This is a frequent occurrence during spectral measurement and has the effect of broadening the peak with resultant degradation of C and Λ_E. The degradation occurs through the increased background continuum included under the peak, and possible difficulties in defining the edges of the peak.

The effect has widely varying consequences, depending upon the uniformity of gain drift, rate of drift and the imminence of other peaks and discontinuities. As a demonstration of the effect, a simple uniform drift rate is assumed for a peak situated upon a uniformly varying continuum.

Let the channel shift of the peak be k channels during the count time T. The increase in B to be accounted for is B' where

$$B' = \left(k + \frac{v R_E}{d}\right) b T \qquad \ldots\ldots\ldots 6.7$$

b = background count rate in counts/channel/min.

* using the positive term in the quadratic solution only

This results in an increase in the value of σ_w^2 to $\sigma_w'^2$ the extent of which is dependant upon the particular measurement technique used.

Substituting equation 6.7 into equation 6.5 gives the modified value A_E' where

$$A_E' = \frac{1}{\epsilon_{PM} C T}\left(2\left[k + \frac{v R_E}{d}\right]bT + \frac{1}{2C^2} + \sigma_w'^2 + \frac{1}{2C}\left(\frac{1}{C^2} + 8\left[k + \frac{v R_E}{d}\right]bT + 4\sigma_w'^2\right)^{1/2}\right)^{1/2} \quad \text{---6.8}$$

The quantity A_E' varies approximately as the square root of the peak shift in high background counting conditions. For this case, the effect is similar to the broadening of resolution considered in section 6.5.1.

6.3 Spectrum Measurement Technique

Several techniques are available for analysis of spectral information. These are divided into the analysis of the complete energy spectrum and the analysis of the full energy peak.

6.3.1 Measurement of the Total Spectrum

Analysis based upon the total spectrum can allow the maximum information to be obtained about the source. The common technique employed is that of stripping from the spectrum the spectral response expected for a monoenergetic gamma ray normalised to the energy and intensity of each observable full energy peak. Shafroth (1967) has considered this in some detail for NaI(Tl) spectrometers and similar techniques have been considered for Ge(Li) spectrometers, in particular by Helmer, Metcalf, Heath and Gazier (1964), Heath (1966), Helmer, Heath, Schmittroth, Jayne and Wagner (1967) and Barnes (1968). These strippings are effected most commonly using least squares techniques. The method is satisfactory when most of the spectrum is source generated and the natural background contribution is small. Difficulties are encountered though when the spectrum is dominated by natural background events for then there is little advantage to be gained. As the substance of this thesis is oriented to low level counting, the analysis has been restricted to the full energy peak alone.

6.3.2 Measurement of the Full Energy Peak

Several techniques have been evaluated for peak measurement using computer assistance. The least squares technique is again commonly used

(Black 1969). Ciampi, Daddi and D'Angelo (1968) assume a Gaussian shape peak and fit this using a maximum probability technique on to the full energy peak under investigation. However, the peak shape frequently deviates from a Gaussian and systematic errors can be incurred. Huang, Osman and Ophel (1969) avoid this problem by fitting a pre-measured peak shape onto the test spectrum. The advantage of both these techniques is that overlapping peaks may be separated. However, all these analyses require computer assistance and in low level measurements, the peak shape may be considerably distorted by poor statistics.

Another technique relies upon the projection of the continuum from either side of the peak to obtain a measure of the value of under the peak. Thompson (1969) has developed a simple method but it is only effective for a uniform background continuum. A more general version is developed below which may be used manually in its simpler version or more fully using a computer.

6.3.2.1 Calculation of the Background Under the Peak

Fig. 6.1 shows the measurement technique adopted for a full energy peak. A measurement of the continuum under the peak is performed by projecting a value from the side windows WX and YZ chosen on each side of the peak. The measured value B has a standard deviation of σ_B where

$$\sigma_B = \left(B + \sigma_w^2 \right)^{1/2} \qquad \ldots\ldots\ldots 6.9$$

An nth order polynomial is least squares fitted to the side window WX

where

$$\left(y_i \right)_X^w = \sum_{n=0}^{n=n} a_n i^n \qquad \ldots\ldots\ldots 6.10$$

and $\left(y_i \right)_X^w$ = the polynomial value of channel contents in channel i

$a_0 \text{---} a_n$ = polynomial constants for window WX

A similar polynomial is fitted to the window YZ

i.e.

$$\left(y_i \right)_Y^z = \sum_{n=0}^{n=n} b_n i^n \ldots\ldots 6.11 \qquad \text{where } b_0\text{---}b_n = \text{polynomial constants} \\ \text{for window YZ}$$

Fig. 6.1

Peak Measurement Technique Adopted for a Full Energy Peak
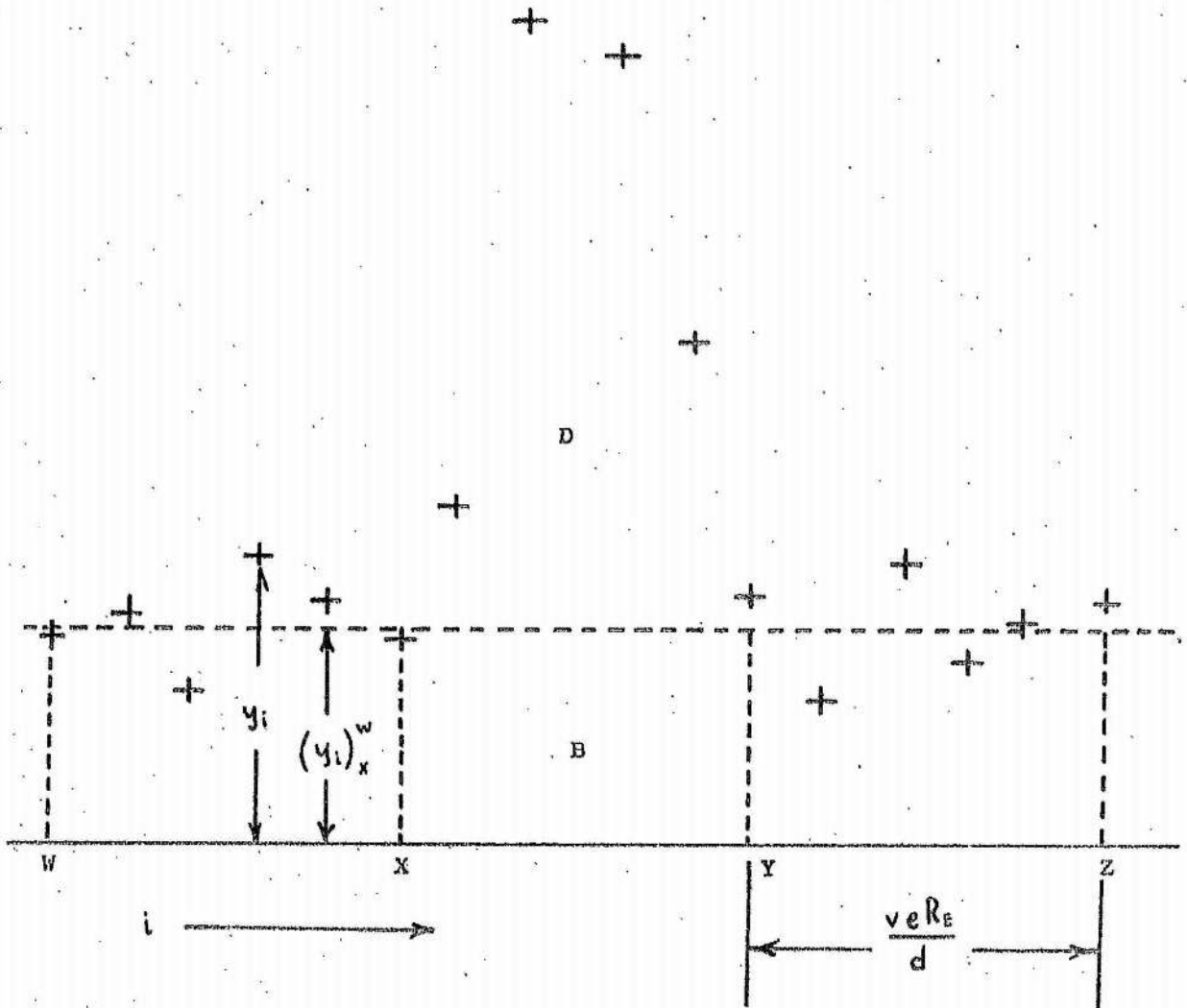
The window width is decided by the prevailing continuum conditions, and in the absence of neighbouring peaks or other discontinuities is usually a maximum of two peak base widths. Measurement has shown that in most cases the increase in window width beyond this brings little improvement in sensitivity.

Substitution of the channel contents into 6.10 and 6.11 enables solution, by determinants, of the constants $a_0 \cdots a_n$ and $b_0 \cdots b_n$ to give the least squares fit of $(y_i)_x^w$ onto the data points in WX and similarly for YZ, i.e. if

$$D_{wx} = \begin{vmatrix} \frac{ve R_E}{d} & \sum i & \cdots & \sum i^{n-1} & \sum i^n \\ \sum i & \sum i^2 & \cdots & \sum i^n & \sum i^{n+1} \\ \vdots & \vdots & & \vdots & \vdots \\ \sum i^{n-1} & \sum i^n & \cdots & \sum i^{2n-2} & \sum i^{2n-1} \\ \sum i^n & \sum i^{n+1} & \cdots & \sum i^{2n-1} & \sum i^{2n} \end{vmatrix} \qquad \cdots\cdots 6.12$$

where e = ratio of window width to peak base width.

Hence $\frac{ve R_E}{d}$ = number of pairs of data points used in window.

$$a_0 = \begin{vmatrix} \sum y_i & \sum i & \cdots & \sum i^{n-1} & \sum i^n \\ \sum (i y_i) & \sum i^2 & \cdots & \sum i^n & \sum i^{n+1} \\ \vdots & \vdots & & \vdots & \vdots \\ \sum (i^{n-1} y_i) & \sum i^n & \cdots & \sum i^{2n-2} & \sum i^{2n-1} \\ \sum (i^n y_i) & \sum i^{n+1} & \cdots & \sum i^{2n-1} & \sum i^{2n} \end{vmatrix}_x^w \times D_{wx}^{-1}$$

and for $a_1 \cdots a_{n-1}$ so that finally $\qquad\qquad \cdots\cdots 6.13$

$$a_n = \begin{vmatrix} \frac{ve R_E}{d} & \sum i & \cdots & \sum i^{n-1} & \sum y_i \\ \sum i & \sum i^2 & \cdots & \sum i^n & \sum (i y_i) \\ \vdots & \vdots & & \vdots & \vdots \\ \sum i^{n-1} & \sum i^n & \cdots & \sum i^{2n-2} & \sum (i^{n-1} y_i) \\ \sum i^n & \sum i^{n+1} & \cdots & \sum i^{2n-1} & \sum (i^n y_i) \end{vmatrix}_x^w \times D_{wx}^{-1}$$

A similar set of equations are established for the constants $b_0 --- b_n$. $\left(y_i\right)_x^w$ and $\left(y_i\right)_Y^z$ are now evaluated at $i = X$ and $i = Y$ respectively giving values of y_X and y_Y.

$\frac{d(y)_x^w}{di}$ and $\frac{d(y_i)_Y^z}{di}$ are obtained by differentiating 6.10 and 6.11 and both are evaluated at $i = X$ and $i = Y$ (termed $\left(\frac{dy}{di}\right)_X$ and $\left(\frac{dy}{di}\right)_Y$ respectively).

A third order polynomial (maximum possible for given data) is now fitted between X and Y using the equations:-

$$
\left.
\begin{aligned}
\left(C_0 + C_1 i + C_2 i^2 + C_3 i^3 \right)_X &= y_X \\[6pt]
\left(C_0 + C_1 i + C_2 i^2 + C_3 i^3 \right)_Y &= y_Y \\[6pt]
\left(0 + C_1 + 2C_2 i + 3C_3 i^2 \right)_X &= \left(\frac{dy_i}{di}\right)_X \\[6pt]
\left(0 + C_1 + 2C_2 i + 3C_3 i^2 \right)_Y &= \left(\frac{dy_i}{di}\right)_Y
\end{aligned}
\right\} \qquad \cdots\cdots\cdots 6.14
$$

where C_0, C_1, C_2, C_3 are constants of the polynomial to be determined.

The constants C_0 to C_3 are evaluated by determinants as for $a_0 ---a_n$ and $b_0 --- b_n$. The background under the peak is

$$
\sum_{i=X}^{i=Y} \left(y_i\right)_X^Y = B
$$

where

$$
B = (Y - X - 1) C_0 + \left(\sum_{i=X+1}^{i=Y-1} i\right) C_1 + \left(\sum_{i=X+1}^{i=Y-1} i^2\right) C_2 + \left(\sum_{i=X+1}^{i=Y-1} i^3\right) C_3 \qquad \cdots\cdots\cdots 6.15
$$

The selection of the order of the polynomials $\left(y_i\right)_X^w$ and $\left(y_i\right)_Y^z$ is dependant upon manual or computer data handling. Manually, orders above third order are tedious to handle. Care must be taken in the computer analysis in that above fifth orders, there can be a tendancy for the fitted equation to oscillate through the data points.

6.3.2.2 Calculation of σ_w

The statistical deviations of each channel contents cause calculable

deviations in the constants a_0 to a_n and b_0 to b_n, termed a_{0E} to a_{nE} and b_{0E} to b_{nE}. In equation 6.13, the standard deviation of elements in the determinant containing y_i are written as

$$
\left.
\begin{aligned}
\sum y_i &\pm \left(\sum y_i \right)^{1/2} \\
\sum i y_i &\pm \left(\sum i^2 y_i \right)^{1/2} \\
&\vdots \\
\sum i^n y_i &\pm \left(\sum (i^{2n} y_i) \right)^{1/2}
\end{aligned}
\right\} \qquad \dots\dots\dots 6.16
$$

The standard deviations of 6.16 give the deviations in $a_0 \cdots a_n$ of a_{0E} to a_{nE} by substituting 6.16 into 6.13, giving

$$
a_{0E} = \begin{vmatrix}
\left(\sum y_i \right)^{1/2} & \sum i & ----- & \sum i^{n-1} & \sum i^n \\
\left(\sum i^2 y_i \right)^{1/2} & \sum i^2 & ----- & \sum i^n & \sum i^{n+1} \\
\vdots & \vdots & & \vdots & \vdots \\
\left(\sum (i^{2(n-1)} y_i) \right)^{1/2} & \sum i^n & ----- & \sum i^{2n-2} & \sum i^{2n-1} \\
\left(\sum (i^{2n} y_i) \right)^{1/2} & \sum i^{n+1} & ----- & \sum i^{2n-1} & \sum i^{2n}
\end{vmatrix} \times D_{wx}^{-1}
$$

and for a_{1E} to a_{nE} so that finally

$$
a_{nE} = \begin{vmatrix}
\dfrac{v \, \alpha \, R_E}{d} & \sum i & ----- & \sum i^{n-1} & \left(\sum y_i \right)^{1/2} \\
\sum i & \sum i^2 & ----- & \sum i^n & \left(\sum i^2 y_i \right)^{1/2} \\
\vdots & \vdots & & \vdots & \vdots \\
\sum i^{n-1} & \sum i^n & ---- & \sum i^{2n-2} & \left(\sum i^{2(n-1)} y_i \right)^{1/2} \\
\sum i^n & \sum i^{n+1} & ---- & \sum i^{2n-1} & \left(\sum i^{2n} y_i \right)^{1/2}
\end{vmatrix} \times D_{wx}^{-1}
$$

$$\dots\dots\dots 6.17$$

and similarly for b_{0E} to b_{nE}.

The constants a_{0E} to a_{nE} and b_{0E} to b_{NE} are inserted into equation 6.10 to determine the variations of y_X and y_Y and $\left(\dfrac{dy}{di} \right)_X$ and $\left(\dfrac{dy}{di} \right)_Y$. Equation 6.14 is recalculated with these modified values to determine the resulting deviations of the constants $c_0 \cdots c_3$, namely c_{0E} to c_{3E}. With these constants σ_w is calculated to be

$$
\sigma_w = (Y - X - 1) c_{0E} + \left(\sum_{i=X+1}^{i=Y-1} i \right) C_{1E} + \left(\sum_{i=X+1}^{i=Y-1} i^2 \right) C_{2E} + \left(\sum_{i=X+1}^{i=Y-1} i^3 \right) C_{3E} \quad \dots\dots 6.18
$$

6.3.2.3 Calculation of the Full Energy Peak Area

With a knowledge of B and σ_w^-, the peak area is simply calculated as

$$D = \sum_{i=X+1}^{i=Y-1} y_s - B \pm \left(\sum_{i=X+1}^{i=Y-1} y_s + B + \sigma_w^2 \right)^{\frac{1}{2}} \quad i.e. \pm \sigma_D \text{ where } \sigma_D = \text{standard deviation to } 68\% \qquad \ldots\ldots\ldots 6.19$$

where y_s = measured channel contents in channel i between X and Y.

Where the background continuum is approximately linear or where an approximate determination of counting limits is required a straight line solution can be fitted which allows quick determination. For many applications this can give sufficiently accurate results, but is dependant, in part, upon the number of channels in the peak and the spectral complexity.

This technique of peak background measurement has been tried satisfactorily on several examples (section 6.4). σ_w^- has always had values less than $B^{\frac{1}{2}}$ and has had a limited effect. Generally, σ_w^- takes values of $\sim 0.4 B^{\frac{1}{2}}$ for $e = 1$. Hence if this replaces σ_w^- in equation 6.5 a reasonable approximation of A_E may still be calculated.

6.4 Experimental Determination of the Sensitivity Limits

This section demonstrates the use of the equations derived in sections 6.2 and 6.3.

6.4.1 Use of the Background Projection Technique

As a check on the technique of estimating the background continuum under the peak, measurements were made upon sections of continuum taken from three spectra. Table 6.1 shows the continua used. A peak base width of ten channels is taken in the centre of each continuum. On each side of the base width a side window is taken also of one peak base width. A simple fit was made on the side windows to measure the peak base continuum as considered in section 6.3.2.1. Table 6.2 shows the results calculated for the three continua. It is observed that a simple manual and linear fit on relatively uniform continua is sufficient to obtain a satisfactory value for B. This is satisfactory for a uniform continuum, but for curved fits computer analysis is necessary. Figs. 6.2a and 6.2b show two typical fits made by computer.

Table 6.1

Three Continua used for Manual Calculation of the
Background Projection Technique

Channel	Low Background	Medium Background	High Background	
330	2	220	2107	
1	2	208	2032	
2	1	232	1871	
3	1	252	2002	
4	3	228	1861	
5	1	236	1910	lower window
6	2	216	1845	
7	1	217	1759	
8	4	216	1768	
9	3	236	1794	
340	0	198	1678	
1	3	229	1760	
2	2	212	1689	
3	5	205	1641	
4	2	213	1558	peak base width
5	2	222	1543	
6	4	224	1599	
7	5	232	1520	
8	5	241	1510	
9	2	242	1530	
350	1	257	1447	
1	3	243	1391	
2	3	241	1415	
3	2	254	1385	
4	1	229	1421	upper window
5	2	267	1349	
6	1	230	1256	
7	2	251	1307	
8	1	235	1276	
359	1	209	1192	

$T = 100$ min

$v = 2$

$e = 1$

$R_E = 5$ keV

Fig. 6.2a

Typical Side Window Fit made by Computer
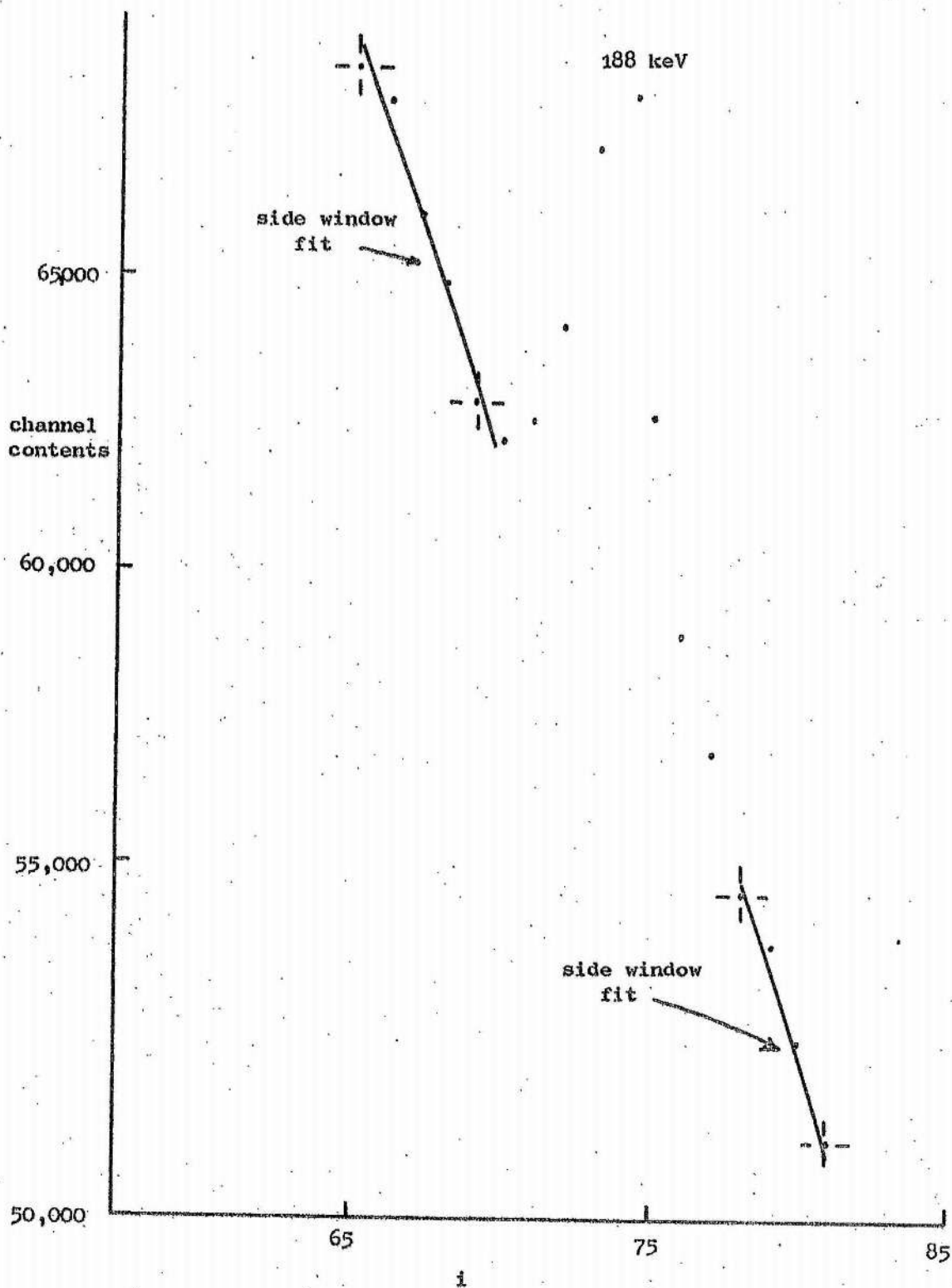
Fig. 6.2b   Computer Fit on a Further Peak in the Spectrum
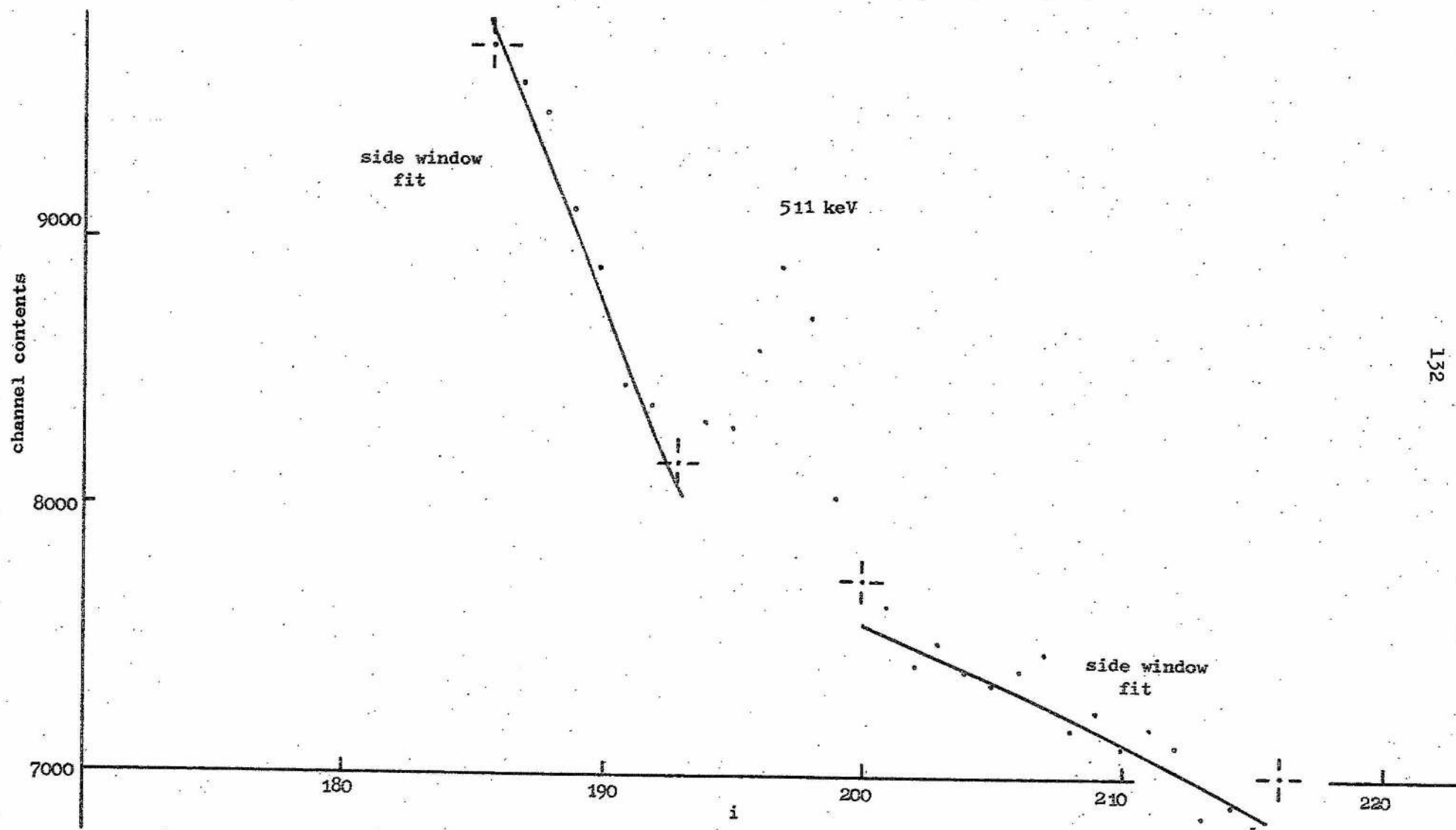
Table 6.2

Data Calculated from Table 6.1

Background Level	Actual B	Predicted B	σ_w	Difference between predicted and true B	$B^{1/2}$	$(B+\sigma_w^2)^{1/2}$
low	30	26	2.67	− 4	5	6
medium	2218	2420	19.40	+202	50	53
high	16028	15936	47.40	− 92	127	131

6.4.2 The Minimum Detectable Peak Area

For a given background level, energy resolution, T and C the minimum detectable peak area may be calculated. However, when the statistical fluctuations of the background are similar to the peak height, it becomes difficult to define when a peak is just observable. This becomes partly observer dependant and varies from experimenter to experimenter.

As a simple demonstration of the minimum detectable peak area, the following simple experiment was performed. A ^{137}Cs source was counted in fixed geometry with the 7.4 cm^3 detector. The source was remeasured (for identical count times and source detector geometry) and a ^{60}Co source was moved in steps towards the detector, thus increasing the background continuum while maintaining the ^{137}Cs counts in the peak constant. This was continued until the peak was considered unobservable. Table 6.3 shows the area of the peak calculated with increasing background together with C. Selected spectra (for differing C) are shown in Fig. 6.3. Spectrum 1 is quite clear and spectra 5 and 6 are still observable though becoming indistinct for peak measurement. The peak in spectrum 7 is just observable (C ∿ .27) while that in spectrum 11 is considered unobservable. As an approximate guide, it is taken that potential peaks calculated to have C ∿ ⅓ or greater may be background fluctuations and it is difficult to decipher the peak from the continuum.

The clarity of the peak is dependant upon the number of channels used in the peak (ideally optimum as considered in section 3.3.3). It is observed that the peak base width is reduced as C increases (table 6.3).

6.4.3 The Prediction of Sensitivity Limits of Ge(Li) Spectrometers

The prediction of the minimum acceptable activity depends upon

Table 6.3

Constant Area Peak Remeasured on an Increasing Background

Spectrum Number	S	B	D	σ_D	Peak Base Width	C
1 *	234	75	159	18.0	6 (channels)	0.11
2	270	120	150	20.0	6	0.13
3	305	132	173	22.0	6	0.12
4	361	198	163	25.0	6	0.15
5 *	491	308	182	29.0	7	0.16
6 *	627	475	152	34.0	5	0.22
7 *	821	675	146	40.0	5	0.27
8	1220	1061	159	49.5	4	0.31
9	2078	1860	218	65.0	5	0.30
10	1872	1660	212	61.5	4	0.29
11 *	2747	2530	213	74.5	4	0.35

* These spectra shown in Fig. 6.3

the repeatibility of the parameters of equation 6.5 in the prediction spectrum and the source + background spectrum. In general ϵ_{PA}, C, T and R_E are maintained constant with little difficulty.

However, the maintaining of the background continuum is difficult if a significant part of the continuum is source generated. In cases where the major contribution is from natural background or other interfering sources and the detector has a good peak to Compton ratio, the continuum level is representative of the source plus background measurement, within statistical variations. In this case direct predictions are made satisfactorily.

The use of equation 6.5 is demonstrated by the following example. The 7.4 cm^3 active volume detector was used to measure standard shape ^{137}Cs sources made up with standard bottles in an easily reproducible geometry. In this configuration ϵ_{PA} was measured to be .0008 for ^{137}Cs gamma rays.

The background continuum at 662 keV was measured for several different experimental arrangements (Table 6.4) for the 7.4 cm^3 detector. From this data, the resolution and the measured value of ϵ_{PA}, the minimum acceptable activities of ^{137}Cs were calculated for a pre-chosen C and T (Table 6.4). Sources of these strengths were manufactured from a standard liquid concentrated ^{137}Cs source and carefully diluted in distilled water to an estimated

Fig. 6.3

Peak of Constant Area Situated Upon an Increasing Background

Fig. 6.3 (cont.)

700

counts

650

600

spec 11
C = 0.35

i
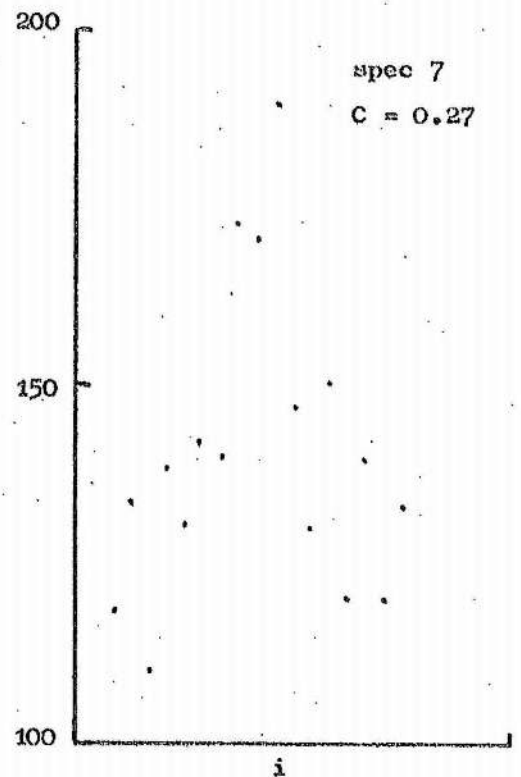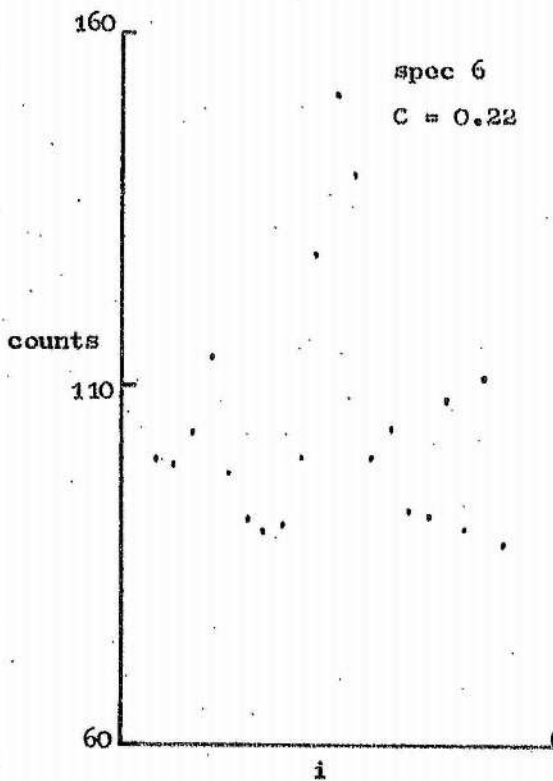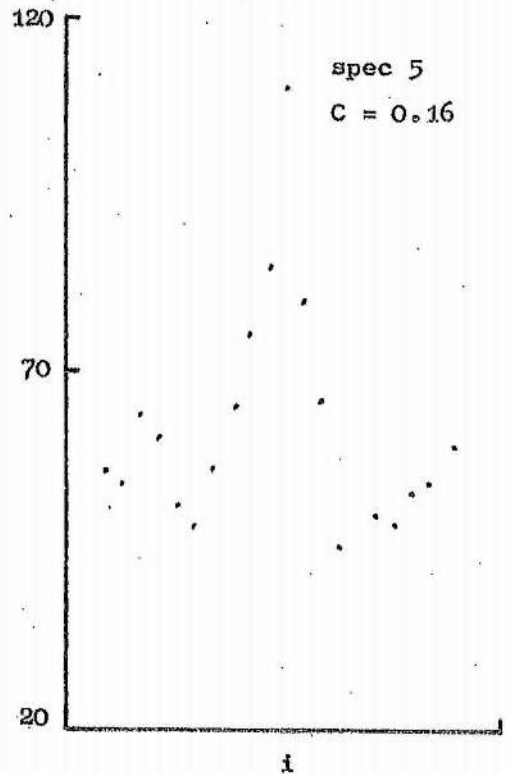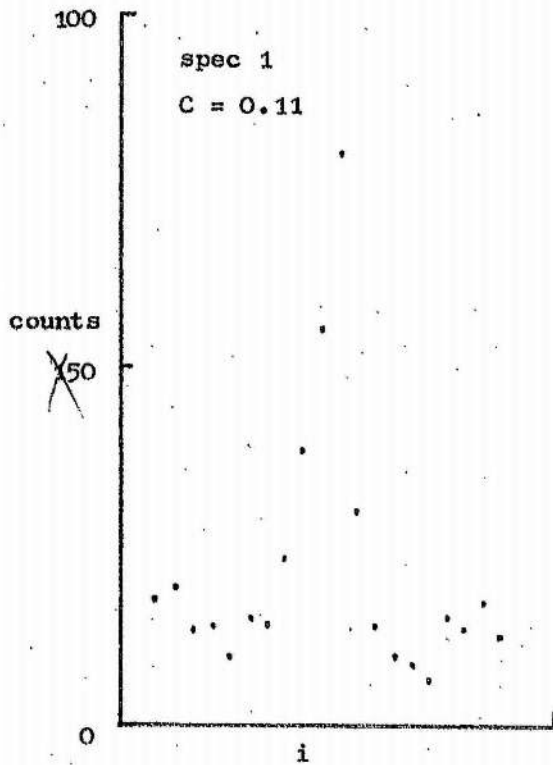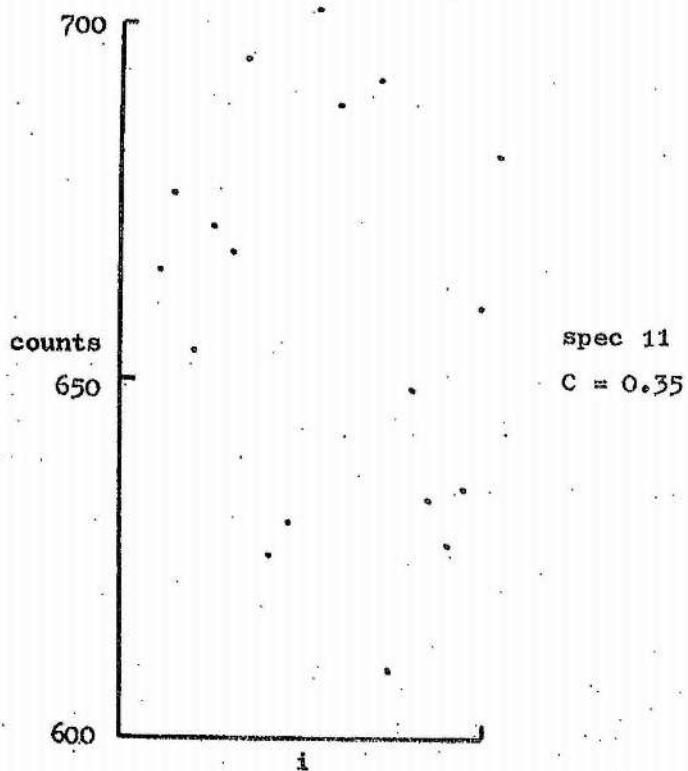
Table 6.4

Comparison of Predicted and Achieved Activities

Background Condition	Measured Background (under peak)	Predicted Source Strength	Measured Source Strength	Set C	Measured C	Count Time	Expected A_E for $C=\frac{1}{3}$
No shield, plus ^{60}Co source	1901 cpm	70 nCi	68 nCi	0.10	0.10	50 min	26 nCi
No shield	3.93 cpm	3.6 nCi	3.8 nCi	0.10	0.09	50 min	2.3 nCi
5cm lead	0.2 cpm	120 pCi	140 pCi	0.20	0.17	600 min	65 pCi
10cm lead	0.11 cpm	70 pCi	70 pCi	0.20	0.20	600 min	42 pCi

error of $\pm 5\%$ and counted for the set times. From these spectra, the activities were calculated and tabulated together with C in Table 6.4. It is observed that the values satisfactorily compare, confirming the use of this equation for these counting conditions.

The minimum detectable activity $(C \sim \frac{1}{2})$ of ^{137}Cs was also calculated and tabulated to show the level at which ^{137}Cs may be considered just observable above background continuum.

6.5 The Effect of the Major Counting Parameters

Equation 6.5 shows that the sensitivity limits are dependant upon several parameters, namely:-

1) Energy Resolution (R_E)
2) Statistical Precision (C)
3) Background Continuum (B)
4) Absolute Full Energy Peak Efficiency (ϵ_{PA})
5) Count Time (T)

Each of these has a different effect upon A_E and consideration of equation 6.5 determines the significance and effect of each parameter.

6.5.1 Energy Resolution

A good energy resolution detector allows superior spectral analysis and optimum statistical precision. The peak base width is expressed as $\frac{v R_E}{d}$, neglecting background effects and gain drift.

Let B_k represent the background continuum, in counts per channel, under the peak. Then assuming a uniform continuum, the background B is

$$B = \frac{B_k \, v \, R_E}{d} \qquad \text{counts} \qquad \ldots\ldots\ldots 6.20$$

As the energy resolution broadens, B is assumed to increase linearly. This simplification of the practical case yields the approximate effect of energy resolution on A_E. Equation 6.20 is substituted into equation 6.5 to give

$$A_E \, \epsilon_{PA} \, T = \frac{1}{C}\left(\frac{2 B_k \, v \, R_E}{d} + \frac{1}{2C^2} + \sigma_w^2 + \frac{1}{2C}\left(\frac{1}{C^2} + \frac{8 B_k \, v \, R_E}{d} + 4 \sigma_w^2 \right)^{1/2} \right)^{1/2} \qquad \ldots\ldots\ldots 6.21$$

Fig. 6.4

The Variation of $A_E \times \epsilon_{pq} \times T$ with R_E for Various Background Levels (c = 0.1)

139
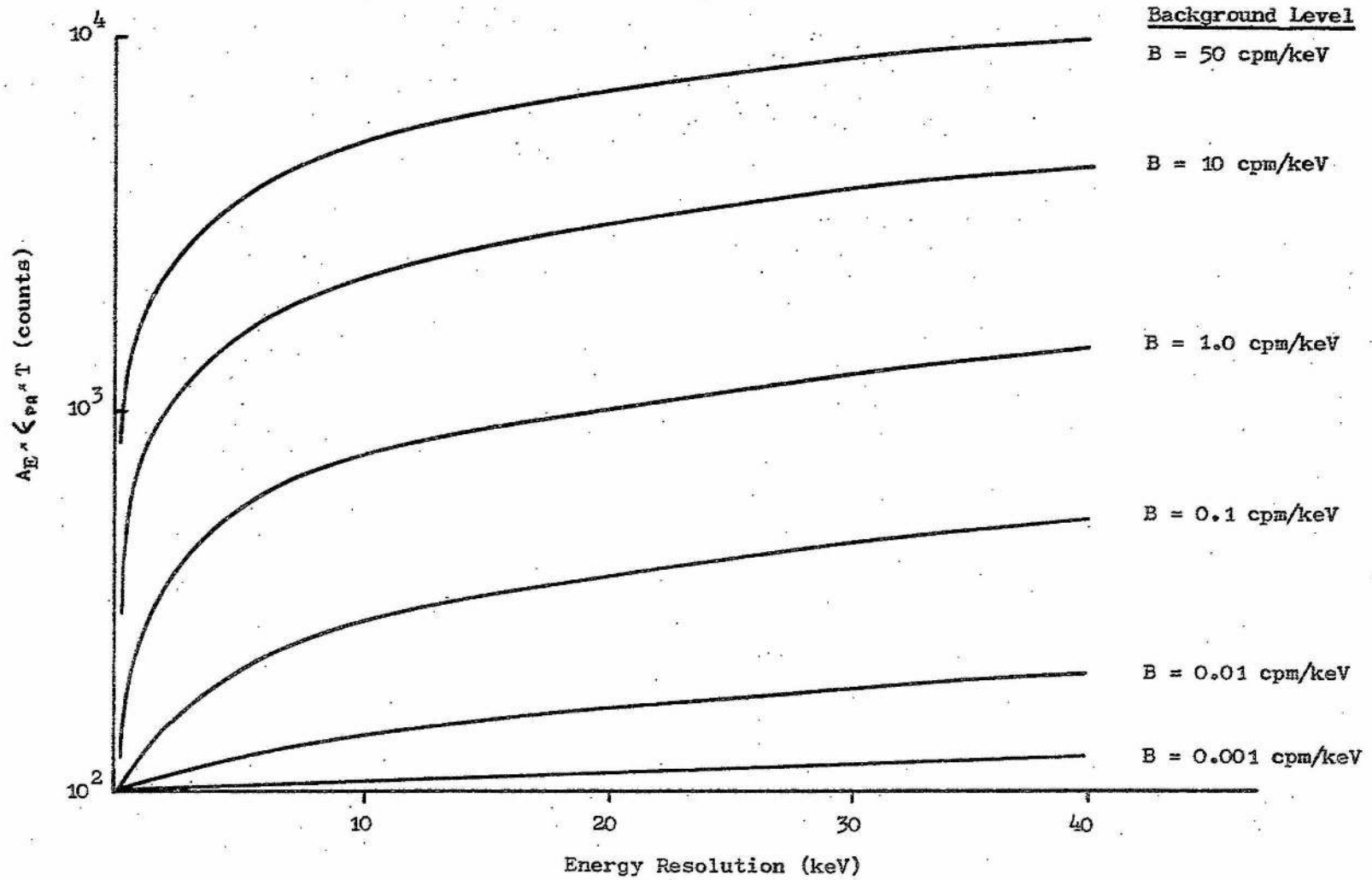
All parameters are held constant while the energy resolution is increased.   Equation 6.21 is plotted for varying R_E, B_k and $\sigma_w \sim 0.4B^{\frac{1}{2}}$. Fig. 6.4 shows the variation of $A_E \leq_{PA} T$ with resolution for differing background levels and with $C = 0.10$.   The energy resolution range is extended to cover both NaI(Tl) and Ge(Li) spectrometers.   The background levels are those ranging from low level experiments (Shafroth 1967, Watt and Ramsden 1964) to high count rate experiments.

The following observations are made on Fig. 6.4:-

1) Very high energy resolution counters have the best low level capabilities.   As the resolution falls below 10 keV, the rate of improvement in sensitivity increases rapidly.   Halving the resolution of a Ge(Li) detector has a greater effect than halving the resolution of a NaI(Tl) detector.

2) In very low level background conditions, improvements in energy resolution has less effect, except in the presence of interfering peaks.

3) Consideration of equation 6.5 and Fig. 6.4 shows that the effect of energy resolution is strongly dependant upon the statistical precision required.

6.5.2 Statistical Precision

This parameter has considerable effect on A_E and the precision should be carefully justified before the experiment is performed.   Fig. 6.5 shows the variation of A_E with C, plotted directly from equation 6.5, for different background levels.   All other parameters areheld constant.

The following observations are made on Fig. 6.5:-

1) As C increases, A_E rapidly decreases at a rate depending upon the particular background level.

2) At low background levels (B → 0) A_E varies approximately as $\frac{1}{C^2}$, which is a commonplace result.   Thus a factor of 10 drop in precision results in a factor of 100 improvement in A_E.

6.5.3 Background Continuum

The continuum under a peak has two basic contributions, namely natural background and that source generated.

Fig. 6.5

The Variation of A_E with C for Different B
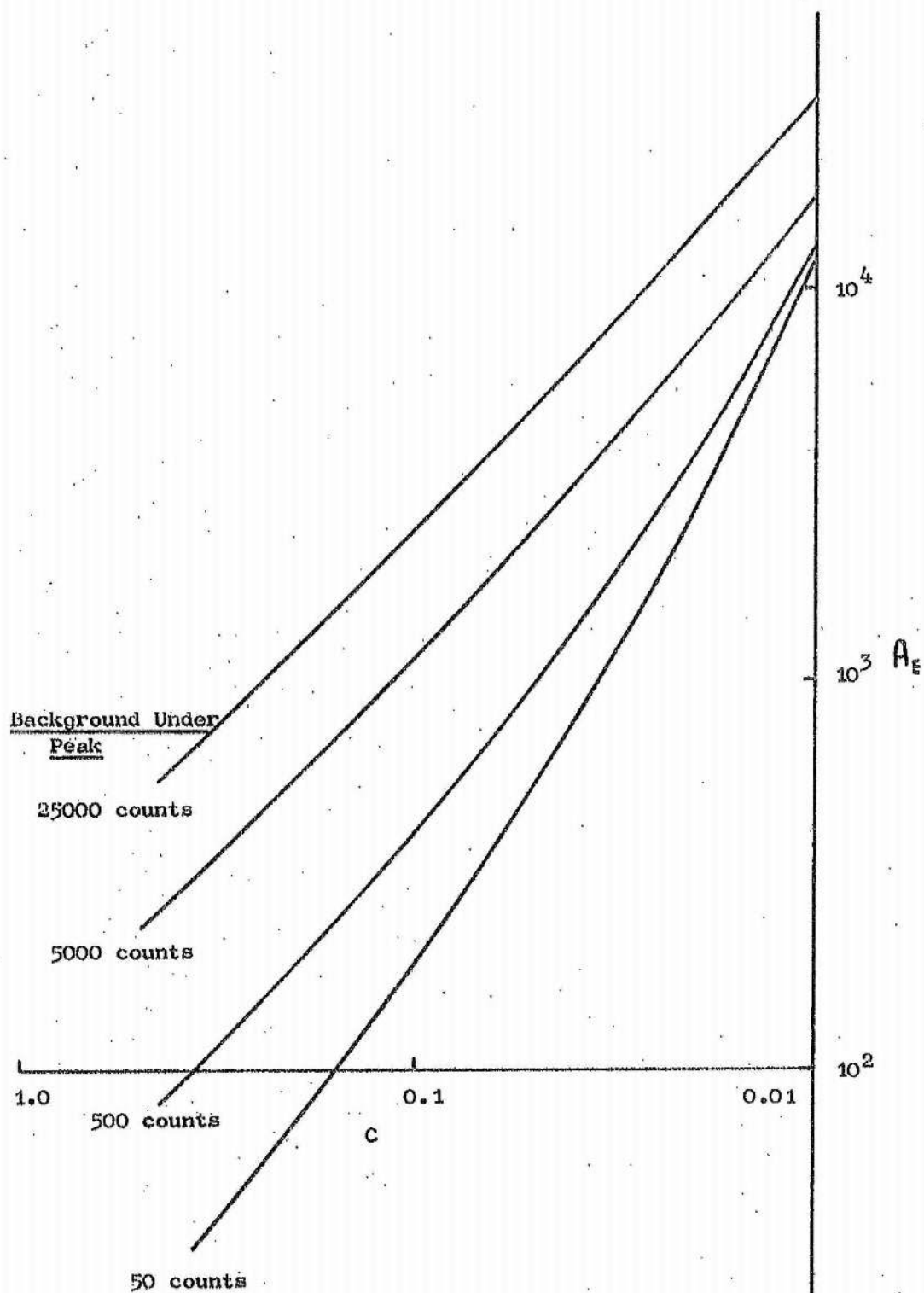
Natural background origins have been intensively investigated
and documented (Eisenbud 1963, Adams and Lowder 1964, Watt and Ramsden 1964
and Shafroth 1967) using gas and scintillation detectors.   In a given count-
ing environment, there is a background flux of radiation B_{FE}, a function of
energy.   As the flux intensity increases, there is a corresponding increase
in B_{DE}, the continuum measured by the detector in that counting environment.
The relation between B_{DE} and B_{FE} changes if the sensitive volume of the
detector changes.   As an approximation it is assumed that the relation
between B_{FE} and sensitive volume is linear, to demonstrate the effect of
sensitive volume size.

When B is largely source generated, background shielding has little
effect and can even degrade the spectrum through scattering in the shield.
For natural background, shielding is useful and the effect of shielding is
calculable.

Consider a spectrometer in which the shielding is increased while
the detector characteristics are held constant with the dominant contribution
to B being from B_{FE}.   Equation 6.5 is plotted for decreasing levels of B.
Fig. 6.6 shows the variation of A_E with B for C = 0.1 and 0.01.   The lower
background levels shown are those typically recorded (Shafroth 1967) with
very efficient shielding.

The following observations on the effect of B on A_E are made:-

1) A large drop in background does not bring a corresponding drop in
the minimum acceptable activity.

2) Fig. 6.6 illustrates the general result that little improvement
in accuracy is gained by making the signal to background ratio
greater than $\sim$ 1.0

It is seen that the application of massive shielding produces diminishing
returns in improvement in spectral response.   Bearing in mind the cost of
such shielding, the cost of a spectrometer should be carefully balanced
between detectors and shield.

6.5.4 Absolute Full Energy Peak Efficiency

The effect of ϵ_{PB} on A_E is partly dependant upon the background
origins.   Source generated continua can be considerable.   When this dom-
inates and ϵ_{PB} is increased, the source generated continua and peak counts
also increase in rough proportion, partially offsetting the improvement in A_E.

Fig. 6.6

The Variation of A_E with Background Continuum
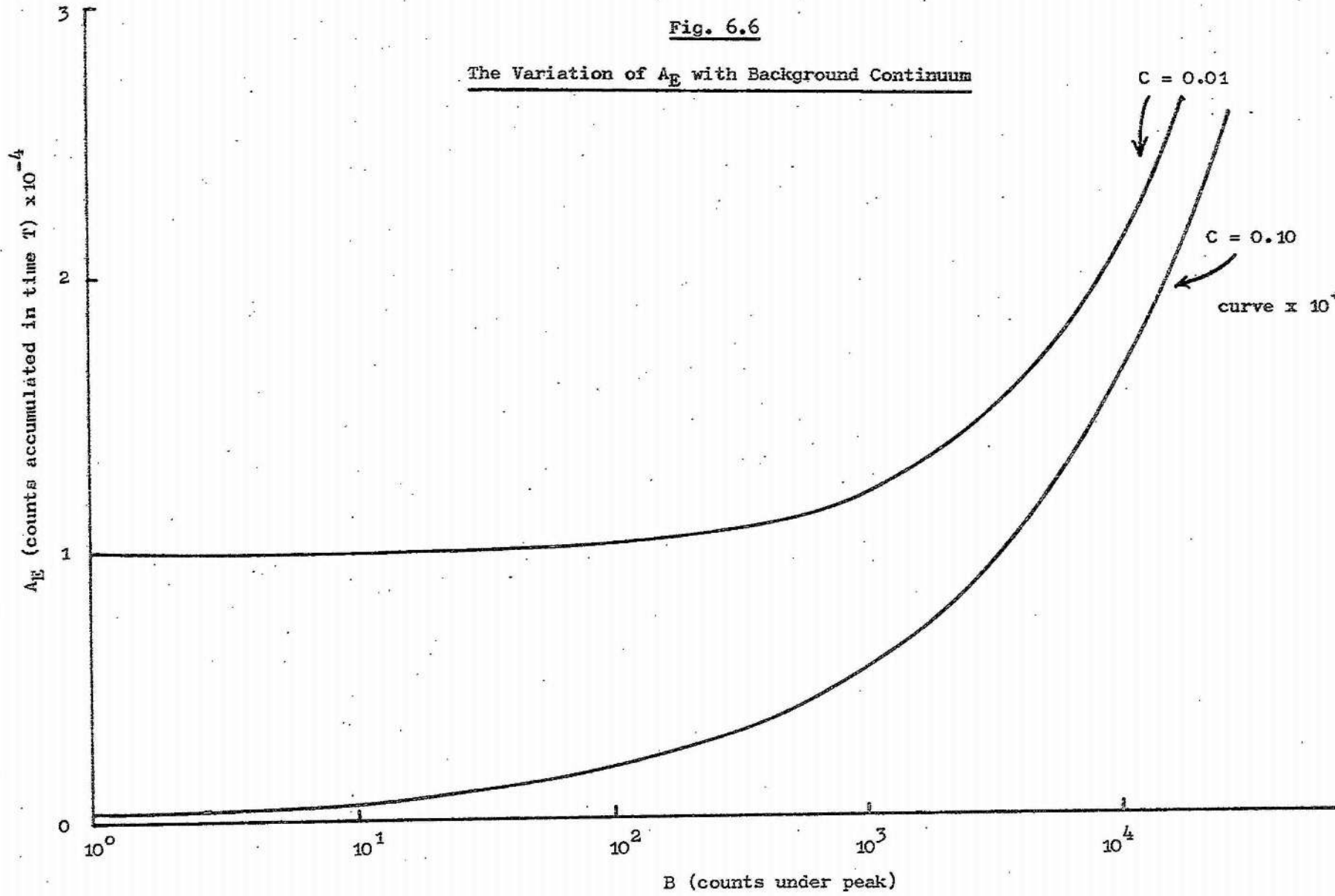
When the background is largely environmental, then an increase in ϵ_g at constant sensitive volume yields an approximately corresponding decrease in A_E. The significance of an optimised geometrical efficiency for low level measurement is thus evident. When the only means of increasing ϵ_{PA} is by increasing the volume of the detector, the background level will similarly increase. Fig. 6.7 shows the calculated variation of A_E with ϵ_{PA} for different levels of B, assuming a pre-optimised ϵ_g.

The following observations are made on ϵ_{PA} :-

1) The optimisation of geometrical efficiency can yield considerable improvements in sensitivity.

2) The increase of efficiency has its greatest effect when measuring weak activities in low level environments.

The above calculations consider small sources placed near the cryostat end window. The case often arises of improving the source counts by increasing quantity of source material (if available). The effects of using larger volume sources are demonstrated by the data obtained in section 5.3.2 for the 7.4 cm^3 detector. When ϵ_{PA} was measured for each volume source, the natural background was also measured over a 10 hour period for that geometry with the source replaced by distilled water and with the addition of 5cm of lead shield. Using this background data, the data for ϵ_{PA} of section 5.3.2 and setting C = 0.2, A_E was calculated for differing energies and volume sources. Table 6.5 shows the variation of minimum acceptable activity for differing energies and volumes.

From this data, the improvement gained (in cpm/ml) can be observed when a liquid source is concentrated (say by evaporation) from 1660 ml to 0.5 ml . Table 6.6 shows the variation of minimum acceptable activity with sample reduction. Certain individual variations in the data are caused variations in the background spectrum. Practical measurements may have other variations due to denser source material, different energies, and inhomogenieties within the material being measured.

Consider the case when 1 photon is emitted per disintegration. Then sample reduction (assuming no activity loss) at 569 keV improves the sensitivity from 0.34 pCi/ml to .08 pCi/ml while for the 1333 keV line the sensitivity is improved from 0.27 pCi/ml to 0.11 pCi/ml. These general levels could be much improved using larger crystals and better shielding.

It is observed that in spite of large volume reductions, the sensitivity is changed by less than an order of magnitude, making low level

Fig. 6.7

Variation of A_E with ϵ_{PA} for Different Background Levels (C=0.10)
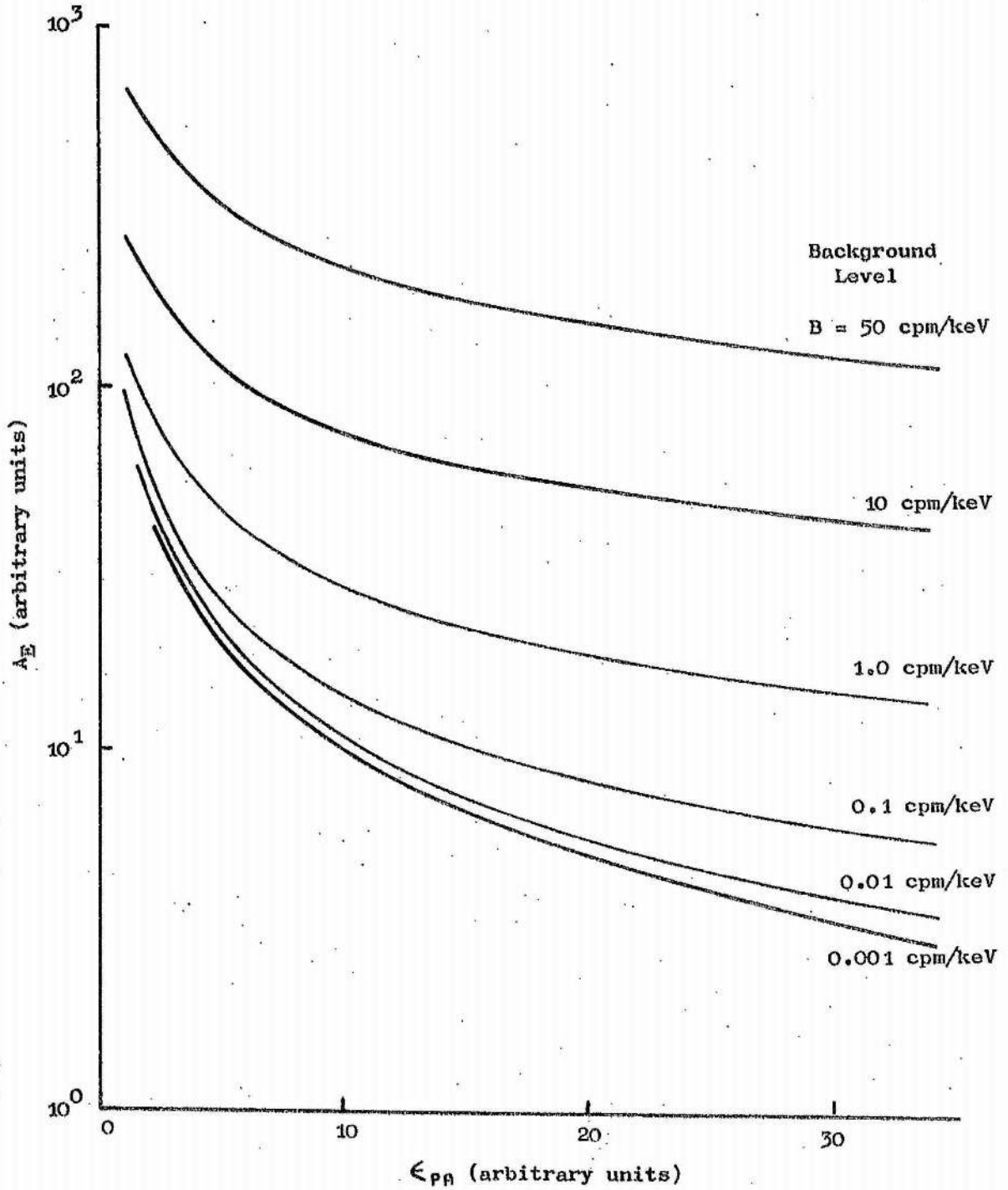
Table 6.5

Variation of A_E* (expressed in γ /min from source) with Energy and Total Source Volume

Source Volume (ml)	569 keV	605 keV	802 keV	1173 keV	1333 keV	1365 keV
0.5	229	254	333	440	415	356
180	402	541	619	700	635	615
380	540	623	783	835	750	855
800	784	825	1070	1010	875	1040
1160	957	1000	1280	1090	920	1175
1660	1270	1230	1625	1090	985	2220

* for C = 0.2,   T = 600 minutes

5cm thick lead shielding

Table 6.6

Variation of A_E (in γ /min / ml of source) as a liquid source is Evaporated to Concentrate its Volume from 1660 ml to 0.5ml

(Calculated from Table 6.5)

Source Volume (ml)	569 keV	605 keV	802 keV	1173 keV	1333 keV	1365 keV
0.5	0.177	0.153	0.20	0.27	0.25	0.21
180	0.242	0.33	0.37	0.42	0.38	0.37
380	0.33	0.37	0.47	0.50	0.45	0.52
800	0.47	0.50	0.64	0.53	0.53	0.63
1160	0.57	0.60	0.77	0.66	0.55	0.71
1660	0.77	0.74	1.00	0.66	0.59	1.30

activity measurements without volume reduction possible.

6.5.5 Count Time

The effect of count time is simply assessed on the assumption that, within statistical variations, a doubling of count time doubles the value of the background continuum to be accounted for. Fig. 6.8 is a graph showing the variation of A_E with T for differing background levels. Virtually any activity may be measured if one is prepared to wait long enough and the system stability is sufficient. The choice of count time for low level measurements is ultimately governed by the numbers of samples, cost of spectrometer time and apparatus availability, unless a short half life isotope is being measured. The greatest effect of count time is for low background levels (Fig. 6.8). It is also observed that a doubling of count time does not correspondingly reduce A_E.

The above analysis is valid while the isotope half life is long compared with T. The case is now considered where the half life is comparable with T. An optimum count time is calculated on the basis that if the count time is too short then the statistical precision of D is impaired and if it is too long then σ_D^- is impaired through excess B. An expression may be derived for C where B and D are functions of T. This is differentiated with respect to T and the minimum value determined to give the best T.

The optimum choice of T depends upon a foreknowledge of the isotope expected. An exact optimum is difficult to calculate if there are many differing isotopes measured in the one sample and the continuum is also time dependant. As a simple illustration the following example is considered.

Consider a full energy peak having an initial count rate d_o decaying with a decay constant λ_p situated upon a background continuum with a constant count rate under the peak of b_K and a decaying component with a decaying component initially of b_o with a decay constant λ_b

The count rate in the full energy peak at time T is d_t where

$$d_t = d_o e^{-\lambda_p T}$$

$$\cdots\cdots 6.22$$

The count rate in the background continuum under the peak at time T is b_t where

$$b_t = b_K + b_o e^{-\lambda_b T}$$

$$\cdots\cdots 6.23$$

148

Fig. 6.8

Variation of A_E with T for Different Levels of B and C = 0.1
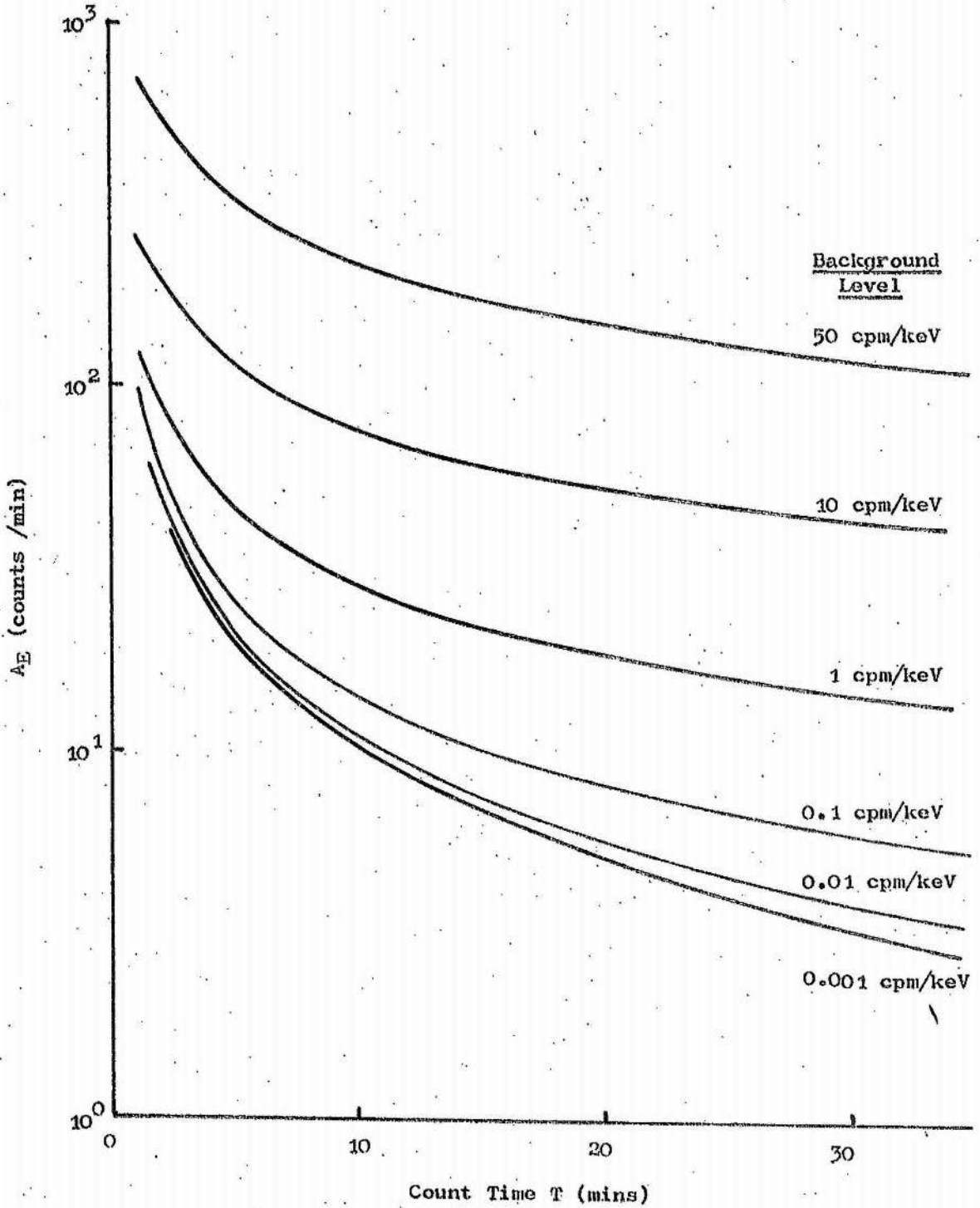
Integration of 6.22 and 6.23 yields D and B at Time T,

i.e.
$$D = \frac{d_o}{\lambda_D}\left[1 - e^{-\lambda_D T}\right] \qquad \ldots\ldots\ldots 6.24$$

and

$$B = b_K T + \frac{b_o}{\lambda_b}\left[1 - e^{-\lambda_b T}\right] \qquad \ldots\ldots\ldots 6.25$$

Also,
$$C = \frac{\sigma_D}{D} = \frac{(s+B)^{1/2}}{D} = \frac{(D+2B)^{1/2}}{D} \qquad \ldots\ldots\ldots 6.26$$

(neglecting σ_w)

Substituting 6.24 and 6.25 into 6.26 yields

$$C = \frac{\dfrac{d_o}{\lambda_D}\left[1 - e^{-\lambda_D T}\right] + 2b_K T + \dfrac{2b_o}{\lambda_b}\left[1 - e^{-\lambda_b T}\right]}{\dfrac{d_o}{\lambda_D}\left[1 - e^{-\lambda_D T}\right]} \qquad \ldots\ldots\ldots 6.27$$

C is a minimum when $\dfrac{dC}{dT} = 0$ and hence T optimum.

Differentiating 6.27 with respect to T and equating to 0 gives

$$\frac{d_o}{2\lambda_D}\left[1 - e^{-\lambda_D T}\right]\left(d_o e^{-\lambda_D T} + 2b_K + 2b_o e^{-\lambda_b T}\right)$$

$$= \left(\frac{d_o}{\lambda_D}\left[1 - e^{-\lambda_D T}\right] + 2b_K T + \frac{2b_o}{\lambda_b}\left[1 - e^{-\lambda_b T}\right]d_o e^{-\lambda_D T}\right) \qquad \ldots\ldots\ldots 6.28$$

This reduces to give

$$\frac{d_o}{2b_K} + \frac{2\lambda_D T}{1 + e^{-\lambda_D T}} + \frac{2b_o\lambda_D(1 - e^{-\lambda_b T})}{b_K\lambda_b(1 - e^{-\lambda_D T})} = e^{\lambda_D T} \qquad \ldots\ldots\ldots 6.29$$

If the background is purely constant then the decay constant λ_b is infinite and hence for a decaying source count upon a constant continuum 6.29 reduces to

$$\frac{d_o}{2b_K} + \frac{2\lambda_D T}{1 + e^{-\lambda_D T}} = e^{\lambda_D T} \qquad \ldots\ldots\ldots 6.30$$

Equations 6.29 and 6.30 are illustrated by the following example.

Consider a spectrum in which $b_o = b_K = 50$ c.p.m. and $d_o = 10$ c.p.m. Let $\dfrac{0.693}{\lambda_D} = 60$ mins and $\dfrac{0.693}{\lambda_b} = 120$ mins. This data is used to show the variation of C with T in equation 6.27. Fig. 6.9 shows a graph of C against T for a constant background and a decaying background component. Minima

Fig. 6.9

Calculated Example of A_E varying with T for Short Half Life Experiment

A = Case Calculated for Constant Background ($b_c = b_x$)

B = Case Calculated for Decaying Background ($b_t = b_x + b_o e^{-\lambda_L T}$)
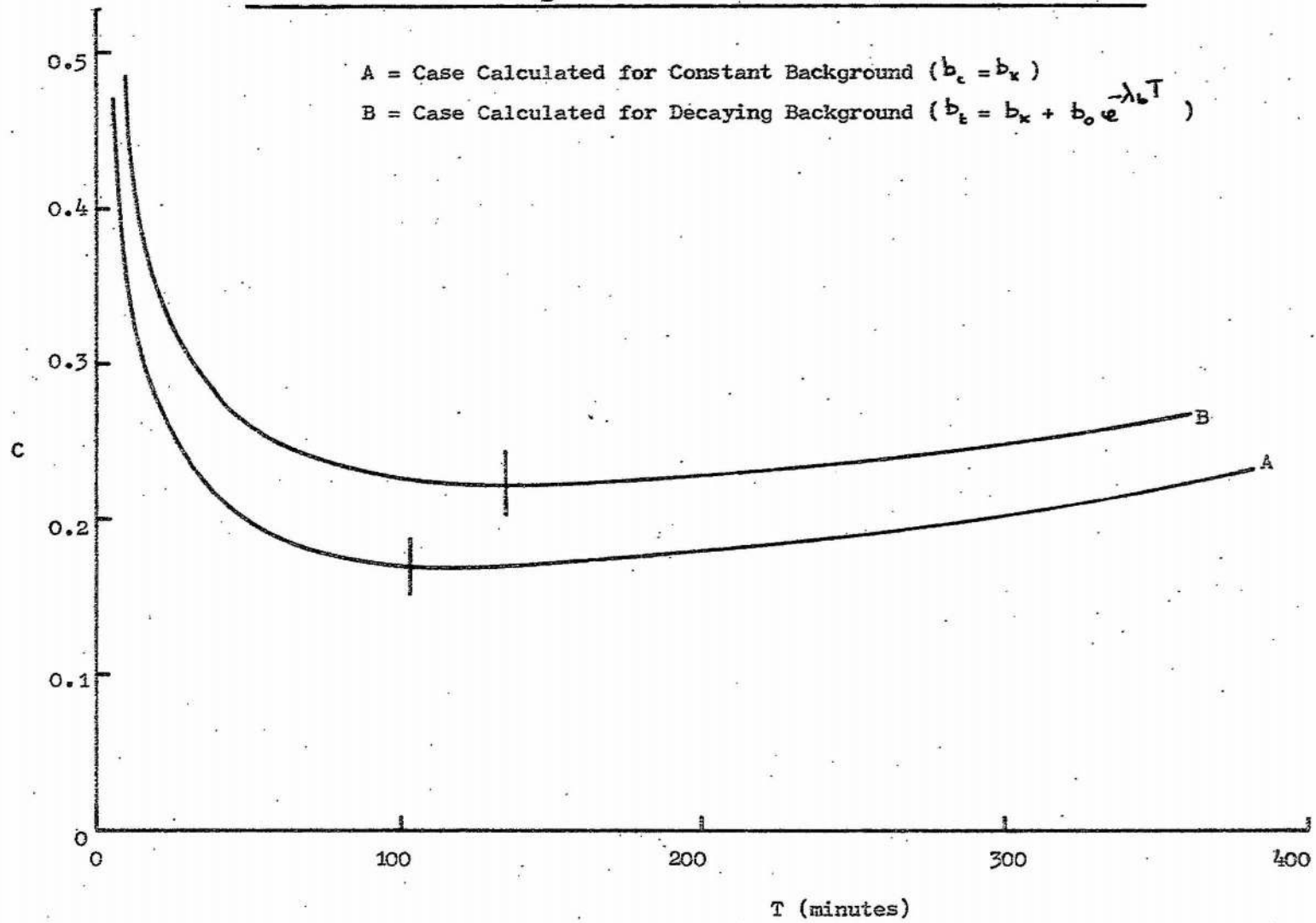
are observed at the values calculated from equations 6.29 and 6.30.

From Fig. 6.9, it will be observed that the minima are shallow so that provided the count time is approximately correct, the experimental precision will be optimum. Because of the shallowness of the minima, a limited number of differing half life isotopes may be counted in near optimum count time conditions.

Chapter 7

The Low Level Counting Capabilities of Ge(Li) Detectors

7.1 Introduction

The lowest level measurements performed with Ge(Li) detectors reported so far were carried out by Phelps, Hamby, Shore and Potter (1968), Potter et. al. (1968), Cooper, Wogman, Palmer and Perkins (1967) and most recently by Lewis and Shafrir (1971) who attained levels of the order of several pCi, using a mixture of massive shielding and anticoincidence shielding. There have also been several low level applications, such as that by Aarkrog and Lippert (1967) who simply used an unshielded Ge(Li) detector to measure fallout samples from the Chinese nuclear tests.

Several counting techniques are applicable to both NaI(Tl) and Ge(Li) systems. The low level counting capabilities of scintillators have been well investigated and described (Watt and Ramsden 1964 and Shafroth 1967). Sonntag (1967) and Nielsen and Perkins (1967) have established very low level spectrometers measuring picocurie activities. However, the systematic optimisation of Ge(Li) detectors for low level counting has not been described to date. Such an evaluation has been performed in this chapter by use of the following criterion. If the introduction of a particular counting technique (i.e. coincidence instead of singles counting) is to be advantageous, then an improved sensitivity must be observed for the same C and T for that source. In many cases, this is determined by application of equation 6.5. A_E is calculated for the Ge(Li) detector in the initial configuration. A_E is then recalculated for the introduction of the new technique under the same source conditions. The ratio of the two must be at least unity and in practice considerably greater to account for the additional expense incurred. The advantage gained by using new equipment should be substantially better than that gained simply, say, by an increase of count time with the initial technique.

7.2 The Use of Massive Shielding for Ge(Li) Detectors

The use of high Z materials to shield detectors from natural and cosmic radiation is the most common and readily applicable technique. Very little detailed information is available on shielding of Ge(Li) detectors and hence experimental work was undertaken.

Fig. 7.1a
Shield Arrangement for the 0.6 cm3 and 20 cm3 Detectors

Small Cable Duct

Shield shaped round Cryostat

Nitrogen Dewar

NaI(Tl) Detector Assembly

3.76 cm dia.

0.6 cm^3 and then 20 cm^3 Ge(Li) Detector

Preamplifier

2.5 cm

7.5 cm

Lead Shield

153
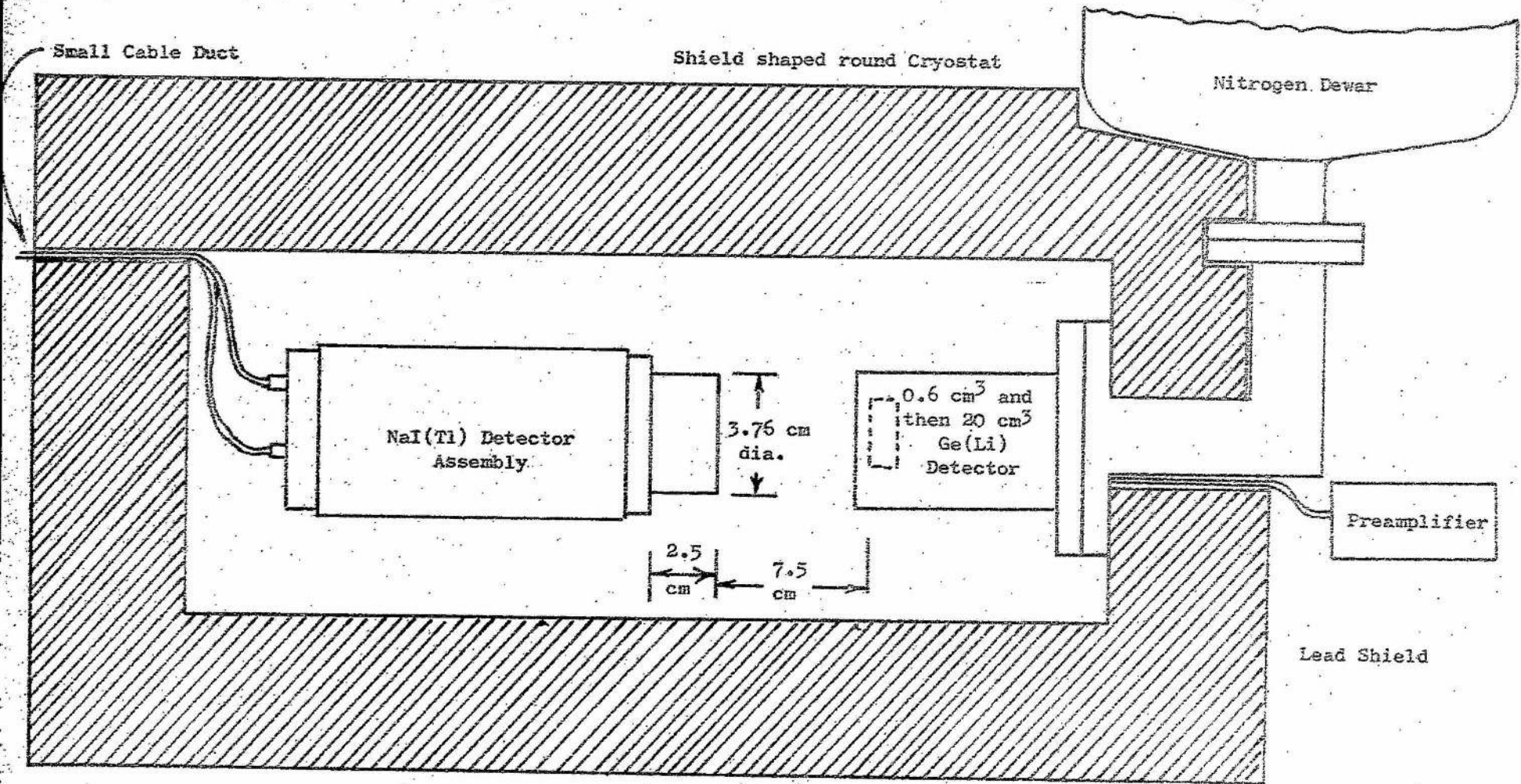
Fig. 7.1b

Shield Arrangement for the 7.4 cm^3 Detector

Preamplifier

Lead shaped
round Cryostat

Iron
support
plate

7.4 cm^3
Detector

7.5 cm

NaI(Tl) Detector
as in Fig. 7.1a

cable duct
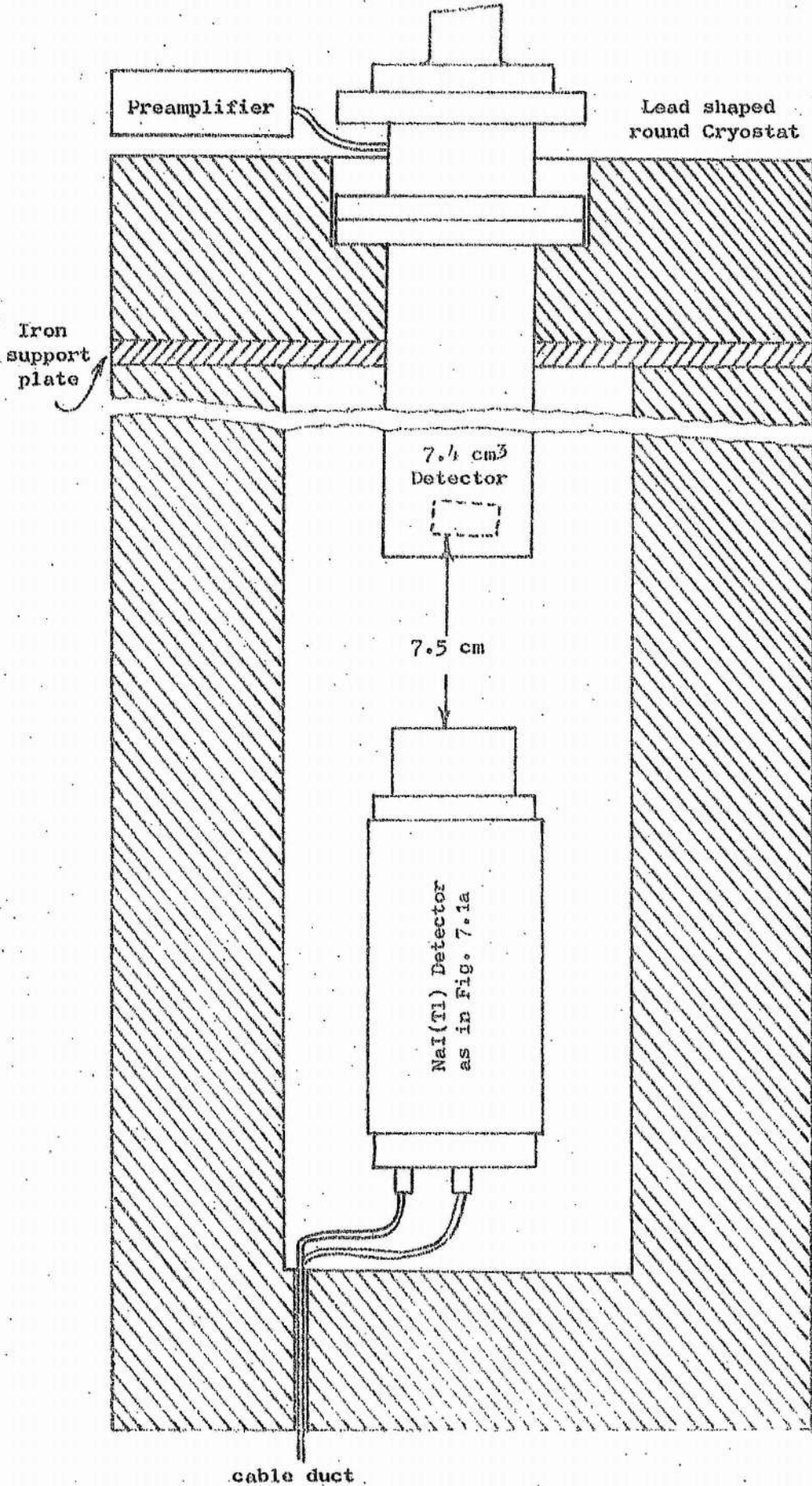
7.2.1 General Requirements

In principle, the shielding studies undertaken with other types
of detectors should be applicable to semiconductor detectors. For measure-
ments in this laboratory lead has formed the basis of shield construction.

The unavoidable use of a cryostat provides an inherent shielding
problem. This entails either complete enclosure of the assembly or the
use of a cryostat with a long cold finger to insert into a low background
enclosure. Either method might result in degraded background levels due
to active materials in the cryostat, especially ^{40}K in the dewar insulation
(Ridley 1967) or penetration of radiation into an incompletely shielded
enclosure. Of the two techniques, the latter is preferred due to the
smaller bulk to shield and the easier task of liquid nitrogen filling.
In addition, the material contamination of the part of the system within
the enclosure is more easily controlled by suitable selection of manufactur-
ing materials.

7.2.2 Experimental Reductions Obtained with Lead for Ge(Li) and NaI(Tl) Detectors

Reproducibility of background levels and reductions between
laboratories are frequently impractical so that for this experiment, the
spectra obtained with Ge(Li) detectors have been compared with those from
a 3.75 cm dia. x 2.5 cm thick NaI(Tl) scintillator in the same enclosure.

Measurements have been undertaken with three Ge(Li) detectors of
0.6, 7.4 and 20 cm^3 nominal sensitive volumes. The same cryostat was used
in each case except for the 7.4 cm^3 detector, installed in the dripfeed
cryostat shown in Fig. 2.2. The NaI(Tl) detector was placed 7.5 cm from
the Ge(Li) detector to minimise interacting scatter. Fig. 7.1a shows the
experimental arrangement adopted for the 0.6 cm^3 and 20 cm^3 detectors while
Fig. 7.1b shows that for the 7.4 cm^3 detector. Spectra were taken from
each detector after a change in the shielding thickness.

7.2.2.1 Results for the 3.75 cm dia. x 2.5 cm thick NaI(Tl) Scintillator

Spectra were taken from each detector as the shielding thickness
was increased in steps from 0 to 10 cm of clean lead. Fig. 7.2 shows the
background spectra obtained for the scintillator up to 2.5 MeV. The total
count rate up to 2.5 MeV is high in comparison with other laboratories,
being a factor of 8 up on counts recorded by Miller, Marinelli, Rowland

p.6

Fig. 7.2

Background Reduction Obtained for the 3.75cmX2.5cm thick NaI(Tl) Detector

(T = 4 hours)

1.46 MeV

0.662 MeV

Counts

No Shield

10% Lead

Energy (MeV)

157

Fig. 7.3

Background Reduction Obtained for the 0.6cc Ge(Li) Detector
in the Same Environment as the Scintillator (Fig. 7.2) (T = 15 hours)

No Shield

Counts x 10⁻¹
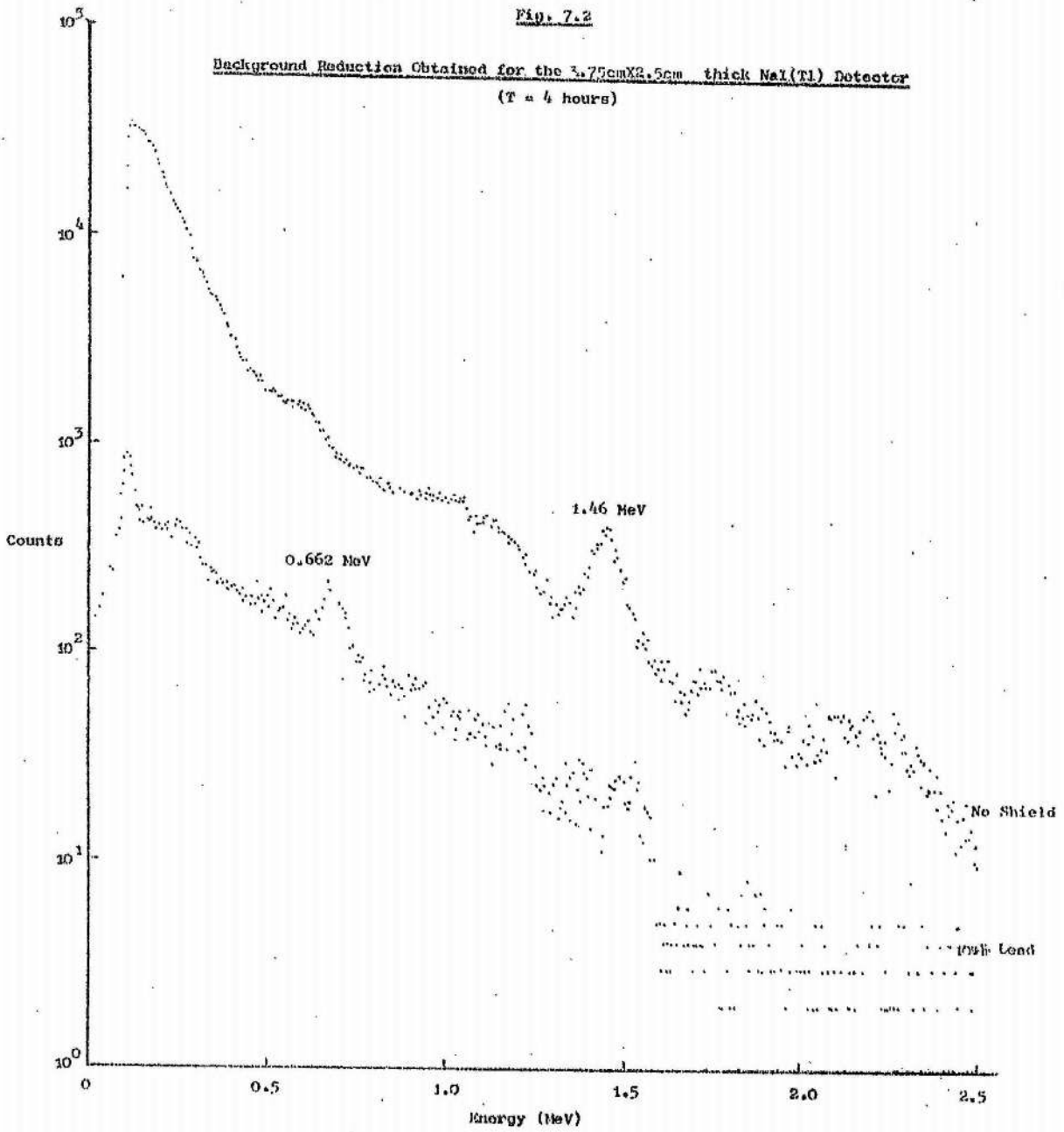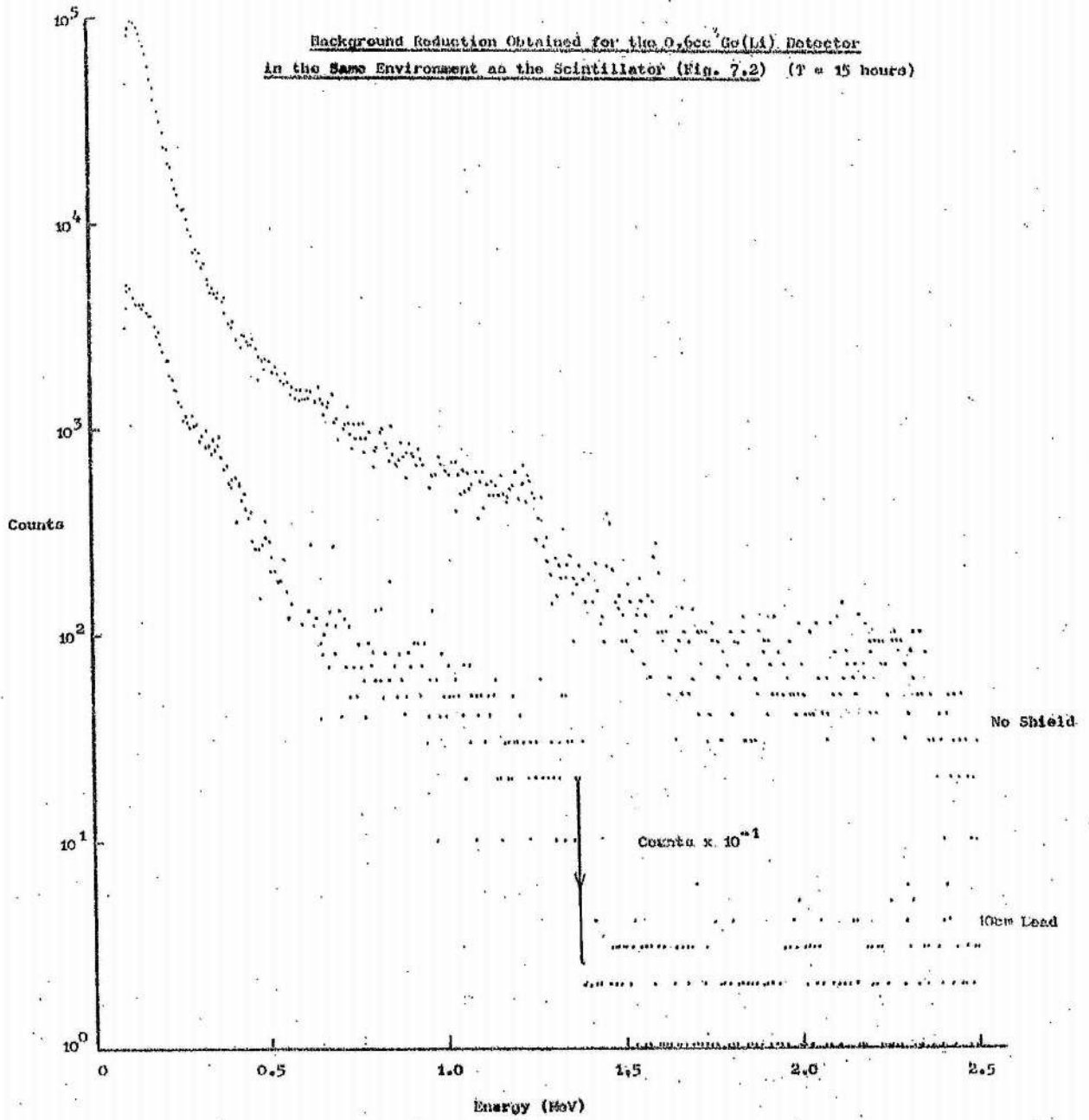
10cm Lead

Fig. 7.4

Variation of L for the 0.6 cm³ Ge(Li) Detector and the Scintillator

(from Figs. 7.2, 7.3)

L

11.10

9.1

2.5

10cm Clean Lead

5cm Clean Lead

5cm Unclean Lead

Main Isotopes Removed
from Store

No Background   shield

0-0.25   0.5 -0.75   1-1.25   1.5-1.75   2.0-2.25   2.25-2.5
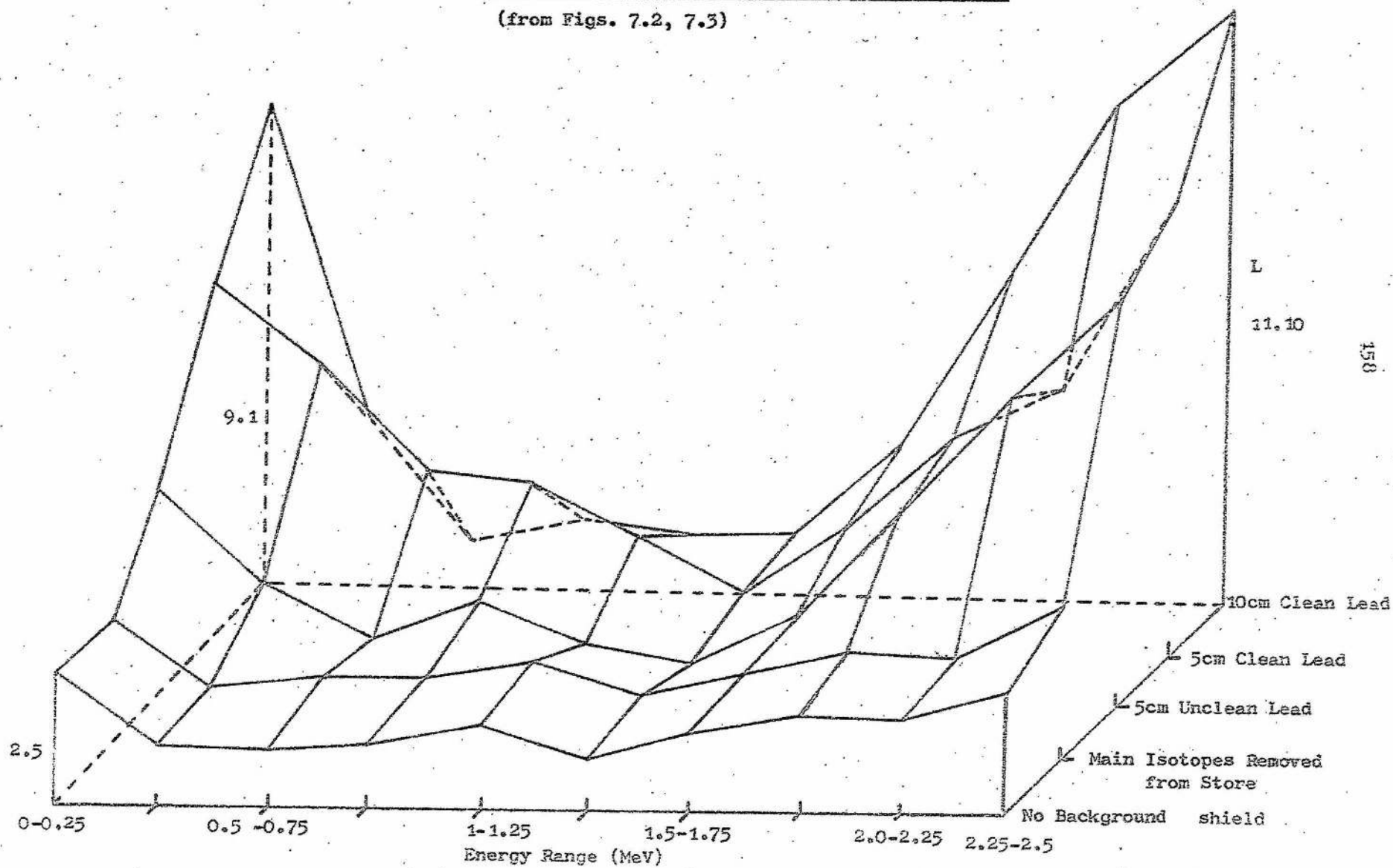
Energy Range (MeV)

Fig. 7.5

Comparison of Backgrounds of the $7.4cc^3$ Ge(Li) and NaI(Tl) Detectors
for 5cm Lead Shielding (T = 10 hours)
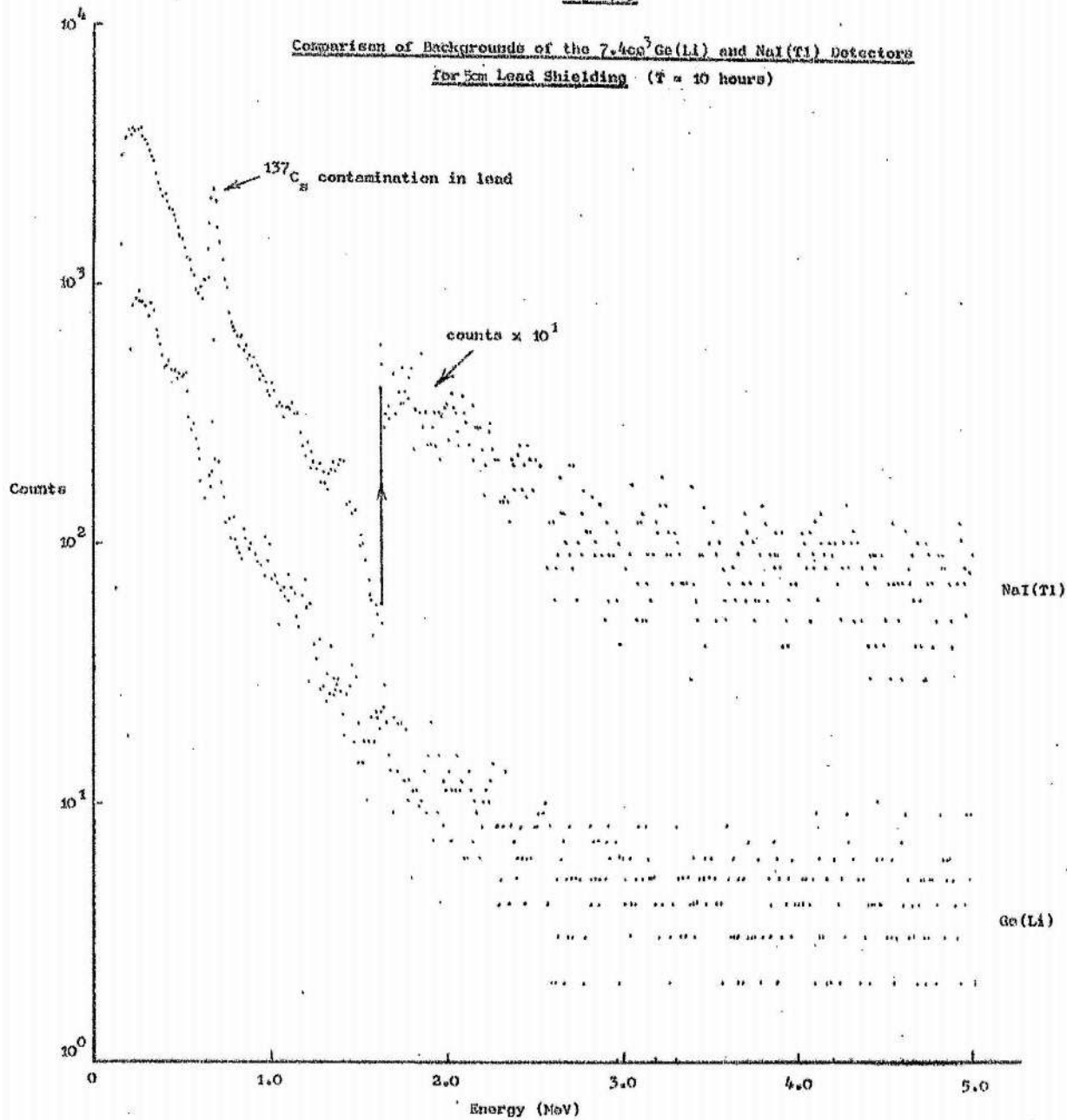
Fig. 7.6

Variation of L for the 7.4 cm^3 Detector and the Scintillator

Energy (MeV)
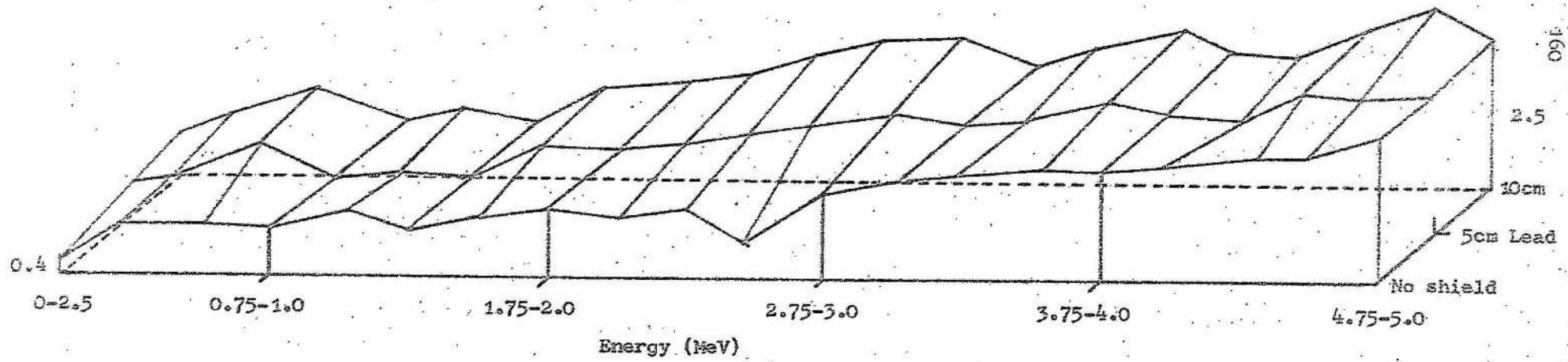
and Rose (1956) for the same size detector and energy range. This is attributed to the location of the laboratory and a nearby isotope store. However, the overall reduction obtained compares favourably, giving a total count rate reduction factor of 22 from 3810 cpm to 150 cpm. The origins of the peaks appearing in the reduced spectrum are probably due to contaminants in the lead used.

7.2.2.2 Results for the Ge(Li) Detectors

The results were, as far as possible, obtained in similar conditions to the scintillator. Fig. 7.3 shows the background recorded for the 0.6 cm^3 detector. The total background count for a 2.5 MeV energy range was reduced by a factor of 11 from 170 cpm, with no shield, to 15 cpm with 10 cm lead.

Parker (1969) uses counts/cm^3/ unit time/unit energy to specify a low level environment. This may be used in this instance to effect a comparison between the scintillator and the semiconductor by comparing their count rates per cm^3 of sensitive volume for equivalent energy ranges. Fig. 7.4 is a graph of the variation of the ratio L for different energies and shielding conditions for the 0.6 cm^3 detector and the scintillator,

where $L = \dfrac{\text{counts/cm}^3\text{/min/.25 MeV measured by the Ge(Li) detector}}{\text{counts/cm}^3\text{/min/.25 MeV measured by the NaI(Tl) detector}}$

It is observed that the Ge(Li) detector has a higher count rate per unit volume than the scintillator for all energies up to 2.5 MeV.

The experiment was repeated with the 7.4 cm^3 crystal (Fig. 7.1b). Fig. 7.5 shows the background recorded for 5 cm lead shielding compared with the scintillator in the same enclosure and with the energy range extended to 5.0 MeV. Some ^{137}Cs contamination in the lead is evident. L was plotted for this detector as for the 0.6 cm^3 detector and is shown in Fig. 7.6. The total background count rate dropped a factor of 15 from 382 cpm to 25 cpm (Table 7.1). This detector shows smaller L values than those for the 0.6 cm^3 detector and less variation with energy for the 10 cm shield thickness.

The above experiment was also repeated for the 20 cm^3 Ge(Li) detector. Fig. 7.7 shows the background spectra with the energy range extended to 5.0 MeV to observe higher energy background variations. Unfortunately, it was not possible to extend the energy range for the 0.6 cm^3

Table 7.1

Comparison of Background Reduction Factors for the Detectors Used

Detector	No Shielding (cpm)	10cm Lead (cpm)	Background Reduction Factor
NaI(T1) (29cm^3)	3810	150	22 over 2.5 MeV 20 over 5.0 MeV
Ge(Li) 0.6cm^3	170	15	11
* 7.4cm^3	382	25	15
* 20.0cm^3	759	53	14

* Compared over 5.0 MeV Range

detector since re-installation of this detector into the horizontal drip-feed cryostat was not feasible.   A background reduction of a factor of 14 was achieved with the total count rate changing from 759 cpm to 53 cpm for the 2.5 MeV range and similarly for the 5 MeV range.

Fig. 7.8 shows the variation of L for the 20 cm^3 detector over a range of 5.0 MeV for different shield thicknesses.   The variation in counts/cm^3 of sensitive volume is not as marked in this case as for the 0.6 cm^3 detector.

7.2.2.3   General Observations on Results

1) More effective background reductions are obtained for NaI(T1) than germanium for equivalent thicknesses of lead shielding (Table 7.1).

2) Some peaks observed by the germanium were not necessarily observed by the NaI(T1) (Fig. 7.7 compared with Fig. 7.2).

3) For the detectors used, the Ge(Li) detectors generally exhibit more counts per unit volume than the NaI(T1) in equivalent conditions.   The difference is dependant upon energy, shielding thickness and detector size.

4) It was found that substantial improvements in background counts were obtained when the lead bricks used had their faces sanded off which removed surface contaminants.

163

Fig. 7.7

Background Reduction Obtained for the 20cm³ Ge(Li) Detector in the
Same Environment as the Scintillator   (T = 10 hours)
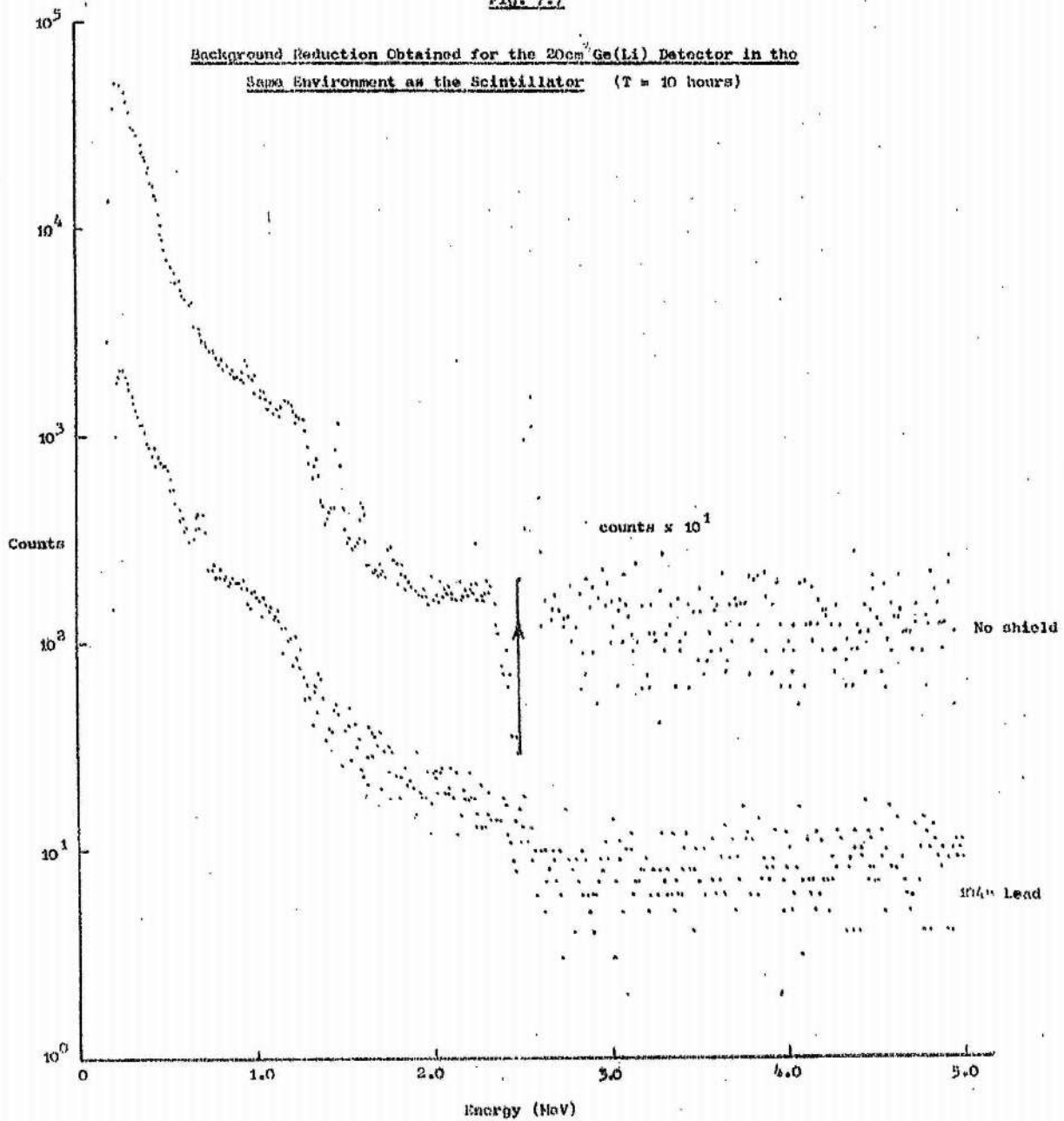
Fig. 7.8

Variation of L for the 20 cm³ Detector and the Scintillator

Energy Range (MeV)
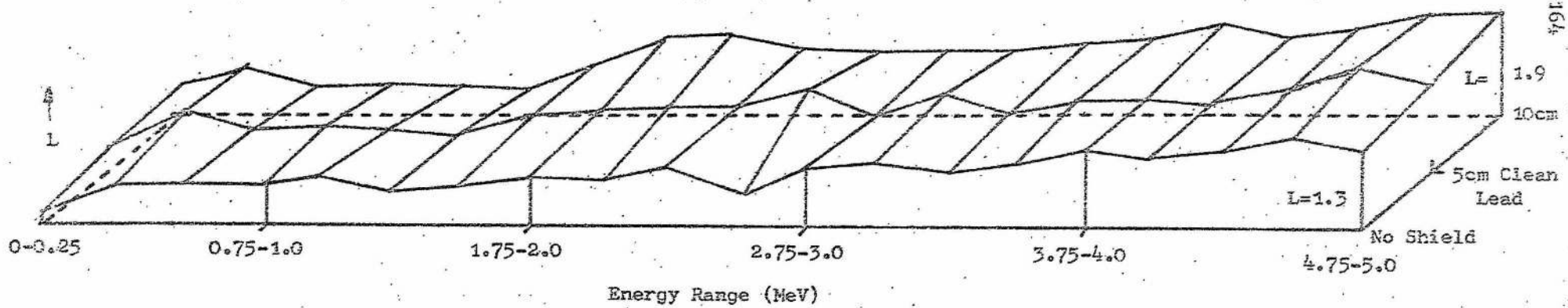
7.2.2.4 Discussion

For the 0.6 cm³ detector, observations 1) and 2) in section 7.2.2.3 infer an inherent noise source associated with the detector, not reducible by shielding. Observation 2) appears erroneous when it is considered that the use of germanium detectors demands high purity materials and that the higher efficiency NaI(Tl) detector should readily detect nearby contamination.

For the 0.6 cm³ detector, observation 3) is not consistent with the ratio of H.V.L. (Fig. 5.5) of germanium and NaI. However, for the 20 cm³ detector, whose dimensions are similar to the NaI(Tl) detector used, there is a rough consistency in results when compared with Fig. 5.5

The 7.4 cm³ detector gave variations of L that fell between that for the 0.6 cm³ and 20 cm³ detector. The explanation for this may lie with the incomplete shield surrounding the detectors and with the material thickness required to absorb a high energy cosmic particle. Application of shielding will remove most of the environmental radiation so that the remainder is associated with the shield and detector contaminants and high energy penetrating particles interacting directly with the detector or in the shield. A high energy particle (E > 10 MeV) may only deposit part of its energy in a detector if insufficient sensitive material is available. The resulting pulse is superimposed on the lower energy part of the background spectrum giving extra counts at lower energies and fewer at higher energies. For thicker detectors the effect would be smaller and occurring at higher energies. The smaller the detector the greater the likely effect.

From an investigation of the leakage current in a Ge(Li) detector Armantrout (1966) has pointed out that pulses could be generated by a detector due to sudden minor surface breakdowns giving charge pulses. The onset of these pulses may be well before a general voltage breakdown point. This should result in pulses at the lower energy end of the spectrum. This will also be dependant upon the particular surface treatment and hence vary greatly between detectors.

7.2.3 Improvements in the Minimum Acceptable Activity Using Massive Shielding

The use of massive shielding always improves A_E since B is reduced while the other parameters remain constant.

Fig. 7.9

Variation of A_E with Shielding and Energy for the Detectors Used
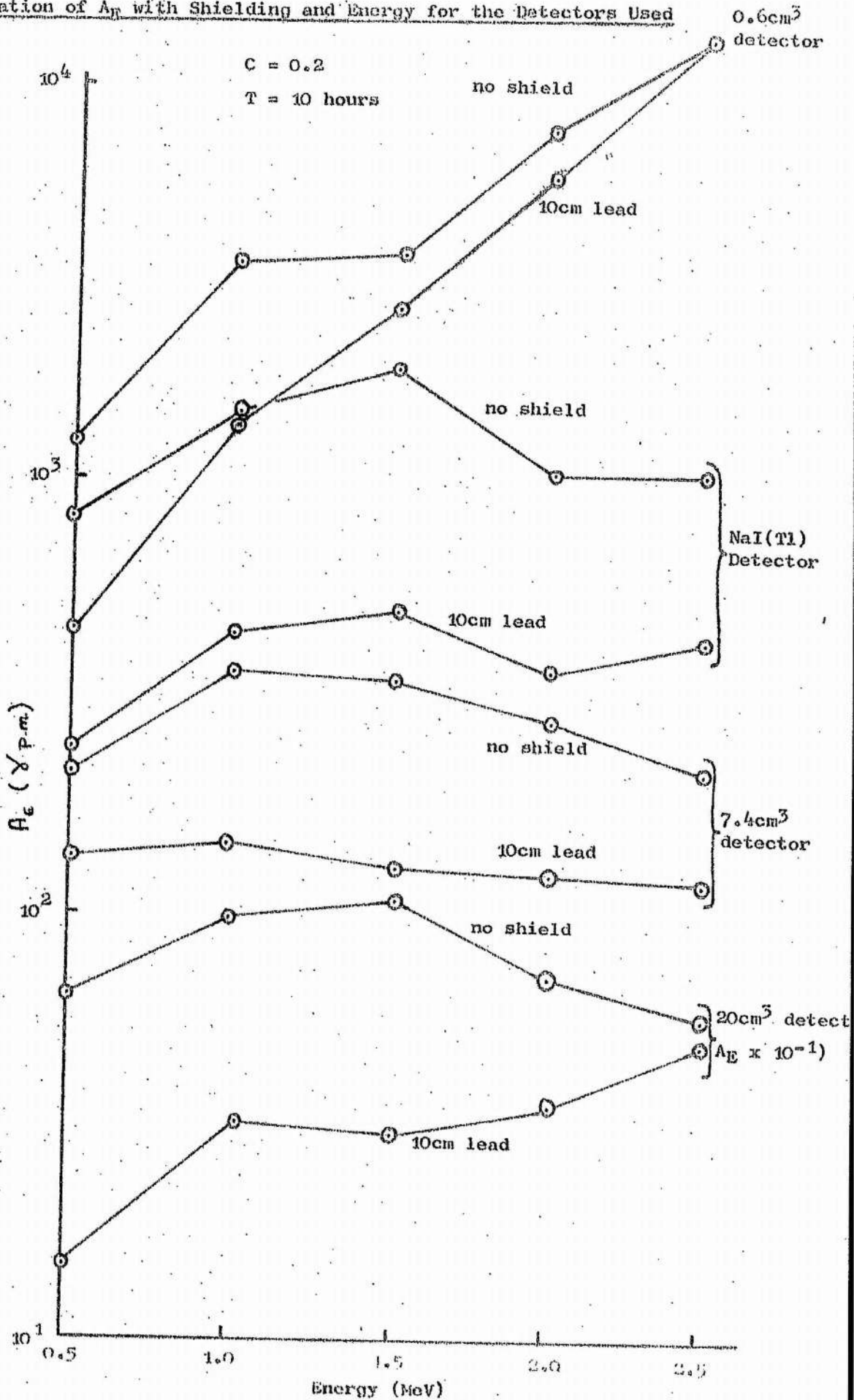
From a knowledge of the background levels measured in sect. 7.2.2, the values of $\in_{PA}$ for the detectors used and their energy resolutions, the improvements in sensitivity limits may be calculated. A_E was calculated for various energies before and after the application of shielding. Fig. 7.9 shows the variation obtained for a count time of 10 hours and C = 0.2. The following observations are made on Fig. 7.9:-

1) A large drop in background does not result in a correspondingly large drop of detection limits (Tables 7.1 and 7.2).

2) The shielding is most effective at lower energies ($>$ 1.5 MeV).

3) The lower efficiencies at higher energies for smaller detectors are compensated by lower background counts and superior energy resolution. This may be appreciated by consideration of Table 7.2 and Fig. 7.9 which show only a maximum reduction factor of four in A_E at 0.5 MeV between the shielded detectors, in spite of large differences in $\in_{PA}$.

<div align="center">Table 7.2</div>

<div align="center">Sensitivity Predictions for the Detectors Used</div>

Detector	Energy Resolution (keV)	$\in_{PA}$ at ^{137}Cs	Reduction Factor in A_E at 0.50 MeV
NaI(Tl)	93	.002	3.5
0.6cm^3	3	.00005	2.3
7.4cm^3	4.5	.0008	1.7
20.0cm^3	17	.00065	4.0

The results of Table 6.4 were obtained for the 7.4 cm^3 detector in the shield described in section 7.2.2.

7.2.4 Results Expected for Larger Detectors

The advent of higher performance detectors with $\in_{PA}$ exceeding that of 3.75 cm dia x 2.5 cm thick NaI(Tl) detectors allow sensitivity limits well below those demonstrated in Fig. 7.9 to be achieved. Consider A Ge(Li) detector with $\in_{PA}$ similar to that of the NaI(Tl) used and an energy resolution of 2.0 keV. Fig. 7.10 shows a graph of the variations

Fig. 7.10

A_E Calculated for Higher Quality Detectors

$C = 0.2$

$T = 10$ hours

solid counter

well counter

A_E (γ p.m.)

Energy (MeV)
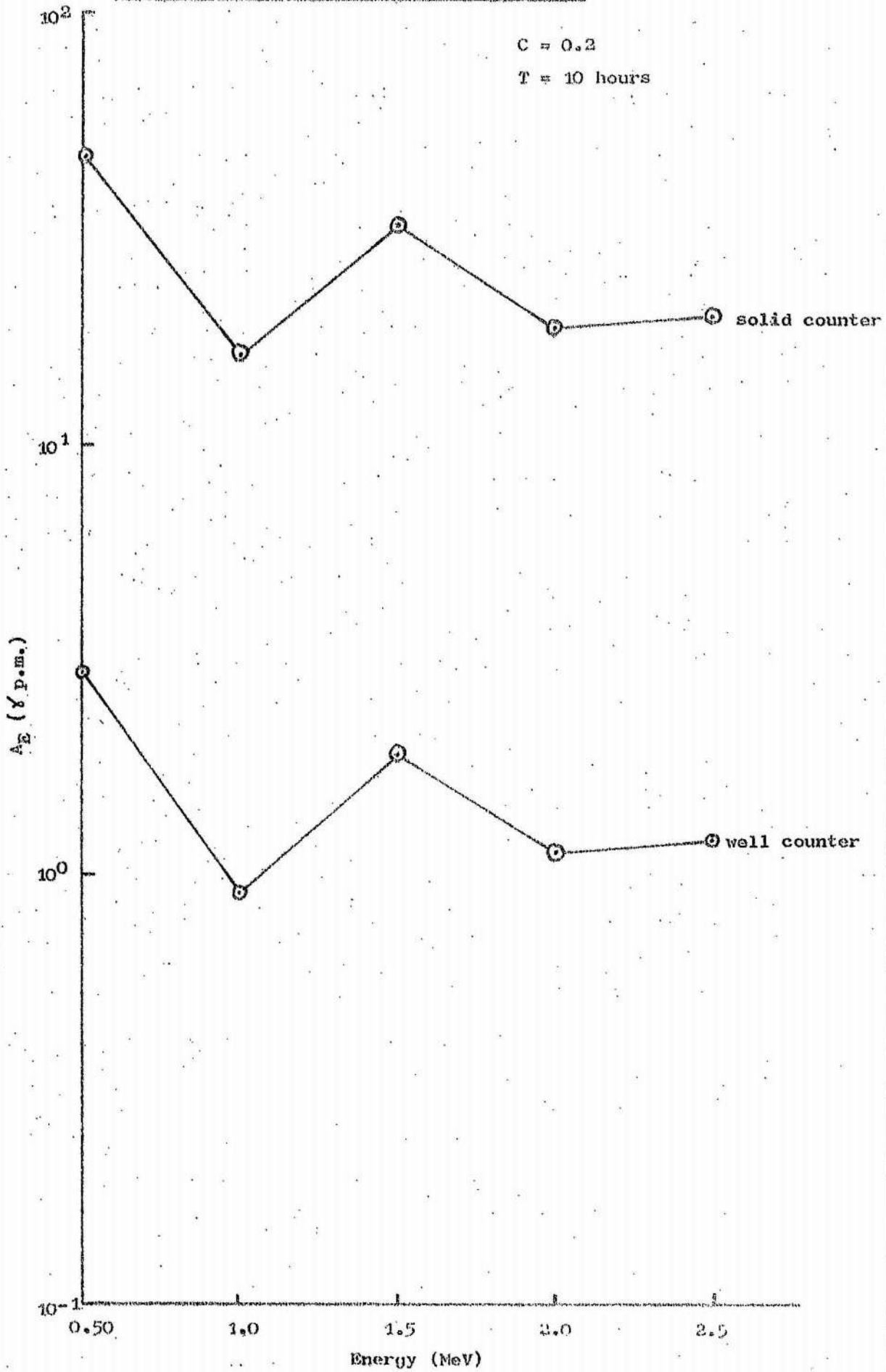
of expected sensitivity with energy assuming the same background as for
the NaI(Tl) detector.   The upper line represents sensitivity limits for
a conventional Ge(Li) detector.   The lower line represents sensitivity
limits for a coaxial well counter exhibiting a greater absolute efficiency
though of similar active volume.   For the background levels measured,
activity measurements of a few pCi are possible (1 pCi = 2.2 γpm assuming
1 γ emitted per disintegration).   Background reductions of a factor of
50 - 100 should be possible so that the above detectors in improved
environments should have improved sensitivity levels.   Cooper, Rancitelli
and Perkins (1969) have succeeded in detecting 1 pCi of ^{137}Cs in 4000 min
count time with a similar detector to the solid one of Fig. 7.10.

Accurate prediction is difficult but it is evident that large
($>$ 50 cm^3) high resolution detectors carefully designed should be capable
of accurately measuring several pCi in times of 10 hours.

These results agree with those of Phelps et. al (1968), Cooper
et. al. (1968), Potter (1969) and Lewis et. al. (1971) who have measured
activities in the range 2 - 40 pCi of ^{137}Cs for small ($<$ 10 cm^3) sources.
Unless longer counting times can be tolerated ($>$ 2000 minutes) sample
reduction appears unavoidable if limits of less than 10 pCi total activity
for C = 0.1 are desired.

7.3   The Use of Coincidence Techniques in Improving Sensitivity Limits

Coincidence techniques are useful for determining gamma-gamma or
particle-gamma events in a high random background count rate.   The technique
has been used with Ge(Li) detectors with some success (Malm, Tavendale and
Fowler 1965, Ewan, Graham, McKenzie 1966 and Ostertag, Miehe, Henck and
Siffert 1968).   However, the loss of counting efficiency (Shirley 1968)
has restricted their use to medium activity ($\sim$ 1μCi - 50 μCi) measurements.
This section evaluates the use of the technique for lower level measurements.

7.3.1   Conditions for Coincidence Counting

A minimum of two detectors are required depending upon the number
of coincident emissions. α - γ, β - γ, or γ - γ measurements may
be undertaken satisfactorily by suitable selection of the appropriate detec-
tors and isotopes.   The same counting principles apply to all coincidence
measurements.   Consider the case for two detectors:-

Let τ = coincidence resolving time of the apparatus,

B_1 = background count under the peak in time T in the singles mode for detector 1,

B_2 = background count under the peak in time T in the singles mode for detector 2.

Then in the coincidence mode, the accidental coincidence count rate is B_c

where $B_c = \dfrac{2\,B_1 B_2\,\tau}{T}$ .... 7.1 - Wapstra (196

B_c assumes only random background counts and hence assumes the best case. If one detector has no energy discrimination, then B_1 is extended to represent the total count.

If ϵ_{PA1} = absolute full energy peak efficiency at energy E_1 for detector 1 and ϵ_{PA2} = absolute full energy peak efficiency for detector 2 at energy E_2 of interest

Then the efficiency in the coincidence mode assuming no spatial correlation

is $\epsilon_c = \epsilon_{PA1}\,\epsilon_{PA2}^{*}$ .... 7.2 - Wapstra (1966)

The use of equations 7.1 and 7.2 allows the calculation of the expected coincidence efficiency and background of the detectors before the experiment is performed. Hence effective prediction is possible.

The detector configuration adopted depends upon the angular correlation of the emitted particles. Due to the lowered counting efficiency (equation 7.2) the greatest possible attention should be paid to optimisation of the source-detector geometry yet without incurring multiple scatter between detectors (Giesler, McHarris, Warner and Kelly 1971).

7.3.2 Criteria for the Use of Coincidence Counting

As stated, the introduction of a new counting technique must result in an improvement in A_E for the same count time and statistical precision. For coincidence counting this criterion is easily determined.

If A_1 represents the minimum acceptable activity of a particular isotope for detector 1) in the singles mode then from equation 6.5,

$$A_1 = \frac{1}{\epsilon_{PA1} C T}\left(2 B_1 + \frac{1}{2 C^2} + \sigma_{w1}^2 + \frac{1}{2C}\left(8 B_1 + 4\sigma_{w1}^2 + \frac{1}{C^2}\right)^{1/2}\right)^{1/2} \qquad \ldots\ldots\ldots 7.3$$

and similarly for detector 2).

* assuming 100% gamma emission per disintegration

When detectors 1) and 2) are used in coincidence then the minimum acceptable activity in the coincidence mode is A_c where

$$A_c = \frac{1}{\epsilon_{p\theta 1}\epsilon_{p\theta 2}CT}\left(\frac{4T B_1 B_2}{T} + \frac{1}{2C^2} + \sigma_{cw}^2 + \frac{1}{2C}\left(\frac{16 B_1 B_2 T}{T} + 4\sigma_{cw}^2 + \frac{1}{C^2}\right)^{1/2}\right)^{1/2} \quad \ldots\ldots 7.4$$

by substitution of 7.1 and 7.2 into 6.5 where σ_{cw}^2 is the peak measurement variance under coincidence conditions.

Equation 7.4 determines A_c for a random background contribution and using the dual parameter analyser described in section 3.2.2. In the case where a single parameter analyser is used then the coincidence spectrum from one detector is observed using pulses received from the other detector system gated on to the relevant full energy peak. Equation 7.4 is modified when a background contribution containing coincident events is present.

Coincidence counting is advantageous if

$$\frac{A_1}{A_c} > 1 \quad \text{and/or} \quad \frac{A_2}{A_c} > 1 \qquad \ldots\ldots\ldots 7.5$$

In practice, this ratio should be substantially greater than 1 to justify the not inconsiderable cost of coincidence equipment. This is partly dependant upon the importance of the sample under test.

7.3.3 Sensitivity Limits with $\alpha - \gamma$ Counting

If the isotope being measured is the only α emitter, then the effective background count may be of the order of 1 count per hour. Hence to a good approximation, this contribution may be ignored resulting in a minimum acceptable activity of A_α where

$$A_\alpha \sim \frac{1}{\epsilon_\alpha C T}$$

$\ldots\ldots$ 7.6 from equation 6.5 where ϵ_α = absolute full energy peak efficiency of the α detector.

Using a germanium detector, in coincidence with the α detector, the criterion of equation 7.5 becomes

$$\frac{A_\alpha}{A_{c\alpha}} \text{ or } \frac{A_1}{A_{c\alpha}} = \epsilon_\alpha C\left(2B_1 + \frac{1}{2C^2} + \sigma_{w1}^2 + \frac{1}{2C}\left(8B_1 + 4\sigma_{w1}^2 + \frac{1}{C^2}\right)^{1/2}\right)^{1/2} > 1 \qquad \ldots\ldots\ldots 7.7$$

α - γ coincidence measurements have been undertaken with solid state detectors to improve the counting capabilities of the spectrometer, in particular by Borodetzky, Merdinger, Armbruster (1966), Nelson and Zyskowski (1966) and Lalovic, Ajdacic, Pai and Petrovic (1966). As a demonstration of the technique the small Ge(Li) detector (0.6 cm^3 active volume) was used in the configuration described in section 3.2.2 to measure ^{241}Am by γ counting and by α - γ coincidence counting. For the 60 keV gamma rays and C set to 0.2 and T = 10 hours the minimum acceptable activity was 830 pCi in the singles mode and with no massive shielding. Coincidence counting was then performed by the addition of a silicon surface barrier detector for which ϵ_α = 0.3. $\epsilon_{P\beta}$ for the 0.6 cm^3 detector was 0.01 at 60 keV giving $\epsilon_{c\alpha}$ =.003. For the same C and T, A$_c$ was found to be 15 pCi, giving an improvement factor (equation 7.7) of 55.

The high counting efficiency of the surface barrier detector for α particles results in this being an effective low level technique for Ge(Li) detectors. If the silicon detector alone were used to detect the α particles then, in the above conditions, A$_\alpha$ $\sim$ 0.15 pCi which is much lower than A$_1$ or A$_c$ (assuming adequate source preparation). The criterion of equation 7.7 would indicate that for this particular measurement, the silicon detector is the best choice, unless the α - γ transition or γ energy were of particular interest. These results are degraded if additional particle backgrounds are present although the high α efficiency should still result in a substantial improvement.

7.3.4 Sensitivity Limits with β - γ Counting

β - γ emitters are very common radionuclides. Low level spectrometry with β - γ coincident measurements has been undertaken, by Englert Everling, Eakins and Hatch (1966) and Rodel (1968) using scintillators. The criterion for its advantage is similar to that of section 7.3.3. However the natural background of β particles is much greater than that of α particles.

Assuming that the β detector (of absolute efficiency ϵ_β) is used purely to effect coincidence counting, no background coincident events are present, and the results are measured from the Ge(Li) spectrum, the minimum acceptable activity of the Ge(Li) detector in the coincidence mode is A$_{c\beta}$ where

$$A_{c\beta} = \frac{1}{\epsilon_{P\beta}\epsilon_\beta CT}\left(\frac{4TB_1B_\beta}{T} + \frac{1}{2C^2} + \sigma_{c\beta w}^2 + \frac{1}{2C}\left(\frac{16B_1B_\beta T}{T} + 4\sigma_{c\beta w}^2 + \frac{1}{C^2}\right)^{1/2}\right)^{1/2}$$

and where σ^2_{cpw} is the measurement variance for the coincident peak,

yielding the criterion of $\dfrac{\beta_1}{\beta_{c\beta}}$ and/or $\dfrac{\beta_\beta}{\beta_{c\beta}} > 1$

It is possible for ϵ_β to approach 0.5 if source absorption is small. The resulting coincidence efficiency can then approach $0.5\epsilon_{p\beta_1}$. As background reductions greater than a factor of 10^4 are often possible with coincidence counting then, where applicable, the introduction of the technique generally yields substantial improvements.

Assuming a substantial background reduction is achieved, then the expression for $A_{c\beta}$ may be approximately rewritten as

$$A_{c\beta} \, \nu \left(\epsilon_{p\beta_1} \, \epsilon_\beta \, C^2 T \right)^{-1} \qquad \qquad \ldots \ldots 7.8$$

Substitution of typical values (say $\epsilon_\beta = 0.33$, $\epsilon_{p\beta_1} = 3 \times 10^{-3}$, $C = 0.2$ and $T = 600$ minutes) gives $A_{c\beta}$ reaching easily obtainable values of ν 40 coincident events per minute, which could represent activities as low as ν 20 pCi.

With the appropriate isotopes and source preparation, this technique shows promise for low level measurement for appropriate sources and source preparation.

7.3.5 Sensitivity Limits with γ - γ Counting

γ - γ counting with Ge(Li) detectors, has been used for medium activity measurements, Ostertag, Miehe, Coche (1968), Ewan et. al. (1966), Palms, Venugopala, Wood (1968) and Malm et. al. (1965), with some success. However, the low coincidence efficiency using two Ge(Li) detectors places severe limitations on the coincidence count rate, and coincidence measurements have been performed by replacing one of the Ge(Li) detectors with a NaI(Tl) scintillator (Ramayya 1966 and Miehe et. al. 1966) or a plastic scintillator (Chase 1968).

The criterion for the advantage of γ - γ coincidence counting is calculated as in section 7.3.2. As an illustration of the problem of γ - γ counting, two Ge(Li) detectors (7.4 cm^3 and 20 cm^3 nominal volume) were used to measure the coincidence gamma rays from ^{60}Co. Table 7.3 shows the characteristics of the two detectors measured in the singles mode. The coincident events were measured using the experimental arrangement of section 3.2.2 with a resolving time of $\tau = 1\mu$ sec. Table 7.4 shows the experimental and predicted variations of efficiency and background in the

coincidence mode. The background count rate has been reduced by a factor of 70,000 for the 20 cm^3 crystal but has resulted in an overall loss of efficiency of a factor of 1600. In consequence, the minimum acceptable activity has been degraded from 40 nCi to 0.98 μCi, a factor of 25 (for T = 100 min and C = 0.1). This result could be improved with larger detectors and/or longer counting times in the lower energy range.

Table 7.3

Singles Chacteristics of Two Detectors Used for

Coincidence Measurement of ^{60}Co

Detector	Efficiency	Background* count under peak	Case 1 A_E (T=100 min C=0.1)	Case 2 A_E (T=600 min C=0.2)	Resolution
7.3 cm^3	1.17 MeV .0006	473 cpm	23.5 nCi	4.7 nCi	5.0 keV
	1.33 MeV .00052	397 cpm	25.1 nCi	4.8 nCi	5.0 keV
20.0 cm^3	1.17 MeV .00090	2467 cpm	35.9 nCi	8.2 nCi	17.0 keV
	1.33 MeV .00076	2309 cpm	41.0 nCi	8.5 nCi	17.0 keV

* Artificially high with interfering sources

Unless excessive (10^4 to 10^5 counts per second) interfering background count rates are encountered, detectors of this efficiency are not suitable for coincidence counting below 1 μCi for count times of less than 100 min and 50 nCi for 10 hour count times. For larger background reductions, the resolving time τ may be improved by two orders of magnitude to a few nanoseconds (Pigneret, Samueli and Sarazin 1966, Graham, McKenzie and Ewan 1966, and Balland, Pigneret, Samueli and Sarazin 1968). In this circumstance, the random count rate may almost be neglected provided that there are no interfering peaks or scatter between crystals. In this case the sensitivity limit $A_{c\gamma\gamma}$ varies as

$$A_{c\gamma\gamma} \sim \left(\epsilon_{pa1} \epsilon_{pa2} C^2 T \right)^{-1}$$

.... 7.9

Table 7.4

Results of the Two Detectors in the Coincidence Mode

Peak	Experimental Background	Predicted Background	Experimental Efficiency	Predicted Efficiency	Case 1 A_c (T=100 min C=0.1)	Case 2 A_c (T=600 min C=0.2)
1.17 MeV in 7.4 cm^3 1.33 MeV in 20 cm^3	0.026 cpm	0.033 cpm	0.55×10^{-6}	0.46×10^{-6}	0.98 μCi	62 nCi
1.33 MeV in 7.4 cm^3 1.17 MeV in 20 cm^3	0.0396 cpm	0.036 cpm	0.56×10^{-6}	0.47×10^{-6}	0.96 μCi	60 nCi

		7.4 cm^3 Det.	20 cm^3 Det.
Background reduction factor	=	13,000	70,000
Efficiency reduction factor	=	1,200	1,600
A_E degradation factor (Case 1)	=	40	25
A_E degradation factor (Case 2)	=	13	7

7.3.6 Discussion

The loss of efficiency in the coincidence mode dominates the choice of a coincidence technique to measure a weak activity. This is particularly so for $\gamma - \gamma$ measurements with two Ge(Li) detectors where the sensitivity may be seriously reduced. The situation can be improved by using a scintillator instead of one of the Ge(Li) detectors to improve A_c.

$\alpha - \gamma$ and $\beta - \gamma$ coincidence counting, where appropriate, can offer low sensitivity limits due to the large background reduction while maintaining reasonable values of $\epsilon_{c\alpha}$ and $\epsilon_{c\beta}$ provided suitable source preparation is possible.

In general, coincidence techniques are used where there is a large interfering source generated background whereas massive shielding is used when the source total activity is small and natural background dominates. Calculation with equations 7.1 - 7.9 are a guide to the choice of technique.

7.4 The Effectiveness of Pulse Shape Discrimination

The technique, first introduced to semiconductor detectors by Funsten (1961), has met limited use in some laboratories. The technique operates by rejecting slow rise time pulses from the detector, which are generally due to charge loss and cause spectrum degradation.

7.4.1 Background Reduction Obtained

The potential reduction obtainable is dependant upon the particular detector used. The poorer the quality of the detector, the greater the reduction expected with this technique. Widely varying results have been reported. Michaelis and Schmidt (1966) and Tamm, Michaelis and Coussieu (1967) obtained background reductions of a factor of three, while Abe, Kawamura and Mutsuro (1968) and Swinth, Phillip and Hoitink (1968) obtained factors of improvement of 0.2 to 0.3 over an energy range 300 - 1800 keV. They also found that the reduction was significant only up to 0.7 of the energy of the peak being examined. Strauss, Larsen and Sifter (1966) demonstrated reduction factors of 2, independant of energy. The reductions achieved in this laboratory (Parish 1969) are energy dependant, being about 0.2 for most energies, increasing to 4 at lower energies (100 keV).

7.4.2 The Sensitivity Limit Improvements Obtainable

The application of pulse shape discrimination always results in an

improvement in sensitivity as B is reduced with no degradation of the other parameters. In the application of pulse shape discrimination, no loss of counting efficiency should be observed. Using the improvement factors of section 7.4.1 sensitivity improvements are calculable and may be separated roughly into two categories:-

1) $2B \gg \frac{1}{2C^2}$. In this case (high background conditions) a change in B dominates the other parameters and equation 6.5 may be considered roughly as

$$ A_E \sim \frac{1}{\epsilon_{PR} C T} \sqrt{2B} $$

.... 7.10

Considering the maximum published reduction factor of B reducing to $\frac{1}{3}B$ gives an improvement in A_E (for same ϵ_{PR} , C and T) of a factor of $\sim \sqrt{3}$.

2) $2B \ll \frac{1}{2C^2}$. In this case (low background conditions) a change in B causes only a very small change in A_E. Hence the technique is unsuitable for low level measurements.

7.4.3 The Significance for High Quality Detectors

Due to the rapid improvement in detector quality and size (in the past two years) available on the commercial market, the effectiveness of pulse shape discrimination as a background reduction technique is reduced. The potential sensitivity improvements are small compared with alternative techniques.

However, it should also be noted that this technique is the only one available that does not impede experimental access to the crystal. In addition, the technique is useful for diagnostic measurements on crystals and when combined with collimated gamma ray beam techniques, may be extended for various uses.

7.5 Anticoincidence Shields for Low Level Measurements

Anticoincidence shields have met several applications (Arnell, Hardell and Hasselgren 1966, Camp 1969, Cooper and Brownell 1967 and Lewis et. al. 1971) and are now a relatively common feature in the field of γ - ray spectroscopy. This section considers their effectiveness for low level activity measurements.

7.5.1 Basic Operational Conditions for Low Level Measurements

The anticoincidence shield serves the dual purpose function of the reduction of source generated Compton continuum in the detector and the rejection of some natural background events. The source placed inside the shield for optimum ϵ_{PR} results in the lowest level measurement (Wogman, Robertson and Perkins 1967 and Phelps et. al 1968). The continuum reduction is a mixture of Compton suppression and natural background suppression and for very low level measurements ($<$ 10 pCi) is dominated almost entirely by the latter.

The other major area of application is for activities $>$ 0.5 μCi where the source is external to the shield and collimated (Hasselgren 1966, Kantele, Martilla and Hattola 1967 and Grenier and Pousier 1968). These latter measurements used mainly for the Compton suppression mode) are often used for activation analysis and analysis of spent reactor fuel elements. While the principle of operation of the shield is similar for both high and low activity measurement, the results (through different continuum origins) require different considerations.

7.5.2 Internal Source Measurements

The use of anticoincidence shielding for weak activity measurements relies largely upon the effectiveness of the shield for natural background suppression. Phelps et. al (1968 and Cooper et. al (1968) have used anti-coincidence methods for weak activity measurements and typify the results generally obtained for internal source measurements. A general survey has been undertaken on these spectrometers by Camp (1969).

The shield itself has some natural shielding effect through the sheer bulk of the scintillator, but the main effectiveness is observed by measuring the background spectrum with the shield switched on and then off. The measurements of Cooper et. al. (1968) typify results with a 2ft. thick NE102 plastic phosphor. Table 7.5 shows the calculated improvements from Cooper's data as a function of energy for a constant C, ϵ_{PR} and T. When the main continuum contribution is from natural background then the sensitivity improvement is as in column (2). When there is a significant contribution from Compton scatter, then a greater reduction is achieved — columns (3) and (4).

The maximum improvement in sensitivity is roughly a factor of 4 or alternatively a factor of 4 improvement in precision is obtained for activity measurements up to 0.5 μCi.

Table 7.5

Approximate Improvements Gained by the use
(Cooper et. al. 1968) of a Large Plastic NE102 Shield

Energy (MeV)	(1) Reduction factor for natural background	(2) Sensitivity Improvement factor	(3) Compton Continuum Reduction Factor	(4) Sensitivity Improvement Factor
0.200	2.7	1.7	~	~
0.400	2.3	1.5	14.0	3.7
0.600	2.2	1.5	17.5	4.1
0.800	2.4	1.6	16.0	4.0
1.000	1.8	1.33	20.0	4.5
1.200	2.1	1.43	10.0	3.1
1.400	1.9	1.4	10.0	3.1
1.600	1.8	1.33	10.0	3.1

Internal source measurements can be complicated by the rejection of coincidence events as this results in partial suppression of coincidence gamma rays. The effective value of $\leqslant_{p\Omega}$ is reduced and this must be taken into account when determining the contribution of these isotopes. However, Camp (1969), Cooper, Rancitelli and Perkins (1969) and Cooper (1970) point out that this can have certain advantages in identification of unknown isotopes by preferential suppression of dominating isotopes, and in removal of escape peaks.

Very careful optimisation of anticoincidence techniques has resulted in the above workers obtaining 10 - 40 pCi measurements regularly and Cooper et. al. (1969) measuring as low as 1 pCi of [137]Cs.

7.5.3   External Source Measurements

The use of the shield with an externally placed source is generally restricted to higher activity sources due to the low $\leqslant_{p\Omega}$ inherent in this geometry. The dominant mode of suppression is largely Compton suppression.

A range of reductions have been reported for different shields which depend upon the design of the shield, the size of the Ge(Li) detector and the type of scintillator used. Reduction factors have varied from two

(Cooper and Brownell 1967) to sixteen (Kantele and Suominen 1966). Camp (1969) has observed that the reduction also depends significantly upon the ratio of sensitive to insensitive material in the Ge(Li) detector. The results of Cooper et. al. 1968 typify the reductions obtainable and Table 7.5 (columns (2) and (4)) shows the resulting reduction and the approximate sensitivity limit improvement derived from the use of the shield. In this case, the improvements gained are not affected by coincident gamma ray emissions as in the case of internal source measurements although escape peaks will still be suppressed.

Minimum acceptable activities for this arrangement are in the range nCi to μCi and hence is not suitable for very low level measurements.

7.5.4 The Combination of Anticoincidence and Pulse Shape Discrimination Techniques

The overall peak height to Compton edge ratio of an anticoincidence spectrometer is the product of the peak to Compton ratio of the detector and the reduction obtainable by the shield. Hence a 20:1 peak to Compton detector in a shield giving a 16:1 reduction factor results in an overall peak to continuum ratio of 320:1. The combination of pulse shape discrimination and anticoincidence shielding does not yield a similar product relationship (Swinth et. al. 1968). This is due to the fact that some of the Compton scatter events suppressed by the shield are also rejected by the discriminator. As the effects of pulse shape discrimination are marginal for good detectors, the combination of techniques only yields marginal improvement over the use of the anticoincidence shield alone.

7.5.5 Discussion

Anticoincidence shields, though generally improving A_E, when used for natural background reduction have limited ranges of improvement. Larger improvements are obtainable when the Compton suppression mode is significant. The most versatile shield for preferential suppression of coincidence gamma rays (Hasselgren 1966) is one which can be adapted to both internal and external source measurements. The combination of massive shielding and anticoincidence methods has resulted in the lowest level measurements yet made with a Ge(Li) detector to date, Cooper et. al (1969), who measured 1 pCi of ^{137}Cs.

7.6 The Use of Pair Spectrometers

The technique of pair spectrometry using scintillators (Pringle, Roulstan and Standil, 1950) is well established and was first demonstrated using Ge(Li) detectors by Ewan and Tavendale (1964).   Its application is limited (Souminen and Kantele 1968) both in energy range and sensitivity. The method is evaluated below.

7.6.1 Conditions of Use for the Pair Spectrometer

The pair spectrometer is of use only when the double escape peak efficiency of the detector is significant ($>$ 1.5 MeV).   The double escape peak efficiency of the spectrometer is a function of the detector sensitive volume and depth, the geometrical efficiency of the two scintillators and the presence of any insensitive material.

There are two modes of operation for a pair spectrometer.   The first is the rejection of triple coincidence events.   This gives suppression of double escape peaks and some continuum (including Compton events) suppression for no change in ϵ_{PA} for the central detector.   In the second mode triple coincidence events are accepted.   This gives an escape peak spectrum with large continuum reductions.   The mode relies on the use of escape peaks for intensity and energy determinations of the initial incident gamma ray. It is possible to collect events for both modes simultaneously (by a suitable arrangement of electronic modules) and store the information in separate halves of the pulse height analyser.   The choice of operating mode is a function of the energy of interest, spectral complexity and the double escape peak efficiency of the detection system.

7.6.2 Change of Counting Parameters During Operation

The observed variations of counting parameters are a function of the mode of operation adopted.

7.6.2.1 Rejection Mode

This particular mode is commonly used (Grenier and Poussier 1968) and can be simultaneously operated and combined with the anti Compton mode. (Auble, Beery, Berzins, Beyer, Etherton and Kelley 1967).   Camp (1969) has investigated the operation of these spectrometers.   Camp (1969) obtained good results for a carefully optimised system giving suppression factors of 40 on the double escape peaks, and a single escape peak reduction factor of 6, independant of energy above 1.50 MeV.   The continuum was reduced a

Fig. 7.11

Simple Pair Spectrometer Made with Two
7.5cm x 7.5cm NaI(Tl) Scintillators

source

shield

Ge(Li) Detector
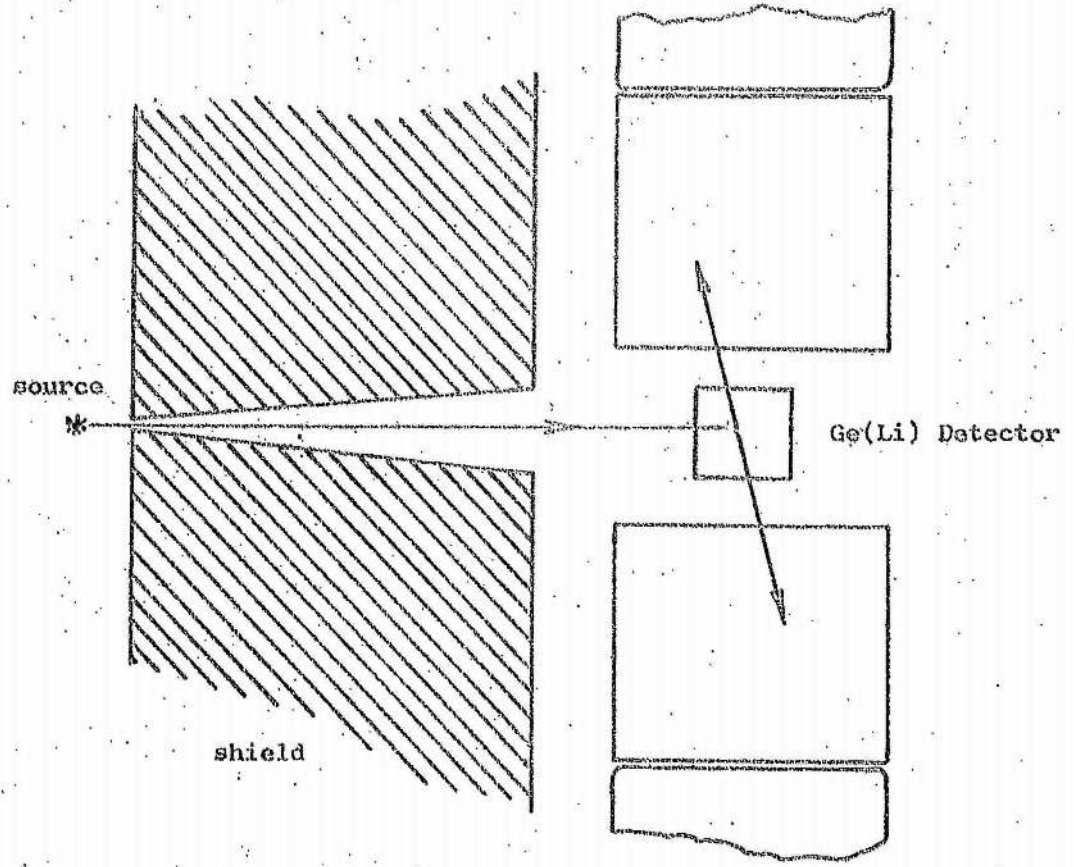
Optimised "Split Halves" Pair Spectrometer by Camp (1969)

Ge(Li) Detector

shield

source
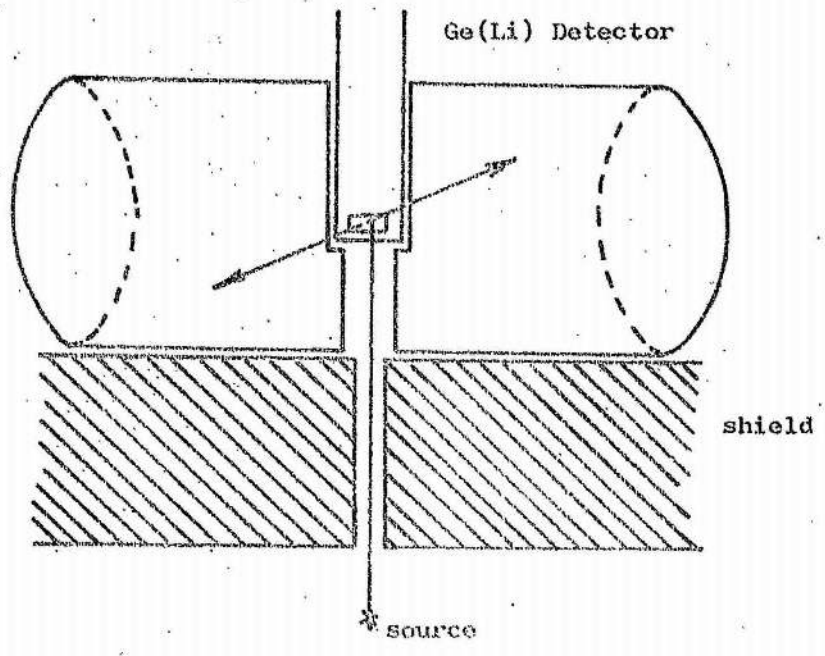
factor of 12 above 1.0 MeV and a factor 4 at .075 MeV. This was obtained with the "split halves" arrangement shown in Fig. 7.11. Cheaper arrangements (Fig. 7.11) using two 7.5 cm x 7.5 cm NaI(Tl) scintillators and an existing Ge(Li) detector can be made with the loss of a certain amount of performance.

There is no reduction of ϵ_{PR} for this counting mode.

7.6.2.2 Acceptance Mode

The choice of this mode is dependant upon the absolute double escape peak efficiency (ϵ_{PP}) of the central detector, and the absolute efficiency of detection of the two annihilation quanta of the scintillators (ϵ_s). Camp (1969) estimated an upper limit for ϵ_s of 0.23, but in general this is smaller, being 0.05 using the 7.5 cm x 7.5 cm NaI(Tl) scintillators. The absolute double escape peak efficiency of the pair spectrometer is ϵ_{PSP} where $\epsilon_{PSP} = \epsilon_{PP}\epsilon_s$, and hence has values ranging 0.05 ϵ_{PP} to 0.23 ϵ_{PP}.

A large continuum reduction may be effected with this technique. Camp (1969) using the "split halves" system achieved energy dependant reductions varying from a factor 55 at the double escape peak of interest to a maximum of 350 between escape peaks. The energy resolution of the system was unaffected for both operational modes of the spectrometer.

7.6.3 The Effects on Sensitivity Limits

The effects on sensitivity limits are only roughly calculable for pair spectrometers due to the difficulty in the accurate predicition of the variations of efficiency and backgrounds.

7.6.3.1 Rejection Mode Effects

The introduction of this mode always results in an improvement in sensitivity as B is reduced for no loss of ϵ_{PR} . However, the inherently poor source detector geometry (Fig. 7.11) invalidates the use of this technique for very low level measurements. Hence, this is used (Alexander, Broude, Hausser and Sharpey-Shafer 1968) for higher ($> 1 \mu$Ci) activity measurements. In this case, where the continuum level and complexity dominates equation 6.5, the maximum improvement factor is given approximately as

$$\frac{A_1}{A_{PAIR}} \sim \sqrt{\frac{12 B}{B_1}} \sim 3.5$$

for the same C and T and from the data of Camp (1969).

Fig. 7.12

Maximum Efficiency Loss Tolerated for a

Given Background Reduction Factor

$C = 0.2$

$T = 10$ hours

Initial B Under Peak

10^3 10^4 10^5 10^6

$\frac{B_1}{B_p}$

$\frac{\epsilon_{pa}}{\epsilon_{pep}}$
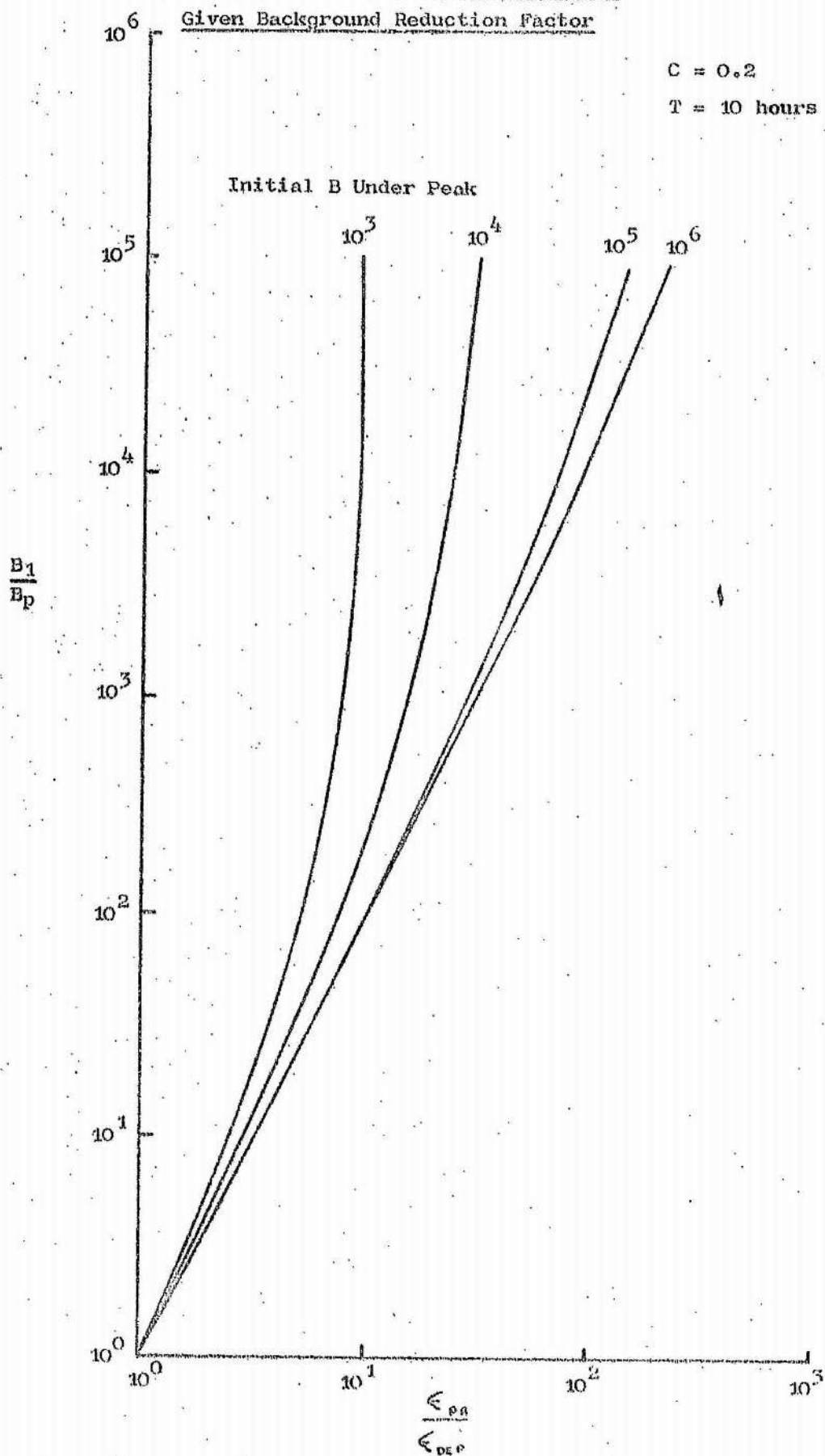
This compares with that of the anticoincidence shield and the combination results in this improvement being extended over several MeV.

7.6.3.2 Acceptance Mode Effects

The introduction of this mode does not result in an improvement unless the background reduction achieved more than offsets the results of differences between ϵ_{PA} and ϵ_{DEP}. This problem may be considered as follows. The sensitivity limit in the singles mode is A_1 for a given B, ϵ_{PA}, R_E, C and T. The resulting pair mode operation gives A_p for levels of B_p with R_E, C, T remaining constant. The efficiency loss exactly balances the background reduction when

$$\frac{A_1}{A_p} = \frac{\epsilon_{PP}\,\epsilon_s \left(2B_1 + \frac{1}{2C^2} + \sigma_{w1}^2 + \frac{1}{2C}\left(8B_1 + 4\sigma_{w1}^2 + \frac{1}{C^2} \right)^{\frac{1}{2}} \right)^{\frac{1}{2}}}{\epsilon_{PA}\left(2B_p + \frac{1}{2C^2} + \sigma_{wp}^2 + \frac{1}{2C}\left(8B_p + 4\sigma_{wp}^2 + \frac{1}{C^2} \right)^{\frac{1}{2}} \right)^{\frac{1}{2}}} = 1 \qquad \ldots\ldots\ldots 7.11$$

but of course must be > 1 for advantage. The variation of maximum tolerable efficiency loss ($\frac{\epsilon_{PA}}{\epsilon_{DEP}}$) for a given background reduction ($\frac{B_1}{B_p}$) is observed by plotting these ratios from equation 7.11 with typical parameter values inserted. Fig. 7.12 shows the result, recalculated for different initial levels of B_1. The curves may be considered as the limiting values governing the choice for a new counting system. In practice, this analysis can represent any counting technique by replacing ϵ_{DEP} and B_p with the expected values of the proposed counting technique. The overall efficiency reduction factor must always be less than that shown in Fig. 7.12 for improvement to be possible.

The following observations are made on Fig. 7.12 and the data of section 7.6.2.2:-

1) The efficiency reduction factor that is tolerable is greater for higher background levels.

2) For a factor of 5 orders of background reduction only 2 orders of magnitude of efficiency reduction at best are tolerable.

3) The major benefit of this technique is the removal of interfering peaks giving simpler spectral analysis.

4) The levels of Camp (1969) (section 7.6.2.2) gives the following results:

One pair spectrometer gave an efficiency reduction of 12.5 and a continuum reduction of 100. However, the resulting sensitivity was degraded a factor of 0.30. For another spectrometer with a

resulting efficiency reduction factor of 5 and a background reduction factor of 55, the resulting sensitivity level was improved a factor of 2 (ignoring the improvement due to removal of interfering peaks). This generally is the minimum tolerable improvement acceptable in practice (ignoring effects of interfering peaks) as this small improvement can often be obtained in the singles mode by an extension of count time. With these spectrometers, careful design is paramount for improvement of any significance to be observed. The poor absolute efficiency of both techniques limits their useful measurements to activity levels greater than several μCi.

7.7 Compton Scattering (Duode) Spectrometers

The use of the duode duode was first introduced with Ge(Li) detectors by Sever and Lippert in 1965. Since then, various forms have been tried with varying degrees of success, in particular by Broude, Hausser, Malm, Sharpey-Schafer and Alexander (1969) and Larsen and Strauss (1970). Their use and the results obtained are now considered.

7.7.1 The Configurations Encountered

Two detectors (or independantly operating sections of a single Ge(Li) detector) are used, placed near to each other and coincidence events from the two signifies collection of multiple scatter events. The incident radiation must be collimated on to one section or detector only, thereby resulting in a poor value of $\epsilon_{p\rho}$. Fig. 7.13 shows some of the configurations fabricated. The useful energy range of these devices is limited to regions where the Compton cross-section interaction is significant and multiple scattering with Compton events is significant (0.4 MeV – 2.0 MeV). The variation in geometry affects the angle of scatter acceptable causing an additional energy dependance of the results.

7.7.2 The Parameter Variations Observed for the Duode

The technique has an inherently poor $\epsilon_{p\rho}$ due to the necessity for source collimation. The configurations shown in Fig. 7.13 cover the range of systems available and are used to illustrate the resulting parameter variations. Table 7.6 shows the efficiency and background reductions in the continuum obtained for the various geometries.

Fig. 7.13

Some Configurations of Duodes Giving Differing Results
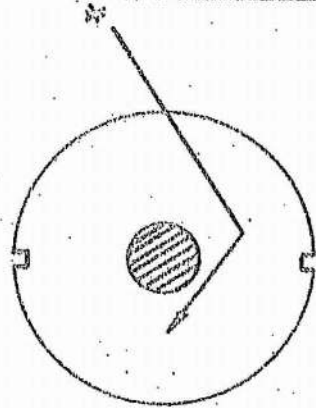
Kraner and Chase
(1968)
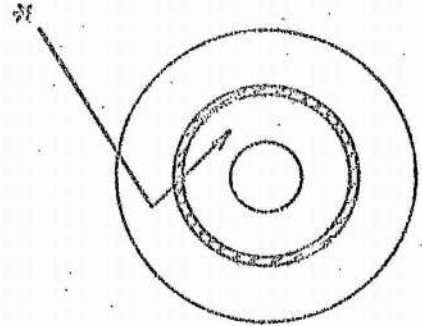
Palms, Wood and Puckett
(1968)
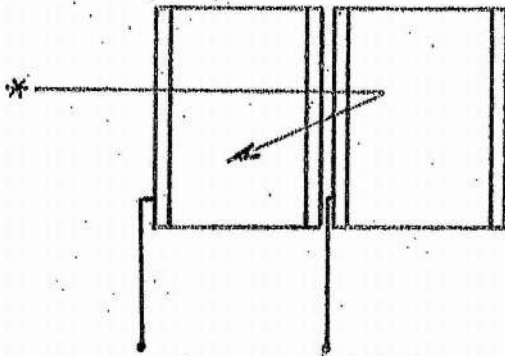
Sayers and Baicker
(1968)
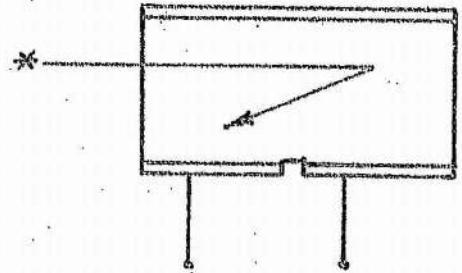
Gruhn, Kane, Kelly,
Kno and Berzins
(1967)
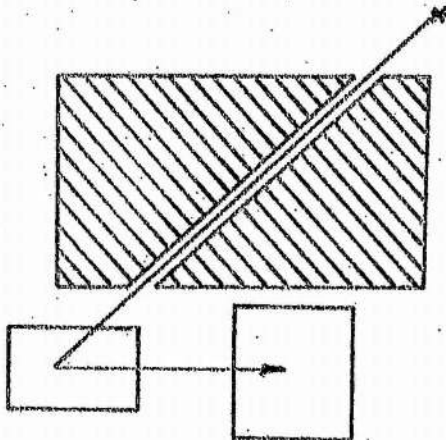
Kantele and Suominen
(1967)
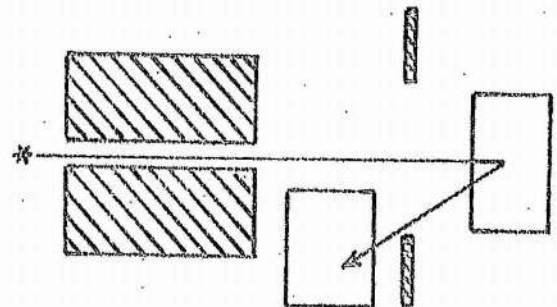
Hick and Pepelnik
(1969)

Table 7.6

Minimum Background Levels where the use of Each

Duode begins to be Effective

Author	Background Reduction Factor	Efficiency Loss Factor	Minimum initial backgrd. level where duode gives an improvement (C=0.2)
Kraner and Chase (1968)	12	4	always gives a degradation
Palms, Wood and Puckett (1968)	20	5	10^8 counts
Sayers and Baicker (1968)	26	7 - 10	always gives a degradation
Gruhn, Kane, Kelly, Kno, Berzins (1967)	100	10	10^6 counts
Kantele and Suominen (1967)	5000	100	10^9 counts
Hick and Pepelnik (1968)	3500	30 - 40	7×10^4 counts

The continuum is dominated, as in pair spectrometry, by source generated events and the technique is most useful in removing this contribution. However, due to the coincidence requirements a large natural background reduction is also effected.

It is observed that the greater the continuum reduction, the greater is the efficiency reduction. This is a function of the range of angle of scatter accepted by the detector.

It is possible for the overall energy resolution of system to be degraded as the use of effectively two detectors and preamplifiers requires very careful matching.

7.7.3 The Conditions where Sensitivity Limits are Improved

The inherently low $\xi_{p\beta}$ instantly invalidates the use of duodes for low level measurements. However, these devices may be of use in higher background conditions, this being decided by the criterion of Fig. 7.12. For a given detector there is a minimum background count under the singles peak for which the introduction of the duode mode instead of the singles mode of the incident detector just improves the counting sensitivity. Table 7.6 shows the calculated minimum background levels for each duode. It is observed that the use of two of these systems always gives degradation

while the remainder are of use only in very high background levels. The contrast is obtained by comparison of the results of Kantele and Suominen and Hick and Pepelnik where although the former obtain a larger background reduction factor, their greater efficiency loss makes its use contraversial. The duode of Hick and Pepelnik is usable to activities of a few μ Ci.

7.8 The Comparison Between Ge(Li) and NaI(Tl) Detectors

General comparisons between Ge(Li) and NaI(Tl) detectors are frequently misleading due to the differing applications, experimental configurations, spectral complexities and environmental conditions commonly encountered. However, comparisons may be made for a specific measurement as in the following low activity measurements with a singles spectrometer capable of use with both semiconductor and scintillation detectors.

A 7.5cm dia. x 7.5cm thick NaI(Tl) scintillator background spectrum was measured for 600 minutes in a massive shield* made of 15cm thick pre war steel. The background counts under the expected positions of the ^{137}Cs and ^{60}Co peaks were measured and tabulated in Table 7.7. Background levels for Nuclear Enterprises 40cm^3 and a 100cm^3 Ge(Li) detectors were evaluated from the considerations of section 7.2 and tabulated (Table 7.7). $\in_{PA}$ was measured at different source-detector distances to observe the effects of optimum and parallel beam geometries. Table 7.8 shows $\in_{PA}$ for each detector for 1 cm, 20 cm and 40 cm source-detector distances and also shows A_E calculated for each geometry and detector.

Table 7.7

Background and Energy Resolution Characteristics of Three Detectors

Detector	Energy Resolution (0.662 MeV)	Energy Resolution (1.33 MeV)	Continuum in peak base width at 0.662 MeV	Continuum in peak base width at 1.33 MeV
7.5cm x 7.5cm NaI(Tl)	49.0 keV	99.0 keV	9920 counts	3600 counts
40cm^3 Ge(Li)	1.8 keV	2.1 keV	40 counts	9.5 counts
100cm^3 Ge(Li)	2.2 keV	2.8 keV	108 counts	24 counts

* at Nuclear Enterprises Ltd., U.K.

Table 7.8

The Variation of A_E and $\epsilon_{p\beta}$ for the Detectors of Table 7.7 at ^{137}Cs and [60]Co Energies for C = 0.2, T = 600 min.

Source-Detector Distance		NaI(Tl)	40cm^3 Ge(Li)	100cm^3 Ge(Li)	$A_E(\gamma pm)$ NaI(Tl)	$A_E(\gamma pm)$ 40cm^3 Ge(Li)	$A_E(\gamma pm)$ 100cm3 Ge(Li)
1 cm	[137]Cs	0.118	0.0055	0.014	10.5	19.7	9.5
	[60]Co	0.063	0.0029	0.071	12.1	29.0	14.5
20 cm	[137]Cs	0.0032	0.00016	0.00042	385.0	680.0	325.0
	[60]Co	0.0019	0.00009	0.00022	400.0	940.0	490.0
40 cm	[137]Cs	0.00094	0.00005	0.00012	1310.0	2160.0	1040.0
	[60]Co	0.00054	0.000026	0.00006	1420.0	3280.0	1665.0

It is observed that the scintillator has a high sensitivity in the absence of interfering peaks and is roughly comparable to the 100cm^3 Ge(Li) detector. However, the presence of more than 3 - 4 peaks below 1.5 MeV may seriously degrade the scintillator performance. The detector choice is strongly influenced by the spectral complexity. The levels in Table 7.8 can be varied by using larger detectors, longer count times and reducing the source detector distance below 1cm. The above levels are supported by the data of Cooper et. al (1969) who achieved levels of 1 pCi with a Ge(Li) detector and of Sonntag (1967) and Nilsson and Perkins (1967) who measured 0.2 pCi with scintillators.

Other comparisons may be made for practical cases by substitution of the appropriate data. $\epsilon_{p\beta}$ must be predicted accurately due to its direct relation with A_E. Errors in the prediction of B are minimised as B has a root relation with A_E.

To undertake a full comparison, the above brief example should be recalculated for a wide range of detector sizes and system conditions, accounting also for more complex spectra.

Table 8.1

Summary of Counting Techniques Analysed by the Criterion Technique

Technique	Useful Activity Range Measurable (C=0.2, T=10 hours)	γ Isotope Restrictions	Effectiveness with γ Energy	Effectiveness with Background Level
Massive Shielding	∿ 5pCi to ∿ 20μCi	no limitation	all energies	all levels of background
Anticoincidence Shield + Massive Shield (i) Internal Source (ii) External Source	(i) ∿ 1pCi to ∿ 0.5μCi	γ - coincidence suppression	∿ 50 keV to several MeV	all levels
	(ii) ∿ 1μCi to several Ci	no limitations	∿ 50 keV to several MeV	all levels
Pulse Shape Discrimination	> several nCi	no limitations	∿ 50 keV to several MeV	nominal at low background levels
Coincidence Counting (i) α - γ (ii) β - γ (iii) γ - γ	(i) ∿ pCi to ∿ 100μCi	α - γ emissions only	decreasing with increasing energy	most effective at high background levels
	(ii) ∿ pCi to ∿ 100μCi	β - γ emissions only	decreasing with increasing energy	most effective at high background levels
	(iii) ∿ 20nCi to ∿ 100μCi	γ - γ emissions only	effective at lower energies (<500 keV)	most effective at high background levels
Duodes	> 1μCi	no limitations	∿ 400 keV to ∿ 2 MeV	at best only usable >10⁴ counts under peak
Pair Spectrometer (i) Acceptance Mode (ii) Rejection Mode	(i) ∿ 10μCi to Several Ci	no limitations for γ's of appropriate energy	above ∿ 1.5 MeV	for complex spectra and high level background
	(ii) ∿ 1μCi to Several Ci	as for acceptance mode	above ∿ 1.5 MeV	medium to high background levels

191

Conclusion

A substantial amount of attention has been paid in this work to measurement and diagnosis of detector characteristics and faults. This is due to the inherent fragility of the Ge(Li) detector system and the difficulty in discerning an organised fault finding and correction procedure from present literature. Direct measurements (leakage current, detector capacity, etc.) allow the experimenter to obtain optimum performance and undertake necessary repairs and reconditioning.

Emphasis has also been placed upon the detector absolute full energy peak efficiency due to its prime significance in low level activity measurements and its easy degradation through poor fabrication technique.

This thesis has broadly defined the inherent low level capabilities of several counting techniques using Ge(Li) detectors. Table 8.1 summarises these capabilities. The data is calculated for detectors in the range $20 - 40 \text{cm}^3$ sensitive volume and $3 - 5$ keV energy resolution. Variations from these estimated sensitivities are obtained for detectors outside these ranges and/or the use of different C and T.

For a specific spectrometer, accurate predictions may be made using its experimentally measured parameters and its minimum detectable activity is determined by setting $C \sim \frac{1}{2}$ in the calculations. This may also be used to evaluate further extensions to be added to that spectrometer. The techniques which are most effective for low level counting are those that maintain a high value of ϵ_{PA}. These are massive shielding, anticoincidence shielding and, where applicable, $\alpha - \gamma$ and $\beta - \gamma$ coincidence systems.

A considerable amount of further work is required to fully evaluate background levels of Ge(Li) detectors. Using the techniques developed in this thesis, a full low level counting evaluation of Ge(Li) detectors, in comparison with other types of detectors, may now be undertaken.

Appendix I

Publications and Conference Papers Resulting from this Thesis

1) Anomolous Effect in a Lithium Drifted Germanium Semiconductor
   G Walford and C.E. Doust 1968

   Electronics Letters Vol. 4 No. 1, 12

2) A Method for the Rapid Calibration of Germanium Spectrometers
   G. Walford and C.E. Doust 1968

   Nucl. Instr. and Meth. 62, 353

3) Defects in Ge(Li) Detector Efficiencies
   G.V. Walford and C.E. Doust 1968

   Proceedings of a Meeting on Special
   Techniques and Materials for Semi
   conductor Detectors
   Ispra, Italy EUR 4269e, 103

4) A Determination of the Relationship between Efficiency and Volume
   of a Ge(Li) Detector and a Proposed Eddy Current Technique for
   Depth Testing the p-i-n Contours of the Crystal
   G.V. Walford and C.E. Doust 1969

   Nucl. Instr. and Meth. 67, 272

5) Ge(Li) Gamma Ray Detectors for Environmental Activity Measurements
   G.V. Walford 1970

   Presented at the Second Congress of
   the International Radiation Protection
   Association, Brighton U.K.

6) The Direct Evaluation of Low Level Counting Techniques Employing
   Ge(Li) Detectors
   G.V. Walford, D.T.W. Aliaga-Kelly and W.B. Gilboy 1971

   Presented at the I.E.E.E. Nuclear
   Instrumentation for Research and Develop-
   ment Science Symposium, November 1971,
   San Francisco, U.S.A.

7) The Low Level Counting Capabilities of Ge(Li) Detectors
   G.V. Walford and W.B. Gilboy

   Nucl. Instr. and Meth.   In preparation

Appendix II

Some Isotopes Suitable for Calibration of Ge(Li) Spectrometers

It has become apparent that with the higher energy resolution of Ge(Li) detectors, many gamma ray energies previously used for calibration of scintillators are inadequately known for semiconductor detectors. The following table contains some readily obtainable isotopes of known intensity and energy that have been successfully used for semiconductor calibration purposes.

Energy Range (keV)	Isotope	Half Life	Reference
8-98	X-ray machine	–	Slivinsky, 1969
30-400	^{133}Ba	7.8 years	Gurfinkel, 1967
60	^{241}Am	458 years	Mowatt, 1969, Paradellis 1969 Tockan 1968
87	^{109}C	470 days	Donnelly 1967, Campbell 1971
89	^{176}Lu	2.1 years	Donnelly 1967
90-3500	^{75}Se	120 days	Gearke 1971
92-1650	^{82}Br	35 hours	Gearke 1971
122-1409	^{152}Eu	12.4 years	Mukherjee 1969, Mowatt 1970
122-136	^{57}Co	270 days	Michaelis 1968, Mowat 1969 Drexler 1967, Paradellis 1969 Campbell 1971
123-1824	^{154}Eu	16 years	Paradellis 1969, Tokcan 1968
145	^{141}Ce	32.5 days	Black 1967, White 1968, Campbell 1971
165	^{139}Ce	140 days	Donnelly 1967, Black 1967 Campbell 1971
188-2446	^{226}Ra in equilibrium with daughter products	1617 years	Walford 1968, Wallace 1969 Mowatt 1970
214-1032	^{131}Ba	11.5 days	Paradellis 1969
215-443	^{180m}Hf	5.5 hours	Kane 1967, Mowatt 1969, Paradellis 1969, Sprouse 1965

Calibration List (cont.)

Energy Range (keV)	Isotope	Half Life	Reference
320	^{51}Cr	27.8 days	Black 1967
402	^{75}Se	127 days	Paradellis 1969
412-1090	^{198}Au	2.69 days	Black 1967, Donnelly 1969, Campbell 1971
432-727	^{108m}Ag	5 years	Kane 1967
477	^{7}Be	53 days	Black 1967
513	^{85}Sr	64 days	Black 1967, Campbell 1971
569-1430	^{207}Bi	8 years	Black 1967, Fox 1965
583-2614	^{208}Tl	3.1 minutes	Kane 1967, Henck 1968
662	^{137}Cs	28 years	Donnelly 1969, Henck 1968 Michaelis 1968, Mowatt 1969, Barker 1967, Tokçan 1968, Campbell 1971
690	^{203}Hg	46 days	Michaelis 1968, Mowatt 1969, Tokçan 1968, Campbell 1971.
768	^{95}Nb	35 days	Black 1967
834	^{54}M	324 days	Barker 1967, Black 1967, Michaelis 1968, Mowatt 1969, Campbell 1971
845-3440	^{56}Co	77.2 days	Barker 1967, Gearke 1971
892-1118	^{46}Sc	84 days	Black 1967, Freeman 1966
934	^{92}Nb	350 years	Black 1967
1115	^{65}Zn	245 days	Black 1967, Campbell 1971
1173-1333	^{60}Co	5.25 years	Barker 1967, Freeman 1966, Henck 1968, Michaelis 1968, Mowatt 1969, White 1968
1222-1554	^{182}Ta	111 days	White 1968
1280	^{22}Na	2.6 years	Black 1967, Freeman 1966, Kane 1967, Michaelis 1968, Mowatt 1969, Paradellis 1969, Tokçan 1968

Calibration List (cont.)

Energy Range (keV)	Isotope	Half Life	Reference
1290–1298	^{41}Ar	1.8 hours	White 1968
1368–2754	^{24}Na	14.9 hours	Kane 1967
1596–2909	^{140}La	40 hours	Tokcan 1968
1836	^{88}Y	108 days	Black 1967, Henck 1968, Michaelis 1968, Mowatt 1969, Tokcan, Campbell 1971
2614	^{228}Th	1.91 years	Kane 1967
1000–10,000	$^{53}Cr(n,\gamma)^{54}Cr$	--	Kane 1967, White 1968
3560	$^{9}Be(p,\alpha\gamma)^{6}Li$	--	Young 1971
4438	$^{12}B(\beta^{-})^{12}C$	--	Camp 1967
4440	$^{15}N(p,\alpha\gamma)^{12}C$	--	Young 1971
5240	$^{16}O(^{3}He,\alpha)^{15}N$	--	Camp 1967
5270	$^{14}N(d,p)^{15}N$	--	Camp 1967
5298	$^{14}C(d,p,\beta^{+})^{15}N$	--	Camp 1967
6130	$^{19}F(p,\alpha\gamma)^{16}O$	--	Young 1971
7480	$^{9}Be(p,\gamma)^{10}Be$	--	Young 1971
7639–7624	$^{56}Fe(n,\gamma)^{57}Fe$		Princetown Gamma-Tech 1968
9170	$^{13}C(p,\gamma)^{14}N$	--	Young 1971, Camp 1967

Appendix III

Anomolous Effect in a Ge(Li) Detector

Introduction

Unexplained phenomena are frequently observed in the character-
istics of Ge(Li) detectors.   Some of these generate degradation of perfor-
mance, while the effect reported here resulted in an improvement in the
detector performance.   This effect, of negative differential resistance,
was observed in two planar Ge(Li) detectors mounted in this laboratory,
the first showing a 4% current reduction, the second showing one of 33%.
Fawcett and Paige first reported the phenomena in n type germanium in 1967.
This appendix describes a brief investigation of the second detector.

The Phenomenon

Both planar Ge(Li) detectors were of similar dimensions, having
drift depths of $\sim$ 3 mm. and with total volumes of approximately 3 cm^3.
Both were also mounted using conventional techniques and contacts were
established with indium foils and indium-gallium eutectic.   The first
detector was urgently required for other experiments and hence could not be
evaluated fully.   The second detector was subsequently mounted in the same
cryostat and the effect was observed when routine measurements were taken
after cooling.

Fig. III.1 shows the current-voltage and the capacity-voltage
characteristics measured.   Above 260 volts, a sharp current decrease is
observed that is stable and reproducible.   As a check on the effectiveness
of charge collection and the field across the intrinsic region, the peak to
Compton ratio, resolution and pulse height output for ^{60}Co were measured with
increasing bias, the results being plotted in Fig. III.2.

This data is typical of normal detectors showing that the bias is
being satisfactorily applied across the intrinsic region after the onset of
the negative slope in the current characteristic.

Fawcett and Paige (1967) observed the effect between 27 - 77°K.
Hence it was decided to observe the behaviour of the detector in this
temperature range by replacing the liquid nitrogen with liquid helium, and
after evaporation of the helium, measuring the characteristics as the cryostat
warms up.

Fig. III.1

Current-Voltage and Capacity-Voltage Characteristics
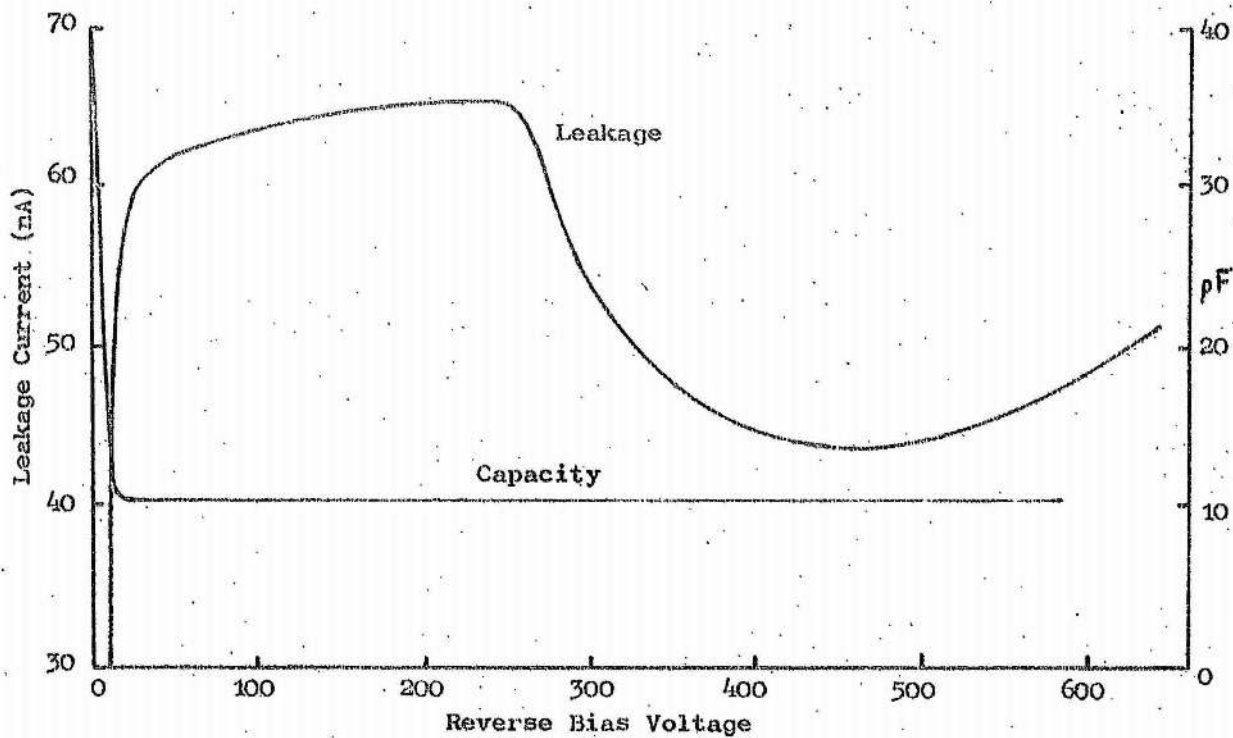
of the Second Detector

Fig. III.2

The Variation of Pulse Height, Energy Resolution and
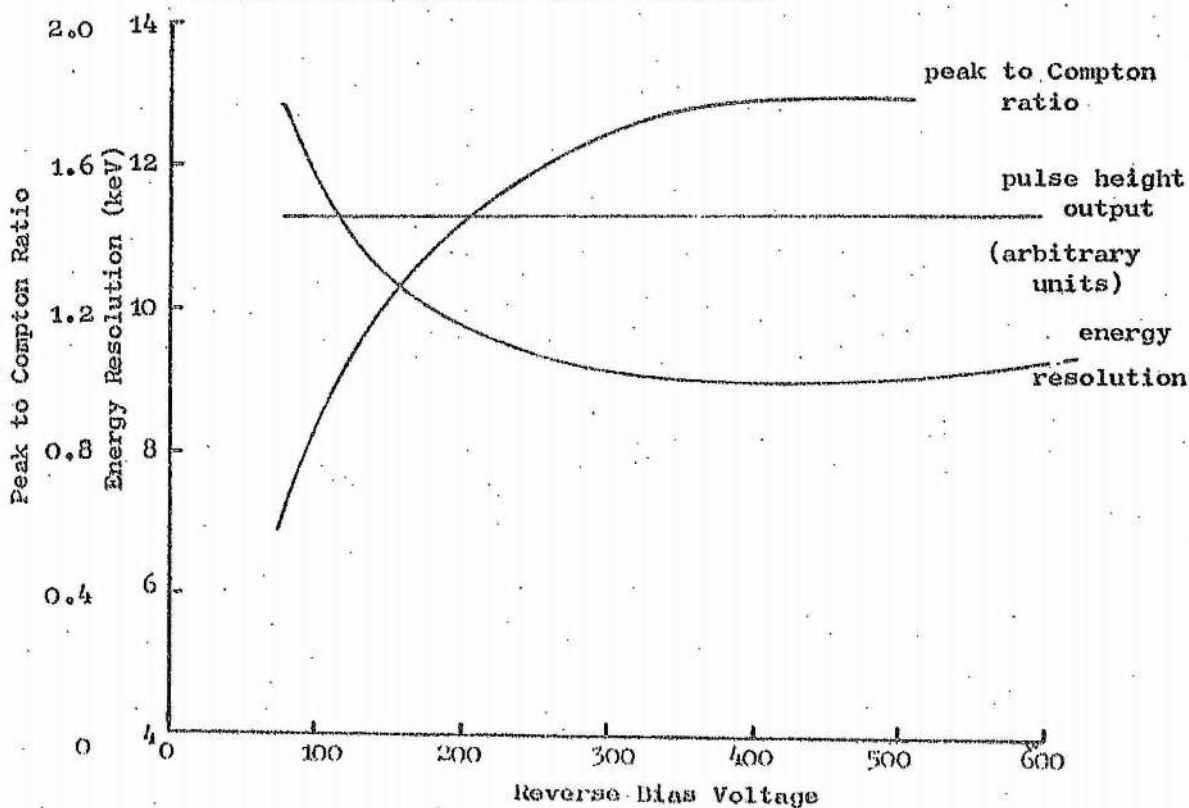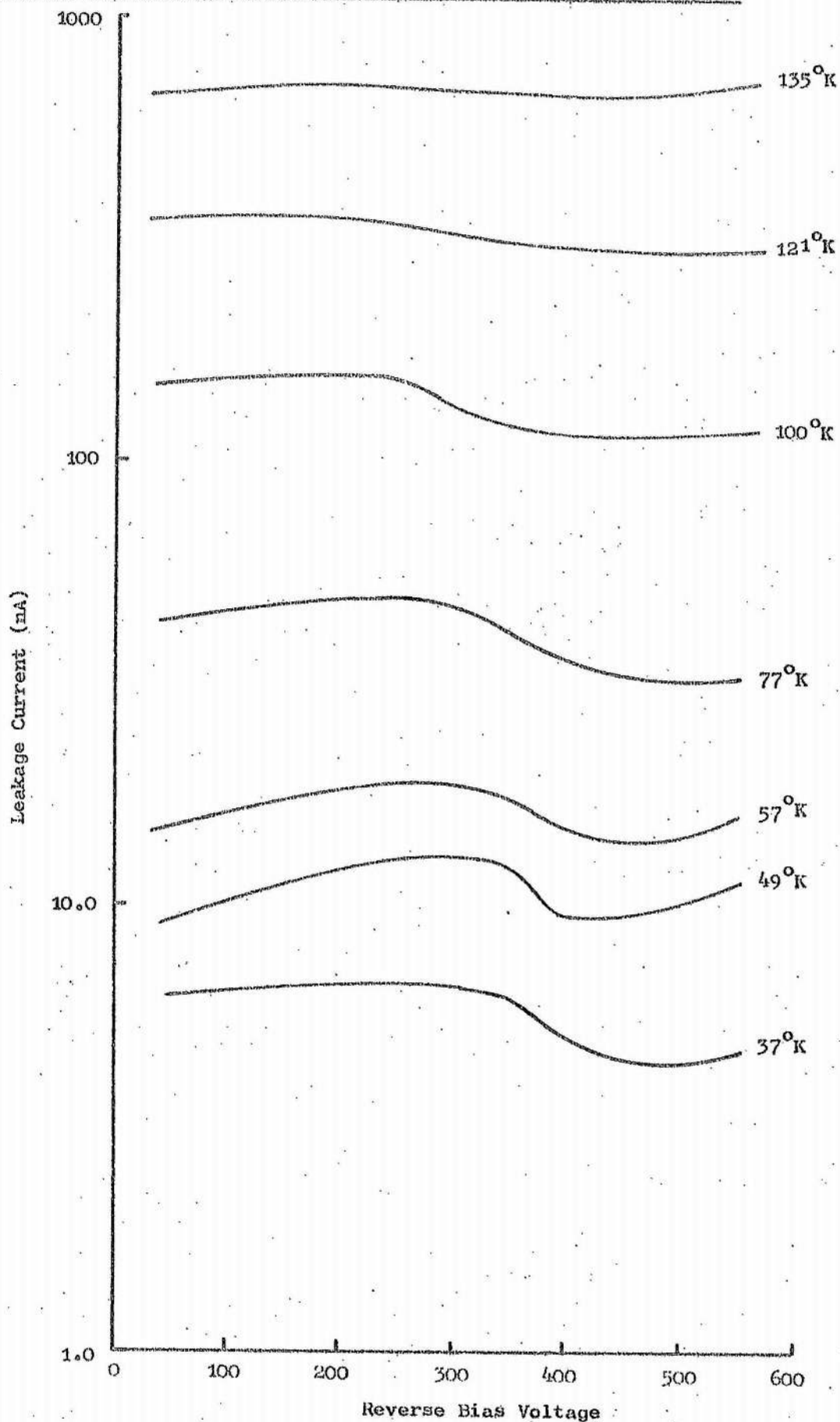
Peak to Compton Ratio with Reverse Bias

Fig. III.3

The Current-Voltage Characteristic Measured from 37°K to 135°K

The cryostat was designed for use with liquid nitrogen, and hence the lowest temperature obtained (measured by a thermocouple placed near the detector) was 37°K. Fig. III.3 shows the current-voltage characteristic plotted at temperatures between 37°K and 135°K above which the characteristic shape was lost. Fig. III.4 shows the variation of the onset threshold with temperature. A minimum threshold voltage is observed at $\sim 120^{\circ}$K.

After the detector had approached room temperature, liquid nitrogen was added to return it to 77°K. Outgassing in the cryostat however resulted in surface contamination giving the detector leakage characteristic of Fig. III.5 at 77°K. The original shape shown in Fig. III.1 can still be observed superimposed upon the excess leakage due to the contamination.

The surface contamination was removed by warming the detector once more to room temperature and pumping the cryostat with a molecular sieve pump. Fig. III.6 shows the resulting current-voltage characteristic after the crystal had been returned to 77°K. It is observed that the original characteristic is regained. The typical slow current fall with time at constant voltage (for the crystal at 77°K) is also observed in both Figs. III.5 and 6.

Discussion

This effect has either bulk, surface state or detector contact origins.

During a warming and cooling cycle, the compensation profile and surface states may change so that should the effect originate from either of these, the curve shape is permanently affected. For this detector, this is not the case. The behaviour of this detector is normal with the exception of the current-voltage characteristic. The remaining possibility by this argument is that of the contacts. Ridley (1967) has considered that the applied contacts might have an additional junction, inadvertently generated say by oxide layers on the indium or germanium, precipitation in the n-layer or contamination on the n or p-layer. Such effects would change the charge injection properties, though they would also be expected to result in potential drops across the junctions.

Bonch-Bruevich (1967) has developed a theory explaining that a space charge might be built up in the intrinsic region, giving an electrical domain that repels injected charge. The conditions however to set up such a state would be highly dependant upon the compensation profile and intrinsic region countours making it highly sensitive to warming and cooling.

Fig. III.4

Variation of Threshold Voltage with Temperature

Fig. III.5

Degraded Current-Voltage Characteristic at
77°C after the First Temperature Cycle

20 hours after
1st temperature
cycle

60 hours after
1st temperature
cycle

Leakage Current (nA)

260

250

240

230

220

210

O   100   200   300   400   500   600

Reverse Bias Voltage
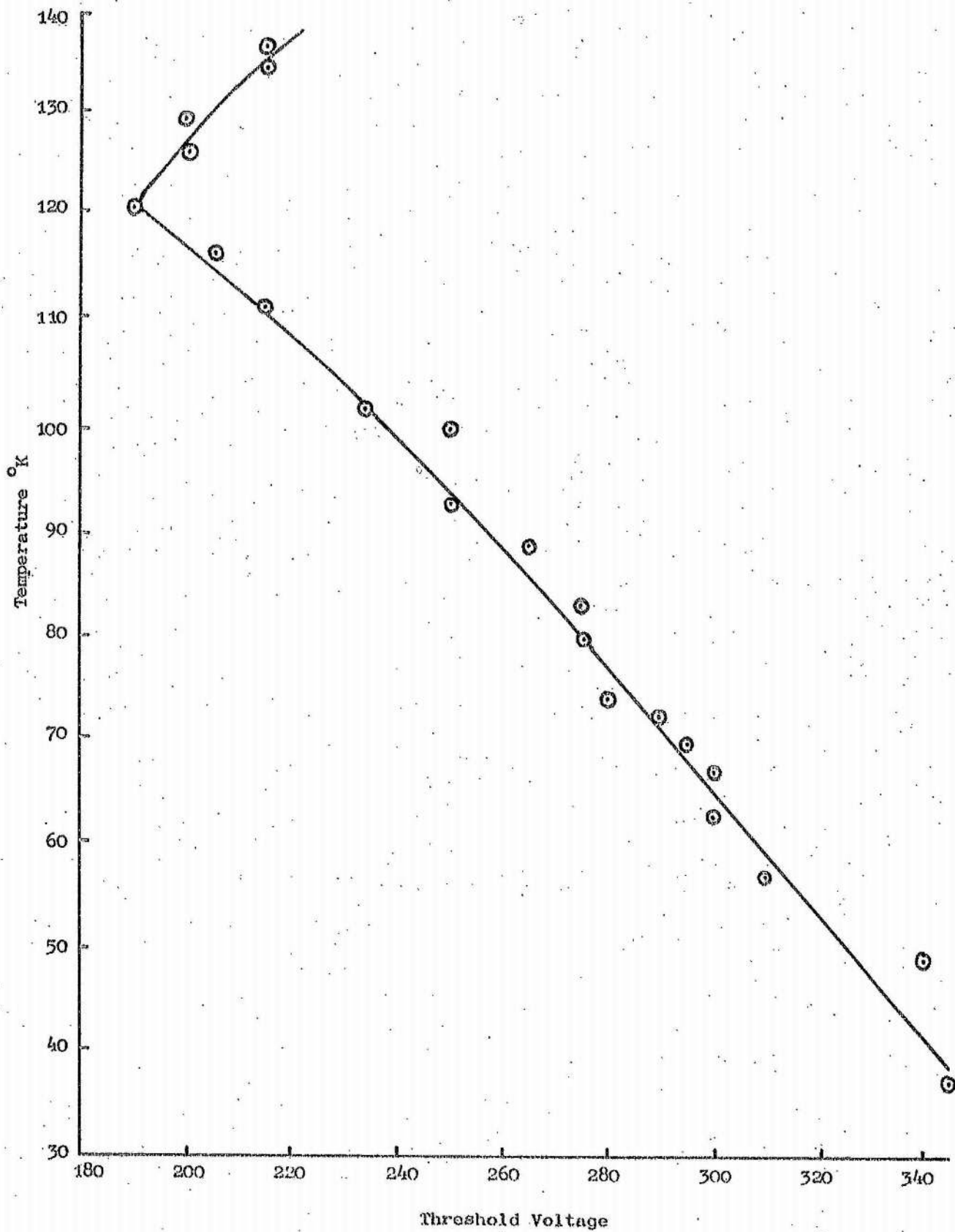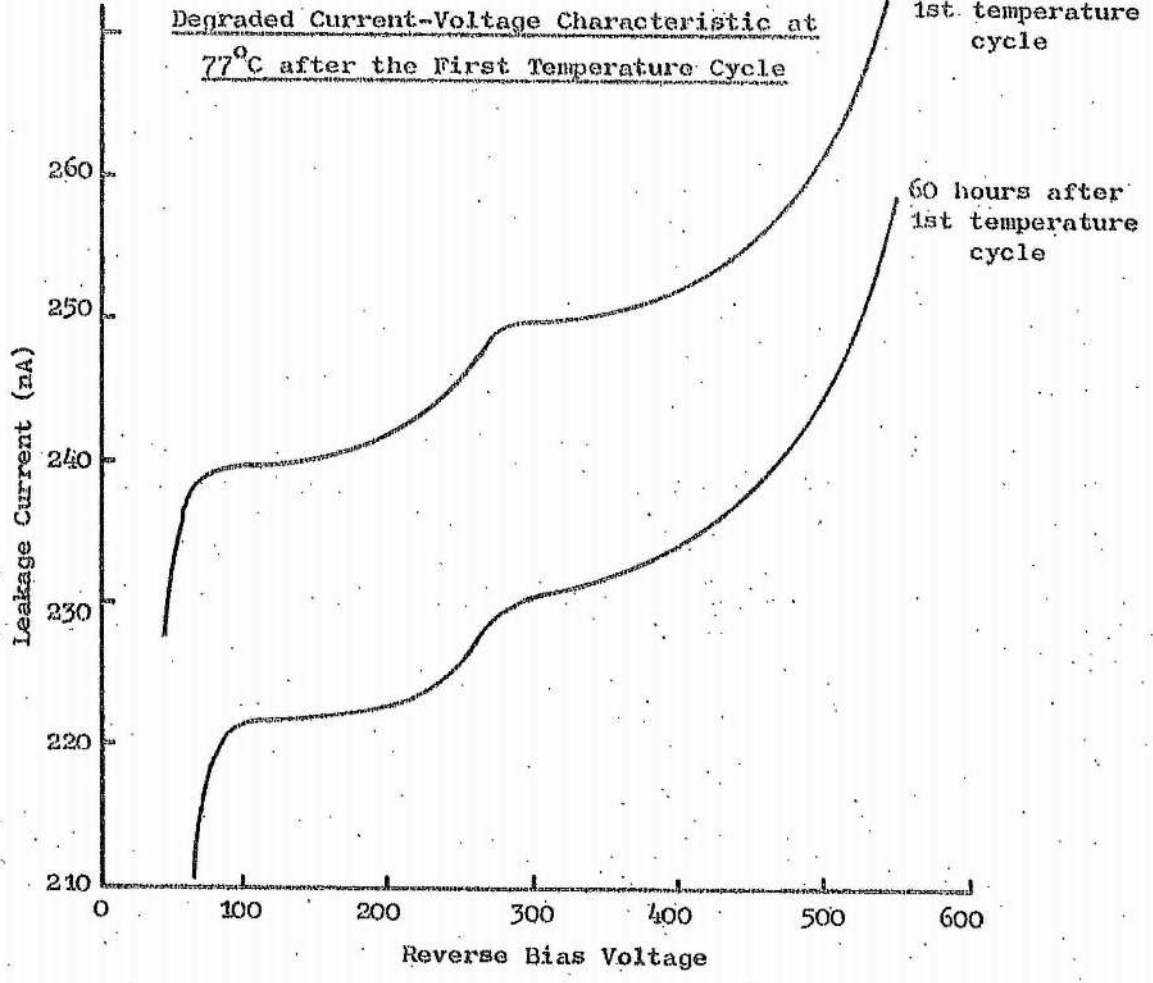
Fig. III.6

The Recovery Observed in the Current-Voltage Characteristic of Fig. III.5

140

130

120

110

100

90

Leakage Current (nA)

20 hours
after 2nd
temperature
cycle

60 hours
after 2nd
temperature
cycle

O   100   200   300   400   500   600

Reverse Bias Voltage
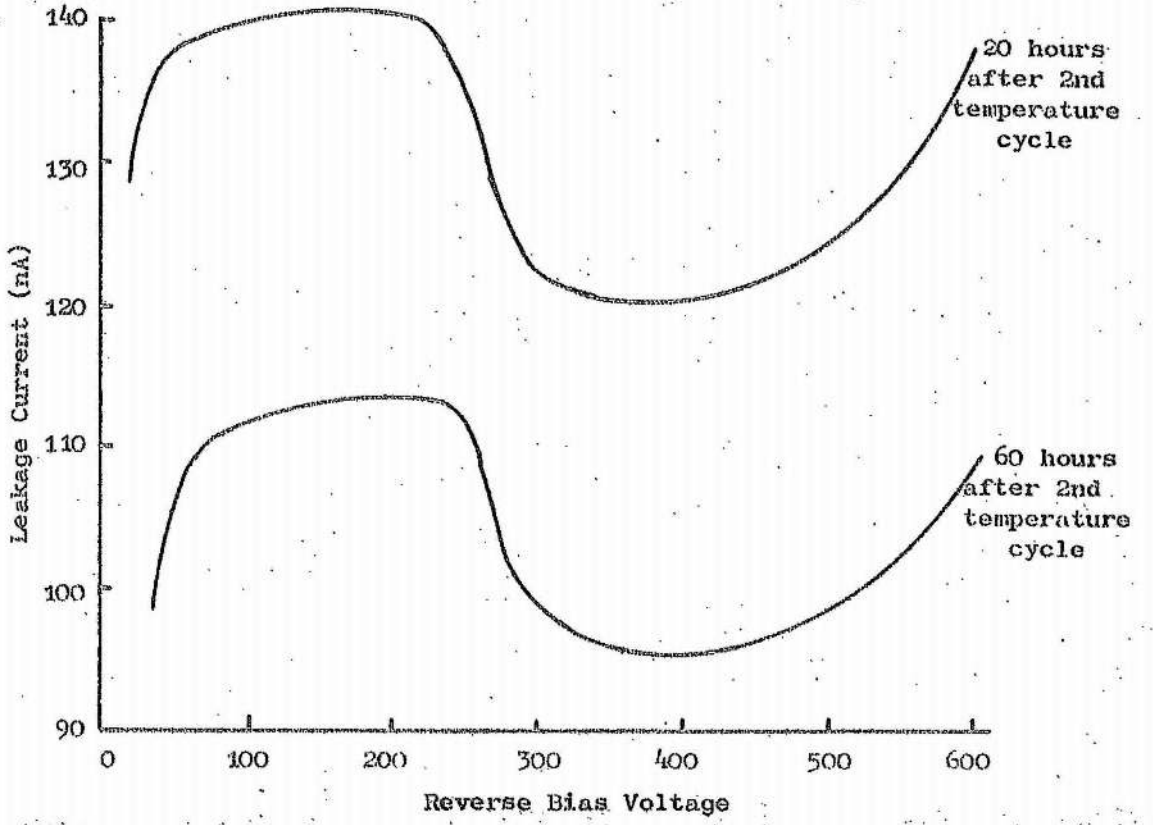
Conclusion

It is difficult to determine the exact origin of this anomolous defect. The demounting of the detector revealed no unusual conditions. Should such an effect be reproducible then it could lead to improved detector performances since the minimum leakage occurs at a reasonable value of collection field.

This problem is illustrative of many of the unexplained effects sometimes observed with Ge(Li) detectors. Only partial measurement is possible without interference with the detector environment causing permanent changes in detector characteristics.

Appendix IV

The Use of Scatter in Determining the Depth of a Source in a
Homogeneous Medium with a Ge(Li) Detector

G.V. Walford and C. Laubereau*

Introduction

Nearly all applications with Ge(Li) detectors rely on measurement of full energy peaks, utilising the high energy resolution potential of the spectrometer. However, the high energy resolution potential also allows accurate definition of the scatter contribution to the spectrum. This appendix describes one application utilising scatter to determine the depth of a source in a homogeneous medium. This has possible application in medical measurements in tumor depth analysis and similar types of problem.

Theory

For a gamma ray to be registered in the full energy peak of a spectrum its entire energy must be deposited in the sensitive volume of the detector. If the gamma ray undergoes a low angle scatter (Fig. IV.1a) then it is removed from the peak to a position below corresponding to the energy loss of the scatter event. An increase in medium thickness increases the proportion of scatter events and decreases the proportion of full energy peak events (Fig. IV.1b).

A measure of the scatter is effected by the ratio G, defined in Fig. IV.1b and its variation with depth is calculated as follows.

Consider a layer, thickness dx, x inside a medium thickness g The forward low angle scatter from dx is dS,

where $dS = I \mu_c \, dx$ and I = incident gamma ray flux at dx

μ_c = forward scatter coefficient for a defined energy range

of scatter.

* Institut für Strahlenschutz,
Gesellschaft für Strahlenforschung,
8042 Neherbery/b Munchen,
Ingolstädter Landstrasse 1,
West Germany.

Fig. IV.1a

Schematic Diagram of the Low Angle Scatter Origins

in a Homogeneous Medium

cryostat housing

Ge(Li) detector

air

scatter
γ ray

direct γ ray

medium

dx

g

x

source
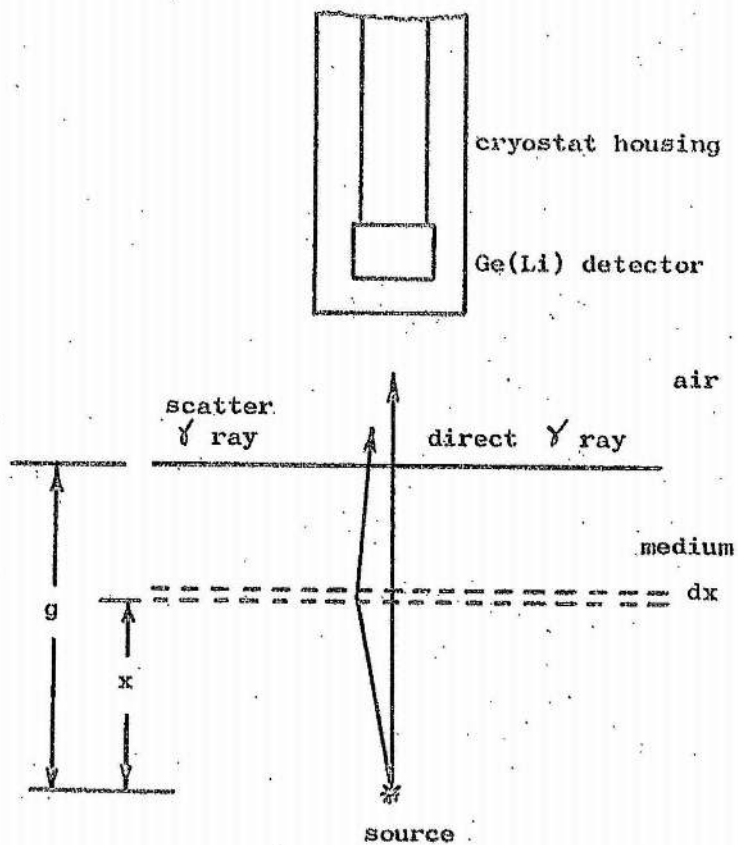
Fig. IV.1b

Spectral Measurement of Scatter and E

no interfering medium

interfering medium between
source and detector

$$G = \frac{\text{counts min}^{-1} \text{ between AB}}{\text{counts min}^{-1} \text{ between AC}}$$

C

A B
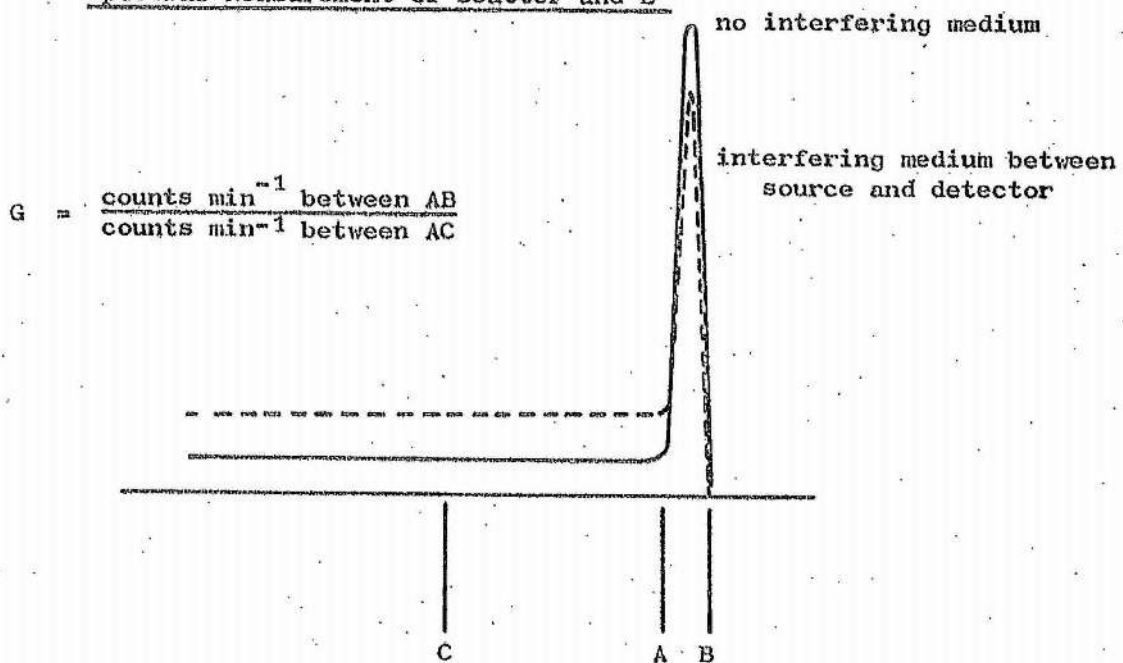
If μ_t = total interaction coefficient for that medium and energy, then e.g. IV.1 is rewritten as

$$dS = I_0 e^{-\mu_t x} \mu_c \, dx$$

The scatter reaching the detector from dx is approximately

$$dS \, e^{-\mu_t(g-x)} = I_0 e^{-\mu_t g} \mu_c \, dx \qquad \ldots\ldots \text{ IV.2}$$

Integration of IV.2 for x varying 0 to g gives the total scatter, S_t , reaching the detector defined by the value of the forward scatter coefficient

$$\text{Hence } \quad S_t = I_0 e^{-\mu_t g} g \, \mu_c$$

The total scatter events in the energy window (AC) is approximately

$$\qquad\qquad\qquad\qquad \ldots\ldots \text{ IV.3}$$

$$S_t \in_{PT} + B_s \qquad\qquad \text{where } B_s = \text{additional continuum not associated with the medium}$$

The counts in the peak region (AB) are

$$\qquad\qquad\qquad\qquad \ldots\ldots \text{ IV.4}$$

$$\in_{PI} I_0 e^{-\mu_t g} + B_p \qquad\qquad \text{where } B_p = \text{additional counts not associated with the source.}$$

Therefore it is useful to define the ratio G of the counts in the region AB, AC as

$$G = \frac{\in_{PT} I_0 e^{-\mu_t g} + B_p}{\in_{PT} I_0 g \mu_c e^{-\mu_t g} + B_s} \qquad\qquad \ldots\ldots \text{ IV.5}$$

B_p is ignored as it is generally small compared with the peak counts. B_s is frequently comparable with the scatter component. The variation of G with g depends upon the choice of AC and hence μ_c . In general, the peak area has always been found to be several times larger than the scatter component and hence, G will have an approximate variation with g of e^{-x}.

The above analysis is valid if the variation of $\in_{px}$ and μ_t is small in the energy region BC.
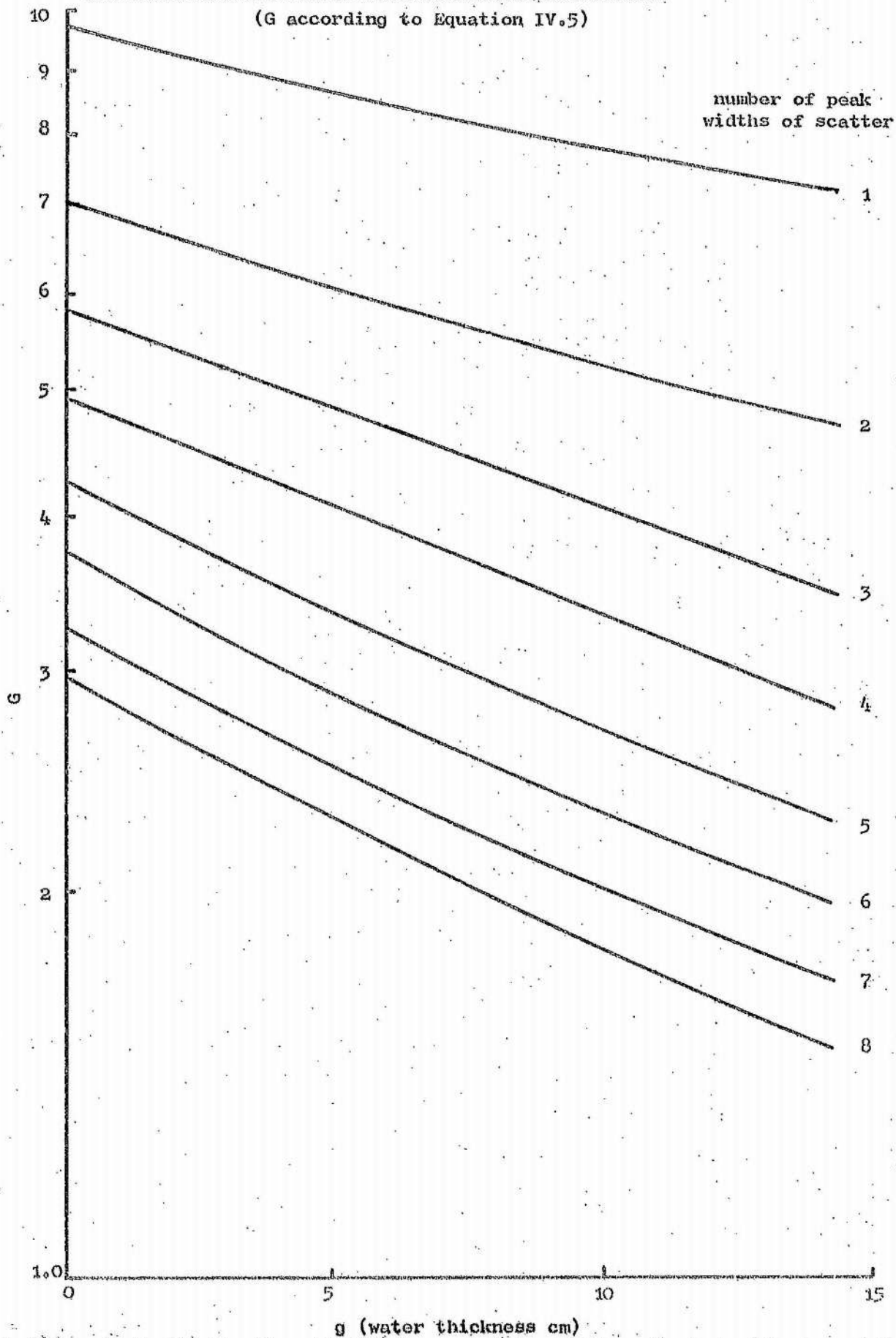
If B_s can be subtracted then the ratio G can be rewritten as

$$G = \frac{e^{-\mu_t g}}{g \mu_c e^{-\mu_t g}} = (g \mu_c)^{-1} \qquad\qquad \ldots\ldots \text{ IV.6}$$

Fig. IV.2

Variation of G with Water Thickness and Width of AC

(G according to Equation IV.5)

number of peak
widths of scatter

G

g (water thickness cm)

Both equations IV.5 and IV.6 are of use. Equation IV.5 holds if the scatter component B_S cannot be subtracted directly.

As g increases, G decreases. With a precalibration, the depth of the source in an unknown medium may be determined from a single measurement, which can be used to correct for source attenuation. The range AC includes all scatter up to a certain maximum angle, defined by the energy loss of the scatter event. Careful positioning of C allows a desired degree of "self-collimation" to be achieved.

Experiment

To demonstrate the technique a ^{137}Cs source was measured at a fixed distance (25 cm) from a Ge(Li) detector, and full energy peak counts, scatter and hence G, were measured. Water, in increasing thickness, was inserted between the source and detector (Fig. IV.1a) and the appropriate parameters measured. Water was chosen in this instance to provide an approximate tissue equivalent absorber. For each water thickness, G was measured for several values of AC. The detector (active volume 7.4 cm^3, 4.5 keV resolution on ^{137}Cs) had a peak base width of 10 keV at 662 keV. AC was measured in terms of peak base widths below the full energy peak.

The experiment was repeated with a lead collimator to determine the feasibility of extended source measurements.

Results

Fig. IV.2 shows the variation of G measured for different water thicknesses and AC. A marked variation of G is observed over all water thicknesses used and all AC. The variation is approximately logarithmic, according to the theory developed. Fig. IV.3 shows the variation of G for the experiment repeated with a collimator inserted next to the detector. With the collimator in place, G was calculated only for AC = AB. Variations in G are still observed, but are reduced due to the additional scatter from the lead.

The collimator was simple, being a 5 mm diameter hole drilled in a 5.0 cm thick lead block. For a source-detector distance of 25 cm, the spatial resolution was approximately 2.0 cm. Careful design would improve this figure an order of magnitude, though this would impose restrictions upon AC since the maximum scattering angle would be limited.

Fig. IV.3

The Variation of G with Water Thickness with a Lead Collimator and AC = AB

(G according to Equation IV.5)
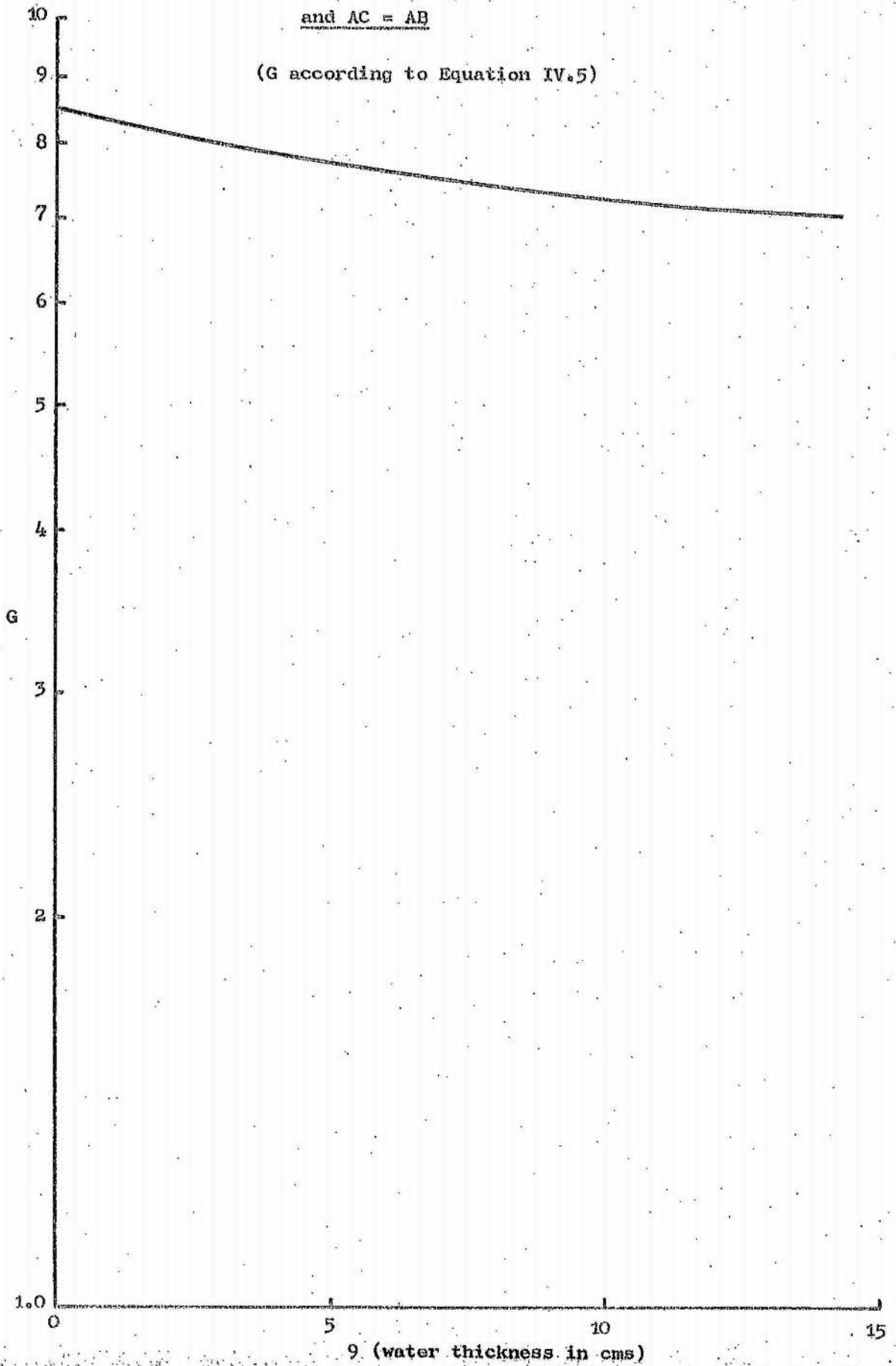
Discussion

The technique is workable in the conditions set by this experiment. It is possible to take a thickness measurement without touching the absorbing medium. For the technique to become of practical use, the following points must be considered:

1) <u>Accuracy</u>. The calculation of G involves the comparison of two counts which results in a standard deviation for G. Counts in excess of 10^3 must be accumulated in AC and AB if the depth is to be determined (without collimator) to within 5% standard deviation since a small variation in G leads to a larger variation in calculated thickness.

   When collimated, the detector had an absolute full energy peak efficiency for ^{137}Cs of 3×10^{-5} resulting in an uncertainty in G of 20% for a 100 μ Ci source and $T = 5$ min. For larger detectors (> 40 cm^3) and for larger source strengths (compatible with organ uptake measurements) then the uncertainty in G can be improved to 2% giving a thickness measurement deviation of $\sim$ 4%.

2) <u>Media</u>. This experiment was performed with water. It is possible to use other materials (Peterson 1970). Since this method relies only on the Compton effect, the scattering cross-section depends only on the number of electrons in the absorber. Hence, results should be expected to be similar for various elements if the thickness is expressed in electrons per cm^3. Further experimentation is necessary to experimentally determine the variations for different media and for different energies.

3) <u>Energy Variation</u>. The forward Compton scattering cross-section (per electron) is independant of energy. Hence similar results would be expected for other energies. It is interesting that the method is almost totally insensitive to total absorption processes (photoelectric and pair production) in the absorber. The method "picks out" the Compton effect even if it is only a small percentage of the total number of interactions.

4) <u>Collimation</u>. If a source profile is required, then collimation is essential. Careful design is required to optimise spatial resolution and minimise scatter from the collimator material. The use of a collimator always degrades the precision of G.

Fig. IV.4

Schematic Layout for a Direct Measurement of G and g
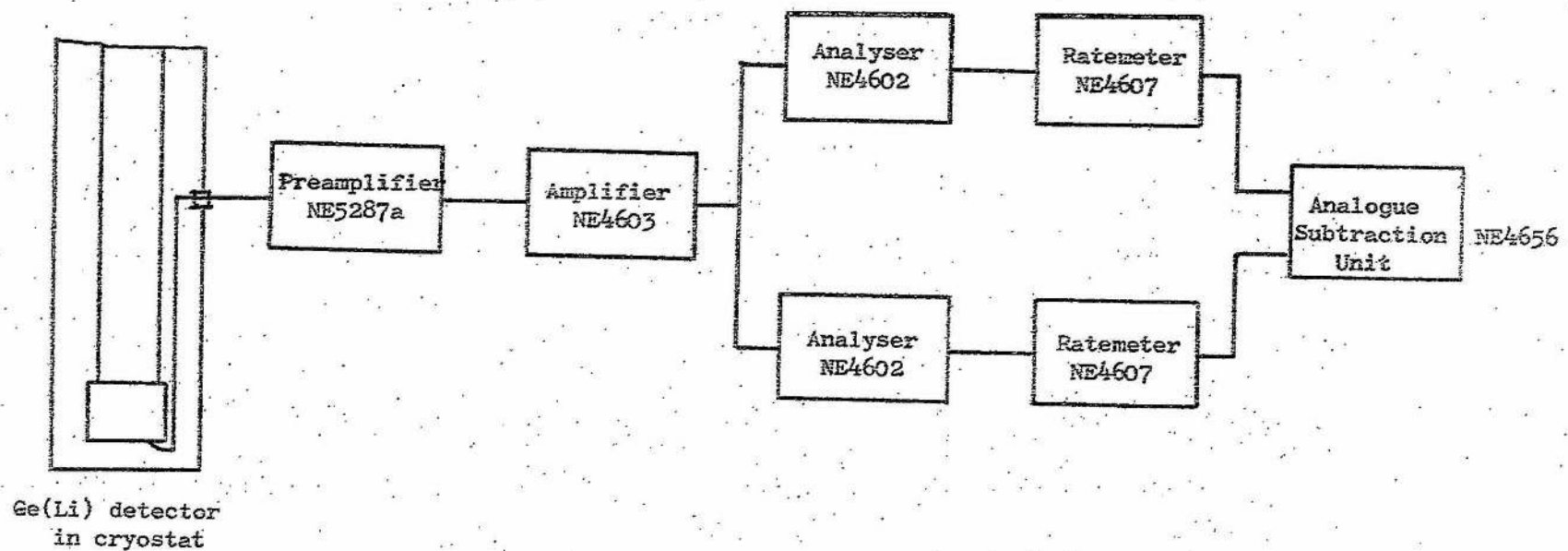
5) Instrumentation. Instrumentation may be arranged to give direct
readings of depth and source attenuation. Fig. IV.4 shows a
schematic layout for a proposed system. After amplification by
the pulse amplifier (NE4603), the pulses are fed to two single
channel analysers, one set on AB and the other on AC. The outputs
are then fed into two ratemeters (NE4607) set to give a logarithmic
output and the resulting voltages are then fed into the analogue
subtraction unit (NE4656). Here, the log signals are subtracted,
and the difference is proportional to log G. The output scale
can be directly calibrated in depth or attenuation factor.

Conclusion

This experiment demonstrates the use of forward scatter measure-
ments with Ge(Li) detectors to measure source depths in media. Several
other applications may be considered, some in medical measurement.

The instrumentation is simple and can be constructed from readily
available units.

Further work is required to fully define the potential of the
technique.

Appendix V

A Proposed Detector Configuration Combining Well and Duode Geometries

Introduction

This detector design is proposed to obtain the maximum flexibility from a spectrometer, thereby giving optimum use for a wide range of measurements. Well counters (sect. 5.3.3) have been developed to optimise source-detector geometry and duodes (sect. 7.7) to try to improve the resulting peak to Compton ratio. The combination of these geometries should allow a number of possible counting configurations.

Proposed Structure

A co-axial detector is used (either single ended or true co-axial geometry) with the p core removed to make a well counter. The n-layer is split to give the geometry of Fig. V.1a. This results in two separately operated halves (Fig. V.1b) for the one detector. Arrangement of the end cap (Fig. V.1c) allows insertion of sources into the well. The electrical coupling of the two halves can be such that the outputs can be separate or summed.
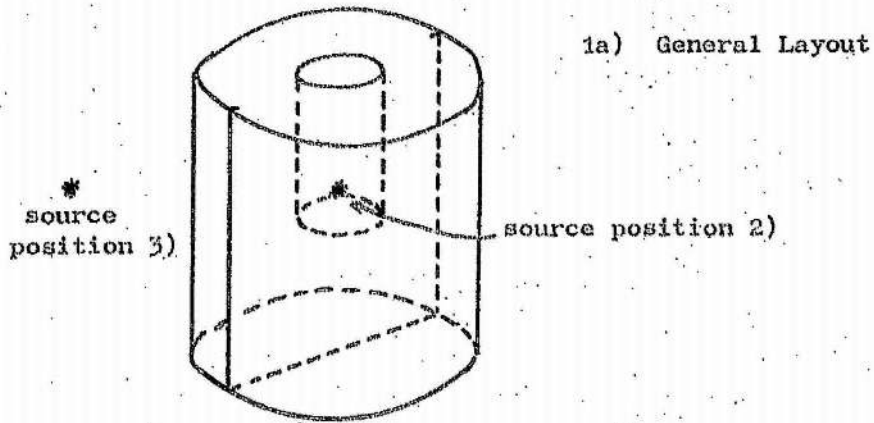
Methods of Operation

There are three basic modes of operation for this device.

1. Both halves summed together, with the source in position (1) or (2). In this mode, the detector operates as a conventional well detector with an optimum source-detector geometry.

2. Both halves operating in coincidence, source in position (2). Coincidence gamma rays only are accepted allowing preferential measurement of such $\gamma - \gamma$ sources as ^{60}Co, ^{46}Sc. The proximity of each half to the source gives a high geometrical efficiency.

3. Both halves in coincidence, source in position (1) or (3). This mode is used for only non-coincidence gamma rays, utilising the principle of the duode. It is appreciated (sect. 7.7.3) that the duode offers little real advantage. However, the principles of operation involved illustrate a wide range of physical processes and as such can be a valuable teaching aid.

Fig. V.1

Schematic Arrangement of the Coaxial Well Duode

* source position 1)

1a)   General Layout

source
position 3)

source position 2)

1b)   Electrical Arrangement
of the Detector

OV

-Ve

n layer
split

source position 1)*

OV

source
position 3)

source position 2)

1c)   Arrangement of the
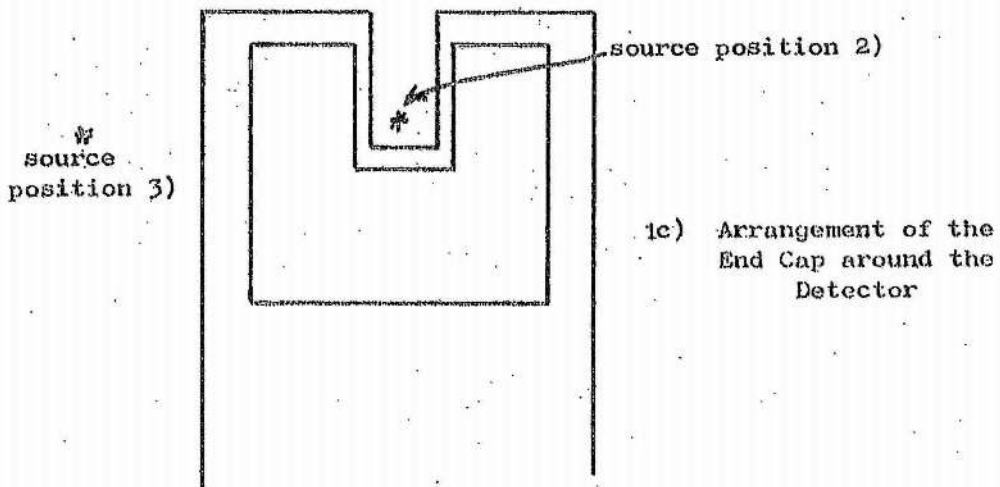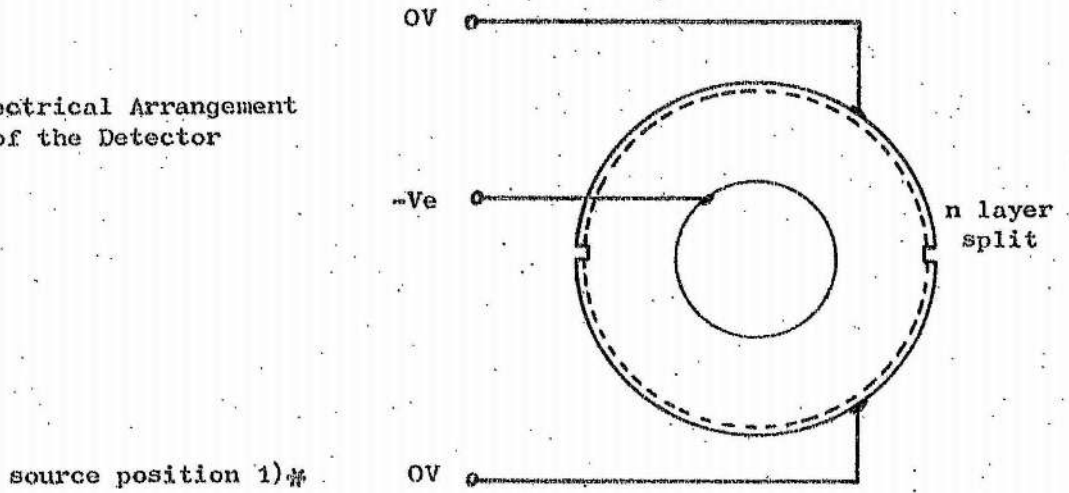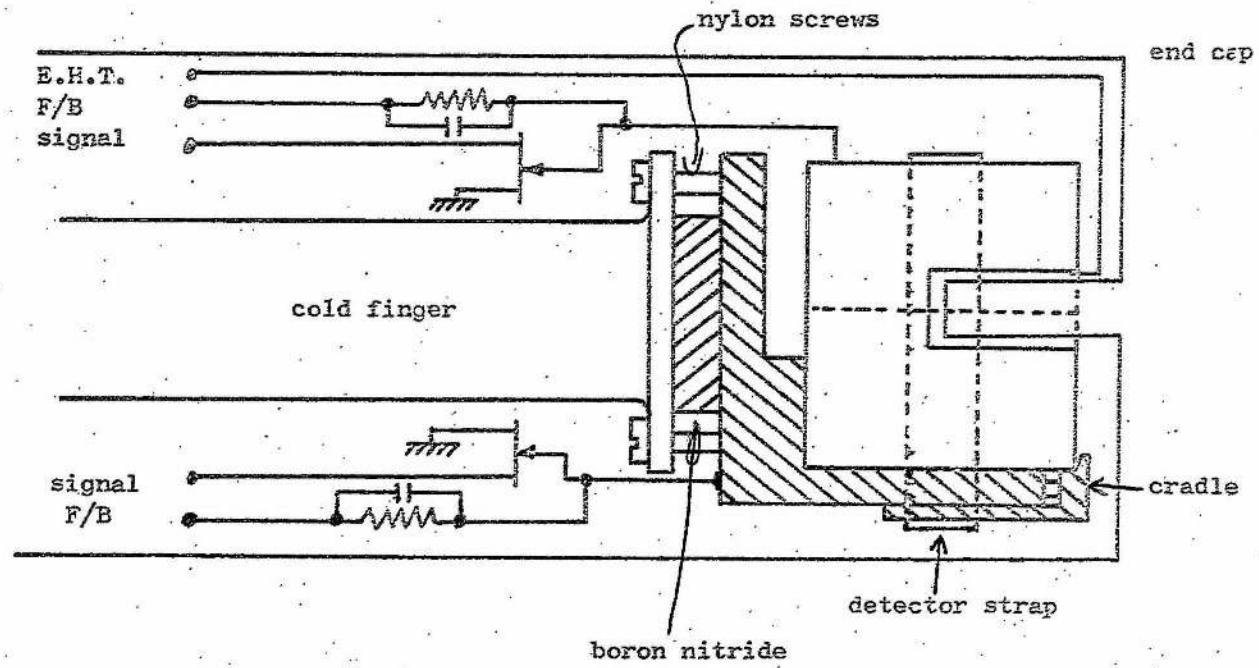End Cap around the
Detector

Fig. V.2

Proposed Mounting Arrangement of the Well Diode

Spectrometer Construction

The coaxial detector is fabricated by cutting the well in the ingot and then diffusing the lithium either in the well or on the outside circumference. Lithium is drifted, in the first case from the well outwards and vice-versa for the second case. When the lithium has drifted through, the i-p contact is re-established by gold evaporation or a gallium diffusion. The outside layer is then split as in Fig. V.1b by a diamond saw, or ultrasonic drill.

Fig. V.2 shows the mounting arrangement. The reverse bias is applied to the well, the two split layers being the signal contacts. Signals are routed to the preamplifier input stages as shown. The detector is held in an adjustable cradle with a nylon strap. The cradle is electrically isolated from earth with a ceramic insulator, boron nitride being a suitable material for this purpose.

Ingots are readily available up to 55 mm. dia. so that large systems can be made with well diameters in excess of 12 mm and still allow 15 mm drift depths. Resolution capabilities of 2 - 3 keV should be possible with the sum operation peak to Compton ratios of 30 to 1 obtainable.

Conclusion

This system, though more expensive ($\sim$ 20% estimate) than the equivalent volume conventional detector, allows several types of application that are only possible with two detectors. In addition, the source-detector geometry is optimised to its fullest extent, allowing the widest range of source activities to be measured.

References

AARKROG, E and LIPPERT, A. F., 1967, Nature, 213, 1001.

ABE, K. KAWAMURA, N., and MUTSURO, N., 1968, Nucl. Instr. and Meth., 63, 105.

ADAMS, F., 1968, J. Belge. Radiol., 51, 40.

ADAMS, J.A.S., and LOWDER, W.M., (Eds.), 1964, The Natural Radiation Environment, University of Chicago Press.

AKUTAGAWA, W., and ZANIO, K., 1968, IEEE Trans. Nucl. Sci., NS-15, no.1, 266.

ALBERGER, D.E., 1968, Nuclear Structure, Eds. Hossain, A., and Rashid, H.A John Wiley and Sons Inc., 273.

ALEXANDER, T.K., BROUDE, C., HAUSSER, O., and SHARPEY-SCHAFER, J.F., 1968, Nucl. Instr. and Meth., 65, 169.

ALLEN, K.W., 1966, Lithium Drifted Germanium Detectors, I.A.E.A., Vienna, STI/PUB/132, 142.

ANDERS, O.U., 1969, Nucl. Instr. and Meth., 68, 205.

ARKADEVA, E.N., MASLOVA, L.V., MATVEEV, O.A., and RYVKIN, S.M., 1967, Fiz. Tekh. Poluprov., 1, 805.

ARMANTROUT, G.A., 1966a, IEEE Trans. Nucl. Sci., NS-13, no.1, 84.

ARMANTROUT, G.A., 1966b, IEEE Trans. Nucl. Sci., NS-13, no.1, 370.

ARMANTROUT, G.A., 1969, UCRL 71508.

ARMANTROUT, G.A., 1970, Met. Trans., 1, 659.

ARMANTROUT, G.A., and THOMPSON Jr., H.W., 1970, IEEE Trans. Nucl. Sci., NS-17, no.3, 165.

ARNELL, S.E., HARDELL, R., and HASSELGREN, A., 1966, I.A.E.A., Vienna, Lithium Drifted Germanium Detectors, STI/PUB/132, 185.

AUBLE, R.L., BEERY, D.B., BERZINS, G., BEYER, L.M., ETHERTON, R.C., and KELLY, W.H., 1967, Nucl. Instr. and Meth., 51, 61.

BAKER, N.A., 1969, Fabrication of Lithium Drifted Detectors, M.Sc. Thesis, University of Surrey.

BALLAND, J., PIGNERET, J., SAMUELI, J.J., and SARAZIN, A., 1968, IEEE Trans. Nucl. Sci., NS-15, no.1, 411.

BARKER, P.H., and CONNOR, R.D., 1967, Nucl. Instr. and Meth., 57, 147.

BARNES, V., 1968, IEEE Trans. Nucl. Sci., NS-15, no.3, 437.

BENOIT, R., and BERTOLINI, G., 1968, Semiconductor Detectors, Eds. Bertolini, G., and Coche, A., North Holland Publishers, 201.

BERTOLINI, G., and COCHE, A., 1968, (Eds.) Semiconductor Detectors, North Holland Publishers.

BISHOP, G.R., 1958, Nucl. Phys., 5, 358.

BLACK, W.W., 1969, Nucl. Instr. and Meth., 71, 317.

BLACK, W.W., and HEATH, R.L., 1967, Nucl. Phys. A90, no.3, 650.

BOCK, E., EUR3630.

BONCH-BRUEVICH, V.L., 1966, Soviet Phys.-Solid State, 8, no.2, 290.

BORNAND, B., 1968, CEA-Bib-90.

BRANDENBERGER, J.D., 1969, Nucl. Instr. and Meth., 69, 271.

BROUDE, C., HAUSSER, O.H., MALM, H., SHARPEY-SHAFER, J.F., and ALEXANDER, T.K., 1969, Nucl. Instr. and Meth., 69, 29.

BROWN, W.L., and WAGNER, S., 1966, (Eds.) Semiconductor Materials for Gamma Ray Detectors, Conf. 660663.

BROWNRIDGE, J., and McLOUGHIN, D., 1968, Nucl. Instr. and Meth., 60, 116.

BUHLER, S., and MARCUS, L., 1967, Nucl. Instr. and Meth., 50, 170.

CAMP, D.C., 1967, UCRL 50156.

CAMP, D.C., 1969a, Semiconductor Nuclear Particle Detectors and Circuits, NAS 1593, 693.

CAMP, D.C. 1969b, UCRL 71825.

CAMPBELL, J.L., O BRIEN, P., and McNELLES, L.A., 1971, Nucl. Instr. and Meth., 92, 269.

CAMPBELL, J.L., SMITH, H.J., and MACKENZIE, I.K., 1971, Nucl. Instr. and Meth., 92, 237.

CAPPELLANI, F., OSTIDICH, A., and RESTELLI, G., 1970, Nucl. Instr. and Meth., 79, 170.

CAPPELLANI, F., and RESTELLI, G., 1968, Proceedings of the Meeting on Special Techniques and Materials for Semiconductor Detectors, Ispra, EUR 4269e, 55.

de CASTRO-FARIA, N.V., and LEVESQUE, R.J.A., 1967, IEEE Trans. Nucl. Sci., NS-13, no. 3, 363.

CHAPMAN, G.T., 1967, Nucl. Instr. and Meth., 52, 101.

CHARTRAND, M.G., and MALM, H.L., 1967, AECL 2764.

CHASE, R.L., 1967, Nuclear Pulse Spectrometry, McGraw Hill.

CHASE, R.L., 1968, Rev. Sci. Instrum., 39, 1318.

CIAMPI, M., DADDI, L., and DANGELO, V., 1968, Nucl. Instr. and Meth., 66, 102.

CLINE, J.E., 1968, IEEE Trans. Nucl. Sci., NS-15, no.1, 198.

COLEMAN, J.A., 1966, Lithium Drifted Germanium Detectors, I.A.E.A., Vienna, STI/PUB/132, 37.

COLES, R.E., 1968, Private Communication, AWRE, Aldermaston.

COOPER, J.A., 1970, BNWL-SA 2940.

COOPER, J.A., RANCITELLI, L.A., and PERKINS, R.W., 1968, BNWL-SA 2876.

COOPER, J.A., RANCITELLI, L.A., PERKINS, R.W., HALLER, W.A. and JACKSON, A.L., 1968, BNWL-SA 2009.

COOPER, J.A., WOGMAN, N.A., PALMER, H.E., andPERKINS, R.W., 1968, Health Physics, 15, 419.

COOPER, J.A. WOGMAN, N.A., and PERKINS, R.W., 1968, IEEE Trans. Nucl. Sci., NS-15, no.3, 407.

COOPER, R.D., and BROWNELL, G.L., 1967, Nucl. Instr. and Meth., 51, 72.

CROUTHAMEL, C.E., ADAMS, F., and DAMS, R., 1970, Applied Gamma Ray Spectrometry, 2nd. Ed., Pergamon Press.

DAVIES, D.E., and WEBB, P.P., 1966, IEEE Trans. Nucl. Sci., NS-13, no.1,72

DAVISSON, C.M., and EVANS, R.D., 1951, Phys. Rev., 81, 404.

DAY, R.B., DEARNALEY, G., and PALMS, J.M., 1967, IEEE, Trans. Nucl. Sci., NS-14, no.1, 487.

DEARNALEY, G., 1967, Private Communication, AERE, Harwell.

DEARNALEY, G., HARDACRE, A.G., and ROGERS, B.D., 1968, Proceedings of the Meeting on Special Techniques and Materials for Semiconductors, Ispra, EUR 4269e, 267.

DEARNALEY, G., HARDACRE, A.G., and ROGERS, B.D., 1969, Nucl. Instr. and Meth., 71, 86.

DEARNALEY, G., and NORTHROP, D., 1966, Semiconductor Counters for Nuclear Radiations, 2nd. Ed., E. and F. Spon Ltd., London.

DE WIT, R.C., and McKENZIE, J.M., 1968, IEEE Trans. Nucl. Sci., NS-15, no.3, 352.

DOLEV, A., ADAM, G., and KATRIEL, J., 1969, Nucl. Instr. and Meth., 68, 176.

DONNELLY, D.P., BAER, H.W., REIDY, J.J., and WIDENBECK, M.L., 1967, Nucl. Instr. and Meth., 57, 219.

DREXLER, G., and PERZL, F., 1967, Nucl. Instr. and Meth., 48, 332.

DZELEPOW, B.S., and ZHUKOUSKY, N.N., 1958, Nucl. Phys. 8, 250.

EISENBUD, M., 1963, Environmental Radioactivity, McGraw Hill.

EL-SHISHINI, M., and ZOBEL, W., 1966, IEEE Trans. Nucl. Sci., NS-13, no.3, 359.

ELAD, E., and NAKAMURA, M., 1968, IEEE Trans. Nucl. Sci., NS-15, no.3, 477.

ELLIOT, G., 1966, Brit. J. Appl. Phys., 17, 167.

ELLIOT, J.H., 1961, Nucl. Instr. and Meth., 12, 60.

ELLIS, R., 1968a, Proceedings of the Meeting on Special Techniques and Materials for Semiconductor Detectors, Ispra, EUR 4269e, 81.

ELLIS, R., 1968b, Private Communication, AWRE Aldermaston.

ELLIS, R., 1969, Private Communication, AWRE Aldermaston.

ENGLERT, T.J., EVERLING, F., EAKINS, G.W., and HATCH, E.N., 1966, Ames. Lab. 15-1478.

EWAN, G.T., GRAHAM, R.L., and MACKENZIE, I.K., 1966, IEEE, Trans. Nucl. Sci., NS-13, no.3, 297.

EWAN, G.T., and TAVENDALE, A.J., 1964, Can. J. Phys., 42, 2286.

FAIRSTEIN, E., and HAHN, J., 1965, Nucleonics, 23, no.7,56.

FAIRSTEIN, E., and HAHN, J., 1965, Nucleonics, 23, no.9,81.

FAIRSTEIN, E., and HAHN, J., 1965, Nucleonics, 23, no.11,50.

FAIRSTEIN, E., and HAHN, J., 1966, Nucleonics, 24, no.1,54.

FAIRSTEIN, E., and HAHN, J., 1966, Nucleonics, 24, no.3,68.

FANO, U., 1947, Phys. Rev., 72, 26.

FAWCETT, W., and PAIGE, E.G.S., 1967, Elec. Lett., 3, (11) 505.

FORCINAL, G., and MEULEMAN, J., 1970, Semiconductor Detectors for Nuclear Radiation, Technische Universitat Munchen, 62.

FOWLER, L.L., and TOONE, R.J., 1964, AECL 2569.

FOX, R.J., 1966, IEEE Trans. Nucl. Sci., NS-13, no.3, 367.

FOX, R.J., and WILLIAMS, I.R., 1965, Nucl. Instr. and Meth., 35, 331.

FRANKE, H.F., 1969, Nucl. Instr. and Meth., 72, 107.

FRECK, D.V., and WAKEFIELD, J., 1962, Nature, 193, 669.

FREEMAN, J.M. and JENKIN, J.G., 1966, Nucl. Instr. and Meth., 43, 269.

FUNSTEN, H.O., 1962, IRE Trans. Nucl. Sci., NS-9, no.3, 190.

GEARKE, R.J., CLINE, J.E., and HEATH, R.L., 1971, Nucl. Instr. and Meth., 91, 349.

GIBBONS, P.E., 1966, Lithium Drifted Germanium Detectors, I.A.E.A. Vienna, STI/PUB/132, 42.

GIBBONS, P.E., Proceedings of the Meeting on Special Techniques and Materials for Semiconductor Detectors, Ispra, EUR 4269e, 31.

GIBBONS, P.E., and IREDALE, P., 1967, Nucl. Instr. and Meth., 53, 1.

GIBBONS, P.E., and HOWES, J.H., 1969, Nucl. Instr. and Meth., 73, 221.

GIBBONS, P.E., HOWES, J.H., and PYRAH, S., 1966, Nucl. Instr., and Meth., 45, 332.

GIESLER, G.C., McHARRIS, C., WARNER, R.A., and KELLEY, W.H., 1971, Nucl. Instr. and Meth., 91, 313.

GLASGOW, P., 1970, Nucl. Instr. and Meth., 80, 141.

GORDEN, G.E., BAEDECKER, P.A., and DRAW, J.C., 1968, MIT-905-125.

GORODETZKY, S., MERDINGER, J.C., and ARMBRUSTER, R., 1966, Onde Elec., 46, 964.

GOULDING, F.S., 1961, NAS-NRC, pub 871.

GOULDING, F.S. Nucleonics, 22, 54.

GOULDING, F.S., Nucl. Instr. and Meth., 43, 1.

GOULDING, F.S., and HANSEN, W.L., 1961, Nucl. Instr. and Meth., 12, 249.

GOULDING, F.S., and HANSEN, W.L., 1964, IEEE Trans. Nucl. Sci., NS-11, no.1, 286.

GRAHAM, R.L., MACKENZIE, I.K., and EWAN, G.T., 1966, IEEE Trans. Nucl. Sci., NS-13, no. 1, 73.

GRENIER, G., and POUSSIER, C., 1968, CEA-R-3652.

GRUHN, C.R., KANE, J.V., KELLY, W.H., KNO, T., and BERZINS, G., 1967, Nucl. Instr. and Meth., 54, 268.

GUINN, V.P., 1968, G.A. 8013.

GUNNERSEN, E.M., 1967, Rep. Progr. Phys., 30, 27.

GURFINKEL, Y., and NOTEA, A., 1967, Nucl. Instr. and Meth., 57, 173.

HALL, R.N., 1966, Semiconductor Materials for Gamma Ray Detectors, Conf. 660663, 27.

HALL, R.N., BAERTSCH, R.D., and SOLTYS, T.J., 1968, NYO-3870-1.

HANSEN, W.L., and JARRETT, B.V., 1964, UCRL 11589.

HANSEN, W.L., PEHL, R.H., RIVET, E.J., and GOULDING, F.S., 1969, UCRL 19326.

HARCHOL, M., 1969, Private Communication, Nuclear Enterprises Ltd.

HARSHAW Inc., 1970, Private Communication, Solon, USA.

HASSELGREN, A., 1966, Nukleonik, 8, 443.

HEATH, R.L., 1964, Scintillation Spectrometry Gamma Ray Spectrum Catalogue, Vol. 1, IDO-16880-1.

HEATH, R.L., 1966, Nucl. Instr. and Meth., 43, 209.

HEATH, R.L., BLACK, W.W., and CLINE, J.E., 1966a, Nucleonics, 24, 241.

HEATH, R.L., BLACK, W.W., and CLINE, J.E., 1966b, IEEE Trans. Nucl. Sci., NS-13, no.3, 445.

HELMER, R.G., HEATH, R.L., SCHMITTROTH, L.A., JAYNE, G.A., and WAGNER, L.M 1967, Nucl. Instr. and Meth., 47, 305.

HELMER, R.G., METCALF, R.L., HEATH, R.L., and GAZIER, G.A., 1964, IDO 17015.

HENCK, R., GUTKNECHT, D., SIFFERT, P., DE LAET, L., andSCHOENMAEKERS, W., 1970, IEEE Trans. Nucl. Sci., NS-17, no.3, 149.

HENCK, R., SIFFERT, P., and COCHE, A., 1968, Nucl. Instr. and Meth., 60, 343.

HENCK, R., SIFFERT, P., MIEHE, J., and COCHE, A., 1969, Nucl. Instr. and Meth., 74, 169.

HENCK, R., STAB, L., LOPES da SILVA, G., SIFFERT, P., and COCHE, A., 1966, IEEE Trans. Nucl. Sci., NS-13, no.3, 245.

HICK, H., and PEPELNIK, R., 1969, Nucl. Instr. and Meth., 68, 240.

HOLLANDER, J.M., 1966, Nucl. Instr. and Meth., 43, 65.

HOTZ, H.P., MATHIESEN, J.M., and HURLEY, J.P., 1965, Nucl. Instr. and Meth., 37, 93.

HUANG, F.C.P., OSMAN, C.H., and OPHEL, T.R., 1969, Nucl. Instr. and Meth., 68, 141.

KANE, W.A., and MARISCOTTI, M.A., 1967, Nucl. Instr. and Meth., 56, 189.

KANTELE, J., MARTTILA, O.J., and HATTULA, J., 1966, Nucl. Instr. and Meth., 39, 194.

KANTELE, J., and SUOMINEN, P., 1966, Nucl. Instr. and Meth., 41, 41.

KANTELE, J., and SUOMINEN, P., 1967, Nucl. Instr. and Meth., 56, 351.

KEMMER, J., 1968, Nucl. Instr. and Meth., 64, 268.

KLEIN, C.A., 1968, IEEE Trans. Nucl. Sci., NS-15, no.3, 214.

KINGSTON, R.H., 1956, J. Appl. Phys., 27, 101.

KRANER, H.W., and CHASE, R.L., 1968, IEEE Trans. Nucl. Sci., NS-15, no.3, 381.

LALOVIC, B., 1967, Nucl. Instr. and Meth., 47, 173.

LALOVIC, B., AJDACIC, V., PAI, H.L., and PETROVIC, B., 1966, IEEE Trans. Nucl. Sci., NS-13, no.3, 221.

LARSEN, R.N., and STRAUSS, M.G., 1970, IEEE Trans. Nucl. Sci., NS-17, no.3, 254.

LAUBER, A., 1969, Nucl. Instr. and Meth., 75, 297.

LAUBER, A., and MALMSTEN, B., 1970, Nucl. Instr. and Meth., 81, 77.

LEDERER, C.M., HOLLANDER, J.M., and PERLMAN, I., 1967, Table of Isotopes, 6th. Ed., John Wiley and Sons Inc., New York.

LEVY, A.J., 1966, NASA-CR-90545.

LEWIS, S.R., and SHAFRIR, N.H., 1971, Nucl. Instr. and Meth., 93, 341.

LINGEMAN, E.W.A., KONIJN, J., POLAK, P., and WAPSTRA, A.H., 1969, Nucl. Phys., A133, 630.

LOPES DA SILVA, G., HENCK, R., and SIFFERT, P., 1968, Proceedings of the Meeting on Special Techniques and Materials for Semiconductor Detectors, Ispra, EUR 4269e, 65.

McDONALD, A., 1971, Private Communication, Nuclear Enterprises Ltd.

McINTYRE, R.J., 1965, Bull. Amer. Phys. Soc., 10, 124.

McINTYRE, R.J., 1968, IEEE Trans. Nucl. Sci., NS-15, no.1, 6.

McKAY, K.G., 1949, Phys. Rev., 76, 1537.

McKENZIE, J.M., 1969, Index to the Literature on Semiconductor Detectors, NAS Publication, Washington.

McKENZIE, J.M., and DE WIT, R.C., 1968, IEEE Trans. Nucl. Sci., NS-15, no.1, 444.

MALM, H.L., and FOWLER, I.L., 1965, IEEE Trans. Nucl. Sci., NS-13, no.1, 62.

MALM, H.L., TAVENDALE, A.J., and FOWLER, I.L., 1965, Can. J. Phys., 43, 1173.

MARTIN, M., McMATH, T.A., and FOWLER, I.L., 1970, IEEE Trans. Nucl. Sci., NS-17, no.3, 139.

MAYER, J.W., 1968a, Semiconductor Detectors, Eds. Bertolini, G., and Coche, A., North Holland Pub., 445.

MAYER, J.W., 1968b, Second Conference on Nucleonics in Aerospace, Conf. 670714, 1.

MAYER, J.W., 1969a, Semiconductor Nuclear Particle Detectors and Circuits, NAS 1593, 88.

MAYER, J.W., 1969b, Semiconductor Nuclear Particle Detectors and Circuits, NAS 1593, 284.

MAYER, J.W., and GOSSICK, B.R., 1956, Rev. Sci. Instr., 27, 407.

MEYER, H., and HEINZ, W., 1970, Semiconductor Detectors for Nuclear Radiation, Technische Universitat Munchen, 101.

MICHAELIS, W., 1969, Nucl. Instr. and Meth., 70, 253.

MICHAELIS, W., and SCHMIDT, H., 1966, Lithium Drifted Germanium Detectors, I.A.E.A., Vienna, STI/PUB/132, 90.

MIEHE, J.A., OSTERTAG, E., and COCHE, A., 1966, Onde Elec., 46, 801.

MILLER, C.E., MARINELLI, L.D., ROWLAND, R.E., and ROSE, J.E., 1956, IRE Trans. Nucl. Sci., NS-3, no.4, 94.

MONTEITH, L.K., 1964, Rev. Sci. Instrum., 35, 388.

MOWATT, R.S., 1969, Nucl. Instr. and Meth., 70, 237.

MOWATT, R.S., 1970, Can. J. Phys., 48, 2606.

MUGGLETON, A.H.F.M., 1967, Private Communication, AWRE, Aldermaston.

MUGGLETON, A.H.F.M., 1969, Private Communication, AWRE, Aldermaston.

MUKHERJEE, P., and SENGUPTA, A.K., 1969, Nucl. Instr. and Meth., 68, 165.

NELSON Jn., L.C., and ZYSKOWSKI, C., 1966, I.A.E.A. Conf. 661012-20.

NIELSEN, J.M., and PERKINS, R.W., 1967, Monaco (ICSU), STI/PUB/152, 687.

NILSSON, S., 1966, Lithium Drifted Germanium Detectors, I.A.E.A., Vienna, STI/PUB/132, 163.

NITSCHE, E., 1968, Proceedings of the Meeting on Special Techniques and Materials for Semiconductor Detectors, Ispra, EUR 4269e, 137.

OSTERTAG, E., MIEHE, J.A., and COCHE, A., 1968, Onde Elec, 48, 583.

OSTERTAG, E., MIEHE, J.A., HENCK, R., and SIFFERT, P., 1968, IEEE Trans. Nucl. Sci., NS-15, no.3, 413.

PALMS, J.M., VENUGOPALA, P., and WOOD, R.E., 1968, Nucl. Instr. and Meth., 64, 310.

PALMS, J.M., WOOD, R.E., and PUCKETT, O.H., 1968, IEEE Trans. Nucl. Sci., NS-15, no.3, 397.

PANEL DISCUSSION, 1968, Proceedings of the Meeting on Special Techniques and Materials for Semiconductor Detectors, Ispra, EUR 4269e, 283.

PARADELLIS, T., and HONTZEAS, S., 1969, Nucl. Instr. and Meth., 73, 210.

PARIS, P., and TREHERNE, J., 1968, Nucl. Instr. and Meth., 63, 123.

PARISH, H.G.F.S., 1969, Private Communication, University of Surrey.

PARISH, H.G.F.S., 1971, Unpublished Information, University of Surrey.

PARKER, R.P., Private Communication, Royal Marsden Hospital, Sutton, U.K.

PAULY, J., GUZZI, G., GIRARDI, F., and BORELLA, A., 1966, Nucl. Instr. and Meth., 42, 15.

PEHL, R.H., and GOULDING, F.S., 1970, Nucl. Instr. and Meth., 81, 329.

PELL, E.M., 1960, J. Appl. Phys., 31, 291.

PELL, E.M., 1961, Nat. Acad. Sci., Pub. 871, 136.

PERKINS, R.W., and HALLER, W.A., 1967, Symposium on Life Sciences, I.A.E.A., Vienna, 42.

PETERSON, K., 1970, Unpublished Data, University of Surrey.

PHELPS, P.L., HAMBY, K.O., SHORE, B., and POTTER, G.D., 1968, UCRL 50437.

PIGNERET, J., SAMUELI, J.J., and SARAZIN, A., 1966, IEEE Trans. Nucl. Sci., NS-13, no.3, 306.

POENARU, D.N., 1967, Rev. Roum. Phys., 12, 951.

POTTER, G.D., McINTYRE, D.R., and POMERY, D., 1968, Health Physics, 16, no.3, 297.

PRINCETOWN GAMMA TECH, 1968, Nucl. Instr. and Meth., 64, 1.

PRINGLE, R.W., ROULSTAN, K.R., and STANDIL, S., 1950, Phys. Rev., 78, 627.

PRUSSIN, S.G., HARRIS, J.A.., and HOLLANDER, J.M., 1965, Anal. Chem., 37, 1127.

QUARANTA, A., MARTINI, M., and OTTAVIANI, G., 1969, IEEE Trans. Nucl. Sci., NS-16, no.2, 35.

RADEKA, V., 1964, IEEE Trans. Nucl. Sci., NS-11, no.3, 358.

RADEKA, V., 1965, NRP 1184.

RAMAYYA, A.V., VAN NOOIJEN, B., CARTER, H.K., and HAMILTON, J.H., 1966, Nucl. Instr. and Meth., 43, 379.

RESTELLI, G., 1968, Semiconductor Detectors, Eds. Bertolini, G., and Coche, A., North Holland Pub., 11.

RESTELLI, G., and ROTA, A., 1968, Semiconductor Detectors, Eds. Bertolini, G., and Coche, A., North Holland Pub., 75.

RIDLEY, D., 1967, Nuclear Enterprises Ltd. at Physics Exhibition, London.

RIDLEY, D., 1968, Private Commination, Nuclear Enterprises Ltd.

RIDLEY, D., 1969, Private Communication, Nuclear Enterprises Ltd.

ROEDEL, W., 1968, Nucl. Instr. and Meth., 61, 41.

RYVKIN, S.M., MAKOVSKY, L.L., STROKAN, N.B., SUBASHIEVA, V.P., and KHUSAINOV, A.K.L., 1968, IEEE Trans. Nucl. Sci., NS-15, no.3, 226.

RYVKIN, S.M., and MATVEEV, O.A., 1966, Soviet Physics-Doklady, 10, 1116.

SAKAI, E., 1968, IEEE Tran. Nucl. Sci., NS-15, no.3, 310.

SAKAI, E., and FOWLER, I.L., 1968, IEEE, Trans. Nucl. Sci., NS-15, no.3, 327.

SAKAI, E., and FOWLER, H.L., 1967, Appl. Phys. Lett., 10, 268.

SANTHANAM, S., WEBB, P.P., and MONARO, S., 1969, IEEE Trans. Nucl. Sci., NS-16, no.1, 75.

SAUNDERS, E.W., and MAXWELL, C.J., 1967, UCRL 70545.

SAYRES, A.R., and BAICKER, J.A., 1968, IEEE Trans. Nucl. Sci., NS-15, no.3, 393.

SCHELL, K.J., 1970, Semiconductor Detectors for Nuclear Radiation, Technische Universitat Munchen, 1.

SCHELL, K.J., and NIENHUIS, K., 1968, Proceedings of the Meeting on Special Techniques and Materials for Semiconductor Detectors, Ispra, EUR 4269e, 37.

SCHMIDT-WHITLEY, R.D., 1969, Nucl. Instr. and Meth., 70, 227.

SCHROEDER, G.L., KRANER, H.W., and ROBLEY, D., 1966, Science, 151, 815.

SEVER, Y., and LIPPERT, J., 1965, Nucl. Instr. and Meth., 33, 347.

SHAFROTH, S.M., (Ed.), 1967, Scintillation Spectroscopy of Gamma Radiation, Vol. 1, Gordon andBreach.

SHIRLEY, D.A., 1965, Nucleonics, 23, no.3, 62.

SIEGHBAHN, K., 1966, $\alpha \beta \gamma$ Ray Spectroscopy, North Holland Pub.

SKLAVENITIS, L., 1967, CEA-Bib-110.

SLIVINSKY, V.W., and EBERT, P.J., 1969, Nucl. Instr. and Meth., 71, 346.

SONNTAG, C., 1967, Monaco (ICSU) STI/PUB/152, 675.

SPROUSE, G.D., and HANNA, S.S., 1965, Nucl. Phys., 74, 177.

STAB, L., HENCK, R., SIFFERT, P., and COCHE, A., 1965, Nucl. Instr. and Meth., 35, 113.

STRAUSS, M.G., and LARSEN, R.N., 1967, Nucl. Instr. and Meth., 56, 80.

STRAUSS, M.G., LARSEN, R.N., and SIFTER, L.L., 1966, IEEE Trans. Nucl. Sci., NS-13, no.3, 265.

SUOMINEN, P., and KANTELE., 1968, Nucl. Instr. and Meth., 58, 229.

SWINTH, K.L., PHILLIPP, L.D., and HOITINK, N.C., 1968, IEEE Trans. Nucl. Sci., NS-15, no.3, 486.

TAMM, U., MICHAELIS, W., and COUSSIEU, P., 1967, Nucl. Instr. and Meth., 48, 301.

TAVENDALE, A.J., 1964, IEEE Trans.Nucl. Sci., NS-11, no.3, 191.

TAVENDALE, A.J., 1966, Lithium Drifted Germanium Detectors, I.A.E.A. Vienna, STI/PUB/132, 4.

TAVENDALE, A.J., 1970a, Nucl. Instr. and Meth., 84, 314.

TAVENDALE, A.J., 1970b, IEEE Trans. Nucl. Sci., NS-17, no.3, 130.

THOMPSON, C.J., 1969, Nucl. Applications, 6, 559.

TOKCAN, G., and COTHERN, C.R., 1968, Nucl. Instr. and Meth., 64, 219.

TRAMMELL, R., and WALTER, F.J., 1969, Nucl. Instr. and Meth., 76, 317.

TURCOTTE, R.E., and MOORE, R.B., 1969, Nucl. Instr. and Meth., 72, 210.

VERPLANKE, J.C., and VERHEIJKE, M.L., 1970, Semiconductor Detectors for Nuclear Radiations, Technische Universitat Munchen.

VAN-ROOSBROECK, W., 1965, Phys. Rev., 139, 1702.

WAINIO, K.M., and KNOLL, G.F., 1966, Nucl. Instr. and Meth., 44, 213.

WALFORD, G.V., 1970, Second Congress of the International Radiation Protection Association, Brighton, Abs. 346.

WALFORD, G.V., 1971, Semiconductor Nuclear Radiation Detectors, IEE Colloquim on Solid State Devices, London.

WALFORD, G.V., ALIAGA- KELLY, D.T.W., and GILBOY, W.B., 1971,IEEE Nuclear Science Symposium, San Francisco,to be Published.

WALFORD, G.V., and DOUST, C.E., 1968, Proceedings of the Meeting on Special Techniques and Materials for Semiconductor Detectors, Ispra, EUR 4269e, 103.

WALFORD, G.V., and DOUST, C.E., 1968, Elec. Lett., 4, no.1, 12.

WALFORD, G.V., and DOUST, C.E., 1968, Nucl. Instr. and Meth., 62, 353.

WALFORD, G.V., and DOUST, C.E., 1969, Nucl. Instr. and Meth., 67, 272.

WALFORD, G.V., and GILBOY, W.B., 1971, In Preparation.

WALLACE, G., and COOTE, G.E., 1969, Nucl. Instr. and Meth., 74, 353.

WAPSTRA, A.H., 1966, αβγ Ray Spectroscopy, Ed. Sieghbahn, K., North Holland Pub., 539.

WATT, D.E., and RAMSDEN, D., 1964, High Sensitivity Counting Techniques, Pergamon Press.

WEBB, P.P., 1968, IEEE Trans. Nucl. Sci., NS-15, no.3, 321.

WEBB, P.P., GREEN, R.M., FOWLER, I.L., and MALM, H.L., 1966, IEEE Trans. Nucl. Sci., NS-13, no.3, 351.

WEBB, P.P., MALM, H.L., CHARTRAND, M.G., GREEN, R.M., SAKAI, E., and FOWLER, I.L., 1968, Nucl. Instr. and Meth., 63, 125.

WEISBERG, L.R., L.R., and GOLDSTEIN, B., 1968, Second International Conference on Nucleonics in Aerospace, Conf. 670714, 43.

WERNER, S., 1966, Z. Anal. Chem., 221, 85.

WHITE, D.H., GROVES, D.J., and BIRKETT, R.E., 1968, Nucl. Instr. and Meth., 66, 70.

WILLIAMS, D., 1966, AERE-M 1736.

WILLIAMSON, C.F., and ALSTER, J., 1967, Nucl. Instr. and Meth., 46, 350.

WOGMAN, N.A., ROBERTSON, D.E., and PERKINS, R.W., 1967, Nucl. Instr. and Meth., 50, 1.

YAMAZAKI, T., and EWAN, G.T., 1968, Nucl. Instr. and Meth., 62, 101.

YOUNG, F.C., FIGUERA, A.S., and PFEUFER, G., 1971, Nucl. Instr. and Meth., 92, 71.

ZANIO, K.R., and AKUTAGAWA, W.M., 1968, IEEE Trans. Nucl. Sci., NS-15, no.3, 266.

ZANIO, K., AKUTAGAWA, W.M., and MAYER, J.W., 1968, Second International Conference on Nucleonics in Aerospace, Conf. 670714, 140.

ZERBY, C.D., 1960, Proceedings of a Symposium on Total Absorption Gamma Ray Spectrometry, TID 7594, 67.

ZERBY, C.D., 1963, Methods in Computational Physics, Vol 1, Eds, Alda, B., and Fernbach, S., Academic Press, New York, 89.

ZERBY, C.D., and MORAN, H.S., 1962, ORNL 3169.

ZULLIGER, H.R., and AITKEN, D.W., 1970, IEEE Trans. Nucl. Sci., NS-17, no.3, 187.